

H24/3116

MONASH UNIVERSITY
THESIS ACCEPTED IN SATISFACTION OF THE
REQUIREMENTS FOR THE DEGREE OF
DOCTOR OF PHILOSOPHY

ON..... 7 December 2001

.....
for Sec. Research Graduate School Committee

Under the copyright Act 1968, this thesis must be used only under the normal conditions of scholarly fair dealing for the purposes of research, criticism or review. In particular no results or conclusions should be extracted from it, nor should it be copied or closely paraphrased in whole or in part without the written consent of the author. Proper written acknowledgement should be made for any assistance obtained from this thesis.

ERRATA

Global Errata

Multiple citations of authors should be read as chronological order in place of alphabetical.

Example: p.1 line 18 "Ellam & Cox, 1991; Ellam *et al.*, 1992; Hawkesworth *et al.*, 1993" for "Ellam *et al.*, 1992; Ellam & Cox, 1991; Hawkesworth *et al.*, 1993".

Replace instances of " ϵ_{Nd} " with " ϵ_{Nd} "

(Abstract L23; p.69 line 1, 2; p.79 Figure 6.6 caption line 2; p.80 line 1; p.85 line 7; p.86 line 3; p.86 Figure 6.10(a) ordinate axis, Figure 6.10(b) abscissa axis; p.86 Figure 6.10 caption line 1 & line 3; p.88 Figure 6.12 ordinate axis; p.91 Figure 6.13(b) abscissa axis, Figure 6.13 parameter table line 5; p.91 Figure 6.13 caption line 4; p.96 line 7; p.96 Table 6.5 line 1; p.100 line 22, 23, 25, 27; p.101 line 2; p.104 line 13, 21; p.105 Figure 6.16 caption line 4; p.105 Figure 6.16 ordinate axis; p.106 line 15, 17; p.107 Figure 6.17 ordinate axis; p.108 Figure 6.18 ordinate axis; p.108 line 3, 4, 9; p.112 line 15, 22; p.109 Figure 6.19 parameter tables; p.110 Figure 6.20 parameter tables; p.111 Figure 6.21 ordinate axis; p.117 line 20; p.118 line 8; p.119 line 14, 18, 21; p.120 line 10; p.121 line 18, 24; p.122 line 16.)

Replace instances of " $d^{18}O$ " with " $\delta^{18}O$ "

(p.118 line 14, 16, 17, 19; p.120 line 13, 16, 18, 21; p.121 line 26; p.123 line 16.)

Specific Errata

Chapter 3

p.25 line 3 " $\sim 20\mu m$ " for " $\sim 20mm$ "
p.27 line 22 " $2050 \pm 4 Ma (2\sigma)$ " for " $2050 \pm 4 Ma$ "
p.28 Table 3.2 footer " 2σ " for " $2s$ "

Chapter 4

p.39 line 17 "Figure 4.5" for "Figure 4.6 a,b"
p.41 Figure 4.6: Comment: map was constructed from fieldwork conducted as part of this study and also from unpublished field maps of Dr Martin Sharpe (1978-1981).

Chapter 5

p.46 line 16, 19 " Fe_2O_3 " for " Fe_2O_3 "
p.47 line 6 " SiO_2 " for " SiO_2 "
p.47 Figure 5.1 " Fe_2O_3 " for " Fe_2O_3 "
p.48 Figure 5.2 " Al_2O_3 " for " Al_2O_3 "
p.48 Figure 5.2 " Na_2O " for " Na_2O "
p.48 Figure 5.2 " K_2O " for " K_2O "
p.48 Figure 5.2 " TiO_2 " for " TiO_2 "
p.48 Figure 5.2 " SiO_2 " for " SiO_2 "
p.48 Figure 5.2 " Fe_2O_3 " for " Fe_2O_3 "
p.48 line 1 " SiO_2 " for " SiO_2 "
p.49 line 16 " SiO_2 " for " SiO_2 "
p.49 line 18 " Fe_2O_3 " for " Fe_2O_3 "
p.62 line 5 "(Siliceous High Magnesium Basalts or SHMB)" for "(SHMB)"

Chapter 6

p.67 line 18 " β -decay" for "b-decay"
p.72 Figure 6.1 abscissa title " $^{187}Re/^{188}Os$ " for " $^{187}Os/^{188}Os$ "
p.87 Figure 6.11 " $\gamma Os = 0$ " for " $gOs = 0$ "
p.89 line 9 "Jordan, 1981" for "Jordan & Anonymous, 1981"

References

p.131 line 9 read "Jordan, T. H., 1981. Continents as a chemical boundary layer; the origin and evolution of the Earth's continental crust. *Philosophical Transactions of the Royal Society of London, Series A: Mathematical and Physical Sciences*, 301(1461), 359-373."

p.131 line 17 "Kruger, F.J., 1997." for "Kruger, F.J. & Anonymous, 1997."

p.133 line 10 read "Marsh, J. S., Hooper, P. R., Rehacek, J., Duncan, R. A. & Duncan, A. R., 1997. Stratigraphy and age of Karoo basalts of Lesotho and implications for correlations within the Karoo igneous province Large igneous provinces. In: *Continental, Oceanic, and Planetary Flood Volcanism* (eds Mahoney, J.J. & Coffin, M.F.). *Geophysical Monograph*, 100, 247-272."

p.135 line 23 read "Peirson, D. G., 1999. The age of continental roots. In: *International symposium on Composition, deep structure and evolution of continents* (eds van der Hilst, R. D. & McDonough, W. F.), pp. 171-194, Cambridge, MA, United States."

Appendix I:

App. I. p.III line 17 "Carius tubes were heated to 220°C" for "Carius tubes were heated to 240°C"

App I. p VI line 5 "1 ml $Ba(NO_3)_2$ " for "1 ml $Ba(NO_3)_2$ "

App. I(e). p VII line 22 "La Jolla" for "La Jolle"

App I. p VII line 14 " $^{87}Sr/^{86}Sr = 0.71023 \pm 8 (2 sd, n=50)$ " for " $^{87}Sr/^{86}Sr = 0.71023 \pm 4 (1 sd, n=50)$ "

Appendix II:

App. II p. VIII - XIII line 12 " Al_2O_3 " for " Al_2O_3 "

App. II p. VIII - XIII line 14 " Na_2O " for " Na_2O "

App. II p. VIII - XIII line 8 " K_2O " for " K_2O "

App. II p. VIII - XIII line 6 " TiO_2 " for " TiO_2 "

App. II p. VIII - XIII line 11 " SiO_2 " for " SiO_2 "

App. II p. VIII - XIII line 4 " Fe_2O_3 " for " Fe_2O_3 "

ADDENDUM

Chapter 2

p.19 line 25: Comment: Sm-Nd model ages of >3 Ga for sub-calcic garnets reported by Richardson *et al.*, (1993) for the Premier kimberlite were proposed by analogy with similar inclusion assemblages found at the Finsch and Kimberly kimberlite occurrences. Diamond inclusion model ages of these occurrences are defined by relatively well constrained Rb-Sr and Sm-Nd model ages of 2.2-3.3 Ga (Richardson *et al.*, 1984). The model ages of the harzburgite diamond inclusions from the Premier kimberlite, as defined by a poorly correlated Sm-Nd isochron, were in fact older than the age of the earth (Richardson *et al.*, 1993). However, the emphasis of the argument was that the model ages were conceivably as old as the early Kaapvaal craton, which remains a reasonable assertion on the basis that the inclusions at premier remain very similar to those found at Finsch and Kimberly sufficient for Richardson *et al.*, (1993) to propose that they are the same age.

Chapter 6

p.72 Figure 6.1 Read caption as: "Figure 6.1(a) Isochron diagram of B1 whole-rock analyses, (b) Isochron diagram of B2/B3 whole-rock analyses. Error bars at 2s of the mean are shown or entirely contained within the symbol. Isochron calculated using Isoplot/EX program after (Ludwig, 1998) using the algorithms of (York, 1969a; York, 1969b). MSWD = Means Square of Weighted Deviates. gOs = percentage deviation of the isochron initial from the calculated value for the chondritic mantle for the age of Bushveld emplacement (2054 Ma).

p.82 line 1: Comment: Reproducibility ($\pm 0.2\%$) was estimated on the basis of duplication of unknown samples. The errors quoted for analyses of the standards BHQ and NBS-29 are 1s.d.

p.105 Figure 6.16: Comment: all isotopic ratios are plotted at the age of Bushveld emplacement (2050 Ma).

Appendix I:

Appendix 1(d) include:

(viii) Procedure for cleaning steel filament holders and platinum filament wire:

In order to minimise Re-contamination of samples or instrument during-

mass spectrometry the following procedures should be adhere to:

Cleaning of Mass Spectrometer filament holders:

- (1) Using tweezers and metal file remove spent platinum wire from the filament holders
- (2) Place filaments in a small glass beaker
- (3) Transfer to clean lab and cover filament holders with hydrogen peroxide (H₂O₂) and place in ultrasonic for 10 minutes.
- (4) Drain H₂O₂ down acid sink.
- (5) Rinse filaments with MilliQ-H₂O followed by AR-ethanol.
- (6) Dry in oven at 60°C

Cleaning platinum filament wire:

- (1) Take the platinum wire and cut into 18mm long pieces.
- (2) Place the pieces in the quartz glass crucible.
- (3) Cover platinum with potassium pyrosulphate powder.
- (4) Place quartz glass crucible into small muffle furnace
- (5) Heat furnace to 400°C for 1/2 hour then 700°C for further 1 hour
- (6) Turn furnace off and wait until cooled (overnight)
- (7) Add ~20 ml MilliQ-H₂O to the crucible.
- (8) Once the white cake has loosened transfer to a wide necked teflon jar.

- (9) Add a further ~50 ml of MilliQ-H₂O and place on warm hotplate (~60°C) until white cake has completely dissolved
- (10) Rinse thoroughly with MilliQ-H₂O and dry in oven (~60°C) for one hour.

App. I(e).(ii) and (iii) p.VII: Comment: Precision on parent daughter ratios for standard analyses in the Sm/Nd and Rb/Sr isotopic systems was estimated statistically to within 95 % confidence limits as 2 standard deviation (2 sd) of the arithmetic mean of the population of long term international standard analyses (Nd: La Jolla; Sr: SRM987).

Appendix II:

App.II p.VIII-XIII: Comment: The reader should be advised that elements that are conventionally reported in ppm concentrations (Transition Metals e.g Sc, Ti, V, Cr and the REE) have been reported in ppb concentrations for consistency within the table. To convert ppb concentrations to ppm, the values should be divided by a factor of 10³.

Figures and Tables

p.21 Figure 3.1 and caption should be replaced with:

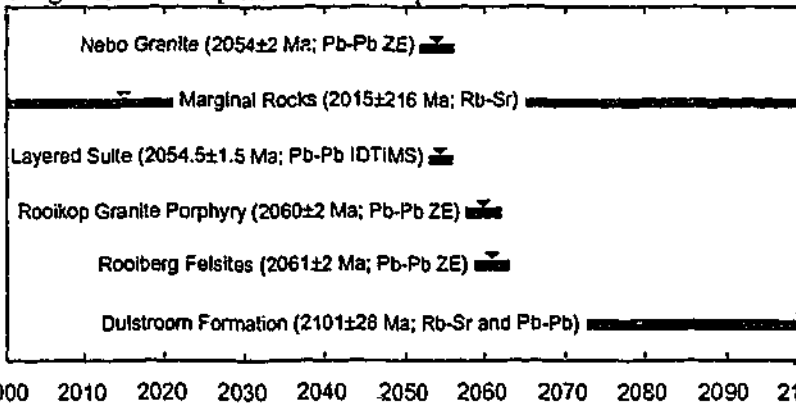


Figure 3.1 Age chart of Bushveld and related rocks illustrating the poor temporal constraint on age of the marginal rocks (Data sources are those from Table 3.1, with the exception of the age of the Layered Suite which is from Harmer and Armstrong 2000). ZE = Single Zircon Evaporation Ages.

Addendum to Figure 5.11 (p.65): Elemental parameters used in modelling primitive mantle - crustal reservoir interaction.

	Nb (ppm)	La (ppm)	Yb (ppm)	Th (ppm)	Source
Lower Crust	5.00	8.00	1.50	1.20	Rudnick & Fountain (1995) ¹
Mid Crust	8.00	17.00	2.30	6.10	Rudnick & Fountain (1995)
Upper Crust	25.00	30.00	2.20	10.70	Taylor and McLennan (1985)
N-MORB	2.33	2.50	3.05	0.12	Sun & McDonough, (1989)
E-MORB	8.30	6.30	2.37	0.60	Sun & McDonough, (1989)
OIB	48.00	37.00	2.16	4.00	Sun & McDonough, (1989)
Shoshonites	0.95	13.5	0.54	1.078	Lin et al., (1989); Pearce et al., (1992)
Average Boninite	0.80			0.26	Cameron et al., (1983) ² ; Lin et al., (1989); Pearce et al., (1992)

¹Rudnick, R. L. & Fountain, D. M., (1995). Nature and Composition of the Continental Crust: A Lower Crustal Perspective. *Reviews In Geophysics*, 33(3), 267-309.

²Cameron, W. E., McCulloch, M. T. & Walker, D. A., (1983). Boninite petrogenesis: chemical and Nd-Sr isotopic constraints. *Earth and Planetary Science Letters*, 65, 75-89.

Addendum to Appendix I(d): (ix) Table of Re-Os Standard Analyses

STD	[Os]ppb	¹⁸⁷ Os/ ¹⁸⁸ Os	2SE(M)	2SE(M)%	[Re]ppb	¹⁸⁷ Re/ ¹⁸⁸ Os	Date	Analyst	Method ¹
WPR-1	16.861	0.14400	0.00071	0.49%				JMCB	DI
WPR-1	16.380	0.14605	0.00035	0.24%	11.635	3.314	Feb-98	LRF	DI
WPR-1	16.866	0.14497	0.00029	0.20%	11.675	3.328	Feb-98	LRF	DI
WPR-1	16.823	0.14473	0.00029	0.20%			Sep-98	LRF	SE
WPR-1	17.019	0.14272	0.00073	0.51%			Sep-98	LRF	SE
WPR-1	16.560	0.14482	0.00029	0.20%			Sep-98	LRF	SE
WPR-1	16.804	0.14491	0.00029	0.20%			Sep-98	LRF	SE
WPR-1	16.729	0.14541	0.00029	0.20%	11.559	3.322	Jan-99	JMCB	SE
WPR-1	16.528	0.14517	0.00029	0.20%	11.745	3.417	Feb-99	JMCB	SE
WPR-1	16.846	0.15135	0.00097	0.64%			Mar-99	JMCB	SE
WPR-1	16.580	0.14427	0.00167	1.16%	11.526	3.342	Apr-99	JMCB	SE
WPR-1	16.556	0.14459	0.00032	0.22%	11.370	3.317	Apr-99	EC (this study)	SE
WPR-1	16.533	0.14484	0.00022	0.15%	11.106	3.243	Jun-99	EC (this study)	SE
WPR-1	16.465	0.14512	0.00022	0.15%	11.274	3.256	Jul-99	JMCB	SE

Summary Statistics

MEAN	16.704	0.14521			11.486	3.317			
STD. DEV.	0.171	0.00192			0.219	0.053			
2SE(M)	0.197	0.00222			0.253	0.062			
2SE(M)%	1.2%	1.5%			2.2%	1.9%			
n	14	14			8	8			

DI = Nitrogen gas distillation; SE = Carbon Tetrachloride (CCl₄) solvent extraction followed by microdistillation

**Parental magmas of the Bushveld Complex,
South Africa**

Edward Alexander Curl

A thesis submitted for the degree of
Doctor of Philosophy

Department of Earth Sciences
Monash University
Australia

June, 2001

Abstract

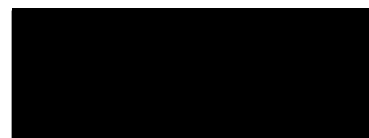
The field relations and geochemistry of the marginal rocks of the Eastern Bushveld Complex suggest that they represent the parental magma compositions of the mineralised layered complex. Re-Os and O-isotope data are consistent with derivation of these magmas mainly from mantle sources and allow only limited scope for assimilation of crustal material. Major and trace element geochemistry support previous interpretations of the marginal rocks as the products of at least two distinct magma types, the first of which relates mainly to broadly pyroxenitic (B1) marginal rocks, the second to dominantly gabbro-noritic rocks, which may be further subdivided on the basis of trace element geochemistry into B2 and B3 groups.

Co-variation within the three marginal rock groups between a number of major and minor elements and elements compatible in the minerals plagioclase, Cr-spinel and orthopyroxene indicates a major role for the fractionation and accumulation of these minerals during magmatic evolution, and these elemental trends have allowed the identification of a parental magma composition for the Bushveld Complex. Comparison of this composition with primary/parental magma compositions from other environments suggests that the marginal rocks have strong similarities to Archaean/Proterozoic siliceous high magnesium basalts (SHMB). They also show affinities with some examples of subduction-related magmas such as boninites and shoshonites.

The conclusion that the parental magmas of the Bushveld Complex were derived mainly from sources within the mantle is based largely on Re-Os and O-isotopic evidence. Although the bulk rock Re-Os isotope systematics of the marginal groups have suffered post emplacement resetting, probably related to activity of hydrothermal fluids, Os-rich chromite mineral separates preserve "mantle-like" chondritic initial Os-isotopic compositions. Similarly, relatively unfractionated oxygen isotope signatures ($\delta^{18}\text{O} \approx +5$) strongly support a dominantly mantle origin. These data, coupled with enriched incompatible trace element signatures, unradiogenic initial ϵNd values (≈ -4) and radiogenic initial $^{87}\text{Sr}/^{86}\text{Sr}$ ratios ($\sim 0.705\text{--}0.707$) favour the conclusion that the marginal rocks were sourced largely from sub-continental lithospheric mantle (SCLM) beneath the Kaapvaal craton. Data from mantle xenoliths in kimberlite pipes which have sampled the SCLM confirm the presence of suitably enriched sources. A recent seismic survey has not only confirmed the presence of thick mantle lithosphere beneath the Kaapvaal, but a zone of low seismic velocity suggests that beneath the Bushveld Complex the SCLM may have been depleted and subsequently re-enriched in response to the Bushveld magmatic event.

Declaration

This thesis contains no material previously accepted for the award of any other degree or diploma in any other university and, to the best of my knowledge, contains no material previously published or written by another person except where due reference is made in the text.



Edward Curl

June, 2001

Acknowledgements

I would like to start by thanking my supervisors in chronological order: David Lambert for co-proposing the project, providing initial inspiration and for assisting in development of the hypothesis. Wolfgang Maier for co-proposing the project, supporting my fieldwork and providing an excellent sounding board for ideas on every aspect of the Bushveld Complex. Neal McNaughton for assisting me with SHRIMP work and for helping to make my stay at University of Western Australia enjoyable and productive. Lastly, I would like to thank Ian Nicholls for associate supervision throughout the project and in particular for his thorough reviews of my work and his support during the writing of this thesis. I would also like to thank Martin Sharpe for an invaluable field tour and access to field maps and Stuart Graham for his comments and discussion.

This project was conducted with financial support from the Australian Research Council and Samancor - Steelpoort Operations (South Africa). Both of these institutions are graciously thanked for their contribution.

All of the staff in the department of Earth Sciences, past and present, have made my studies here both enjoyable and productive. In no particular order I would like to thank Chris Pierson, Florita Heinricus, Peter Moulder, Kirsten Wohlt, Robert Douglas, Louise Frick, John Tsirios, Karen Bond, Monica Walker, Jannene McBride, Adelle Agha and Draga Gelt. I would also like to thank the following academic staff for input and general good naturedness Mike Hall, Ian Cartwright, Dave Gray, Bear McPhail and Steve Beresford. To all the current and past post-graduate students thanks for making my stay here fun. In particular I would like to thank Ali Dean, Geoff Pike, Sam Watkins, Cath Spaggiari, Mary Jane, Mark Tait Jess "The Moose" Trofimovs and Christian Noll for being around.

I would like to thank my fiancée Catherine Kenna for providing me with an enormous amount of encouragement, support and inspiration over the past 3 years. I would also like to thank my sister Alison for "being on the team" and providing fantastic support over the past months. My brother Ollie is thanked for hardware support and general good fun and Arth and Chels are thanked for being there also. My Dad Bruce and my Mum Margaret are thanked for helping me get to where I am today!

Table Of Contents

ABSTRACT	
DECLARATION	
ACKNOWLEDGEMENTS	
CHAPTER 1: INTRODUCTION	1
1.1 STATEMENT OF THE PROBLEM	1
1.2 AIMS OF THE STUDY	1
1.3 SIGNIFICANCE OF THE STUDY	2
1.4 PREVIOUS WORK	3
1.5 CONCEPTUAL FRAMEWORK	4
1.5.1 Relating the marginal rocks to the layered complex	4
1.5.2 Petrogenesis	5
1.6 WORKING HYPOTHESES	5
1.7 THESIS STRUCTURE	6
CHAPTER 2: REGIONAL GEOLOGY	7
2.1 INTRODUCTION TO THE BUSHVELD COMPLEX	7
2.2 STRATIGRAPHY AND SUBDIVISION	7
2.3 REGIONAL GEOLOGY	11
2.4 POST EMPLACEMENT HISTORY OF THE BUSHVELD COMPLEX	13
2.5 CRATONIC SETTING OF THE BUSHVELD COMPLEX	14
2.6 THE MANTLE BENEATH THE KAAPVAAL CRATON	17
2.6.1 Physical features	17
2.6.2 The age of the SCLM	19
2.7 SUMMARY OF REGIONAL GEOLOGY	20
CHAPTER 3: GEOCHRONOLOGY OF THE MARGINAL ROCKS	21
3.1 INTRODUCTION	21
3.2 AGE ESTIMATES FOR THE BUSHVELD COMPLEX	21
3.3 AGE ESTIMATES FOR THE MARGINAL ROCKS	24
3.4 U-Pb SHRIMP GEOCHRONOLOGY OF THE MARGINAL ROCKS	24
3.4.1 Introduction	24
3.4.2 Sample selection	24
3.4.3 Analytical Method	25
3.4.4 Results	26
U-Pb age of the B1 rocks	26
U-Pb age of the B2 and B3 rocks	29
3.5 DISCUSSION OF SHRIMP DATA	31
CHAPTER 4: DISTRIBUTION, MINERALOGY AND PETROGRAPHY OF THE MARGINAL ROCKS	32
4.1 INTRODUCTION TO THE MARGINAL ROCKS	32
4.2 DESCRIPTION OF THE MARGINAL ROCKS	32
4.2.1 The Bushveld Type 1 (B1) marginal rocks	34
Quench textured micro-pyroxenites (BIN)	34
Granular noritic B1 marginal rocks	36
Peridotites (B1-UM)	37
4.2.2 The gabbroic marginal rocks (B2/B3)	39
4.3 DISCUSSION OF FIELD RELATIONSHIPS AND IMPLICATIONS FOR THE MODE OF EMPLACEMENT OF THE BUSHVELD COMPLEX	40
CHAPTER 5: MAJOR AND TRACE ELEMENT GEOCHEMISTRY	45
5.1 INTRODUCTION	45
5.2 MAJOR ELEMENT GEOCHEMISTRY	45
5.2.1 Analytical techniques	45

5.2.2 Results	46
<i>B1 Samples</i>	46
<i>B2 and B3 samples</i>	47
5.2.3 Comment on major element relationships	49
5.2.4 Major element classification	49
<i>Total-alkalies vs. silica classification (TAS)</i>	50
<i>Alkalies-FeO-MgO (AFM) Classification</i>	51
5.3 TRACE ELEMENT GEOCHEMISTRY	52
5.3.1 Analytical techniques	53
5.3.2 Logarithmic variation diagrams	53
<i>Mainly Incompatible Elements</i>	53
<i>Mainly compatible trace elements</i>	54
5.3.3 Multi-element spidergrams	55
<i>B1 samples</i>	55
<i>B2 samples</i>	57
<i>B3 Rocks</i>	58
5.4 PETROGENETIC AFFINITIES	59
5.4.1 Refractory element petrogenetic affinities	59
5.4.2 Incompatible trace element petrogenetic affinities	62
5.5 SUMMARY	64
CHAPTER 6: ISOTOPE GEOLOGY OF THE MARGINAL ROCKS OF THE EASTERN BUSHVELD COMPLEX: IMPLICATIONS FOR PETROGENESIS OF THE PARENTAL MELTS	67
6.1 INTRODUCTION	67
6.1.1 Application of the Re-Os system	67
6.1.2 The application of the Sr-Nd isotopic systems	68
6.2 RESULTS	69
6.2.1 Re-Os Isotopes	69
<i>Analytical Methods</i>	69
<i>Re-Os Results</i>	69
6.2.2 Sr-Nd Isotopes	75
<i>Analytical Methods</i>	75
<i>Rb-Sr Results</i>	76
<i>Sm-Nd Results</i>	78
Oxygen isotopes	80
<i>Analytical Methods</i>	80
<i>O-isotope Results</i>	82
6.3 DISCUSSION	83
6.3.1 Re-Os Isotope Systematics	83
6.3.2 Correlations between the marginal rocks and the Bushveld Complex cumulates	84
<i>Sr-Nd</i>	84
<i>Re-Os</i>	87
6.3.3 Sm-Nd depleted mantle model ages	88
6.4 SR-ND MODELLING	89
6.4.1 Previous models for the generation of the Bushveld magmas	89
6.4.2 Sr-Nd modelling of the marginal rocks	90
6.5 OXYGEN-SR MODELLING	90
<i>Modelling Results</i>	92
6.6 OS-ND MODELLING	92
Modelling Methods	94
The reservoirs	95
<i>Plume Source</i>	95
<i>The Crust</i>	96
<i>SCLM</i>	98
<i>The Depleted Mantle</i>	103
Modelling Results	104

<i>Derivation of the Bushveld from a predominantly plume source?</i>	104
<i>A role for the depleted mantle?</i>	106
<i>SCLM Component in the Bushveld melts?</i>	107
<i>Synopsis of generation of B1 melts</i>	108
<i>Generation of the B2 and B3 melts</i>	109
6.7 SUMMARY	112
CHAPTER 7: DISCUSSION AND CONCLUSION	115
7.1 INTRODUCTION	115
7.2 RELATIONSHIP OF THE MARGINAL ROCKS TO THE LAYERED COMPLEX	115
7.2.1 SHRIMP U-Pb age dating	115
7.3 SUMMARY OF PETROGENETIC INDICATORS	116
7.3.1 Major elements	116
7.3.2 Trace elements	116
7.3.3 Lithophile isotope systematics	117
7.3.4 Re-Os isotopes	119
7.4 ORIGIN OF THE BUSHVELD PARENTAL MAGMAS	120
7.4.1 "Are Bushveld U-type parent magmas boninites or contaminated komatiites?"	120
7.4.2 Nature and origin of the enriched source	120
7.4.3 Evolution of the Bushveld magma series	121
7.5 EXPLORATION/METALOGENIC SIGNIFICANCE	122
7.6 CONCLUSIONS	122
REFERENCES	124
APPENDIX I. ANALYTICAL METHODS	I
Appendix I(a) Sample Preparation	i
Appendix I(b) X-Ray Fluorescence Analysis	i
Appendix I(c) High Resolution Inductively Coupled – Mass Spectrometry (HR ICP-MS)	ii
Appendix I(d) Re-Os Isotopic analyses	ii
(i) Desilicification procedure	iii
(ii) Carius tube loading	iii
(iii) Sample spike equilibration	iii
(iv) Solvent Extraction Technique	iii
(v) Osmium microdistillation for the clean up of Os samples	iv
(vi) Re concentration and clean-up procedure	v
(vii) Negative-Thermal Ionization Mass Spectrometry (N-TIMS)	vi
Appendix I(e) Rb-Sr Isotopic Analysis	vi
(i) Sample preparation	vi
(ii) Rb-Sr Mass spectrometry	vii
(iii) Sm-Nd Mass spectrometry	vii
APPENDIX II. MAJOR AND TRACE ELEMENT DATA	VIII
APPENDIX III. SAMPLE DATABASE	XIV

Chapter 1: Introduction

1.1 Statement of the problem

The field relations, petrology and geochemistry of the marginal group of rocks associated with the Bushveld Complex suggest that they may be genetically related to the Bushveld Complex, and indeed that their chemical composition may in part represent the initial magma composition of the Bushveld intrusion prior to chemical differentiation. The chemical and isotopic characteristics of these rocks are unusual for their apparent intra-continental setting, being similar in some ways to calc-alkaline island-arc type magmas. There are three main models for the origin of these unusual characteristics in the Bushveld Complex and other similar magmas, the critical assessment of which will form the central theme of this thesis. The first invokes the crustal contamination of a mantle derived magma, citing several key aspects of their trace element and isotope characteristics as evidence for this, such as negative Nb anomalies, positive $^{87}\text{Sr}/^{86}\text{Sr}_i$ and non radiogenic initial Nd isotopic compositions (Arndt & Christensen, 1992; Arndt & Jenner, 1986; Barnes, 1989; Kruger & Anonymous, 1997; Sun, 1989). The second hypothesis explains these characteristics as being derived from the contamination of an asthenospheric mantle derived magma, such as a melt from the head of a plume, with a low degree partial melt of the sub-continental lithospheric mantle (SCLM). The low degree partial melt of the SCLM has been termed the "*lamproite component*", likening it's composition to that of ultrapotassic lamproite magmas (Ellam *et al.*, 1992; Ellam & Cox, 1991; Hawkesworth *et al.*, 1993). The final model invokes a composition that is dominated by melting in the SCLM itself, with a heat source and a possible melt component provided by the arrival of a mantle plume at the base of the lithosphere (Lambert *et al.*, 1994).

1.2 Aims of the study

The aims of this study are twofold:

- To further understand the genetic relationships between the marginal rocks and the layered succession of the Bushveld Complex.

- Document and understand the unusual characteristics of the parental magmas in terms of processes operating during magma generation, transport and emplacement.

1.3 Significance of the study

The Bushveld is the largest known mafic/ultramafic layered intrusion in the world, with subsurface outcrop in excess of 60,000 sq. kilometers. Host to the Merensky Reef and UG-2 Chromite layer, containing approximately 90% of the world's platinum reserves, as well as massive reserves of chromium and vanadium, the Bushveld is not only geologically significant, it is also economically highly significant (Eales & Cawthorn, 1996). The fact that the marginal rocks share some of their unusual chemical and isotopic characteristics with several other mineralised layered igneous complexes, suggests that the development of these characteristics may be associated with the generation of magmas predisposed to the formation of platinum group element ore deposits. As such, understanding the processes that led to the development of these characteristics may be integral in understanding the controls on ore formation and localisation. Furthermore, a specific understanding of the parental magma composition is important because the mixing of two compositionally disparate magmas may be instrumental in the sulphide saturation of the magmas leading to the concentration of metals into laterally extensive economic horizons (Irvine *et al.*, 1983; Irvine & Sharpe, 1982; Lambert *et al.*, 1989). Therefore an understanding of the exact nature of these magmas is critical to the full understanding of this process.

The inherent fractionation associated with the development of a mineralogically layered suite of rocks hinders efforts to directly assess the nature and origin of the parental magma(s) to a layered igneous complex on the basis of the cumulate sequence alone. Focusing on the granular (phyric) and quench textured (aphyric) marginal rocks of the Bushveld, this study offers a rare opportunity to study probable examples of the parental magmas(s) to a mineralised layered igneous complex, and to study them for the first time using modern, high precision isotopic and trace element techniques.

The size and inferred volume of the igneous province suggests that the Bushveld Complex may be

related to the presence of a mantle plume beneath the Kaapvaal craton in the early Proterozoic. Thus, this study of the processes that led to the generation of the Bushveld parental magmas provides an unprecedented opportunity to study the processes of interaction between mantle plumes and the continental lithospheric mantle and/or continental crust. In providing a greater understanding of these processes this study will determine the relative importance of these processes in the genesis of the world class mineral deposits hosted by the Bushveld.

1.4 Previous work

The layered suite of the Bushveld has been studied extensively since the discovery of the Merensky Reef deposit in 1924 by Andries Lombaard and Dr Hans Merensky. Major field based studies on the stratigraphy have been conducted *e.g.* (Jackson, 1967), and petrological studies summarised by Eales & Cawthorn, (1996), including an estimation of parental magma composition based on a sample from the marginal suite of rocks by Wager & Brown, (1968). Until 1977 it was believed that the Bushveld and its internal stratification, was derived by the fractionation of a single magma of an Al-tholeiitic composition with the near-liquidus crystallisation sequence olivine-orthopyroxene-plagioclase-clinopyroxene (Irvine, 1970; Wager & Brown, 1968). Hamilton (1977) later recognised a marked upward increase in initial strontium isotopic composition in the cumulate sequence, with several major discontinuities or "spikes" which were correlated with marked changes in mineralogy of the cumulate sequence and, most importantly, with the economic chromitite horizons and the sulphide bearing Merensky Reef. This led to the proposition by several workers that the formation of these economically significant horizons reflected the influx and mixing of two contrasting magmas, the later with significantly more radiogenic initial strontium isotopic compositions (Hamilton, 1977; Harmer, 1985). This recognition sparked a series of studies which aimed to further characterise the magmas involved through the mapping, sampling and analysis of the marginal suite of sills and dykes in both the Eastern (Harmer & Sharpe, 1985; Sharpe, 1981; Sharpe, 1982b) and Western Bushveld (Cawthorn *et al.*, 1981; Davies *et al.*, 1980). Concurrent with these studies of the Bushveld were extensive studies of the Stillwater Complex in Montana, notably by Irvine & Sharpe, (1982), who were able to draw remarkable parallels between the Bushveld and Stillwater complexes in

terms of parental magma compositions, and mixing dynamics. This parallel was later to be confirmed and expanded upon by Lambert *et al.* (1989) and Lambert & Simmons (1987) using the first high precision trace element and Re-Os isotopic data for the Stillwater Complex.

1.5 Conceptual framework

1.5.1 Relating the marginal rocks to the layered complex

This study was founded on the premise that the marginal rocks of the Eastern Bushveld are genetically related to the layered suite. It was proposed by Harmer & Sharpe (1985), Sharpe, (1981), Wager & Brown (1968) and Willemse (1959) that the marginal rocks were compositionally representative of the initial liquid from which the complex crystallised. The validity of this premise was tested as part of this project using several approaches:

Initially, spatial relationships between the marginal rocks and the layered complex were assessed by considering the field relations at 1:10,000 scale and collecting samples, focusing on 3 key localities in the Eastern Bushveld. The field relations observed in this study built on the previous mapping work of Dr Martin Sharpe (Bushveld Institute, University of Pretoria; Harmer & Sharpe, 1985; Sharpe, 1981; Sharpe, 1982a; Sharpe, 1982b). A subset (32) of the field samples collected were analysed for major elements by X-ray Fluorescence Spectroscopy (XRF) and for trace elements, including the Rare Earth Elements (REE), by High Resolution Inductively Coupled Plasma mass spectrometry (HR-ICP-MS). The data obtained were then compared to previously published determinations on the cumulate series (*e.g.* Maier & Barnes, 1997). Notable similarities in the major and trace element chemistry of the two groups supported the possibility that the marginal rocks represent the parental magma compositions.

In order to unequivocally relate the marginal rocks to the layered complex, the geochronology of the rocks was determined by analysing for Re-Os, Rb-Sr and Sm-Nd isotopes on whole rock samples and mineral separates. Intricacies of the thermal/alteration history of the rocks were revealed by these isotope systems leading to some imprecision in the intrusion age determinations, which made it necessary to apply a third technique. U-Pb zircon (SHRIMP)

dating was performed on two representative samples, which produced significantly more precise results. These results were then compared to previous age determinations on the Bushveld Complex, and an assessment of the suitability of the dating methods applied was made. The high precision ages provided by the SHRIMP dating were indistinguishable from existing age estimates of the layered complex and confirmed, in conjunction with the major and trace element similarities, that the marginal rocks were representative of the magma parental to the Bushveld Complex.

1.5.2 Petrogenesis

Having established the genetic relationship of the marginal rocks to the layered complex the geochemistry of the rocks was considered as a petrogenetic indicator, both in the derivation of the initial magma and its evolution to form the various zones of the layered complex. Initially the major and trace element chemistry of each group of rocks was considered separately and comparatively. Once an understanding of the intra-group variation was gained it was possible to identify a representative composition for each group. These compositions were then compared with established earth reservoirs such as mantle and crustal trace element reservoirs and plausible source and contaminant compositions were identified. The isotope data were then used to further constrain possible mantle/crustal sources for the different rocks groups culminating in quantitative models of melting and crustal contamination of mantle derived rocks. This allowed the derivation of a geological model which accounts for the trace element and isotope characteristics of the parental magmas of the Bushveld Complex and also considers geological constraints such as cause/heat source of melting, volume of melting and mode of emplacement.

1.6 Working hypotheses

Based on the trace element and isotope characteristics of the marginal rocks several hypotheses for the genesis of the parental magmas were considered. Those hypotheses are:

- that these magmas represent partial melts of the chondritic asthenospheric mantle which were subsequently contaminated by continental crust during transport and

emplacement into the shallow crust

- that the magmas were derived by melting of a mantle plume which was then contaminated by continental crust
- that they represent partial melts of the sub-continental lithospheric mantle beneath the Bushveld which are either emplaced directly or are contaminated by crust en-route to emplacement.

1.7 Thesis structure

The structure of the thesis broadly reflects the conceptual development of the project. Which was to; (a) establish, unequivocally, the co-genetic relationship of the marginal rocks of the Eastern Bushveld to the mineralised layered complex and then to, (b) examine in detail the petrogenesis of the marginal rocks and propose a geological model for the generation, transport and emplacement of these parental magmas into the chamber represented by the Bushveld Complex. Chapter 2 provides an introduction to the Bushveld Complex and the Kaapvaal Craton; this is followed in Chapter 3 by a detailed description of the field relations, mineralogy, subdivision and petrography of the marginal rocks. Chapter 4 details geochronology of the Bushveld Complex and presents new SHRIMP data on the marginal rocks. Chapter 5 describes the major and trace element geochemistry of the marginal rocks and considers the implication of these finding for possible petrogenetic models for the complex. Chapter 6 further examines petrogenetic models while presenting the isotope geology of the marginal rocks examined in this study. Finally, in Chapter 7 a summation of the principal findings is presented and a global discussion and conclusions on the petrogenesis of the marginal rocks and by implication the Bushveld layered complex, is given.

Chapter 2: Regional Geology

2.1 Introduction to the Bushveld Complex

The Bushveld Complex, located in the north central Kaapvaal craton of South Africa, is the largest known mafic/ultramafic layered intrusion on earth. The Complex has an estimated subsurface expression in excess of 60,000 km² and a composite stratigraphic thickness of over 10 km. It hosts approximately 90% of the world's platinum reserves within the Merensky Reef and UG2 chromitite horizons. It also hosts abundant reserves of chromium and vanadium. As such, the Complex is economically extremely significant (Eales & Cawthorn, 1996). The aim of this chapter is to introduce the reader to the Bushveld Complex and to place it in a regional stratigraphic and tectonic framework.

2.2 Stratigraphy and Subdivision

The mineralogically layered cumulate sequence of the Bushveld Complex is subdivided into 5 zones on the basis of vertical mineralogical and petrological variations (Fig. 2.1). The Lower Zone consists of a layered sequence of dunites and harzburgites, ranging in thickness from zero in parts of the Eastern Bushveld, to over 800 m at the Union section of the Western Bushveld. The thickness is governed largely by the topography of the floor of the complex. The overlying Lower Critical Zone (CZ_L), at an average thickness of 800 m consists predominantly of orthopyroxenites. The sudden first appearance of cumulus plagioclase (Fig 2.2a) marks the base of the 400 m thick Upper Critical Zone (CZ_U), which consists of norites and anorthosites with subordinate orthopyroxenites and harzburgites. Together the Lower and Upper Critical Zones host up to 13 massive chromitite layers (Fig 2.2b) each up to 1.6 m in thickness, with a total combined thickness of 8.3 m at the Union Section in the Western Bushveld. Chromite layers are mined extensively for chromium in the Eastern Bushveld (Eales & Cawthorn, 1996; Lee & Perry, 1988; Maier *et al.*, 2000). In addition the CZ_U hosts the economically important Merensky reef and UG-2 deposits. The 2-3 km thick Main Zone (M₂) is uniformly gabronoritic with minor anorthosite. The 2-3 km thick Upper Zone (U₂) is broadly ferrodioritic in composition and is host to 13 massive vanadiferous magnetite layers, currently being mined for vanadium (Eales & Cawthorn, 1996). The vertical

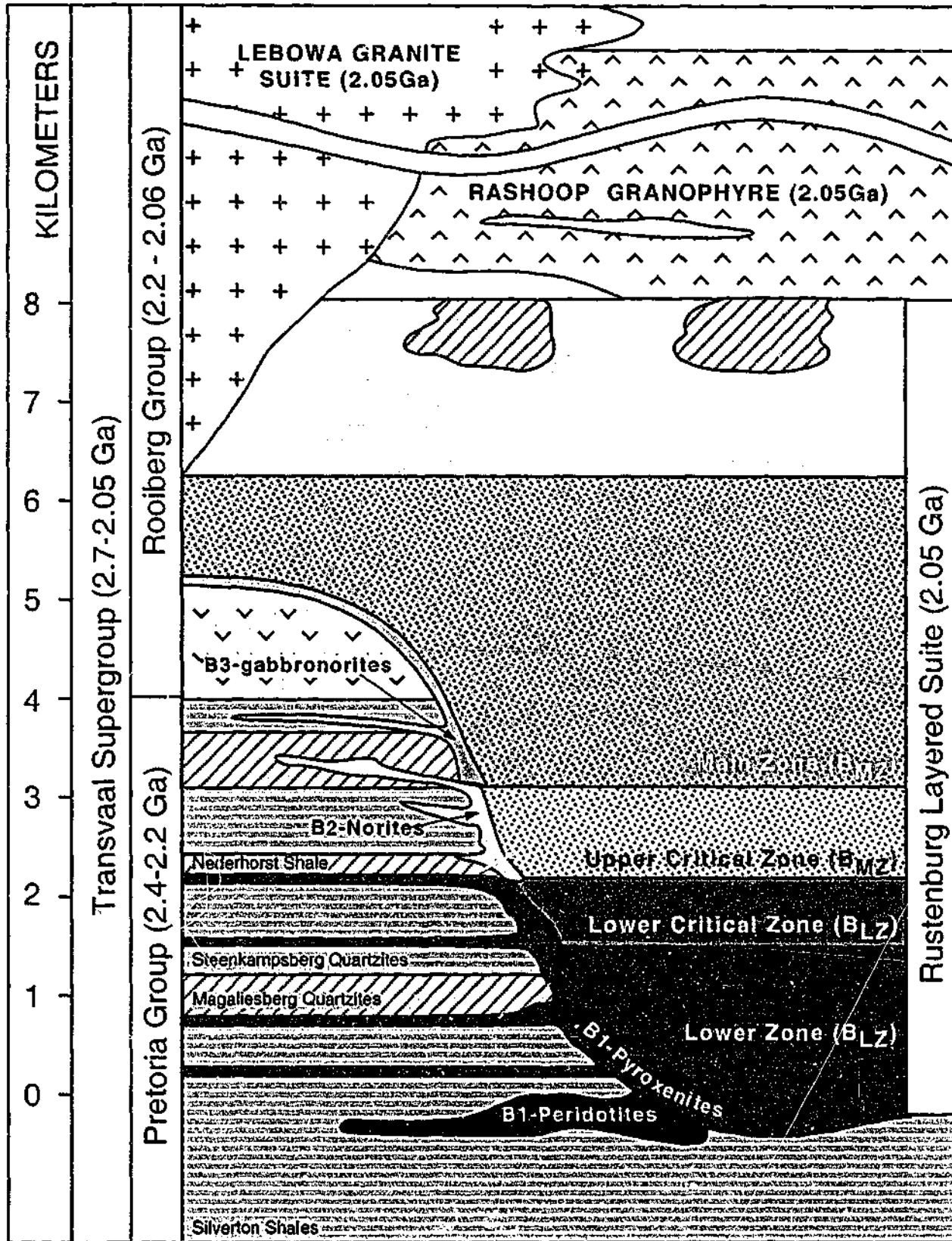


Figure 2.1 Generalised stratigraphy of the Bushveld Complex and associated Transvaal Supergroup sedimentary host rocks (adapted from von Gruenewaldt *et al.* 1985).

lithological/mineralogical variation of the complex is summarised in Figure 2.3.

Two distinct groups of rocks identified as part of the marginal sequence associated with the Eastern Bushveld broadly mirror the compositional development of the Layered Complex from bottom to

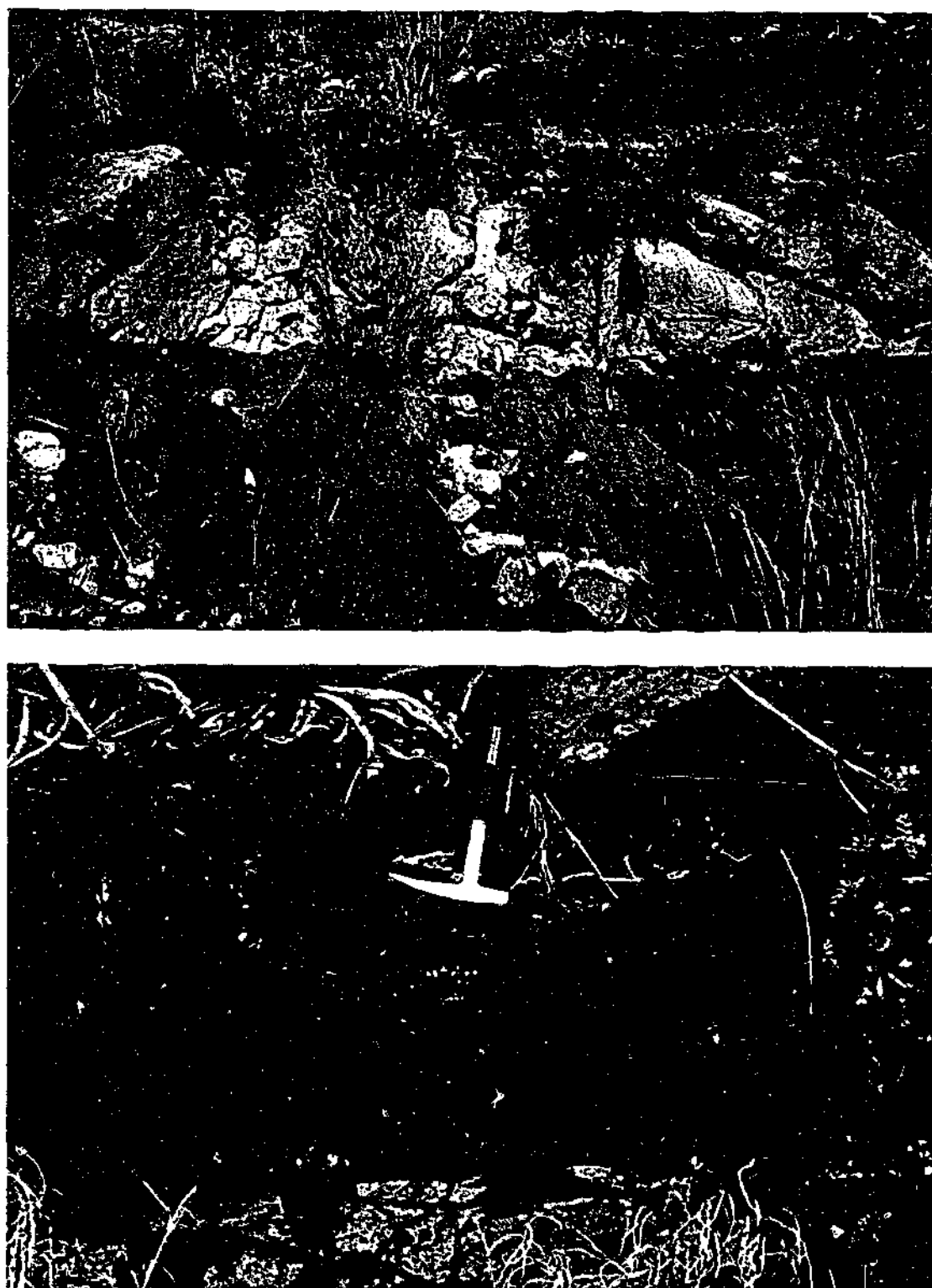


Figure 2.2 Field photographs from key localities in the eastern Bushveld Complex. (a) contact between Lower Critical Zone pyroxenite overlain by the first appearance of plagioclase marking the base of the Upper Critical Zone, (b) massive chromitite horizon (LG4). Both photographs taken at Cameron Section (Cameron, 1978). Pick used for scale measures 40 cm in length.

top The two groups, each consisting of a number of facies, are defined on the basis of their spatial distribution with respect to the Layered Complex, their petrography and their major, minor and trace element geochemistry. The first is a broadly pyroxenitic group (including some peridotites) that borders the Lower Zone and Lower Critical Zone of the complex termed the Bushveld Type 1 (B1) marginal rocks (Sharpe, 1981). The second is a gabbroic group extending upward from the

boundary between the Lower Critical and Upper Critical Zones where plagioclase appears as a cumulus phase, hence the more felsic (gabbroic) character of the associated marginal rocks. The gabbroic group is further subdivided into two groups on the basis of its field relations, and geochemistry. The first of these is the Bushveld Type 2 (B2) marginal group which occur as a thin (<100 m) thick "rind" where the Upper Critical Zone of the Layered Complex abuts the Transvaal sediments. Locally the B2 rocks also occur as shallow sills which are separated from the marginal package by not more than 5 m of quartzite. The second gabbroic group are termed the Bushveld Type 3 (B3) group, occurring as the marginal group to the Main Zone of the Layered Complex. Its mode of occurrence is similar to that of the B2 rocks and indeed B3 gabbros are difficult to distinguish from their B2 counterparts in outcrop.

A schematic map of the Bushveld Complex as a whole is shown in Figure 2.4. As shown, the Bushveld has traditionally been considered as a series of "limbs" or intrusive compartments (Hunter,

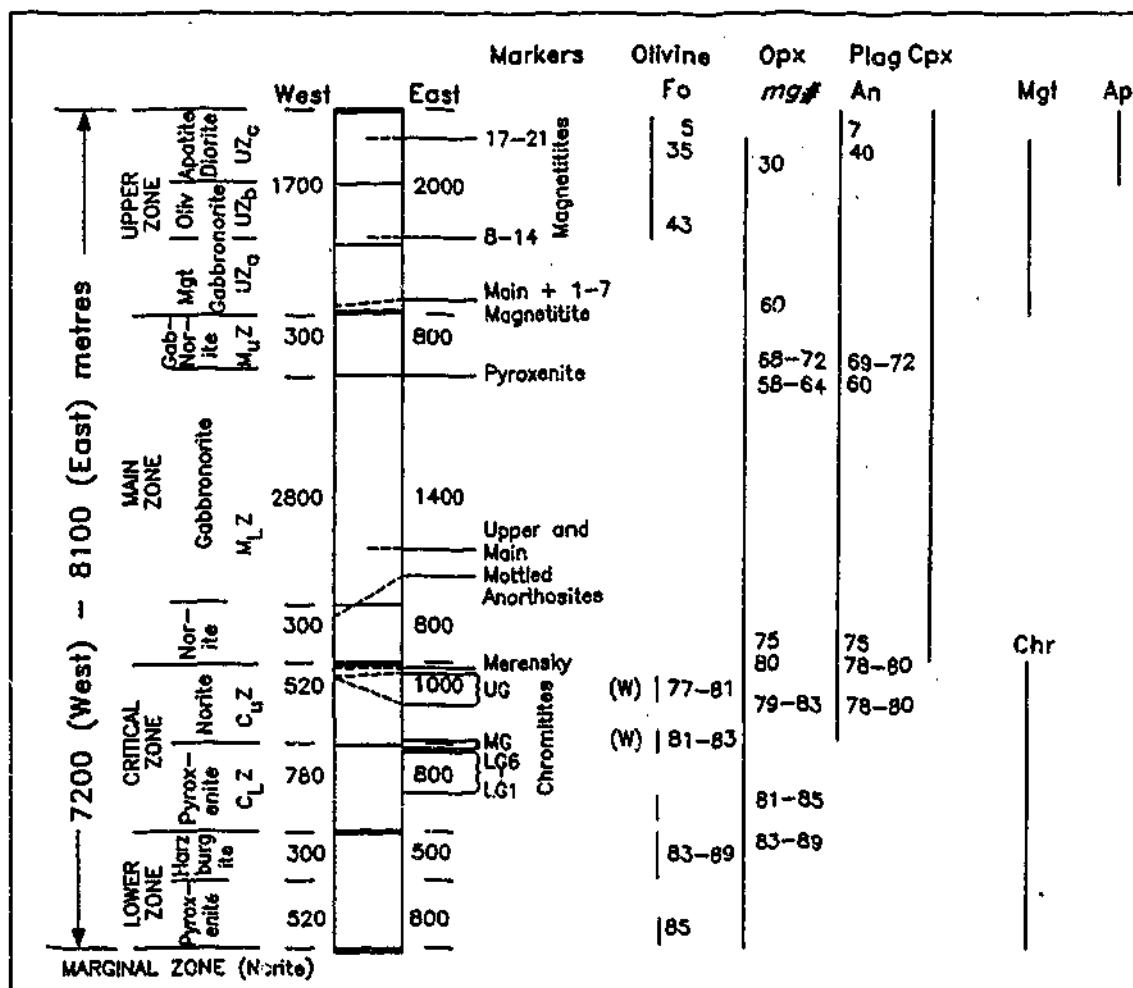


Figure 2.3 Generalised stratigraphic sections through the Eastern and Western Bushveld (as indicated), highlighting appearance/disappearance of main cumulus phases. Generalised trends of cumulus mineral compositions are also shown (Eales & Cawthorn, 1996).

1975; Sharpe & Snyman, 1980). This was based on early gravity data that indicate that the mafic phase was not continuous beneath the cover sequences that now limit the surface expression of the complex (Smit *et al.*, 1962). However, reconsideration of gravity data in the light of isostatic constraints has revealed that it is possible that the Complex was intruded as a single lopolith (pers com. Cawthorn, R.G.). This is supported by aeromagnetic data, which clearly support the fact that the various limbs are interconnected, and indeed that the Bushveld Complex is a single interconnected intrusive body (Fig. 2.5). This is in line with the very similar stratigraphic relationship observed in the two main surface expressions, the Eastern and Western Bushveld (Fig 2.3).

2.3 Regional geology

The Bushveld Complex intruded the Pretoria Group of the upper part of the Early Proterozoic-Late Archaean Transvaal Supergroup at *c.a.* 2.06Ga (U-Pb Zircon Age - Walraven *et al.*, 1990). The total stratigraphic thickness of the Bushveld is *ca.* 8 km. The Transvaal Supergroup is a supracrustal volcanosedimentary sequence estimated to have a total stratigraphic thickness of >15 km. The basement to the Transvaal Supergroup is the Archaean Granite-Greenstone terrain of the Murchison belt, which forms a major component of the northern portion of the Archaean Kaapvaal craton.

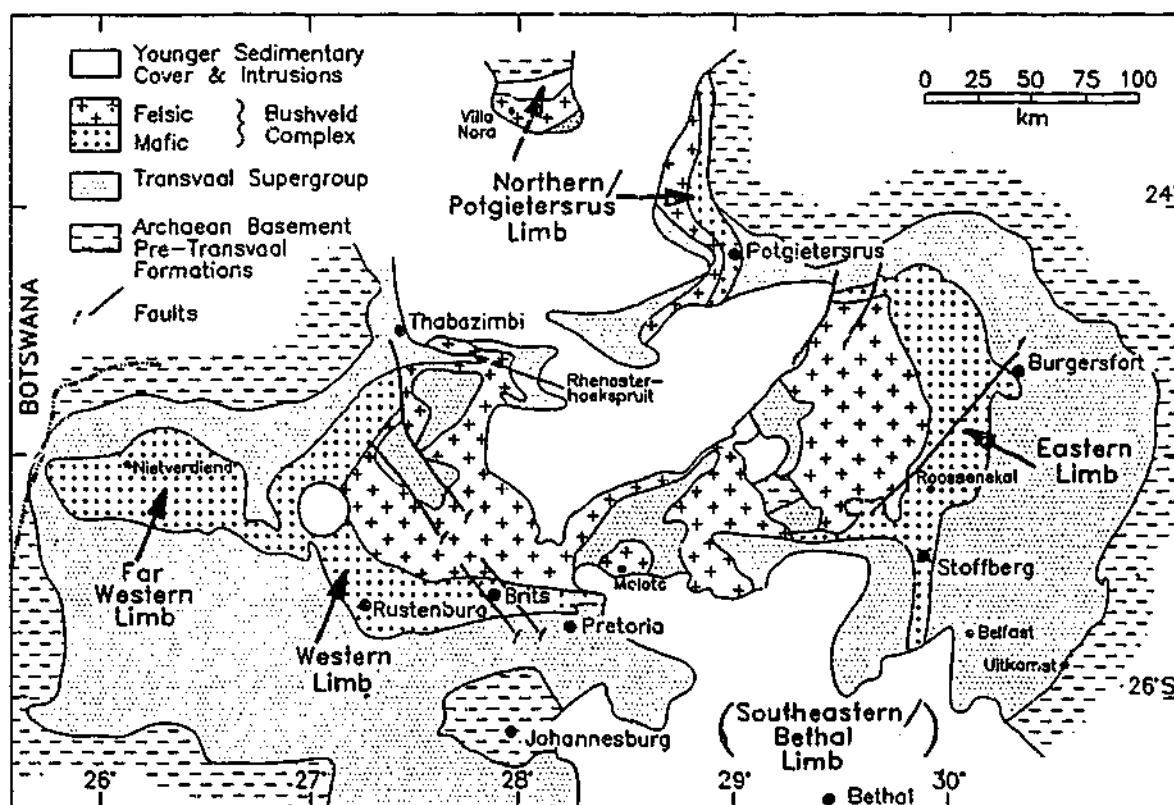


Figure 2.4 Schematic geological map of the entire Bushveld Complex (after Eales & Cawthorn, 1996).

The Transvaal Supergroup up to the base of the Pretoria group was deposited between 2.7 and 2.4 Ga in response to basinal development as a product of a failed rifting event. This rifting event climaxed with the opening of a shallow epeiric sea which provided the depositional environment for the Carbonates which make up much up the lower part of the Transvaal Supergroup (Potgeiter, 1992 *in* McCourt, 1995).



Figure 2.5 Aeromagnetic image of the Bushveld Complex and surrounding geology (modified from excerpt of Ayres *et al.* 1998).

The *ca.*2.25-2.05 Ga Pretoria group was deposited in a half graben setting (Eriksson *et al.*, 1995; Eriksson & Reczko, 1995), related to a rifting event which developed as a result of the positive inversion and re-activation of the ENE trending Thamabizi-Murchison Lineament (TML) (Potgeiter, 1992 *in* McCourt, 1995). The TML is a major crustal scale discontinuity instrumental in the accommodation of stresses caused during the development and stabilisation of the Kaapvaal craton. The TML was particularly important in accommodating stresses associated with the collision of the Kaapvaal with the Zimbabwe craton and the development of the Limpopo belt (Hoal *et al.*,

1995; McCourt, 1995).

The Pretoria group consists of a 7 km thick sequence of shales and quartzites interbedded on the kilometer scale, into which the Bushveld and associated sills were intruded. The intrusive contact of the layered sequence of the Bushveld Complex transgresses the stratigraphy of the Pretoria group (Eriksson & Reczko, 1995) (Fig. 2.1). The sills, particularly those associated with the Lower Zone of the complex, are almost exclusively stratabound and can be traced as far as 100 km into the country rocks of the Transvaal Supergroup (Sharpe, 1981). It has been proposed that the Bushveld Complex was emplaced into a dilational jog system associated with transpressional re-activation of TML during the late stage of deposition of the Pretoria group of the Transvaal Supergroup (DuPlessis & Walraven, 1990).

2.4 Post emplacement history of the Bushveld Complex

The Bushveld and surrounding rocks show little evidence of metamorphism or alteration, other than contact metamorphism associated with the emplacement of the complex itself. There is also little evidence for significant tectonism aside from the intrusion of planar dykes of Karoo age (*ca* 190 Ma; Marsh *et al.*, 1997). There is, however, some evidence to suggest that the Bushveld may have been subjected to a number of relatively minor thermal events for a period of up to 800 Ma after emplacement. An $^{40}\text{Ar} / ^{39}\text{Ar}$ analysis performed by FM Consulting on a magnetite gabbro drill-core sample collected from the Upper Zone of the Western Bushveld (Ref: GSSA LW139), yields an argon step heating plateau age of 2096 ± 12 , with partial overprints at 1750 and 1216 Ma (Burger & Walraven, 1976; Frank Fitch, FM Consulting, pers. com. 2000). Other evidence for overprinting effects has been observed in other samples from the Upper Zone of the Bushveld as well as in granites as far away as Prieska district in the SW of the Kaapvaal craton (Altermann *et al.*, 1992; Burger & Walraven, 1976).

The younger of the three ages represented in the Ar spectra (1216 Ma) may correspond to the

intrusion of the Pilanesberg alkaline complex, the Premier Kimberlite or other such alkaline intrusions, including the Spitskop Complex or the economically significant Phalabowra Complex (Walraven *et al.*, 1990; Harmer, 1999). Although individually these events were probably not thermally significant on a regional scale, the broad spatial distribution of these events implies that they may have been associated with a thermal event that was significant on a regional scale. The origin, or correlation, of the 1750 Ma event is less clear, although there is some evidence in the Kaapvaal for a thermal event at approximately this time. Similar ages are recorded in micas from the Upper Archaean Vryburg formation (1752 ± 37 Ma; Altermann *et al.*, 1992), near Debeerskloof on the SW margin of the Kaapvaal craton. Here the Kheis sub-province of the Namaqua province was deformed during the Black Ridge thrusting episode, the last regional metamorphic event affecting this part of the craton (Altermann & Halbich, 1991). Peak metamorphism associated with the 2.2-1.8 Ga Unbendian convergent margin orogenic event which occurred along the NW margin of the Kaapvaal, was achieved at approximately 1800 Ma (Gibson & Wallmach, 1995). This age of metamorphism is plausibly within error of a 1750 event, given the relatively poor constraint on the exact timing of either event. Again the broad spatial distribution of these coincident age estimates could imply a broader regional thermal event (Gibson & Stephens, 1997).

2.5 Cratonic setting of the Bushveld Complex

The Kaapvaal craton has an area of $\sim 1.2 \times 10^6$ km² the modern extent of which has been defined on the basis of mapping and geophysical investigations (Fig. 2.6). The craton is bounded to the north by its contact with the Zimbabwe craton which is marked by the Mid Archaean Limpopo belt which developed during the collision between the cratons. The western and southern boundaries of the craton are defined by the Rehoboth and Namaqua-Natal mobile belts (respectively) both of which are Proterozoic in age. The eastern margin is defined by the Lembombo monocline, which consists of Jurassic volcanic rocks, erupted during the breakup of Gondwanaland (de Wit *et al.*, 1992). Seismic evidence suggests that the craton has a deep rigid, stable lithospheric root extending to depths of 3-400 km (James *et al.*, 2001), which is further supported by diamondiferous xenoliths brought to the surface by Cretaceous kimberlites which are scattered across the craton.

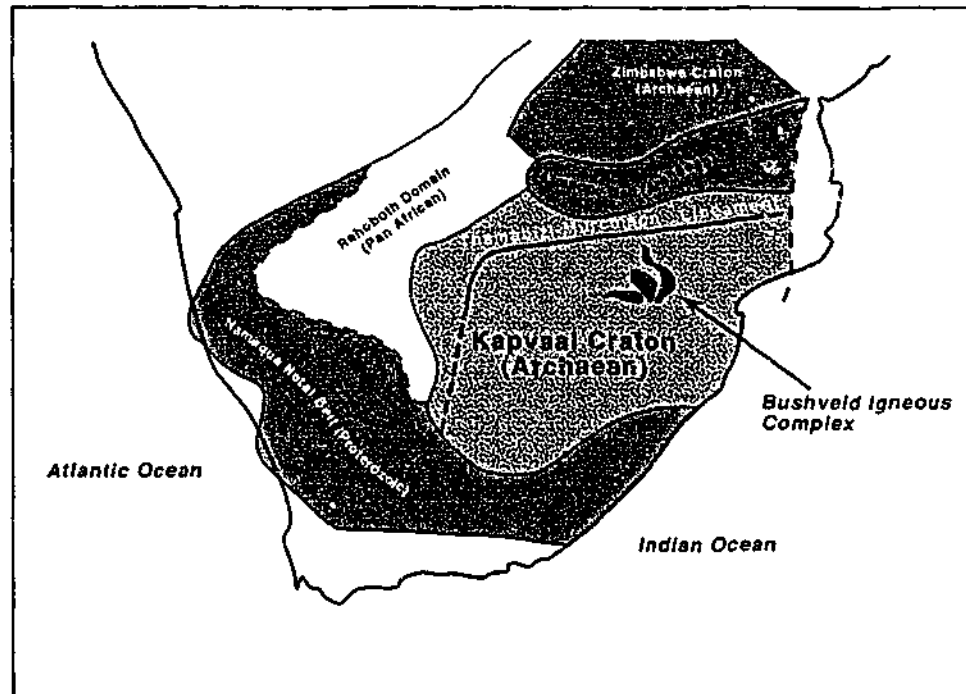


Figure 2.6 Cratonic subdivision and age of the southern African continent (adapted from Hoal *et al.* 1995)

The earliest components of the Kaapvaal craton, the Archaean Gneiss terrain, the southern Barberton greenstone belt and the northern Barberton greenstone belt were accreted early in the period 3.5-3.1 Ga. This early-accreted continental mass, approximately $5 \times 10^5 \text{ km}^2$ in area is referred to as the Kaapvaal shield. The mode of formation of these early continental fragments is envisaged to have involved a process similar to those associated with modern oceanic convergent margins, with one fundamental difference. de Wit *et al.* (1992) proposed that the early oceanic crust was of significantly lower density than modern oceanic crust, on the basis that its greater abundance of ultramafic material and more extensive hydration lead to the development of seafloor alteration assemblages consisting predominantly of relatively low density serpentine minerals. This view is supported in the Kaapvaal craton by the Jamestown ophiolite, a preserved fragment of early oceanic crust within the Barberton Greenstone belt. de Wit *et al.* (1992) propose that the lower density of the oceanic crust resulted in an obduction dominated tectonic regime. Stacking of successive ophiolite sequences and associated burial of earlier sheets would have led to the generation of large volumes of trondhjemite-tonalite magmas (Fig. 2.7). These magmas were then emplaced into the upper parts of the sequence to develop the "granite-greenstone" sequences observed in the Barberton area (Condie, 1981; Smith & Erlank, 1982).

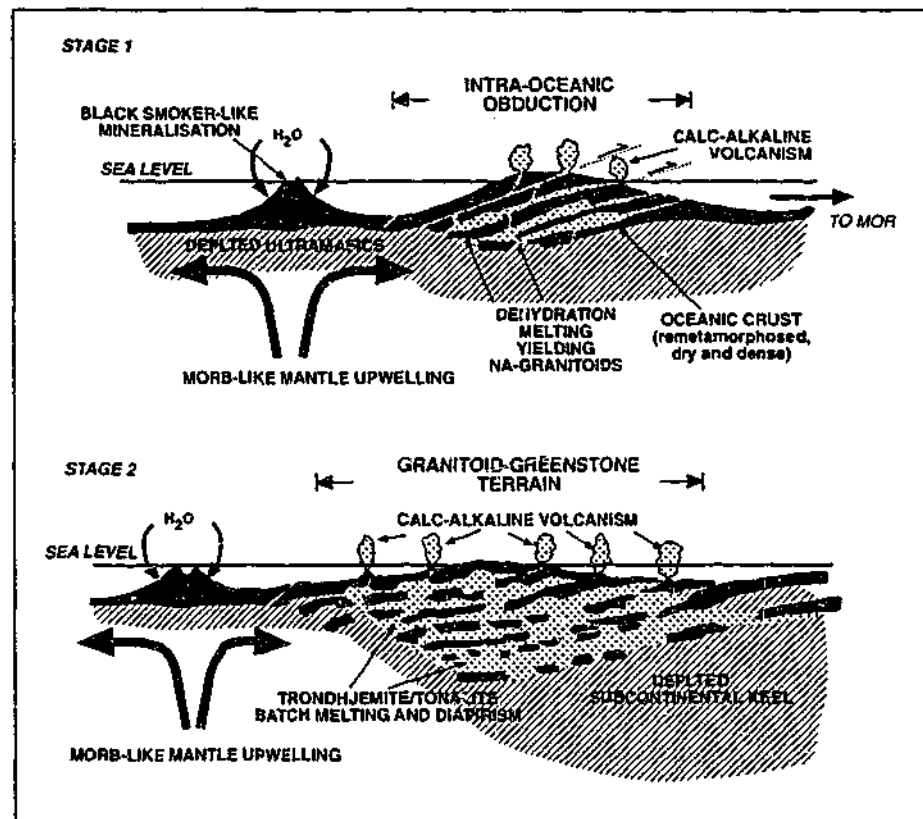


Figure 2.7 Schematic model of intra-oceanic obduction processes resulting in thrust stacking of primitive high MgO oceanic crust (Stage 1). Continuation of this process resulted in load induced subsidence of primitive crustal material causing the generation of vast amounts of tonalite-trondjemite magmas which make up much of the basement of the early Kaapvaal craton (diagram modified after de Wit *et al.*, 1992).

By 3.1 Ga the cratonic fragments had accreted and become sufficiently stabilised to support the development of late Archaean sedimentary basins (*e.g.* Witwatersrand, Pongola and Ventersdorp basins) through extension and passive continental margin development (Walraven *et al.*, 1990).

The next important phase of craton development (2.9-2.7 Ga) culminated in the accretion of several elongate fragments along the northwestern margin of the craton, some of which can be described as "exotic" such as the Murchison belt (an ancient arc-like terrain) and several exotic fragments in the Limpopo belt. The timing of collision between the Kaapvaal and Zimbabwe cratons is constrained by the peak of orogenesis and metamorphism in the Limpopo belt (2.68 Ga), and roughly marks the final stabilisation of the Kaapvaal craton (de Wit *et al.*, 1992).

2.6 The mantle beneath the Kaapvaal Craton

2.6.1 Physical features

Archaean continental regions commonly exhibit elevated S-wave seismic velocity signatures to depths of up to 350 km below the surface of the earth. This suggests that they have deep rigid roots, which are mechanically coupled and may be genetically related to the overlying continent (Gurney, 1990). Jordan (1978) termed these regions below ancient cratons the tectosphere. The Kaapvaal seismic velocity profile is typical of an Archaean craton, starting out with a seismic velocity of 4.3 km s^{-1} for the crust and upper mantle down to depths of $\sim 80 \text{ km}$, which is relatively slow when compared with global continental averages. Beyond 80 km depth the Kaapvaal exhibits a positive velocity gradient of reaching a maximum of 4.6 km s^{-1} between 110 and 220 km depth. Velocity inversion modelling shows that the S-wave seismic velocities are well above global averages down to depths in excess of 350 km (de Wit *et al.*, 1992; Durrheim & Green, 1992). More recent seismic studies of the Kaapvaal confirm these observations and provide some detail of the structure and distribution of the SCLM beneath the Kaapvaal craton (James *et al.*, 2001).

The tomographic images of James *et al.* (2001) reveal high velocity mantle keels that extend to depths of 300 km or more beneath undisturbed regions of the Kaapvaal and Zimbabwe craton (Fig. 2.8). The greatest depths seem to correspond to diamondiferous regions of the Kaapvaal craton, such as in the mantle beneath the diamond mining centre Kimberley, in the central Kaapvaal. Conversely, beneath younger post-Archaean terrains a distinct absence of deep rigid keel structures is noted. In particular beneath the Bushveld Complex, there is a zone of significantly lower seismic velocity, which according to James *et al.* (2001) may be related to the Bushveld magmatic event. The most likely explanation for a zone of low seismic velocity beneath the Bushveld Complex is the re-fertilisation (involving addition of Fe) of the SCLM, lowering the rigidity and seismic velocity (James *et al.*, 2001). Jordan (1988) noted that compositional variation can account for as much as 1% P-wave velocity perturbation, which is similar to that observed in the Bushveld SCLM.

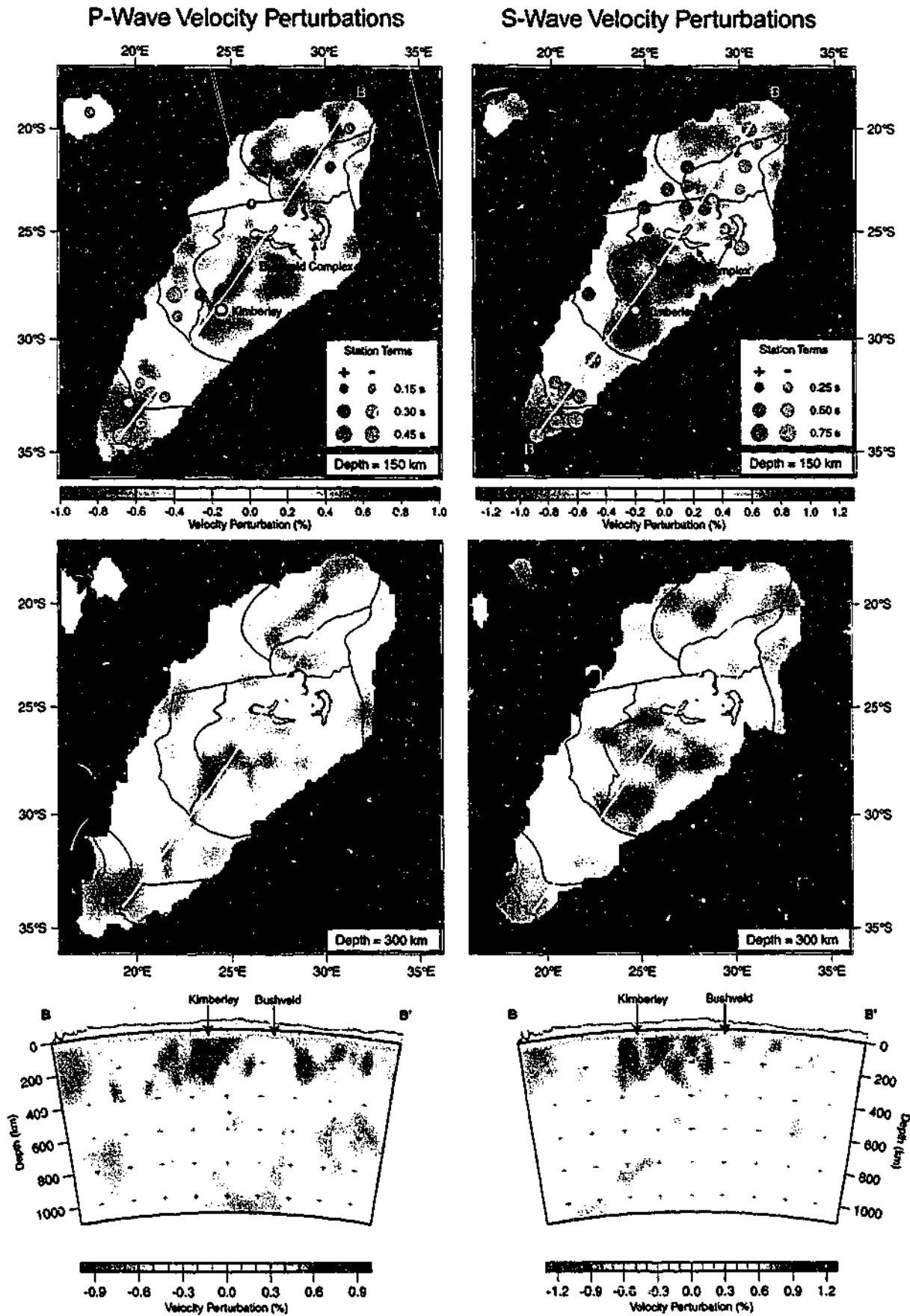


Figure 2.8 S and P-wave seismic velocity maps and profiles of a section spanning the Kaapvaal Craton, the Limpopo Mobile Belt. Marked for reference are the geographic positions of the town of Kimberley and outline of the surface expression of the Bushveld Complex (images compiled by the Kaapvaal Seismic Group as part of the Kaapvaal Project, reproduced with permission of M.J.Fouch, soon to be featured in the publication James *et al.* 2001).

In addition to seismic data, there are several other features of the Kaapvaal craton which suggest that it has a well developed SCLM. Physical sampling of this important region of the upper mantle is provided by xenoliths brought to the surface by the wide variety of kimberlites which have erupted onto the craton over the past 1000 Ma. This has allowed mantle petrologists to study the SCLM beneath the Kaapvaal in great detail. In addition to the geochemical/geophysical evidence for a thick SCLM, heat flow measurements across the Kaapvaal craton reveal, on the whole, relatively low heat flow ($\sim 45 \text{ m W m}^{-2}$). In comparison, surrounding younger mobile belts yield much higher heat flow measurements (80 m W m^{-2}) suggesting substantially thinner lithosphere in these regions (Jones, 1988 *in de Wit et al.*, 1992).

2.6.2 The age of the SCLM

Anderson (1995) proposed that the SCLM may be the product of melt extraction during crust formation. The model presented by de Wit *et al.* (1992) for formation of the early Kaapvaal shield is consistent with this relationship between crust and underlying lithospheric mantle. That is, that the keel beneath the shield represents the residue of early melting which contributed significantly to the volume of early crust. The origin and stability of the SCLM can be attributed to this ancient extraction event, rendering the rocks highly refractory and therefore able to persist for at least 3 Ga, or more, in the case of the Kaapvaal craton (Pearson *et al.*, 1999). The fact that the mantle beneath the Bushveld Complex appears to have been re-enriched might imply that the old SCLM was perhaps partially melted during the Bushveld event and subsequently re-enriched after the Bushveld magmatic event.

The contemporaneous development of the SCLM and the early Kaapvaal craton is supported by Sm-Nd isotopic ages of mineral assemblages encapsulated in diamonds (*diamond inclusion ages*) that are as old as the craton itself. Highly enriched harzburgite (clinopyroxene free) inclusion assemblages from the Premier Kimberlite, which samples the SCLM immediately adjacent to the Bushveld Complex, yield ages $>3.0 \text{ Ga}$ (Richardson *et al.*, 1993). Similarly, Rb-Sr and Sm-Nd

model ages from diamond inclusions found at Kimberley (Bultfontein) and in the Finsch kimberlite centre around 3.2 Ga (Richardson *et al.*, 1984). These model ages suggest that the SCLM chemically separated from the chondritic convecting mantle, probably through differentiation processes associated with partial melting, at around this time.

The radiogenic isotope systems, as they relate to xenolith samples of the SCLM, provide us with useful tools in understanding the enrichment and depletion history of mantle and crustal reservoirs. The Re-Os system is unique with respect to other more commonly used isotopic systems (Rb-Sr, Sm-Nd and U-Pb) in that both the parent and daughter elements are siderophile and chalcophile, and importantly Os is actually compatible during mantle melting. This leads to extreme fractionation of the Re/Os ratio during partial melting events, leading to the time integrated development of strongly contrasting Os isotopic reservoirs in the mantle and crust. Backward projection of present day measured isotopic composition of samples of the SCLM yield ages of separation of the SCLM from the chondritic mantle that are similar to those provided by diamond inclusions (Pearson *et al.*, 1999). The detailed behavior of Os during these processes will be covered in subsequent sections where relevant to the thesis.

2.7 Summary of Regional Geology

The Bushveld Complex, situated in the northwest corner of the Archaean Kaapvaal craton is the largest known mafic/ultramafic intrusive complex in the world, it is also the largest known economic repository of platinum group metals. The Bushveld intrudes the Transvaal Supergroup, a *c.a.* 15 km thick Archaean volcano-sedimentary which initiated in the late stages of craton stabilisation (3 Ga) and continued through until the initiation of Bushveld magmatism (2.06 Ga). Seismic evidence suggests that the Kaapvaal craton is underlain by an extremely thick region of rigid sub-continental lithospheric mantle, which exhibits unusually low seismic velocities in the region of the Bushveld Complex. Isotopic evidence from kimberlite borne xenoliths indicates that the development of the SCLM may have been broadly synchronous with the formation of the craton.

Chapter 3: Geochronology of the marginal rocks

3.1 Introduction

There have been several attempts to unequivocally relate the marginal rocks of the Bushveld Complex to specific sections of the mineralised layered portion of the complex on the basis of either their spatial association with the complex (Sharpe, 1981), or their mineralogical and geochemical characteristics (Cawthorn *et al.*, 1981). In the absence of precise geochronological data none of these have been successful. This chapter presents new geochronological data which provide a precise age of crystallisation of the marginal rocks and thereby allows their relationship to the Bushveld Complex layered rocks to be assessed.

3.2 Age estimates for the Bushveld Complex

Excellent reviews of the geochronology of the Bushveld Complex and related rocks have been provided by Walraven *et al.* (1990) and Walraven (1997), however a brief review will be presented here. A summary of current age estimates is presented in Table 3.1, and the data are illustrated graphically in Figure 3.1.

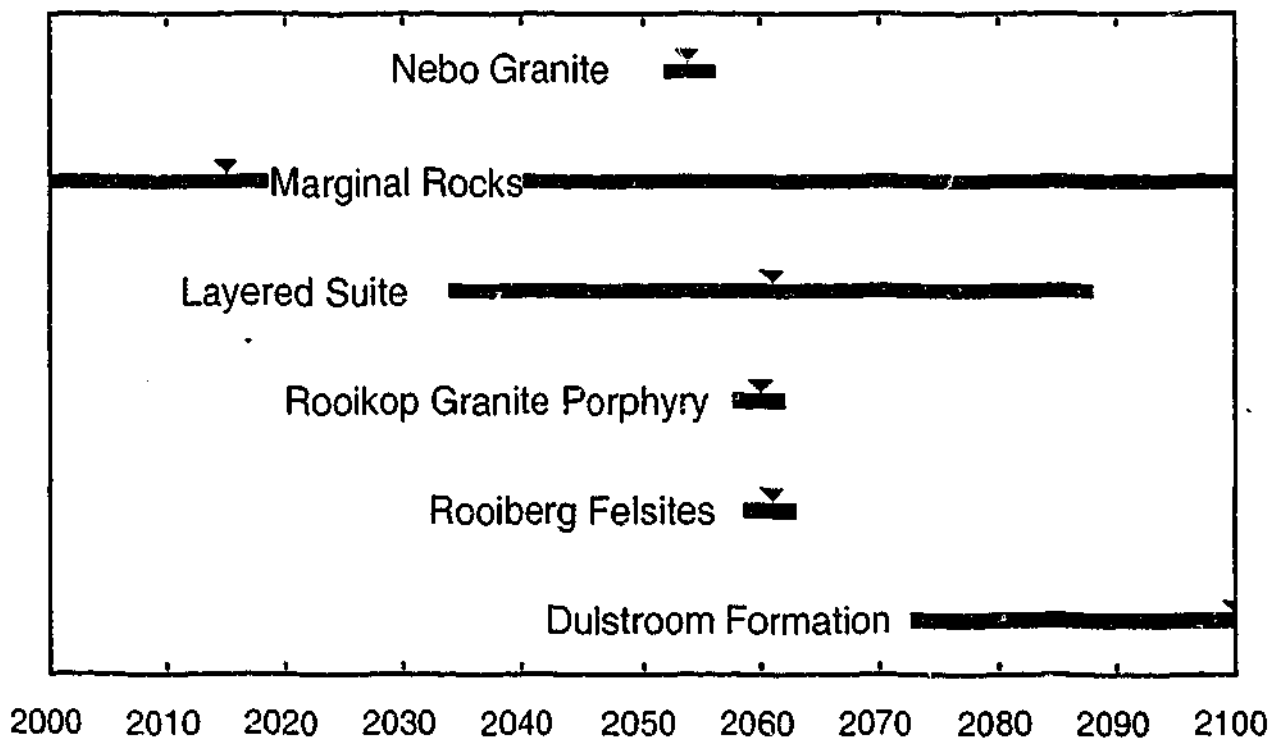


Figure 3.1 Age chart of Bushveld and related rocks illustrating the poor temporal constraint on both the Layered suite and the associated marginal rocks, both best constrained relative to their host rocks and intrusives. (Data from Harmer & Sharpe (1985); Walraven (1997); Walraven *et al.* (1990); Walraven & Hattingh (1993).

Table 3.1 Summary of age estimates for the Bushveld Complex

Rock unit (order of decreasing inferred stratigraphic age) ¹	Relationship to the Bushveld layered complex	Age (Ma)	Method ²	Reference
Dulstroom Formation	Lower Part of Pretoria Group into which the Bushveld intrudes	2101±28	Rb-Sr and Pb-Pb	J.K. Schwetzer Unpublished data in (Walraven, 1997)
Rooiberg Felsites	Roof rocks to the layered complex (predate the complex)	2061±2	Pb-Pb ZE	(Walraven, 1997)
Rooikop Granite Porphyry	Intrusive porphyry postdating Rooiberg felsites	2053±12	Pb-Pb ZE	(Walraven, 1997)
Bushveld Complex				
Layered Suite	Upper Zone	2061±27	"preferred age for Bushveld" Mean Rb-Sr of pre-1990 published ages (n=34)	(Walraven et al., 1990)
Marginal Rocks		2015±216	Whole rock Rb-Sr isochron on lower zone marginal rocks	(Harmer & Sharpe, 1985)
Nebo Granite	Intrudes the core of the layered suite	2054±2	Pb-Pb ZE	(Walraven & Hattingh, 1993)

¹Data presented in order of decreasing geological age as inferred from intrusive / stratigraphic relationships ²ZE: single grain zircon Pb-evaporation ages

The accepted best estimate of the emplacement age of the Bushveld layered complex is 2061 ± 27 Ma (Walraven *et al.*, 1990), which is an average age based on previous Rb-Sr determinations ($n=34$) for the Upper Zone of the Bushveld Complex. Walraven *et al.*, (1990) deemed this the "preferred age for the Bushveld mafic rocks". The Upper Zone rocks were chosen for this age estimate because of their homogeneous initial Sr isotopic ($^{87}\text{Sr}/^{86}\text{Sr}_i$) composition (Kruger *et al.*, 1987). In comparison age corrected $^{87}\text{Sr}/^{86}\text{Sr}_i$ for the Lower and Main Zones vary significantly, possibly reflecting mixing between two isotopically distinct magmas (Harmer & Sharpe, 1985; Irvine *et al.*, 1983; Irvine & Sharpe, 1982). Variable $^{87}\text{Sr}/^{86}\text{Sr}_i$ has led to a wide variety of relatively imprecise Rb-Sr age estimates for the Lower and Main Zones of the Bushveld Complex ranging from 1926 Ma to 2234 Ma (Hamilton, 1977; Harmer & Sharpe, 1985; Kruger & Marsh, 1982).

Several attempts to constrain the minimum age of the Bushveld Complex have been made by analysing zircons from members of the Lebowa granite suite which intrudes the core of the Bushveld Complex, using conventional Pb-Pb multi-grain wet chemistry methods (Walraven *et al.*, 1990; Walraven *et al.*, 1987). These data yield a broad spread of age estimates for the emplacement of the granites ranging from 1400 to 2063 Ma. The source of uncertainty in these ages is that they are based on concordia intercept ages of analyses that are between 45 and 70% discordant. The high uranium contents and associated metamictisation of the zircons has led to substantial Pb-loss causing this discordance. Zonation and possible inheritance of zircon crystals, which cannot be accounted for by conventional methods, probably also contributed to the failure of this method in the determination of reproducible ages for the Lebowa suite of granites (Walraven *et al.*, 1987). Despite this, the upper end of the age range is identical within the uncertainty to the accepted age of the layered complex (Walraven *et al.*, 1990).

The most convincing minimum age constraint for the Bushveld Complex is provided by high resolution age estimates for the Nebo granite (2054 ± 2 Ma), part of the Lebowa suite, which intrudes the core of the mafic phase of the Bushveld Complex and clearly postdates the layered complex (Walraven & Hattington, 1993). The maximum age of 2061 ± 2 Ma is provided by SHRIMP ages on the Rooiberg felsites into which the Bushveld intrudes (Walraven, 1997). These maxima and

minima ages provide the most precise age estimate available for the mafic phase of the complex. McNaughton & Pollard (1993) and McNaughton *et al.* (1993) suggested that the Lebowa granite suite may even represent anatectic crustal melts associated with the transport and emplacement of the Bushveld mafic phase. If this is the case then the age of the layered complex might be closer to that of the Nebo granite (2054 ± 2 Ma).

3.3 Age estimates for the marginal rocks

Absolute age determinations on the marginal rocks have until the present study been poorly constrained. The only absolute age determination is provided by a whole rock Rb-Sr errorchron (MSWD +1000) yielding an age of 2015 ± 216 Ma published by Harmer & Sharpe (1985), which is within error of the accepted age for the Bushveld. However recalculation of this age from the same data, using modern computerised methods (Ludwig, 1998) yields an age of 1873 ± 130 Ma. Either of these estimates yield ages with poor precision which should be treated as first order estimates only.

3.4 U-Pb SHRIMP geochronology of the marginal rocks

3.4.1 Introduction

SHRIMP U-Pb zircon geochronology studies have been undertaken on two samples from the marginal rocks of the Eastern Bushveld, one from the B1 suite of rocks (ECBV15) and the other from the gabbroic (B2/B3) suite (ECBV58). The results show that the two groups are synchronous with each other and compare extremely well with existing estimates of the age of the Bushveld layered complex.

3.4.2 Sample selection

Geochronological samples analysed as part of this study were collected along the Eastern margin of the Bushveld where it abuts the sediments of the Archaean Transvaal sequence. Sampling locations were selected as representative of the particular group of rocks based on the mapping work as detailed in Chapter 3 and on the work of Dr Martin Sharpe (pers. com. 1998; Harmer &

Sharpe, 1985; Sharpe, 1981; Sharpe, 1982a; Sharpe & Hulbert, 1985).

3.4.3 Analytical Method

The U-Th-Pb isotopic composition and absolute abundances in ~20 mm diameter areas of zircon were measured using a sensitive high-resolution ion microprobe (SHRIMP) at Curtin University of Technology. All analyses (n=37; Table 3.2) on the two samples were performed during a single 24 hr analytical session. Calibration of the Pb isotopic ratios was performed in reference to the cz3 standard (564 Ma; Nelson & Myers, 1997). A total of 10 analyses of the standard (excluding setup calibration) were performed at regular intervals throughout the session and were used to calculate the uncertainties on the inter-element isotopic ratios of the unknowns. The precision of measurements on the standard was considered to be excellent, calculated to be 0.99% on the $^{207}\text{Pb}/^{206}\text{Pb}$ ratios measured. Data reduction was performed using the in-house software developed at the Australian National University (RSES-ANU) and the Western Australian Isotope Science Centre (WAISC). The contribution of common lead, that is the component of non-radiogenic Pb presumably incorporated into the zircon at time of crystallisation, is assessed and corrected for. This is done by measuring non-radiogenic ^{204}Pb and subtracting the relative abundances of the other isotopes assuming Pb to have the composition of the standard Broken Hill Pb (Russell, 1975). Ages quoted are calculated from the weighted mean of the $^{207}\text{Pb}/^{206}\text{Pb}$ ratios with uncertainties as 2s (95% confidence interval) on the mean for the individual sample. A detailed description of the analytical procedure is given by Compston *et al.*, (1984) and a sound review of the data treatment is provided by Williams & Claesson, (1987).

Analytical sites on zircon grains were selected by targeting areas with minimal potential Pb loss caused by crystal damage (metamictisation) as a product of radioactive decay of U and Th. These parameters were assessed from transmitted and reflected light photomicrography as well as cathodoluminescence (CL) and backscattered electron (BSE) imaging. Several examples of images recorded are presented in Figure 3.2 and the remainder are presented in Appendix 4 (CD). CL imaging under normal electron beam conditions (*ca.* 15kV-5nA) produced limited response as a product of the low concentrations of U and Th in the crystals. CL imaging at higher energies (*ca.*

25kV), although more successful, was abandoned due to energy damage caused to the surface of the mount. When the few CL images generated were compared to the BSE images of the same grains, little, if any additional information was gained about chemical zonations or surface properties of the grains. BSE images were routinely collected at 15kV, 5nA for all grains, with minimal damage to the coated surface of the mount.

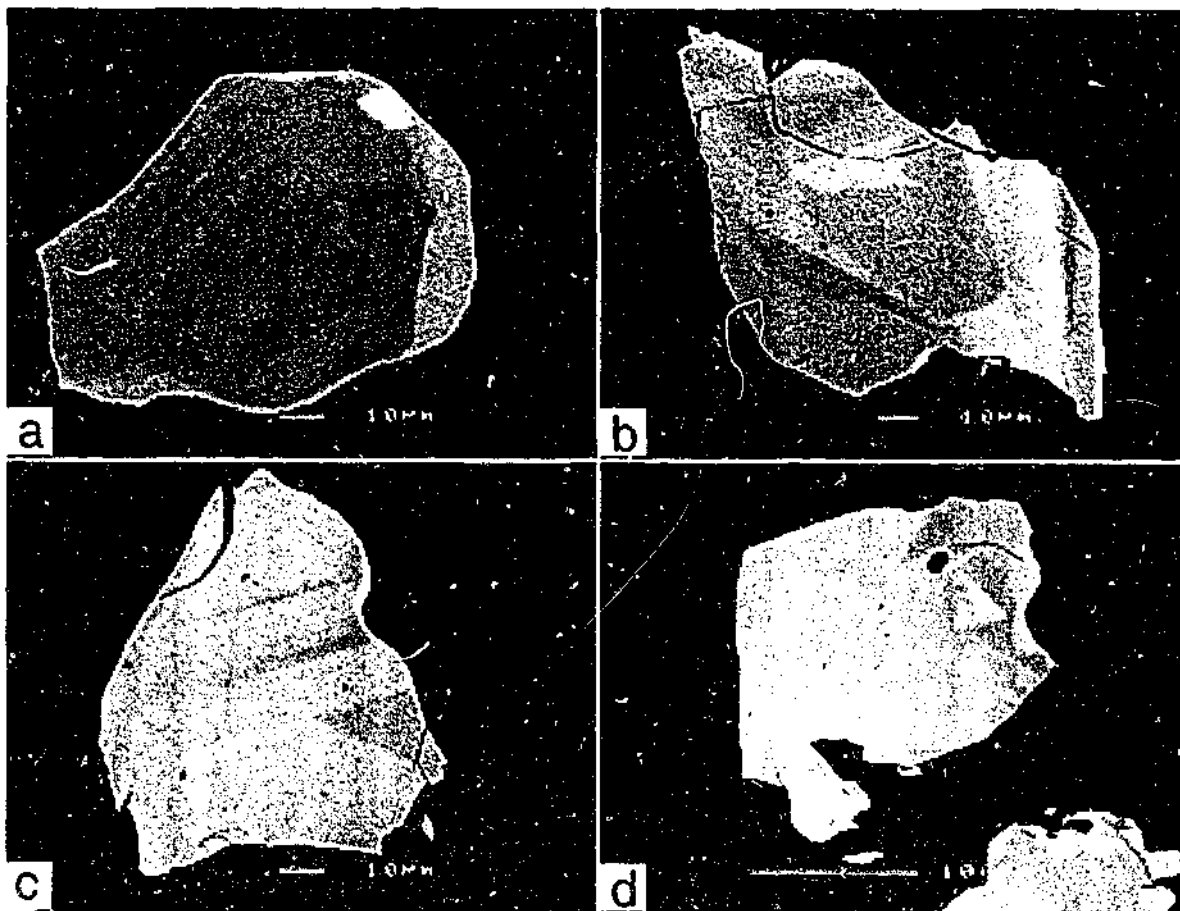


Figure 3.2 Backscattered electron images of zircons separated from sample ECBV15. (a) partially annealed / partially zoned grain, (b-d) totally annealed grains. Images collected at 15kV 5 nA and a 39 mm working distance.

3.4.4 Results

U-Pb age of the B1 rocks

Sample ECBV15 is a B1 marginal norite collected near the basal contact of the Lower Zone of the layered complex. It was sampled from a roadside exposure 2 km east of Steelpoort in the eastern Bushveld. Its location adjacent to the Lower Zone, where it protrudes to form the Burgesfort bulge, identifies it as a B1 sample, although its composition is actually transitional, being not entirely typical of the B1 marginal rocks. This sample is more chemically evolved than the remainder

of the B1 samples, having a slightly higher abundance of plagioclase than other samples from this group, it does however still exhibit similar trace element characteristics to the B1 rocks. This sample was selected for study because of its slightly more evolved composition after several failed attempts at separating zircon from more ultramafic and perhaps more chemically representative samples.

The zircons separated from the sample ECBV15 exhibited weak prismatic habit, evidenced only by occasional concentric zoning patterns on BSE images. The characteristic prismatic form of zircon was obscured in most cases by embayments in the margins of grains. The grains were 100-150 nm in diameter with an aspect ratio of close to unity. The grains were a pale pink to colourless. Very few grains appeared to be metamict, probably owing to the low-moderate concentrations of U (100-300 ppm) and Th (50-400 ppm), also indicated by their pale colour. Their Th/U ratios were 0.5-0.9. BSE electron imaging revealed about half of the grains to be apparently unzoned and the other half to exhibit cryptic zonation, a texture often associated with thermal annealing in zircons (Fig 3.2a *cf.* b-d). Figure 3.2a shows one of the few examples of preserved primary growth zonation, variable annealing at the ends of the grains highlighting the fact that they probably once exhibited primary zonation. It should be noted however, that imaging contrast parameters and digital contrast enhancement of the images used to reveal these zonations (Fig 3.2b-d), may have exaggerated the apparent degree of chemical zonation. Despite the apparent zonation the age determinations reveal a very tight age population indicating that the zonation had little effect on the behavior of the U-Th-Pb system in these zircons.

The $^{207}\text{Pb}/^{206}\text{Pb}$ concordia age of the single population of zircons separated from the B1 sample (ECBV15) is 2050 ± 4 Ma (Fig 3.3a and Table 3.2). The level of discordancy was minimal with all grains falling in the range 97-101 % concordant. The statistical regression on which the age is based on has a mean square of the weighted deviates (MSWD) value of less than unity (0.66), supporting the contention that the zircons are of a singular homogeneous age population. The fraction of measured ^{206}Pb which was calculated to be derived from common Pb is also minimal (<0.07%) rendering the choice of common Pb isotopic composition used in data reduction (Broken

Table 3.2 SHRIMP U-Pb Zircon Analytical Results

Sample	grain-spot	U (ppm)	Th (ppm)	Th/U	4t206 (%)	$\frac{207^*}{206^*}$	$\frac{208^*}{206^*}$	$\frac{206^*}{238}$	$\frac{207^*}{235}$	$\frac{208^*}{232}$	%conc.	Age(Ma)
ECBV15												
10-1	99	57	0.582	0.064	0.1261 ± 7	0.1631 ± 17	0.3733 ± 42	6.490 ± 86	0.1047 ± 17	100	2044 ± 10	
12-1	292	155	0.531	0.043	0.1259 ± 4	0.1492 ± 8	0.3680 ± 36	6.388 ± 69	0.1033 ± 12	99	2041 ± 6	
12-2	160	146	0.914	0.071	0.1269 ± 6	0.2567 ± 15	0.3741 ± 39	6.544 ± 80	0.1051 ± 14	100	2055 ± 9	
13-1	238	199	0.834	0.020	0.1272 ± 5	0.2329 ± 12	0.3718 ± 37	6.520 ± 73	0.1038 ± 12	99	2060 ± 7	
16-1	156	112	0.718	0.001	0.1263 ± 7	0.2041 ± 15	0.3803 ± 40	6.623 ± 82	0.1081 ± 15	102	2047 ± 9	
2-1	299	257	0.859	0.026	0.1265 ± 4	0.2417 ± 9	0.3688 ± 36	6.432 ± 68	0.1038 ± 12	99	2050 ± 5	
20-1	252	190	0.756	0.032	0.1261 ± 5	0.2135 ± 11	0.3699 ± 38	6.434 ± 72	0.1045 ± 13	99	2045 ± 7	
21-1	780	431	0.553	0.005	0.1267 ± 2	0.1552 ± 5	0.3630 ± 34	6.340 ± 62	0.1018 ± 10	97	2052 ± 3	
23-1	212	162	0.766	0.000	0.1264 ± 4	0.2169 ± 10	0.3725 ± 38	6.495 ± 72	0.1054 ± 12	100	2049 ± 6	
27-1	224	196	0.875	0.046	0.1266 ± 5	0.2510 ± 13	0.3580 ± 37	6.249 ± 72	0.1027 ± 12	96	2051 ± 7	
28-1	227	181	0.798	0.000	0.1269 ± 8	0.2293 ± 17	0.3668 ± 45	6.417 ± 91	0.1054 ± 17	98	2055 ± 11	
5-1	169	154	0.911	0.007	0.1261 ± 5	0.2590 ± 13	0.3739 ± 38	6.498 ± 74	0.1063 ± 13	100	2044 ± 7	
51-1	226	160	0.709	0.034	0.1256 ± 4	0.2039 ± 9	0.3796 ± 37	6.627 ± 71	0.1093 ± 12	101	2052 ± 6	
54-1	336	253	0.655	0.023	0.1264 ± 4	0.1857 ± 8	0.3739 ± 36	6.517 ± 69	0.1060 ± 12	100	2049 ± 6	
60-1	152	111	0.729	0.067	0.1262 ± 5	0.2064 ± 13	0.3777 ± 38	6.570 ± 76	0.1070 ± 13	101	2045 ± 8	
61-1	153	137	0.897	0.000	0.1272 ± 4	0.2515 ± 11	0.3738 ± 38	6.557 ± 74	0.1048 ± 13	99	2060 ± 6	
8-1	234	163	0.637	0.000	0.1262 ± 4	0.1980 ± 8	0.3761 ± 38	6.544 ± 71	0.1068 ± 12	101	2046 ± 5	
ECBV58												
10-1	55	25	0.459	0.075	0.1260 ± #	0.1275 ± 25	0.3785 ± 50	6.576 ± 113	0.1052 ± 26	101	2043 ± 17	
13-1	103	73	0.711	0.000	0.1271 ± 8	0.2010 ± 18	0.3677 ± 41	6.444 ± 86	0.1040 ± 16	98	2058 ± 11	
14-1	100	90	0.901	0.021	0.1270 ± 8	0.2541 ± 20	0.3679 ± 42	6.444 ± 89	0.1037 ± 15	98	2057 ± 11	
15-1	91	66	0.730	0.158	0.1259 ± 9	0.1990 ± 21	0.3603 ± 42	6.252 ± 91	0.0982 ± 17	97	2041 ± 13	
16-1	98	74	0.753	0.024	0.1264 ± 8	0.2132 ± 19	0.3668 ± 41	6.394 ± 86	0.1038 ± 16	98	2049 ± 11	
17-1	87	59	0.678	0.000	0.1270 ± 9	0.1924 ± 20	0.3683 ± 42	6.447 ± 92	0.1045 ± 18	98	2056 ± 13	
18-1	43	22	0.510	0.153	0.1240 ± #	0.1440 ± 36	0.3792 ± 52	6.485 ± 132	0.1070 ± 32	103	2015 ± 24	
19-1	111	94	0.850	0.036	0.1272 ± 8	0.2392 ± 18	0.3770 ± 42	6.610 ± 87	0.1061 ± 15	100	2059 ± 10	
21-1	70	39	0.556	0.139	0.1265 ± #	0.1575 ± 25	0.3618 ± 44	6.311 ± 103	0.1026 ± 22	97	2050 ± 17	
23-1	187	129	0.687	0.009	0.1271 ± 5	0.1940 ± 11	0.3693 ± 37	6.472 ± 74	0.1043 ± 13	98	2059 ± 7	
24-1	84	65	0.776	0.081	0.1264 ± 9	0.2158 ± 21	0.3703 ± 42	6.454 ± 92	0.1029 ± 17	99	2048 ± 13	
25-1	71	51	0.720	0.304	0.1249 ± #	0.1933 ± 28	0.3643 ± 43	6.276 ± 102	0.0978 ± 19	99	2028 ± 18	
26-1	92	71	0.775	0.005	0.1274 ± 9	0.2180 ± 20	0.3792 ± 42	6.658 ± 92	0.1067 ± 17	101	2062 ± 12	
27-1	104	55	0.532	0.130	0.1255 ± 8	0.1468 ± 16	0.3703 ± 41	6.406 ± 85	0.1022 ± 17	100	2036 ± 11	
3-1	55	36	0.658	0.107	0.1266 ± #	0.1868 ± 31	0.3890 ± 48	6.770 ± 120	0.1102 ± 24	103	2051 ± 20	
34-1	59	34	0.571	0.076	0.1266 ± #	0.1606 ± 26	0.3735 ± 45	6.519 ± 106	0.1051 ± 22	100	2051 ± 16	
35-1	58	27	0.475	0.074	0.1267 ± #	0.1357 ± 22	0.3756 ± 46	6.562 ± 104	0.1072 ± 23	100	2053 ± 15	
36-1	51	34	0.655	0.010	0.1263 ± #	0.1873 ± 28	0.3814 ± 49	6.642 ± 114	0.1091 ± 23	102	2047 ± 17	
4-1	47	24	0.508	0.000	0.1281 ± 8	0.1424 ± 15	0.3785 ± 48	6.683 ± 99	0.1061 ± 19	100	2071 ± 11	
50-1	95	67	0.708	0.000	0.1260 ± 6	0.2014 ± 14	0.3667 ± 41	6.369 ± 81	0.1043 ± 15	99	2043 ± 9	

All uncertainties quoted are 2s on the arithmetic mean. U-Pb isotopic ratios are corrected for common Pb calculated from the measurement of ^{204}Pb using the Broken Hill common Pb model (Russell, 1975). Analytical procedures and data treatment after Compston et al. (1984).

Hill Pb; Russell, 1975).) of negligible impact on the final age determination. A single analytical point was excluded from the regression and concordia plot. This was done on the basis that it was collected after the last standard measurement and was therefore collected in the absence of two point standard calibration and therefore relied on a projection of the standard curve.

U-Pb age of the B2 and B3 rocks

The B2 sample analysed by U-Pb SHRIMP analysis was collected from a location adjacent to the Upper Critical Zone thereby classifying it as a B2 sample. The sample site is on the Stoffberg-Lydenberg Rd very close to the sampling site of the "initial liquid" sample of Wager & Brown, (1968), as described in Cawthorn & Lee, (1998). The sample is a medium grained granular gabbro-norite typical of the B2 and B3 suite of samples. The zircons recovered, although relatively abundant, were extremely fine (<40 μm). The grains were clear and colourless, reflecting their relatively low abundances of U (50-100 ppm) and Th (50-100), with Th/U typically 0.5-0.8. Despite the marked difference in size, these zircons are very similar in shape and in their cryptic zoning patterns to the B1 zircons. This indicates that; a) their position in the mineral growth paragenesis sequence was probably similar, and b) their thermal/annealing history was probably also the same.

The $^{207}\text{Pb}/^{206}\text{Pb}$ concordia age of the zircons from the B2 sample is 2052 ± 6 Ma (Fig 3.3b, Table 3.2). All data points analysed were included in the regression with no obvious grounds for exclusion of any points. Similar to the B1 sample, the zircons from this sample exhibited a very high level of concordancy and represent a single homogeneous age population. The quality of the age regression is also very good, having an MSWD value of 0.73. The slightly greater uncertainty of the age (± 6 cf. ± 4) is not the product of the slightly lower correlation in the regression, but rather greater analytical uncertainty of the individual data points. This is caused by the lower abundance of U and consequently radiogenic Pb leading to less precise measurements. This comparison is clearly illustrated in the comparison between Figures 3.3a and 3.3b, where the uncertainty boxes in Figure 3.3b are larger than in Figure 3.3a on the same scale. The calculated proportional contribution of non-radiogenic (common) ^{206}Pb was on the whole slightly higher in the B2 sample as a product of the lower overall ^{206}Pb , but more variable than that for the B1 sample (0-0.3% cf. 0.07%). However,

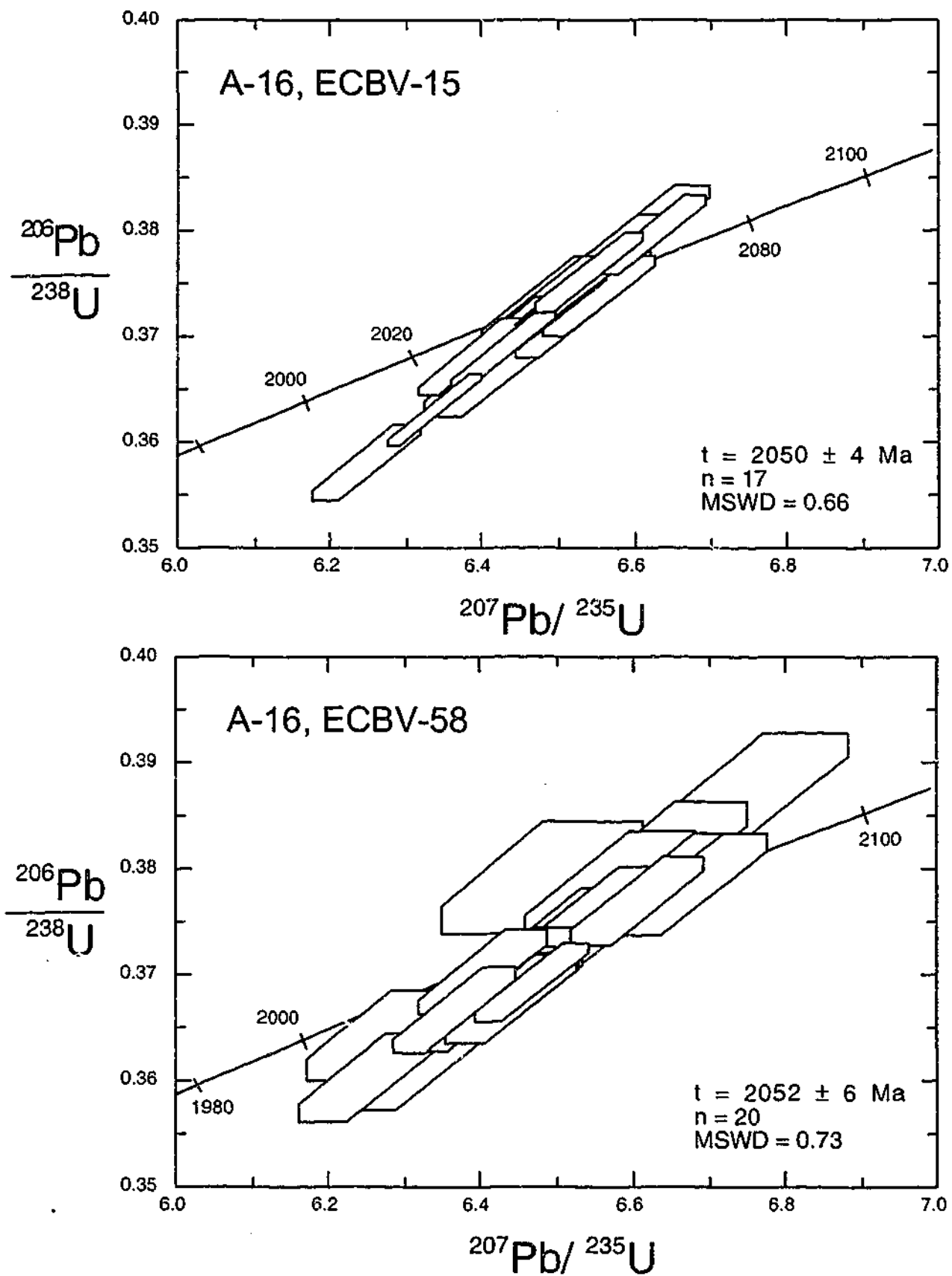


Figure 3.3 Concordia plots for zircon analyses of samples ECBV15 and ECBV58. Error boxes are 2s of the mean for individual point analyses. Ages quoted are calculated according to method described in the text.

even at the upper limits, it is still well below the level where the choice of common Pb model becomes greatly significant in the determination of the age of the rock.

3.5 Discussion of SHRIMP data

The age data presented here clearly place the age of the marginal rocks well within error of the estimated age of the layered complex (2061 ± 27 Ma; Walraven *et al.*, 1990). In light of this evidence and the other previously published evidence relating the marginal rocks to the Layered complex, it seems almost certain that the marginal rocks of the Eastern Bushveld were; a) emplaced at the same time as the layered complex, and b) they are genetically related.

Given the very high precision of the U-Pb SHRIMP ages presented here, they may in fact provide a more accurate age estimate for the emplacement of the layered complex than that of Walraven *et al.*, (1990) (2061 ± 27). The ages presented here are statistically indistinguishable from this age, which itself is close to the age of the Rooiberg (2060 ± 2 ; Walraven, 1997) which, as already noted, were intruded by the Bushveld when they were clearly in a solid state. The minimum age constraint on the layered complex is 2054 ± 4 Ma provided by the Lebowa suite which reconciles well with the age data presented here if the granites were emplaced soon after the crystallisation of the layered complex, as suggested by McNaughton & Pollard (1993) and McNaughton *et al.* (1993). In light of the collateral evidence relating the rocks to the complex, such as mineral and chemical similarities (Cawthorn *et al.*, 1981), strontium isotopic similarities (Harmer & Sharpe, 1985; Kruger, 1994) and field relations (Harmer & Sharpe, 1985; Sharpe, 1982a; Sharpe, 1982c), the age data presented here may in fact be the most precise age determination on the mafic phase of the Bushveld Complex to date.

Chapter 4: Distribution, mineralogy and petrography of the marginal rocks

4.1 Introduction to the marginal rocks

The marginal rocks of the Bushveld Complex occur as both *contact rocks* separating the layered rocks of the Bushveld Complex and the sediments of the Transvaal Supergroup and also as sills that in some cases penetrate as far as 100 km into the country rocks. By far the most common and volumetrically significant occurrence is the contact rocks which occur as a layer of variable thickness ranging over 400 m in thickness around the base of the Lower Zone to less than 10 m in some instances adjacent to the Main Zone. These rocks were originally considered to be simply the product of the quenching of the Bushveld magma(s) against the country rocks (Wager & Brown, 1968). More recent studies, particularly those in the Eastern Bushveld (Sharpe, 1981; Sharpe & Snyman, 1980), have shown them to be part of more complex multi-intrusional event that resulted finally in the emplacement of the Bushveld Complex. In this context their field relations and chemistry led Harmer & Sharpe (1985) to conclude that certain groups of the marginal rocks were the direct antecedents of specific zones within the Layered Complex.

The spatial distribution of the marginal rocks is illustrated in Figure 4.1, and their distribution with respect to the zones of the Layered Complex is illustrated schematically in Figure 2.1. Although this study has focused primarily on the Eastern Bushveld, analogues for at least one of these groups of rocks have been found in the Western Bushveld. A brief summary of the classification and distribution of the marginal rocks will be provided here. For a detailed review the reader is referred to: Harmer & Sharpe (1985); Sharpe (1981); Sharpe 1982 and Sharpe & Hulbert (1985).

4.2 Description of the marginal rocks

The following description of the marginal rocks is based on field observations, transmitted light petrographic analysis and scanning electron microscopy/microprobe analysis (energy dispersive spectroscopy; EDS). Electron imaging and representative microprobe analyses were conducted at the Centre for Microscopy and Microanalysis (CMM) at the University of Western Australia.

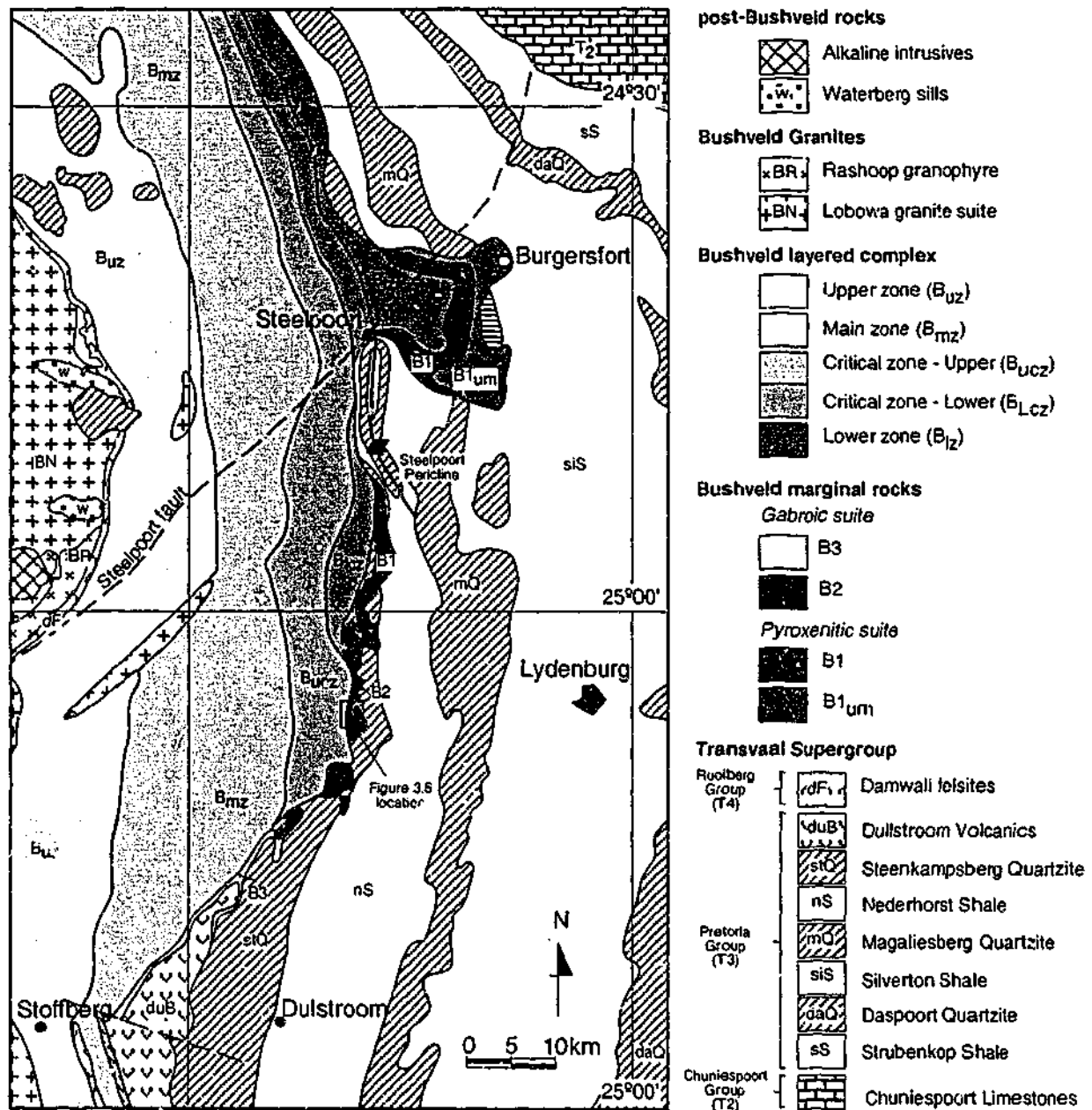


Figure 4.1 Map of eastern contact region of the eastern Bushveld Complex showing the relationship of the various marginal groups to the layered complex and units of the Transvaal stratigraphy. Map constructed 1:1000 field mapping work and mapping work of M. Sharpe (Harmer & Sharpe, 1985; Sharpe, 1978; Sharpe, 1981; Sharpe, 1982a; Sharpe, 1982b; Sharpe, 1982c).

Imaging parameters are as noted in the Figure captions and microprobe analyses were conducted at an accelerating voltage of 15 kV and beam current of 5 nA. Standard calibration was conducted according to CMM in house procedures.

Outcrop of the marginal rocks of the Eastern Bushveld extends for over 100 km, from Stoffberg in the South to Burgersfort in the North (Figure 4.1). Exposure is poor in the area immediately to the south of Burgersfort, where the ultramafic rocks of the marginal and Layered sequences of the Bushveld Complex have undergone intense alteration and extensive erosion. Exposure is

consistently better to the South of Steelpoort where the Complex intrudes the Magalisberg and Steenkampsberg quartzites and the marginal rocks are of more noritic composition. The shallow westerly dip of the quartzites has allowed exposure of the marginal rocks in pods which sit high on the escarpment formed by the relatively competent quartzites.

4.2.1 The Bushveld Type 1 (B1) marginal rocks

The first group identified by Sharpe (1981) was the B1 group, which includes three distinct facies; quench-textured pyroxenites, norites and peridotites. The suite occurs as a package of contact rocks and stratabound sills that envelope the Lower and Lower Critical Zones of the Layered Complex. The peridotite suite appears in some cases to postdate the pyroxenitic and noritic facies and as such were considered as a separate group by Harmer & Sharpe (1985), who proposed that they represent ejections of partially crystallised Lower Zone magma. Here they are considered as part of the same group on the basis of similar isotopic compositions and trace element geochemistry.

Quench textured micro-pyroxenites (BIN)

Quench textured micro-pyroxenites occur as stratabound sills extending as far as 100 km into the floor rocks, apparently emanating from the marginal rocks that envelop the Lower and Lower Critical Zones. The sills are between 10 and 100m in thickness, outcropping as boulders, with in situ outcrop rare. These rocks are common in the Eastern Bushveld, and they have also been documented in the Western Bushveld (Cawthorn *et al.*, 1981). In addition to the samples collected from the Eastern Bushveld Complex as part of this study, a sample was collected from a sill intruding the Magaliesberg quartzite in the area immediately to the south of the Buffelslei dam in the Western Bushveld (ECBV111). This sample was taken from the same sill and close to the sampling site for the "Parental magma to the Bushveld Complex" of Cawthorn *et al.* (1981); Davies *et al.* (1980), (pers.com.Cawthorn, 1998).

The micro-pyroxenite assemblage consists of orthopyroxene + clinopyroxene + plagioclase + quartz \pm chromite. Orthopyroxene occurs as equant to strongly prismatic needle-like phenocrystic grains 2-10 mm in length (Figure 4.2a). These grains are commonly arranged in radial clusters up to 10

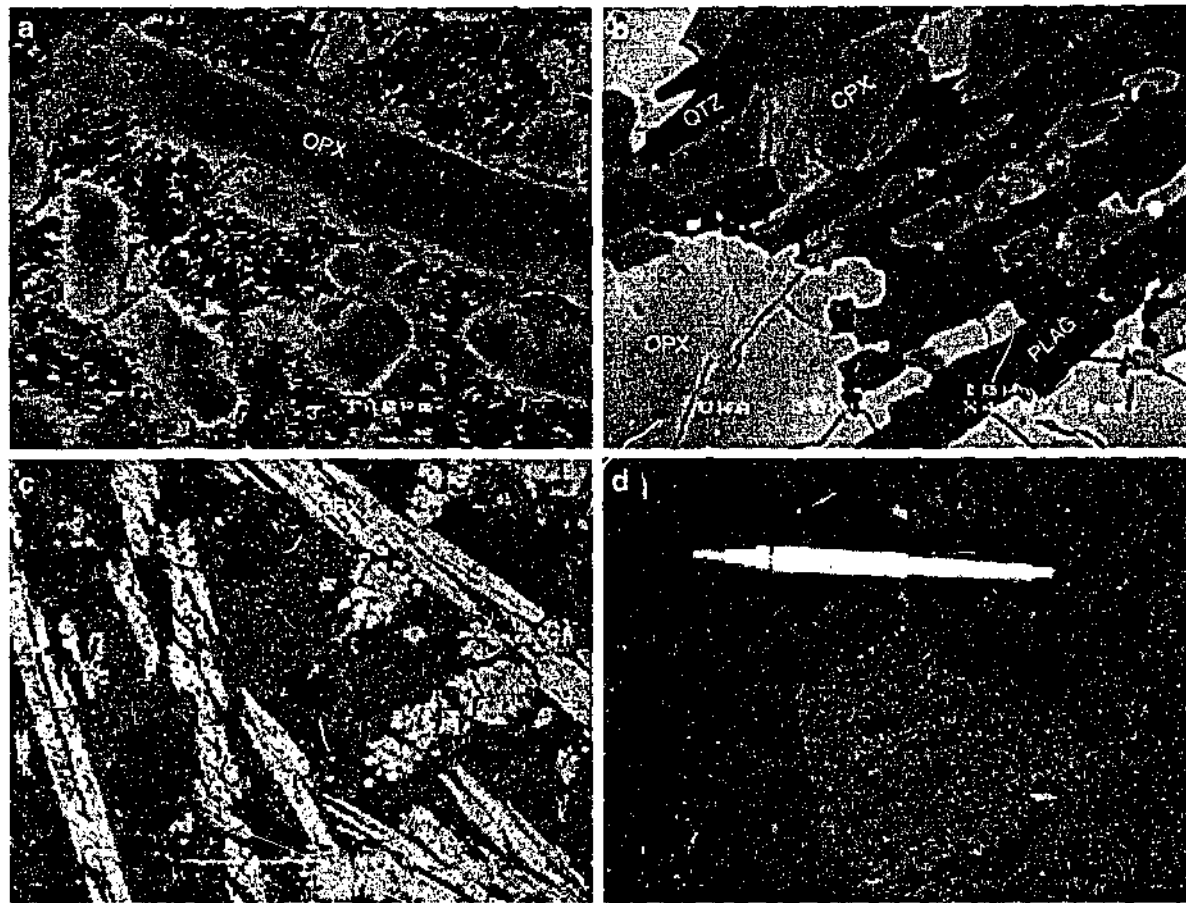


Figure 4.2 Backscattered electron images of two samples of B1 pyroxenite. (a) Sample ECBV18 illustrating zoned elongate crystals of orthopyroxene set in a groundmass of fine grained orthopyroxene, plagioclase, quartz and rare clinopyroxene, (b) detailed view of the same samples showing the textural relations and mineralogy of the groundmass, (c) a finer grained example of a micro-textured B1 pyroxenite (ECBV111), lacking significant zonation in the phenocrystic orthopyroxene, but in general having a lower enstatite No (60-70), close to that of the groundmass. (d) photograph of micro-textured B1 in outcrop showing radial alignment of orthopyroxene growth (pen for scale 15 cm). Mineral codes: OPX - orthopyroxene, CPX - clinopyroxene, PLAG - plagioclase, QTZ - quartz. Magnifications as per scale bars.

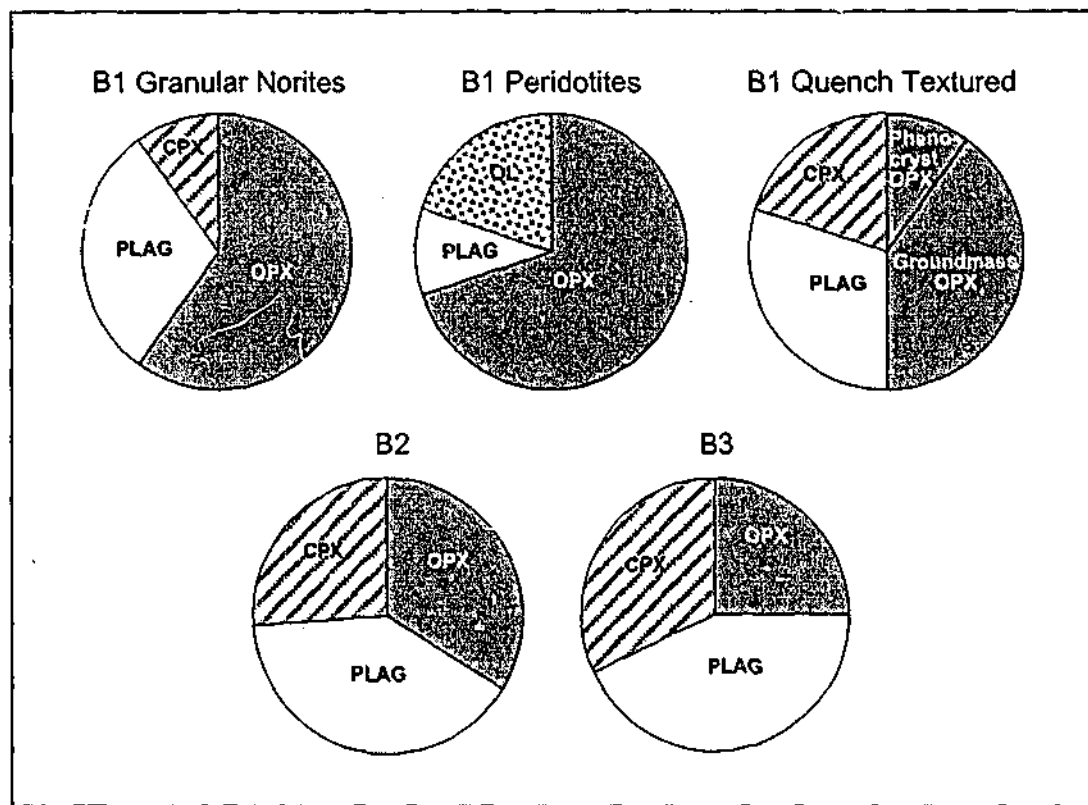
cm in diameter often visible on weathered surfaces, as seen in Figure 4.2d. The orthopyroxene is typically zoned from more magnesium cores to less magnesian rims that are in equilibrium with the groundmass orthopyroxene, indicated by the dendritic margins of some of the phenocrystic grains (Figure 4.2b). Typical modal abundances and mineral compositions are summarised in Figure 4.3 and Table 4.1. The zonation of the phenocrystic orthopyroxene is shown by core-rim tonal variation in backscattered electron images. Brightness within these images is proportional to average atomic number (Z) and hence more Fe-rich rims appear as brighter. The groundmass consists of intergrown laths of orthopyroxene, plagioclase and quartz, with occasional groundmass oikocrystic clinopyroxenes (Figure 4.2b).

The grainsize range of the groundmass within this group of rocks is demonstrated by comparison of Figures 4.2a,b and 4.2c, in which mineralogy and texture are essentially the same, but with

vastly different grainsize in the groundmass. The lack of zoning and partial resorption of prismatic orthopyroxene shown in Figure 4.2c,d is considered to reflect more extensive equilibration between groundmass and phenocrystic pyroxene, which has an average composition similar to the groundmass orthopyroxene. This contrasts with Figure 4.2a,b in which phenocryst orthopyroxene is clearly out of equilibrium with the groundmass.

Granular noritic B1 marginal rocks

The granular pyroxenitic series is exposed as a group of contact rocks and shallow sills that envelops the Lower Zone and Lower Critical Zone of the Bushveld Complex where it is in contact with floor



Rock Group	Major minerals					Accessory minerals		
	Phenocrystic/ Cumulus OPX	Post Cumulus OPX	Plag.	CPX	Olivine	Chromite	Magnetite	Biotite
B1 Granular Norites	60		30	10		<2	-	<1
B1 Peridotites	70		10		20	<5	-	<1
B1 Quench Textured	10	40	30	20		<2	-	-
B2		34	40	26		-	<2	<1
B3		25	43	32		-	<2	<1

Figure 4.3 Pie graphs summarising modal mineral abundances in the marginal rocks. Modal abundance data based on visual estimates of thin sectioned samples (B1) and digital image analysis of tonal variation in backscattered electron images (B2 and B3). Mineral codes: see Figure 4.2 and OL – olivine. Magnifications as per scale bars.

Rock Group	Phenocrystic/ Cumulus OPX (En #)	Post Cumulus OPX (En #)	Cumulus Plagioclase (An #)	Post-cumulus Plagioclase (An #)	CPX (Ca:Mg:Fe)	Olivine (Fo #)
B1 Granular Norites	85-80			56-55	35-40-15	
B1 Peridotites	87-79			75-65	35-50-15	85-80
B1 Quench Textured	Cores 85-80; Rims 70-60	70-60		65-55	45-40-15	
B2		65-55	65-55		43-39-18	
B3		65-55	65-55		46-40-14	

Table 4.1 Representative mineral composition data ranges for principal mineral phases. Data are from averages of Energy Dispersive Spectroscopy (EDS) microanalysis, parameters are described in the text.

rocks of the Needserhorst shale and the Steenkampsberg quartzite. This envelope is particularly well developed in the area surrounding the Burgersfort bulge, where the marginal package is, in places, as thick as 400 m (Figure 4.1). The Burgersfort bulge is a large body of rocks which protrudes from the otherwise smooth basal contact of the Bushveld Complex in the area between Burgersfort and Steelpoort. The body is about 15 km in diameter, consisting of layered dunites and harzburgites of the Lower Zone of the Bushveld.

The B1 norites consist of equant grains of orthopyroxene intergrown with plagioclase with accessory clinopyroxene, quartz, biotite and chromite. Figure 4.4a is an image of a typical granular norite. By comparison with that of the quench textured B1 pyroxenites, the orthopyroxene is relatively unzoned and on the whole less magnesian. With compositions approaching those of the phenocryst rims and the groundmass orthopyroxene of the quench textured samples.

Peridotites (B1-UM)

Apparently, although not unequivocally, post-dating the pyroxenitic series these rocks occur as a series of sills intruding into the sediments and in some cases apparently exhibiting cross-cutting relationships with pre-existing noritic rocks in the area around the Burgersfort Bulge (Figure 4.1). A spectrum of rock types is represented within this group, ranging from pyroxenitic through harzburgitic, to almost dunitic. The pyroxenitic members consist of weakly zoned cumulus orthopyroxene with interstitial plagioclase and minor quartz (Table 4.1; Figure 4.4). The more



Figure 4.4 Backscattered electron images of (a) granular noritic (B1) sample and, (b) peridotite (Harzburgite) sample (B1-UM). Mineral codes: as for Figure 4.2 and 4.3, CHR - chromite. Magnifications as per scale bars.

harzburgitic members consist of subhedral olivine grains up to 1 mm in diameter, poikilitically enclosed by orthopyroxene, with biotite, plagioclase and chromite as common accessories (Figure 4.4b). The chromites occur as both a discrete cumulus phase and as idiomorphic inclusions in olivine and orthopyroxene. The olivines are slightly serpentinised in some cases, but on the whole the rocks are relatively fresh. The more dunitic members are texturally similar to the pyroxenites, but with more abundant slightly more magnesian olivine. Chromite as an accessory phase appears to be most abundant in the more ultramafic members.

Outcrop of the peridotite series around the Burgersfort Bulge is poor, with exposure restricted to occasional disturbances caused by road making, and in a shallow quarry. Although Figure 4.1 depicts the B1-UM series rocks as a contiguous body enveloping the Burgersfort Bulge, the field relations are considerably more complex. The body actually consists of a series of thick (10-40 m) sills interspersed with rafts of quartzite. Although the sills are mineralogically/compositionally very similar and considered to be part of the same intrusive event, their cross cutting relations suggests that they were emplaced progressively rather than as a single intrusion. Some of the sills were found to be internally stratified, whilst others are relatively homogeneous. For example the Zwackwater Sill, visited as part of this study, was found to be internally stratified, consisting of a 1-1.5m basal layer of dunitic material grading upwards into a more harzburgitic series and finally into a noritic top. The total stratigraphic thickness of this sill is thought to be <20m, in contrast to the Aapiesdaorndraai body lying to the NE of the Burgersfort Bulge is as thick as 700m, but is

virtually unstratified, consisting almost entirely of equigranular harzburgites (Sharpe & Hulbert, 1985). Overall the peridotite sill package consists of a complex series of small intrusions that together make up a relatively contiguous body of rocks as indicated in Figure 4.1.

4.2.2 The gabbroic marginal rocks (B2/B3)

The gabbroic rocks consist of a suite of medium to fine grained gabbro-norites that occur where the Upper-Critical and Main Zones of the Bushveld Layered Complex abut the quartzites of the Magalisberg and Steenkampsberg units of the Transvaal Supergroup. They are divided into two groups on the basis of their spatial association with the units of the Layered sequence, and their trace element abundances. They are distinguishable in the field only by their stratigraphic position. Those adjacent to the Upper Critical Zone are termed Bushveld type 2 or *B2* with *B2N* the later denoting the fine grained sub-facies, likewise *B3* and *B3N* refer to those rocks adjacent to the Main Zone (nomenclature after Sharpe, 1981).

Mineralogically the gabbroic rocks can be classified as gabbro-norites, consisting of an equigranular assemblage of plagioclase, orthopyroxene and clinopyroxene, with accessory magnetite, biotite, ilmenite and sulphide. In some of the finer grained rocks oikocrystic growth of orthopyroxene and clinopyroxene enclosing cumulus plagioclase is evident, indicating that plagioclase was the primary liquidus phase with subordinate orthopyroxene and clinopyroxene (Figure 4.6a,b).

The gabbroic group occurs almost exclusively as contact rocks. Where they occur as sills they are rarely separated from their contact counterparts by more than 100 metres of country rock. These relationships are illustrated in Figure 4.7, where the gabbros are shown as a series of contact rocks up to 200 m in thickness, also occurring as shallow sills of similar thickness. It is not entirely clear whether the quartzites that separate the sills from their contact counterparts were still connected to the floor rocks during intrusion, or whether they occur as rafts, although their coplanar relationship with the in-situ floor rocks suggests that they may have been mechanically coherent during intrusion.

The textural differences between the fine grained sub-facies of the marginal rocks (*B2N* & *B3N*) and their coarser grained counterparts probably reflects contrasted cooling rates, as minimal whole

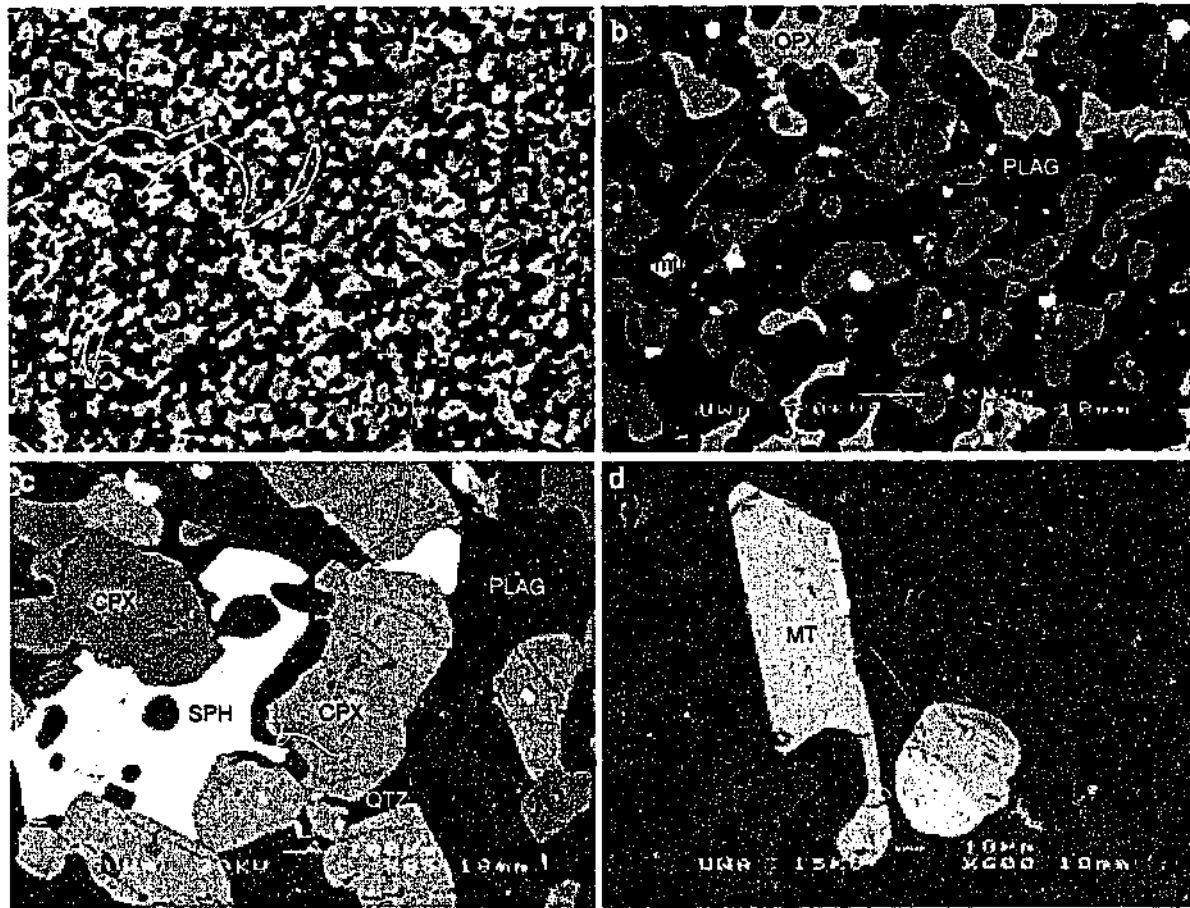


Figure 4.5: Backscattered electron images of samples from gabbroic marginal rocks (a) typical gabbroic marginal rock in thin section, note the presence of large (100-300 μm) oikocrysts of orthopyroxene (lighter shade) and clinopyroxene (darker shade) growing interstitial to plagioclase, (b) more detailed view of the same sample showing rare accessory occurrence of titanomagnetite, (c) detailed view of a B2 sample showing rare occurrence of intercumulus sulphide (SPH - pyrrhotite), and (d) detailed view of secondary alteration of titanomagnetites in a B2 sample. The paler shade is primary titanomagnetite (as marked - MT), whilst the brighter secondary mineral growing around the outside and associated with cracks in the grain to the right is an unidentified secondary iron mineral, probably haematite. Mineral codes: as for Figure 3.2, 3.3 and 3.4, MT - Magnetite. Magnifications as per scale bars.

rock compositional and mineralogical differences are observed. There is field evidence to suggest that finer grained rocks were emplaced before coarse grained equivalents. This is indicated by the presence of fragments of fine grained marginal rocks (B2N/B3N) mechanically included into the coarser grained rocks. The means by which this occurred will be outlined presently.

4.3 Discussion of field relationships and implications for the mode of emplacement of the Bushveld Complex

The field relationships of the marginal rocks indicate a significant time break between the emplacement of the pyroxenitic and gabbroic groups, and by implication their associated zones of the Layered Complex. Furthermore the relationship between the fine and coarse grained gabbroic rocks may provide some insight into the mode of emplacement of the upper part of the Bushveld

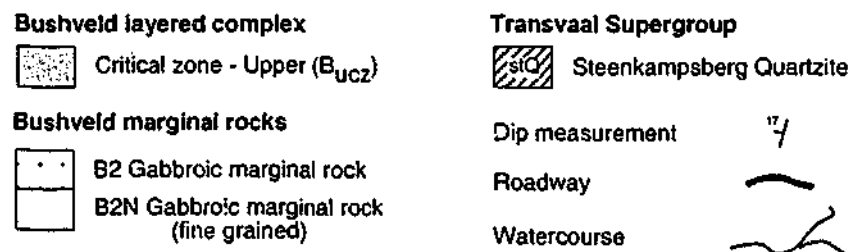
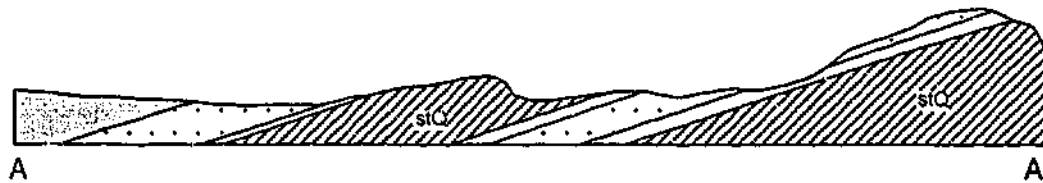
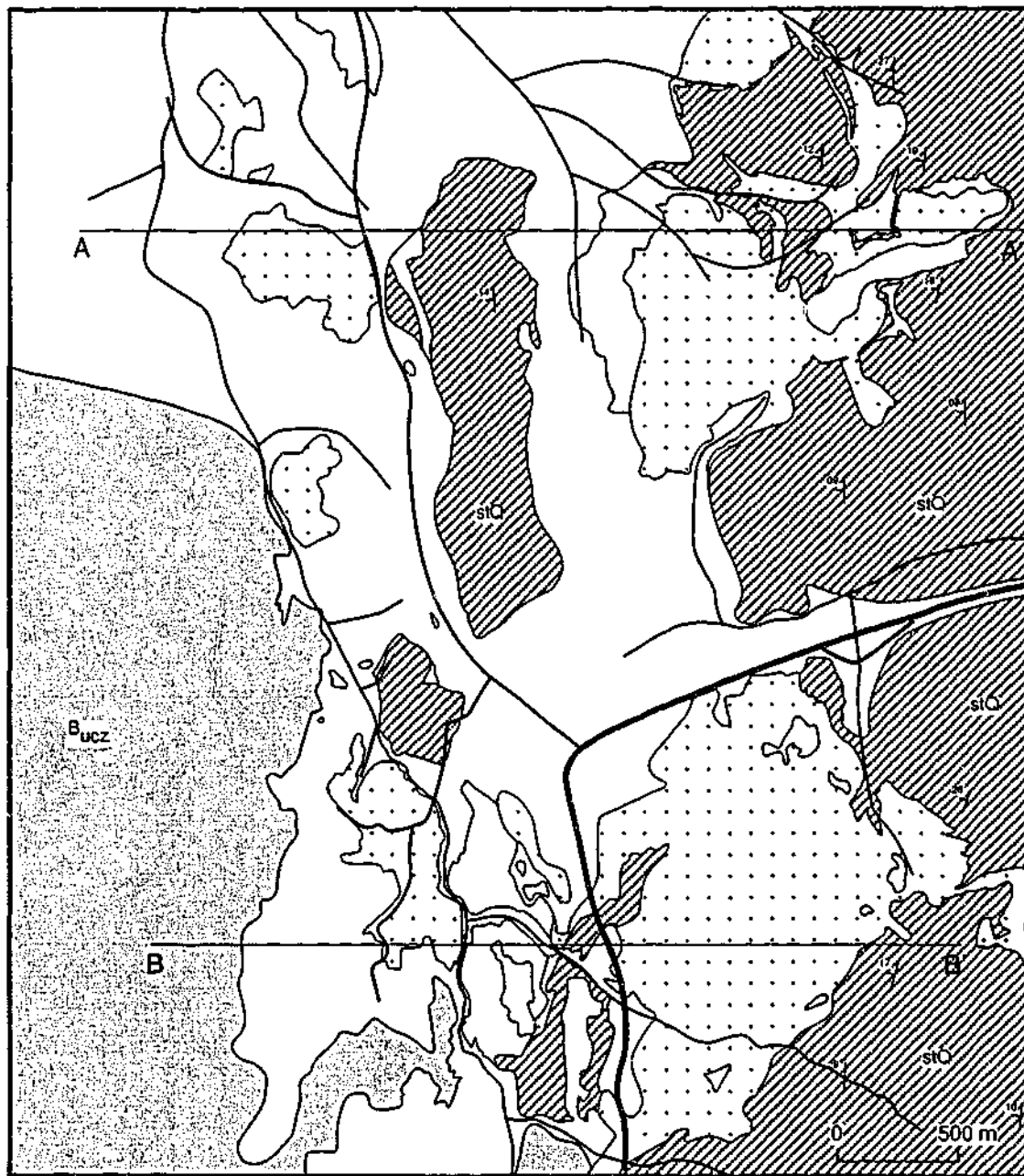


Figure 4.6 Map of Millies farm locality on the Farm Vygenhoek. Illustrates the local variability in the nature of the contact from shallow sills to contact rocks and the variable presence or absence of the fine grained sub facies (Compiled from 1:1000 field mapping. Vertical scale = horizontal scale = scale bar).

Complex.

Insights into the timing of emplacement of the B1 marginal rocks relative to the layered cumulate rocks can be gained from structural relationships in the area to the south of Steelpoort. Sharpe & Chadwick (1982) concluded that deformation of the floor rocks of the Bushveld Complex occurred during the early stages of the emplacement of the Lower Zone, terminating prior to the emplacement of the Upper Critical and Main Zones. This conclusion was reached on the basis of structural relationships observed around the closure of the Steelpoort pericline. This structure has been interpreted as a product of *syn*-intrusional structural deformation of the floor rocks that occurred during the emplacement of the Lower and Lower Critical Zones. The folding resulted in the at least partially lithified layered rocks of the Lower Critical Zone as well as the associated B1 marginal rocks and shallow sills being folded around the closure of the structure. On its western limb the Lower Critical Zone rocks dip steeply to the west, and the Upper Critical Zone rocks which terminate against the steeply dipping cumulates dip to the west at a much lower angle. This indicates a sequence of events that consisted of the emplacement of the Lower and Lower Critical Zones, followed by folding and finally emplacement of the Upper Critical and Main Zones. This places a relative age constraint on the timing of the emplacement of the pyroxenitic marginal rocks as prior to the emplacement of the Upper Critical and Main Zones of the Complex. Similarly, in the area to the north of the town of Vygenhoek the gabbroic rocks are seen to cross cut and quench against rocks of the pyroxenitic group. This confirms that there was a time break sufficient to allow extensive crystallisation of the pyroxenitic marginal rocks prior to the emplacement of the Upper Critical and Main Zones.

The mechanical inclusion of fragments of fine grained gabbroic rocks in their coarse grained counterparts which grade laterally into the Layered Complex, indicates that the fine grained marginal rocks were largely solid when the Complex was intruded. This indicates that an initial smaller volume of magma may have been injected as a sill or dyke along a pre-existing zone of weakness or fracture surface, crystallised and was later intruded by the more massive volume that crystallised to form the Layered Complex, although major and trace element chemistry suggests that the magmas

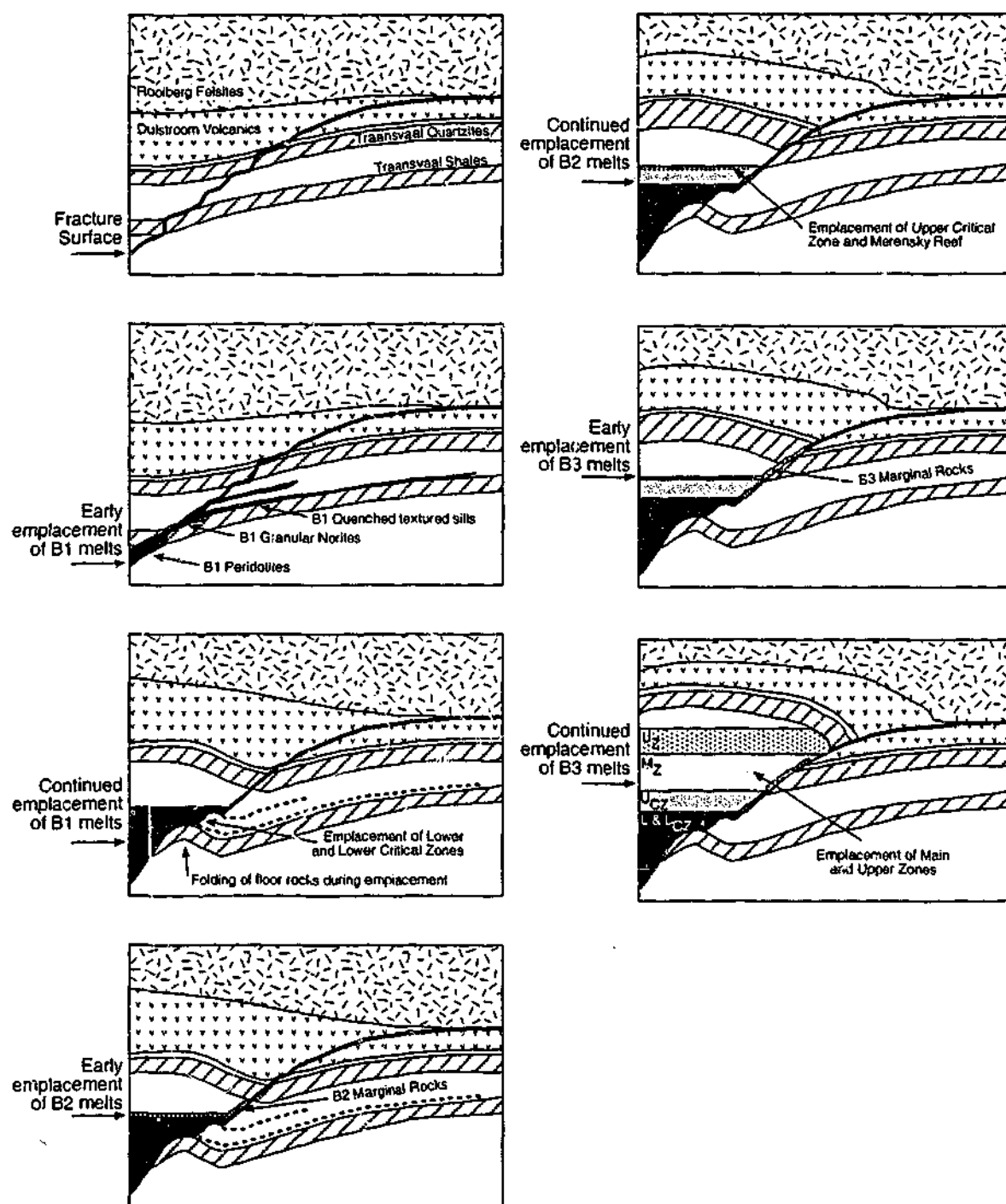


Figure 4.7 Schematic intrusion sequence for the Bushveld Complex – Vertical scale is exaggerated by approximately 5 times (modified after Sharpe 1981). Codes: L & L_{C2} = Lower and Lower Critical Zones, U_{C2} = Upper Critical Zone, M_Z = Main Zone and U_Z = Upper Zone.

were very similar in composition and probably of common origin. The same evidence also precludes the possibility that the marginal rocks may have intruded along the contact of the Complex after emplacement.

The field relationships of the marginal rocks indicate that the emplacement of the Bushveld was an episodic event, summarized schematically in Figure 4.8. The history of the Complex probably began with the emplacement of at least some of the pyroxenitic marginal rocks along concordant

and discordant planes of weakness in the Transvaal rocks, proposed by some to be an unconformity (Walraven *et al.*, 1990). This was followed shortly after by the emplacement of the lower ultramafic portion of the Complex up to the boundary between the Lower and Upper Critical Zones. Concurrent with this was the structural deformation observed in some of the floor rocks, including the evolution of the Steelpoort pericline. This event was followed by the early emplacement of the B2N marginal rocks followed by the larger volume of magma that formed the Upper Critical Zone. The same episodic emplacement of marginal rocks followed by larger volumes of magmas probably resulted in the formation of the B3N marginal series and the Main Zone.

The solidification of the fine grained marginal rocks prior to the next phase of emplacement does not imply that the same relationship existed between the different zones of the Layered Complex. The smaller thickness and lower volume of the marginal rocks means that they would have had a significantly lower thermal mass, and would have consequently cooled much faster than the rocks of the Layered Complex. By the same reasoning the time break between the intrusion of the marginal rocks and the Layered Complex is also not necessarily very long, an assertion supported by the lack of contact metamorphism of the marginal rocks, suggesting a close approach to thermal equilibrium between the marginal rocks and the Complex.

Chapter 5: Major and Trace Element Geochemistry

5.1 Introduction

This chapter explores in detail the major element characteristics of the marginal rocks of the Bushveld Complex and assesses their petrogenetic affinities by comparison with similar rocks from other environments. One of the key elements in understanding the Bushveld Complex is determining the relationships between the contrasted magmas apparently involved in its genesis, and that of other similar layered intrusions. This relates specifically to the so-called U and A-type magmas recognised and in the context of the Bushveld Complex, the B1 (~U-type) and the B2 and B3 (A-type) magma series. The fact that these two magma types occur in a number of intrusive complexes worldwide, in a similar relationship to each other suggests that they are related to a specific set of geological processes. Examples of similar complexes include the Stillwater complex, Montana USA, (Irvine *et al.*, 1983; Lambert *et al.*, 1994) and the Munni Munni Complex, Pilbara Western Australia, (Barnes & Hoatson, 1994). Crystal fractionation and accumulation of certain mineral phases in each of these complexes has had a significant influence on their compositional development and these processes will be explored in detail to determine the genetic relationship between the various groups of marginal rocks.

5.2 Major Element Geochemistry

5.2.1 Analytical techniques

A series of 38 field samples were analysed for major elements. Sample powders were prepared in an agate mill according to the method outlined in Appendix Ia. The sample set was analysed for a suite of 11 major element oxides and 16 minor/trace elements using XRF, the results of which are presented in Appendix II. Analyses were performed at the University of Melbourne, according to the low dilution fused disk method of Haukka & Thomas, (1977) Appendix Ib.

5.2.2 Results

B1 Samples

There exists considerable major and minor element chemical variation within the B1 group of rocks (Table 5.1). The B1 group has MgO concentrations in the range 8 – 33 wt.%, with the peridotites occupying the upper end of this range. The quenched and granular textured B1 samples typically fall in the range 8-15 wt.%. MgO is correlated positively with Cr (Fig. 5.1). Concentrations of Cr are in the range 500-7000 ppm, with the quenched and granular textured samples in the range 500-1000 ppm. Also shown is the field for B1 phenocrystic orthopyroxenes, which lies on a similar trend to the line defined by B1 granular and quenched textured samples, but below the trend for the peridotite samples which pass more towards the field for chromites (*c.a.* 30 wt.% Cr). A strong positive correlation between Ni and MgO is observed in the peridotite samples, and to a lesser extent in the quenched and granular textured samples. The concentration of Ni in the B1 samples is in the range 50-2000 ppm, with the quenched and granular samples having <400 ppm Ni. The field for olivines from the peridotite samples also lies on the same general trend as the peridotite samples. Co also exhibits a positive correlation with MgO.

Table 5.1 Whole-rock compositional ranges for marginal rocks

	<i>B1 Pyroxenites</i>	<i>B1 Peridotites</i>	<i>B2 Norites</i>	<i>B3 Norites</i>
SiO ₂ wt.%	53.27 - 57.05	42.265 - 56.01	46.99 - 59.12	50.55 - 53.92
MgO	8.08 - 14.1	18.57 - 33.88	3.49 - 10.56	6.95 - 8.99
Fe ₂ O ₃	9.95 - 11.08	8.885 - 11.1	10.01 - 14.12	9.59 - 11.99
CaO	5.88 - 7.14	2.39 - 5.4	7.58 - 12.31	9.48 - 11.6
Al ₂ O ₃	10.70 - 13.76	3.97 - 9	13.52 - 16.35	15.42 - 16.35
Na ₂ O + K ₂ O	1.96 - 3.13	0.3 - 2.02	1.32 - 3.37	1.4 - 2.91
Cr ppm	392 - 1874	2438 - 9790	42 - 511	262 - 1094
Ni ppm	165 - 408	646 - 2086	36 - 173	103 - 151
Sr ppm	158 - 250	24 - 145	238 - 456	315 - 355

The elements V, Sc and the oxides CaO and Fe₂O₃ exhibit a broadly negative correlation with MgO in the B1 samples. In general these elements exhibit an inverse relationship to Cr, Ni and Co, that is, those samples high in Cr, Ni and Co generally have lower concentrations of V, Sc, CaO and Fe₂O₃.

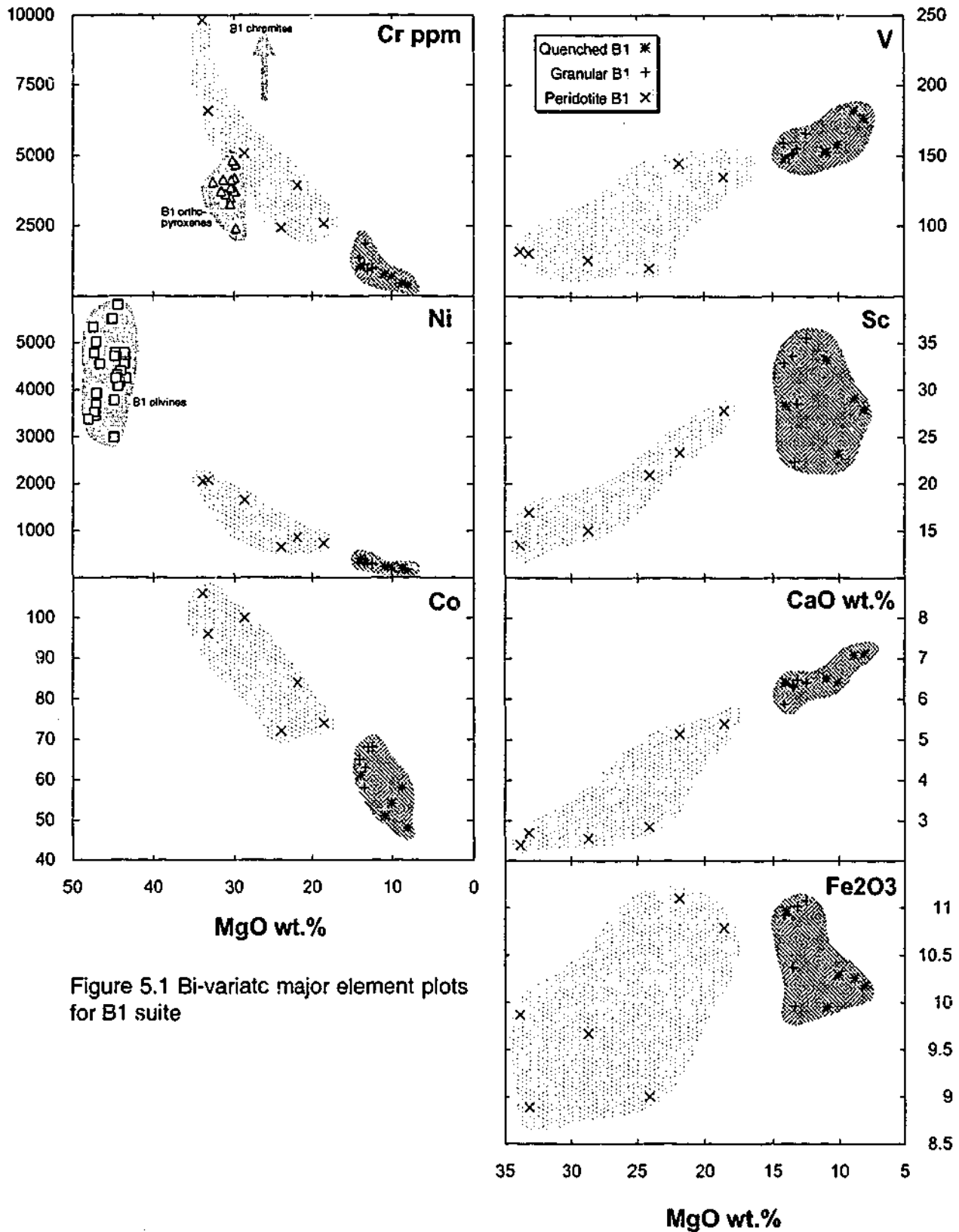


Figure 5.1 Bi-variate major element plots for B1 suite

B2 and B3 samples

The B2 and B3 suite of rocks exhibit a more restricted range in MgO concentrations (4-11 wt.%), which is significantly lower than the B1 group as a whole (Fig. 5.2). The broader range in SiO₂ makes this a more suitable element (oxide) for consideration of the B2 and B3 rocks. The most notable relationships observed in Figure 5.2 are the broad negative correlation of CaO, Al₂O₃, FeO and MgO with SiO₂, and the broadly positive correlation between total alkalis (Na₂O + K₂O) and SiO₂. The other elements plotted, Sr and TiO₂, apparently exhibit no systematic correlation with

SiO₂. To investigate the behavior of TiO₂ in more depth, it was compared with total iron concentration (Fe₂O₃ tot). Although there is apparently no relationship in the case of the B2 samples, there is a positive correlation in the case of the B3 samples.

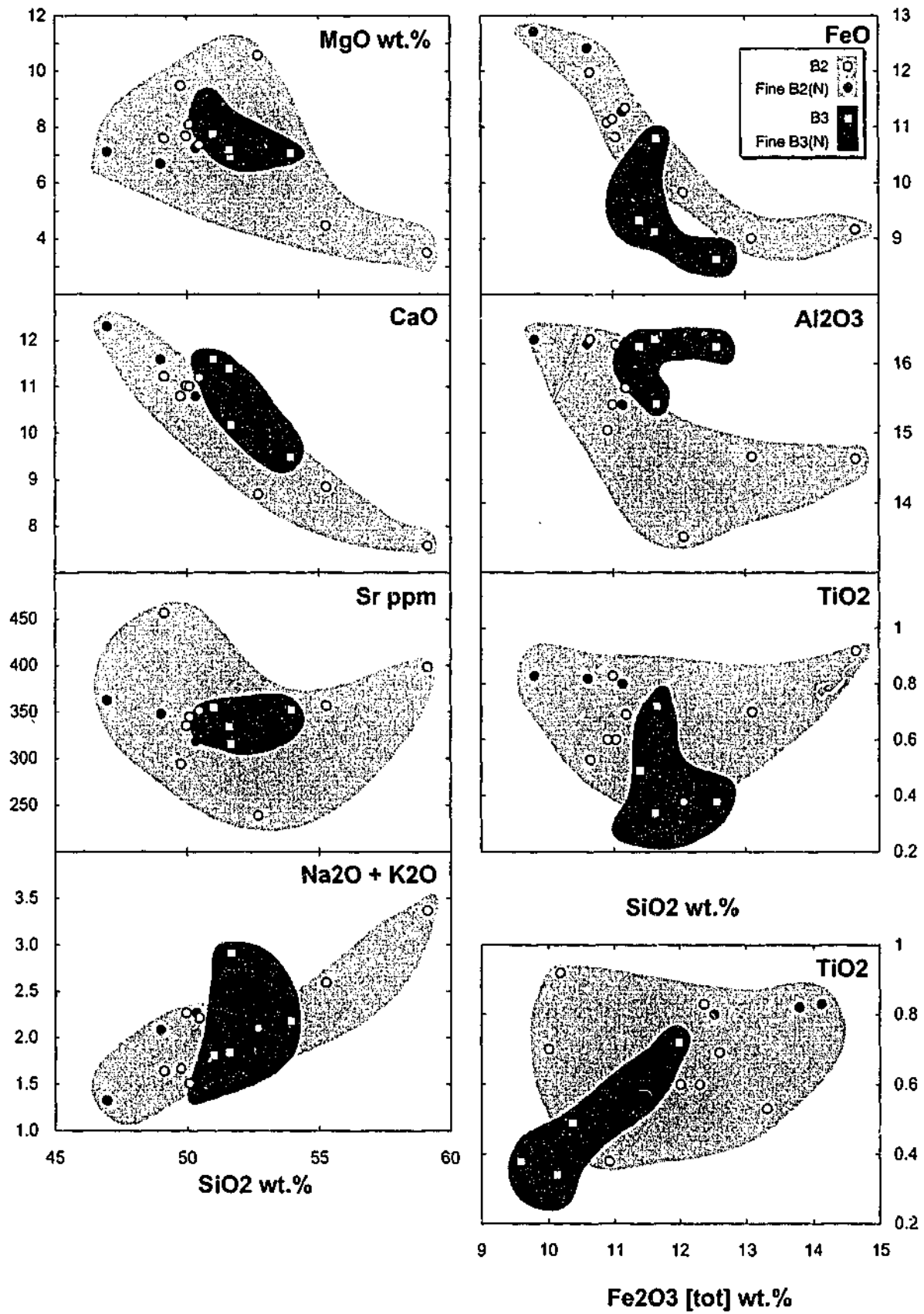


Figure 5.2: Bi-variate major element plots for B2 and B3 suites.

5.2.3 Comment on major element relationships

The positive correlation of MgO with Cr in the B1 rocks, which passes through the measured compositions of phenocrystic orthopyroxene suggests crystal fractionation/accumulation of orthopyroxene was probably highly significant in the development of the magma series. The very high abundance of Cr in some of the peridotite samples is probably the product of accumulation of chromite, also evidenced petrographically. Similarly, the positive correlation between MgO and Ni in the B1 rocks is explained by crystal fractionation/accumulation of olivine. The occurrence of phenocrysts of orthopyroxene with MgO rich cores in the quenched textured B1 samples, suggests that their composition may have evolved from a more MgO rich magma. Likewise the mesocumulate texture in some of the peridotite samples indicates that they are accumulations of olivine and orthopyroxene. Thus, the initial liquid of the B1 suite probably lies somewhere between these two extremes, perhaps approximated by the granular textured B1 samples. The operation of crystal fractionation/accumulation processes is also supported by the negative correlation between MgO and the other elements plotted in Figure 5.1, suggesting that these elements are incompatible in olivine and orthopyroxene.

Negative correlations of SiO₂ with CaO, FeO and positive correlation with alkalis suggest the fractionation/accumulation of plagioclase in the B2 and B3 rocks. Positive correlation between Fe₂O₃ and TiO₂ in the B3 rocks indicates a role for titanomagnetite, also observed in thin section.

5.2.4 Major element classification

Major element classification of the marginal rocks highlights some of the important major element differences between the two groups of rocks. Furthermore, it begins to reveal some of the characteristics which make the marginal rocks unusual, considering their intra-continental setting, and may provide some preliminary insights into their petrogenesis. Several authors have proposed and questioned an affinity between the Bushveld rocks and arc-related calc-alkaline rocks, in particular boninites (Barnes, 1989; Harmer & Sharpe, 1985; Sun, 1989). The classification of the Bushveld rocks by similar means as those which define these melts may give some insight into their possible relationship.

Total-alkalies vs. silica classification (TAS)

Although this type of diagram is not typically applied to the classification of plutonic mafic and ultramafic rocks, it has been used here to chemically correlate the intrusive rocks with their well-documented and well-understood extrusive counterparts.

Caution must be exercised when classifying any rocks that may have suffered major element metasomatism and associated loss or gain of the highly mobile alkali elements, a key parameter in TAS classification. On the basis of petrography the Bushveld marginal rocks have suffered minimal visible alteration, and show none of the characteristics normally associated with significant major element metasomatism, such as sericitisation of feldspars or olivine, or any other significant secondary mineral growth (Kerrick & Wynman, 1997).

A TAS classification diagram for the Bushveld marginal rocks is presented in Figure 5.3. At first glance TAS classification of the marginal rocks does not distinguish the two groups of rocks very effectively with almost complete overlap between them. However if their compositions are considered in terms of their fractionating mineral phases, and estimates of their parental melts are applied, some distinctions begin to become apparent.

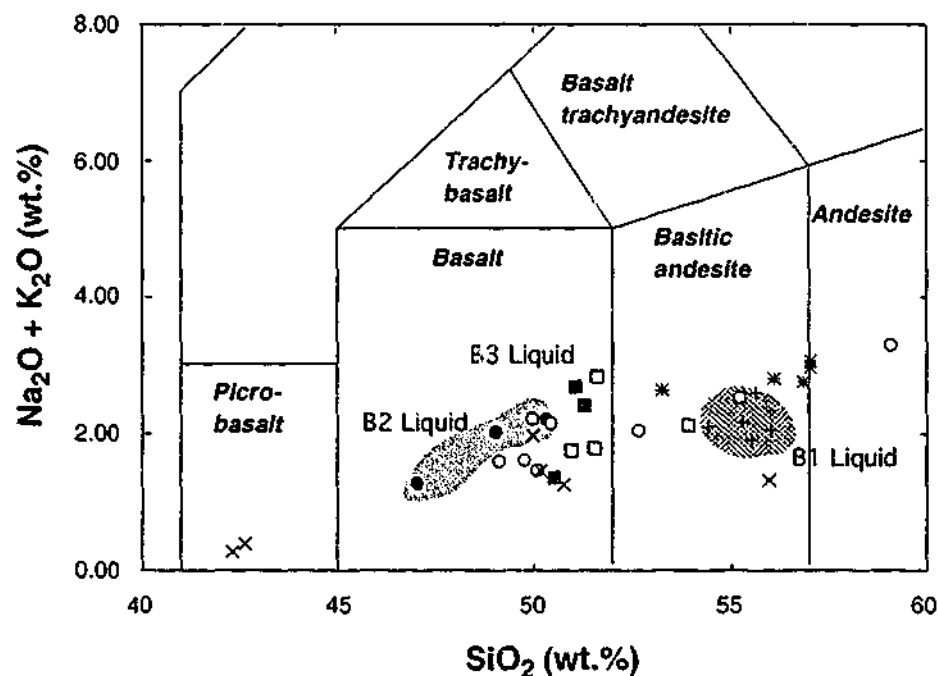


Figure 5.3 Total alkali silica classification (TAS) for marginal rocks (Le Maitre *et al.*, 1989). Symbols as for Figure 5.1.

On the basis of compatible element trends it was noted that the B1 liquid is probably best represented by the granular rocks. The compositional field for these rocks is marked on Figure 5.3 and classifies the B1 melts on the high silica side of the field for basaltic andesites. Similarly there is a wide degree of variability in the composition of the B2 and B3 rocks, again probably the function of variable crystal fractionation/accumulation of plagioclase in this suites of rocks. In so far as the parental melts to the B2 and B3 rocks are represented by the fine grained sub-series (B2N/B3N), they are both classified within the field of basalt, with B3 being slightly more silica rich.

The possible affinity between boninites and the Bushveld B1 melts is supported by the TAS classification (Fig. 5.3), with most boninites falling into the field of basaltic andesites (Crawford *et al.*, 1989). The original proposition by Wager & Brown, (1968) that the Bushveld Complex differentiated from a single melt type of basaltic composition was based on an analysis of a B2 samples, which do indeed plot in the field for basalts. This type of classification highlights some fundamental differences in the major element composition of the Bushveld marginal rocks and supports the idea that the Bushveld crystallised from at least two different magma types.

As useful as TAS classification is, it is not necessarily a definitive classification, as it overlooks MgO variation which is relevant in the classification of mafic and ultramafic rocks. This will be considered next in the classification of the Bushveld marginal rocks.

Alkalies-FeO-MgO (AFM) Classification

A key compositional control on mafic and ultramafic rocks is the composition and modal abundance in ferromagnesian minerals. The AFM diagram serves to classify rocks as tholeiitic or calc-alkaline in consideration of this important characteristic.

The AFM diagram presented in Figure 5.4 effectively differentiates the B1 rocks from the B2 and B3 rocks, primarily as a function of their higher MgO abundances. The broadly linear trend exhibited by the B1 rocks starting from MgO rich compositions, trending more towards FeO rich compositions is clearly the function of crystal fractionation/accumulation of ferromagnesian minerals. The B1

rocks plot in the calc-alkaline fields of the classification scheme of Kuno, (1968) and within the tholeiitic field of the classification of Irvine & Baragar, (1971). The B3 rocks lie in a similar position to the B1 rocks with respect to their alkalis/FeO[*tot*] balance falling into the same classification. The B2 rocks are clearly more strongly tholeiitic than either of the other two suites, plotting within the tholeiitic field of both classification schemes.

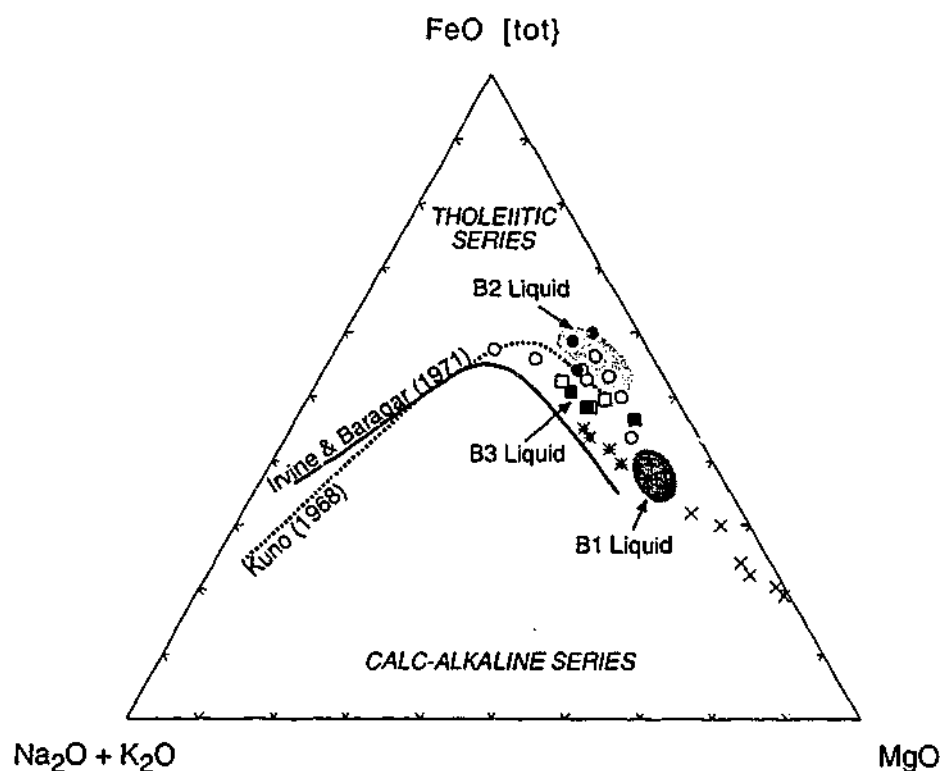


Figure 5.4 Alkali-Total FeO-MgO (AFM) diagram for marginal rocks. Classification fields are referenced as shown. Symbols as for Figure 5.1.

5.3 Trace Element Geochemistry

Perhaps the most important distinguishing characteristics of the B1, B2 and B3 rocks are their absolute and relative trace element abundances. Trace elements not only distinguish the magma types, they actually define to a large extent what constitutes a B1 magma, and by its petrologic association, a U-type magma. Similar to the major elements, the absolute abundances of trace elements have also been significantly affected by crystal fractionation/accumulation processes. However, due to the similar degree of incompatibility of the trace elements that will be considered here, the effect of crystal fractionation/accumulation on the relative abundances, or degree of inter element fractionation, is subtle. This means that the the ratios between elements are controlled primarily by magma source chemistry, degree of partial melting and crustal assimilation. It is for

this reason that many of the hypotheses proposed for the origin of U-type magmas rely heavily on trace element geochemistry.

5.3.1 Analytical techniques

A suite of 37 trace elements were analysed by HR-ICP-MS, including transition metals, lanthanides (REE) and actinides (U, Th). Analysis was performed using an open beaker HF-HNO₃ digestion followed by HR-ICP-MS at the Victorian Institute of Earth and Planetary Sciences (VIEPS) *Trace Analysis Laboratory* at Monash University. Samples were analysed at two dilution factors for optimum sensitivity across the broad range of elemental concentrations. Transition metals were analysed at a dilution of ~1:5000 while less abundant elements such as the REE, Nb and Ta were analysed at a lower dilution of ~1:1000. Full details of the methods and data reduction procedures are presented in Appendix Ic and all data are presented in Appendix IIa.

5.3.2 Logarithmic variation diagrams

Key trace element concentrations have been plotted on logarithmic variation diagrams using Th as a reference element, as it is highly incompatible in all of the major mineral phases observed in the marginal rocks. If the processes occurring in a co-magmatic series of rocks can be described by the Rayleigh Fractionation Equation, then a Log/Log plot of two elements should form a straight line within each stage of crystallisation (~constant D). In addition to this the slope of the straight line can yield a quantitative estimate of the bulk partition value D according to Equation 5.1 (Allegre *et al.*, 1977).

Mainly Incompatible Elements

Elements which plot with a positive slope when compared to Th on a Log/Log plot (Fig. 5.5) can be considered as largely incompatible. The elements Ba, Nb and Rb appear to be largely incompatible across the full spectrum of marginal rocks, suggesting that like Th these elements are not compatible to any significant extent in any of the major mineral phases. Sr exhibits contrasting behaviour between the B1 suite and the gabbroic (B2 and B3) suite. It is highly incompatible in the B1 suite as a whole and compatible in the B2 and B3 rocks with a bulk distribution coefficient of

$$D_c = \frac{(\log C_c^L - \log C_c^0)}{(\log C_i^L - \log C_i^0)} \dots \dots \dots \text{Equation 5.1}$$

Where:

D_c = Bulk distribution coefficient

C_c^L = Concentration of compatible trace element at any stage of the crystallisation process

C_c^0 = Concentration of compatible trace element in the initial liquid

C_i^L = Concentration of incompatible trace element at any stage of the crystallisation process

C_i^0 = Concentration of incompatible trace element in the initial liquid

approximately unity. This behaviour almost certainly reflects the influence of plagioclase as a major liquidus phase in the B2 and B3 rocks. Although Zr and La appear to be behaving largely incompatibly in the B1 and B3 rocks, in the case of the B2 rocks both of these elements may be partially compatible. The fact that these elements exhibit erratic behaviour and unusually high abundances in some samples suggests possible incorporation of accessory phases which are highly enriched in these elements.

Mainly compatible trace elements

Ni and Cr are largely compatible in the B1 rocks probably as a function of chromite, orthopyroxene and olivine fractionation/accumulation. Although not consistently these elements appear to be only moderately compatible in the B2 and B3 rocks having a bulk distribution coefficients of approximately unity.

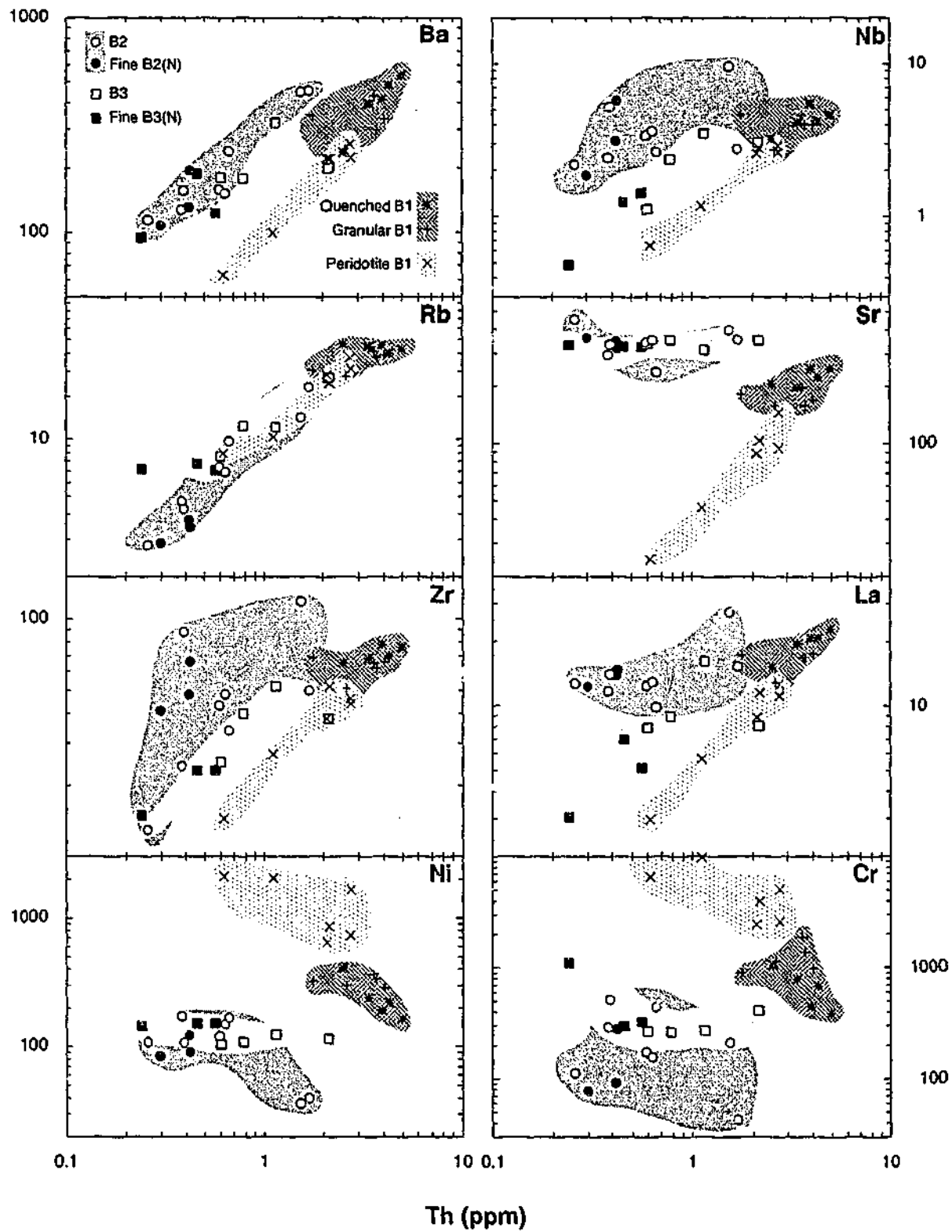


Figure 5.5 Logarithmic variation diagrams for key trace elements as a function of Th.

5.3.3 Multi-element spidergrams

B1 samples

There is a broad range in the REE abundances in the samples measured (Fig. 5.6a), that may be attributed to variable degrees of crystal fractionation/accumulation, and which has led to the development of parallel patterns across this range. Concentrations of La vary by an order of magnitude from 10-100 times chondritic abundance, with a similar degree of variation (1-10)

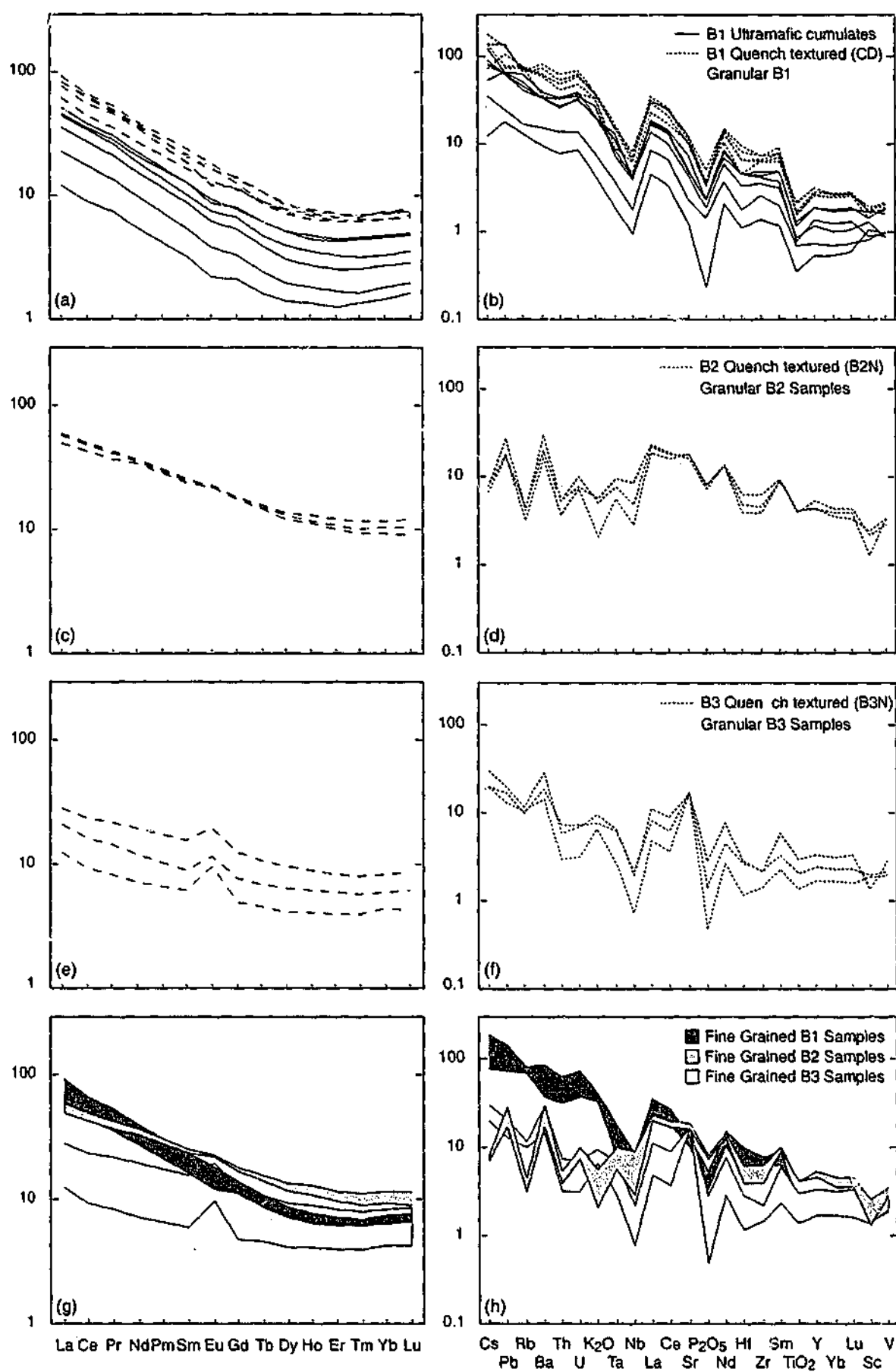


Figure 5.6 Chondrite normalised REE and Primitive mantle normalised Trace Element patterns for Bushveld marginal rocks. Composite Figures (g-h) are constructed from maxima and minima of the fine grained rocks from the respective groups. Chondrite values are those of (Evensen *et al.*, 1978). Primitive mantle values are from (McDonough *et al.*, 1985) and (McDonough-W-F, 1990).

observed for the heavy rare earth elements (HREE). The most notable feature of the REE patterns of the B1 rocks is the extreme fractionation of the light rare earth elements (LREE) with $[Ce/Sm]_N = 2.6-3.5$, coupled with the relatively flat to slightly upwardly concave HREE patterns ($[Er/Yb]_N = 0.83-0.97$). No Eu anomalies are evident in the quenched and granular textured B1 samples, whereas peridotite samples exhibit slightly negative Eu anomalies. Negative anomalies in this instance are most likely to be the product of addition of minor plagioclase.

There is a slight variability in the overall degree of REE fractionation between the granular B1 samples and the quench textured samples. The quench textured samples are slightly more fractionated, having slightly steeper LREE patterns than the remainder of this suite of samples. This may be the function of fractionation of orthopyroxene, which has a greater affinity for the HREE than the LREE.

Primitive mantle normalised trace element data for the B1 samples are presented in Figure 5.6b. The elements are normalised to primitive mantle and arranged in order of decreasing incompatibility during low to moderate degree partial melting (McDonough *et al.*, 1985), with the most highly incompatible elements to the left of the diagram. Therefore a simple partial melting event of low to moderate degree (5-10%), in the generation of a basalt from a primitive mantle source for example, should result in a smoothly sloping pattern decreasing towards the right of the diagram. Similar to the REE the overall abundance of the trace elements has been affected by crystal fractionation/accumulation, whilst the inter-element ratios have remained fairly constant. Patterns for B1 rocks slope gently to the right in an overall sense, as expected, but with several important departures from that overall trend. There are significant negative anomalies in the high field strength elements (HFSE) Ta, Nb, P, Hf and Ti, and positive anomalies in the large ion lithophile elements Cs, Pb and to a lesser extent Ba.

B2 samples

The B2 samples are also enriched in LREE ($Ce/Sm_N = 1.8-2.4$) although not to the same extent as the B1 samples (Fig. 5.6c). There is an obvious difference in the degree of fractionation between

the granular textured (B2) and the finer grained samples (B2N), with the B2N samples having less fractionated REE patterns. The degree of overall fractionation of REE in the B2 samples is substantially less than the B1 samples having $[Ce/Yb]_N = 4.1-6.2$ compared to the B1 samples which range up to 9. The B2 samples also have substantially higher concentrations of the HREE than the B1 samples. Some of the B2 samples exhibit positive Eu anomalies suggesting addition of plagioclase, while the B2N samples do not exhibit Eu anomalies. There is a relatively large range in the overall concentration of the REE in the granular textured samples which is probably due to the cumulus addition of plagioclase. The sample with the lowest concentrations of the REE has the most positive Eu anomaly suggesting that the addition of plagioclase has diluted the concentrations of REE overall while proportionally increasing the concentration of Eu. The origin of the lesser degree of fractionation in the B2N samples is not considered to be a function of plagioclase addition on the basis of textural evidence, thus it would seem more likely that this characteristic was inherited from the initial liquid.

The trace element patterns for the B2 rocks also show a marked departure from those of the B1 samples (Fig. 5.6d) shown comparatively in Fig. 5.6(h). Most notably the concentration of large ion lithophile elements (LILE) in the fine grained B2 samples is significantly lower and more jagged, with a marked negative anomaly in Rb which may be consistent with the addition of plagioclase which can have a relatively high affinity for Ba and Pb. Concentrations of Nb and Ta are broadly similar to the B1 samples, as are the elements through the middle part of the diagram. Notable also is the higher concentrations of Ti to Sc in the B2 rocks.

B3 Rocks

The B3 rocks have the lowest concentration of the REE of all the marginal rocks and they are also the least fractionated. Chondrite normalised REE plots are shown in Figure 5.6(e), and comparatively in Figure 5.6(g). The B3 rocks exhibit a similar relationship between the B3N samples and the B3 samples as their B2 counterparts, that is the B3N rocks are also less fractionated in the LREE than their granular counterparts. The positive Eu anomaly in all of the B3 rocks emphasizes the contribution of plagioclase to the chemistry of these rocks. Variable addition of

plagioclase is probably responsible for the variability in the overall abundance of REE in the B3 suite.

The trace element patterns for the B3 rocks are similar in their LILE abundances to the B2 rocks despite their lower REE abundances. The abundances of the remainder of the trace elements are lower than those of the B2 samples, with the exception of Sr with almost identical in abundances to the B2 rocks, with remarkable consistency through both the B2 and B3 rocks. The LILE patterns for the B3 rocks are smoother than those of the B2 rocks principally on account of the lower abundances of Rb and Cs in the B2 rocks.

While the trace element data presented so far provide some insight into the overall fractionation trends of the Bushveld melts and have allowed the identification of several significant patterns of enrichment and depletion, quantitative comparison of the three magma types and comparison with crust and mantle reservoirs is more difficult. Chondrite and depleted mantle-normalised inter-element ratios can be used as an index of fractionation allowing identification of trends within and between sample datasets. Furthermore, some of the Earth's mantle and crustal reservoirs have been well characterised in terms of certain incompatible inter-element ratios, thus they could act as a source indicator.

5.4 Petrogenetic Affinities

5.4.1 Refractory element petrogenetic affinities

Hickey & Frey (1982) utilised ratios of the elements Al, Ti, Ca, V and Sc in identifying possible melt depletion in the source of western Pacific boninite rocks. Similar to the Bushveld B1 melts, these same boninites exhibit relatively high but variable MgO abundance (4-25 wt.%), and high silica abundances, consistent with low-pressure fractionation of orthopyroxene. The ratios of CaO/TiO₂, Al₂O₃/TiO₂, Sc/Ti, V/Ti are also variable, although not controlled by orthopyroxene fractionation as indicated by the lack of correlation between Cr, Ni or MgO and these ratios. The authors propose that the high ratios of CaO/TiO₂, Al₂O₃/TiO₂, Sc/Ti, V/Ti observed are a function of source depletion, Ti being the most incompatible of all of these elements (Fig. 5.7 a-b). The

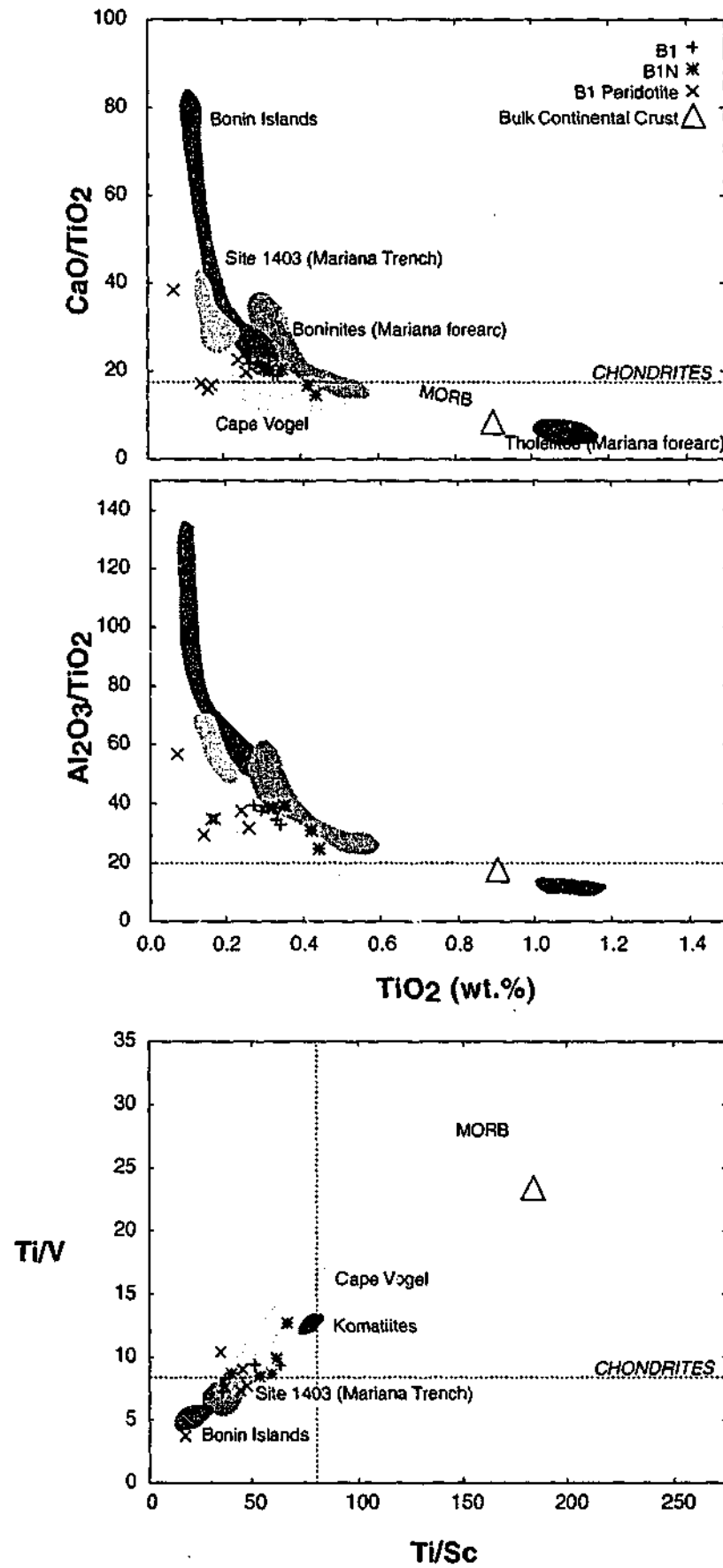


Figure 5.7 Boninite petrogenetic affinities of the Bushveld B1 magmas (data sources after compilation of Hickey & Frey 1982)

substantially supra-chondritic ratios of boninites indicate that the source must be particularly depleted given that the ratios are expected to decrease during boninite melt genesis. Hickey & Frey (1982) propose that the degree of variability in these ratios is the function of either variability in source characteristics, or variability in the amount of Ti introduced during secondary melt re-enrichment

in the source. The later is considered more likely on the basis of the sub-chondritic $\text{Al}_2\text{O}_3/\text{TiO}_2$ and CaO/TiO_2 of the Cape Vogel boninites, in the absence of higher crust-like TiO_2 abundances.

The positioning of the Bushveld B1 magmas in the field of boninites may argue for source enrichment as opposed to crustal contamination in the genesis of the B1 melts on the basis of petrogenetic association. Furthermore, the positioning of the B1 melts with lower abundances of TiO_2 and higher ratios of $\text{Al}_2\text{O}_3/\text{TiO}_2$ and CaO/TiO_2 than the bulk continental crust (also shown) supports this hypothesis. A similar relationship is observed in terms of the transition metals V and Sc (Fig. 5.7 c).

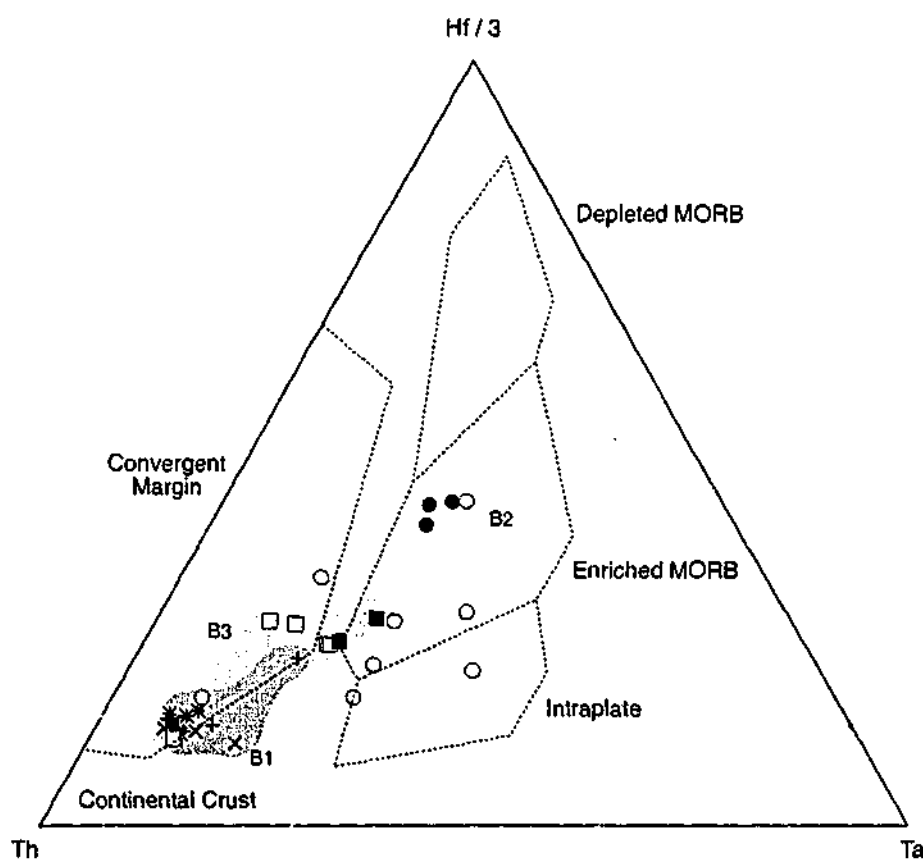


Figure 5.8 Th-Hf-Ta ternary plot of Bushveld marginal rocks. Classification fields are those of Wood, (1980).

Further to the possibility that the Bushveld B1 melts may represent convergent margin melts, they have been plotted on the ternary classification diagram of Wood (1980) (Fig. 5.8). Their positioning in the field of convergent margin magmas support the possibility that they may be derived from a boninite like source.

5.4.2 Incompatible trace element petrogenetic affinities

Several authors have made the comparison between the Bushveld melts and other incompatible element rich melts (Barnes, 1989; Harmer & Sharpe, 1985; Sun, 1989), including those from modern island arcs (boninites) and those interpreted to be the function of crustal contamination of a komatiite melt (SHMB). Certainly there are some similarities between the Bushveld B1 (and B2) melts and SHMB, and less so with boninites. Most notable is the similar abundances and degree of fractionation of the REE in SHMB and the Bushveld melts illustrated in Figure 5.9a. The fields of REE for SHMB overlap completely with those for the B1 and B2 melts, while the B3 have slightly lower abundances, but again with similar fractionation trends. Although some boninites have REE concentrations approaching that of the Bushveld melts, the vast majority are well below the Bushveld melts in their normalised abundances.

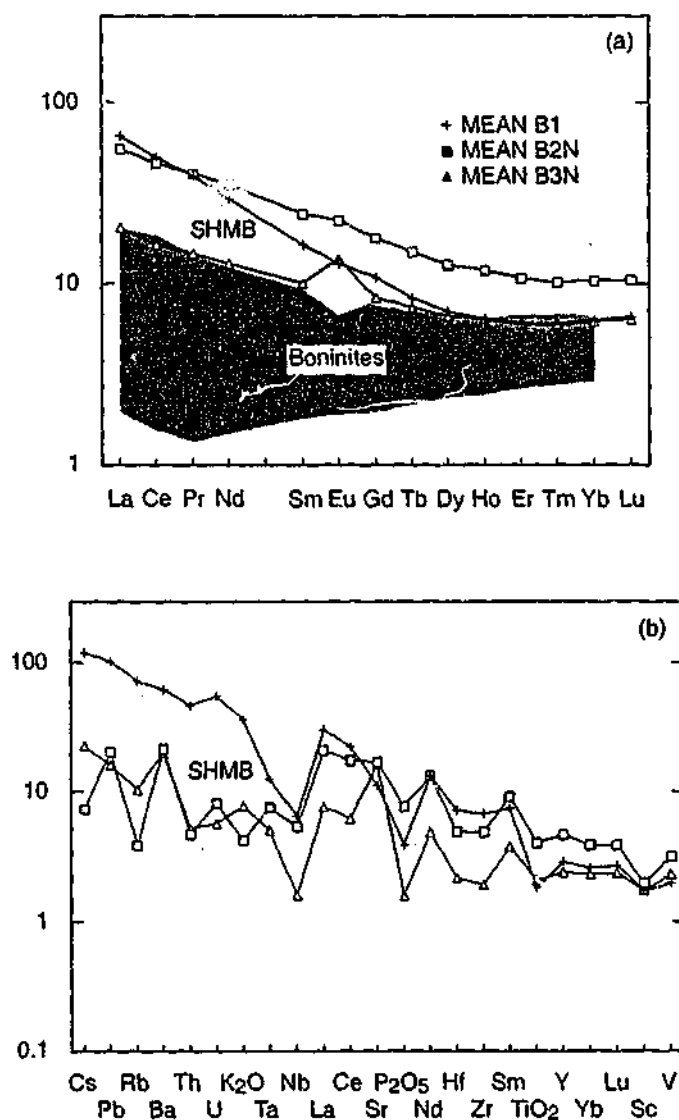


Figure 5.9 (a) REE patterns of average marginal rocks compared with the field for boninites (Cameron *et al.*, 1983) (b) Average incompatible element patterns for Bushveld marginal rocks compared with fields for Siliceous High MgO Basalts (Sun, 1989).

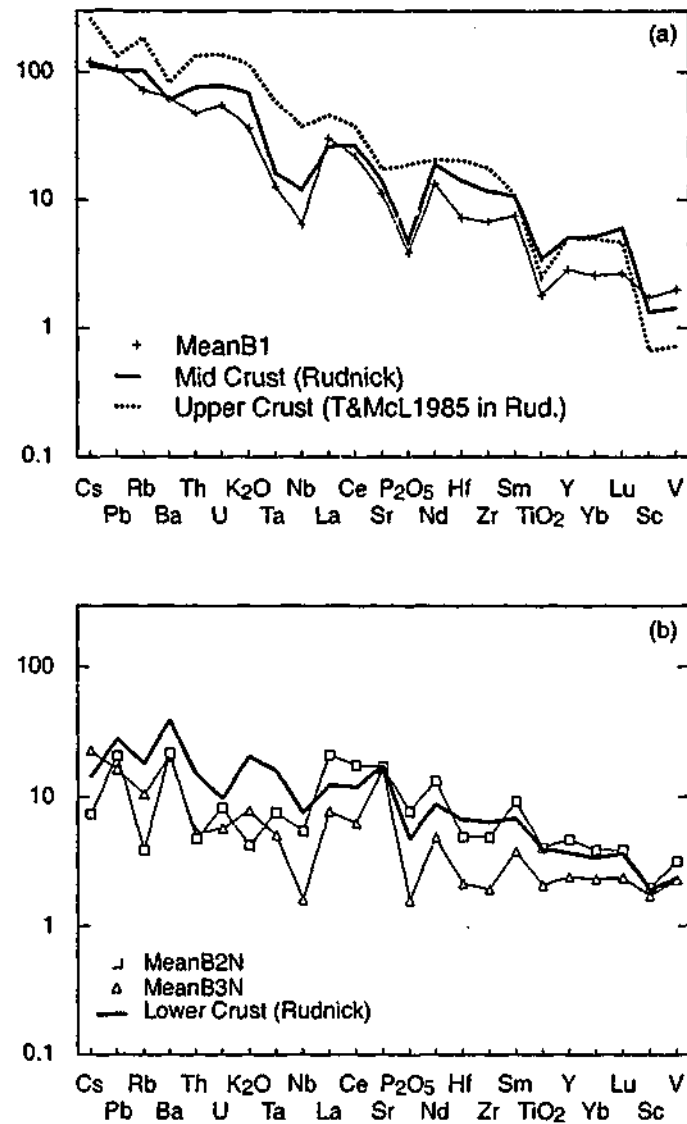


Figure 5.10 (a) Mean incompatible elements for B1 marginal rock compared with estimates of upper crust, and lower crust (b).

Comparison of the incompatible trace element patterns of the B1 Bushveld marginal rocks and published values for SHMB from Western Australia, and Antarctica (Sun, 1989) reveal that like the REE, the trace element patterns of are also very similar (Fig. 5.9b). SHMB have been interpreted as the product of crustal contamination of komatiites (Arndt & Jenner, 1986), which suggests that the Bushveld B1 magmas may also have been the product of crustal contamination of mantle derived magmas. To investigate this further the Bushveld rocks have been compared to the composition of some proposed crustal and mantle reservoirs and mantle derived magmas in terms of trace element patterns (Fig. 5.10). There is a remarkable similarity between the Bushveld B1 magmas and proposed mid crustal compositions (Fig. 5.10a). The most notable similarities are in the depletion of the HFSE and similar levels of LILE enrichment. There are also many similarities between the Bushveld B2 and B3 melts and estimated compositions of the lower crust (Fig. 5.10b),

again similar behavior of the LILE and the HFSE are the most notable. Both of these observations lend support to the hypothesis that the Bushveld melts are intrusive equivalents to Archaean/Proterozoic SHMB (Barnes, 1989).

Several authors have cited negative Nb anomalies, relative to other incompatible elements such as La (Arndt & Christensen, 1992) and Th (Jochum *et al.*, 1991), as evidence for crustal assimilation in the genesis of SHMB, CFB and similar melts including the Bushveld B1. This is supported by the similarities in the comparisons made in Figure 5.10, although the negative Nb anomalies in the B1 melts are of greater magnitude than those in the crustal rocks, perhaps making them difficult to explain by crustal contamination of a mantle derived melt only. To investigate this further the normalised ratio of Th/Nb has been compared with Nb concentration for the marginal rocks and a series of curves modelling the contamination of primitive mantle with continental crust (Fig. 5.11a). The spread of the data is broadly parallel to the abscissa (Nb concentration) indicating that the $[Th/Nb]_N$ ratio is not dependant on the concentration of Nb and is therefore probably independent of crystal fractionation/accumulation processes. The only model curve that approaches the $[Th/Nb]_N$ ratio observed in the B1 rocks is that of the mid crustal contamination of a primitive mantle source. However, this curve does not reach the field of B1 melts until a modelled value of ~40% contamination of the primitive mantle, which is relatively high. Similar results are gained when the ratio of Nb/La is considered as a function of degree of REE fractionation ($[La/Yb]_N$) (Fig. 5.11b). Again the relative abundance of Nb appears largely independent of REE fractionation. Modelling suggests that the composition of the B1 melts can not be modelled by the contamination of depleted mantle with any estimate of the continental crust.

5.5 Summary

The rocks sampled and analysed as part of this study represent a series most likely derived from two or three discrete parental magmas represented by the B1, B2 and B3 marginal rocks. For the most part the intra-group variation can be explained as the product of fractionation, accumulation and addition of various cumulus mineral phases. In the case of the B1 rocks the fractionation/

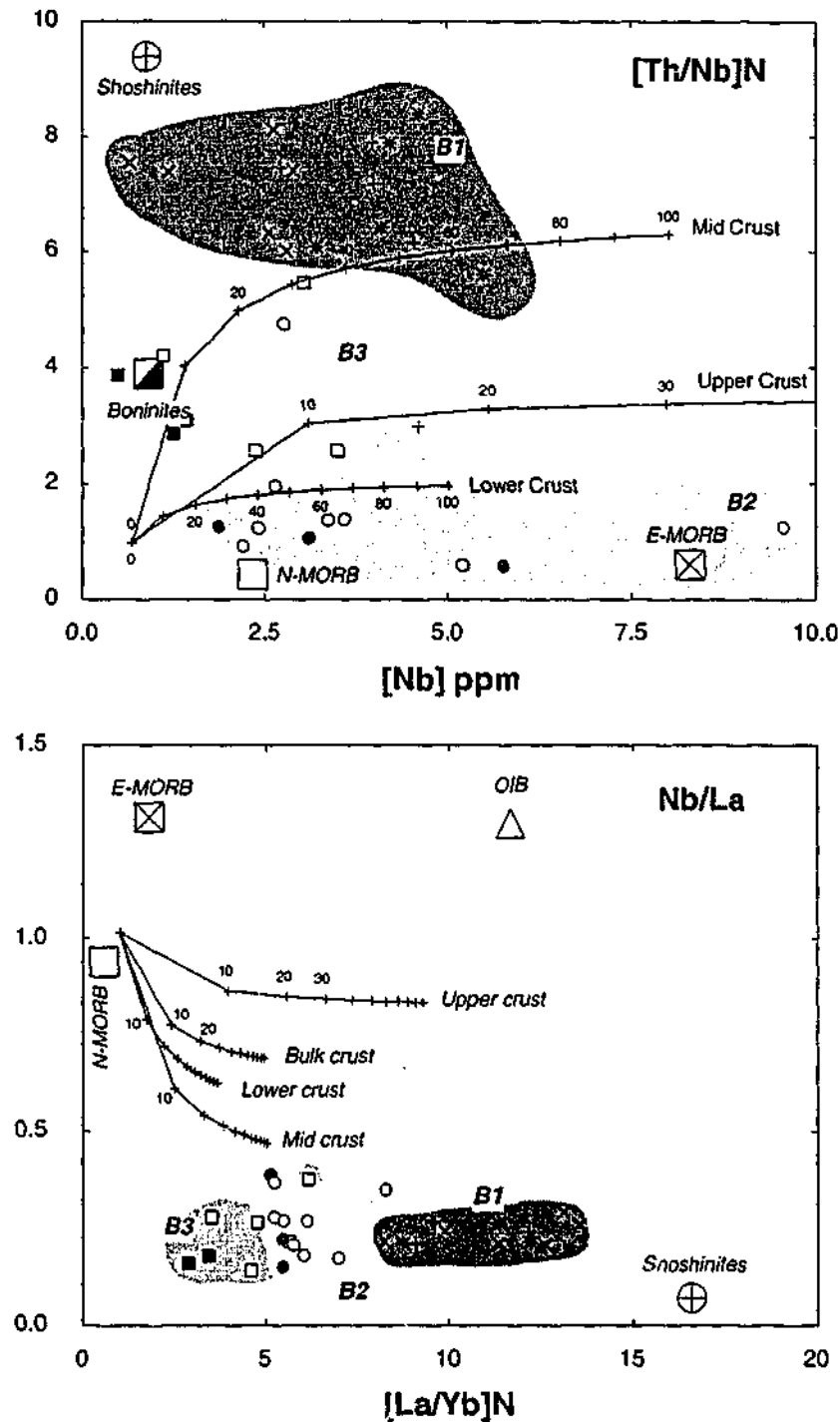


Figure 5.11 (a) $[Th/Nb]_N$ versus $[Nb]$ ppm, and (b) Nb/La versus $[La/Yb]_N$ for the Bushveld marginal rocks. Reservoir data are from Lin *et al.* (1989); Pearce *et al.* (1992); Rudnick *et al.* (1990); Sun & McDonough (1989); Taylor & McLennan (1985). The composition of mid ocean ridge basalts (MORB) and the convergent margin magmas, boninites and shoshinites are also plotted of Figure 5.11. In the case of both $[Th/Nb]_N$ versus Nb and Nb/La versus $[La/Yb]_N$ the compositional estimate of shoshinites is close to that of the B1, perhaps lending support to a boninite-like petrogenesis for the B1 melts.

accumulation of olivine, orthopyroxene and chromite has played an extensive role in the compositional development of the series as a whole. The B1 rocks interpreted to be most representative of the initial liquid are the granular textured B1 rocks. These rocks show limited compositional variation and lie between the fractionated quenched textured samples and peridotite samples in terms of Ni, Cr and MgO. The compositions measured for these samples are very

similar to those reported by Harmer & Sharpe, (1985) as the parental magma to the Lower and Lower critical zones of the Bushveld Layered Complex. Major and trace element characteristics of the B2 and B3 suite suggest that they have been subject to crystal fractionation/accumulation processes involving plagioclase.

The simultaneous occurrence of the three magma types in the one place as part of the same magmatic event suggests that they may be related to one another by some relatively simple geological process, being perhaps ultimately derived from a single parental magma represented by the B1 samples. The commonality between the magma series of the Bushveld Complex and those of some other layered intrusive complexes supports this. The trace element similarity between the Bushveld B1 melts and SHMB implies that contamination of a mantle derived magma may have been responsible for the unusually enriched trace element characteristics of the B1 melts, although the evidence pertaining to the negative anomalies of Nb may contradict this. Major and trace element characteristics are also similar in many ways to some convergent margin magmas, in particular, highly enriched shoshinite magmas.

Chapter 6: Isotope Geology of the Marginal Rocks of the Eastern Bushveld Complex: implications for petrogenesis of the parental melts

6.1 Introduction

The contrast between elemental concentrations in the continental crust and the underlying mantle leads to the fractionation of parent daughter ratios in certain radiogenic isotope systems. In time, these fractionated elemental ratios lead to the development of crustal and mantle reservoirs with unique isotopic compositions. Thus, the radiogenic isotope systems provide a powerful tool in understanding the time integrated evolution of crust / mantle systems. Furthermore, the development of distinctive isotopic reservoirs provides a means of chemically distinguishing magmas sourced from either environment. In addition to fractionation of the radiogenic isotope systems, the formation of crust and mantle reservoirs also fractionates the stable isotopes of oxygen, leading to distinct reservoirs of this element also. These parameters combined allow the assessment of interactions between the crust and the mantle during magma genesis, the main topic of this chapter.

6.1.1 Application of the Re-Os system

Re-Os isotopic studies of the marginal rocks of the eastern Bushveld Complex provide new insight into the genesis of the B1 melts. The fact that Os is one of the six platinum group elements (PGE) also means that the system has the potential to provide insight into the actual source of the PGE that form the ore deposits in the Bushveld Complex. The Re-Os system relies on the β -decay of the parent isotope ^{187}Re to ^{187}Os , which is measured against the stable ^{188}Os (Equation 1). Unlike the lithophile isotope systems (Rb-Sr and Sm-Nd) the Re-Os system is a siderophile/chalcophile system. There are several factors that cause the fractionation of Re from Os in geological systems. While both are chalcophile metals, evidence suggests that Os may have a partition coefficient between sulphide and silicate melt ($D_{\text{sulphide/silicate}}$) 1-2 orders of magnitude greater than Re (Lambert *et al.*, 1998). This means that during sulphide saturated melting Os will be retained in the source rocks to a greater extent than Re. The isolation of some Os (Os+Ir+Ru) enriched sulphides within primary mantle mineral phases may also cause some fractionation due to the preferential concentration of the refractory PGE (including Os) in these phases (Alard *et al.*, 1999). Retention of Os in some highly refractory metal alloys may also contribute to the fractionation of Re from Os

during partial melting (Mitchell & Keays, 1981). The combined effect of these processes is the development of mantle and crustal reservoirs with vastly different Re/Os ratios, and in time vastly different $^{187}\text{Os}/^{188}\text{Os}$ compositions. This acts as a powerful tool in distinguishing between crustal and mantle rocks and is thus relevant to this study of the role of crustal contamination in the genesis of the Bushveld magmas.

$$\left(\frac{^{187}\text{Os}}{^{188}\text{Os}}\right)_{\text{MEAS.}} = \left(\frac{^{187}\text{Os}}{^{188}\text{Os}}\right)_{\text{INITIAL.}} + \left(\frac{^{187}\text{Re}}{^{188}\text{Os}}\right)_{\text{MEAS.}} \left(e^{(\lambda t)} - 1\right) \dots\dots\dots \text{Equation 6.1}$$

Where:

λ = Re Decay Constant 1.67×10^{-11} (Smoliar *et al.*, 1996)

t = Period of decay (years)

6.1.2 The application of the Sr-Nd isotopic systems

Both the Sr and Nd isotopic systems are classified as lithophile isotope systems (Zindler & Hart, 1986). In both systems the parent and daughter isotopes behave incompatibly during mantle melting and are therefore concentrated in crustal rocks. Slightly differing compatibilities during melting in both systems leads to the time integrated development of isotopically distinct reservoirs of Nd and Sr. In the Rb-Sr system, which relies on the radiogenic decay of ^{87}Rb to the stable ^{87}Sr measured in reference to the stable ^{86}Sr the parent element Rb is more incompatible during partial melting than the daughter Sr, leading to elevated Rb/Sr in the crust and consequently elevated $^{87}\text{Sr}/^{86}\text{Sr}$. In contrast, in the Sm-Nd system the daughter element (Nd) is concentrated in the crust with respect to the parent element (Sm). During partial melting, the increasing compatibility of the rare earth elements (REE) with increased atomic number (Z), leads to the generation of partial melts which are enriched in LREE. These melts therefore have Sm/Nd that are lower than the source rocks, leading in time to crustal reservoirs that have unradiogenic $^{143}\text{Nd}/^{144}\text{Nd}$, with complimentary relatively radiogenic mantle reservoirs.

Like the Re-Os system the Sm-Nd system is considered in reference to a model chondritic mantle reservoir, with the initial of a given sample compared to chondritic mantle of the same age. More subtle variations in the Sm-Nd system mean that the comparison is made in parts / ten thousand.

This parameter is termed ϵNd , which is defined as $\epsilon\text{Nd} = \frac{{}^{143}\text{Nd}/{}^{144}\text{Nd}_i}{\text{chondritic uniform reservoir (CHUR) of the same age}} \times 10^4$. In contrast to the Re-Os system negative (ϵNd) values are indicative of a crust like component. Comparison of initial Sr composition to a mantle reservoir is less common due to poor constraint on the evolution of these reservoirs in terms of Sr. In addition greater absolute variation in the calculated initial ${}^{87}\text{Sr}/{}^{86}\text{Sr}$ (${}^{87}\text{Sr}/{}^{86}\text{Sr}_i$), compared to ${}^{143}\text{Nd}/{}^{144}\text{Nd}_i$, renders it less necessary to convert the initial value to a relative measure.

6.2 Results

6.2.1 Re-Os Isotopes

Analytical Methods

The Re-Os concentrations and isotopic compositions were determined using a Carius tube digestion-isotope dilution method. Isotopic ratios were measured on negative ions of the oxides of Re and Os using the Finnigan MAT 262 Thermal Ionisation Mass Spectrometer (TIMS) in the VIEPS Department of Earth Sciences at LaTrobe University, Melbourne Australia. A complete description of the chemical analytical procedures used is provided by Lambert *et al.*, (1998) and revised in Lambert *et al.*, (2000). The method adopted was similar to that of Shirey & Walker, (1995). Approximately 3 g of powder was digested and equilibrated with Re and Os spike in a reverse aqua-regia (3 HNO_3 :2 HCl :1 H_2O) solution sealed in a glass carius tube. Each tube was then placed in a steel vessel and heated to 220° C for 16 hr. Os was then separated from Re (and other matrix elements) using a solvent (CCl_4) extraction method described by Cohen & Water, (1996). Os was further purified by the microdistillation described by Birck *et al.*, (1997). Re is extracted from the same matrix solution after the Os is removed using an anion exchange method, also described in Lambert *et al.*, (1998). Full details of the analytical method are presented in Appendix 1d.

Re-Os Results

Re-Os isotopic data for whole rock powders and mineral separates from the Bushveld marginal rocks are summarised in Table 6.1. The whole rock concentration ranges for Re and Os in the two

Table 6.1 Re-Os abundances and Os isotopic compositions for whole rock samples and mineral separates from the Bushveld marginal rocks.

Sample Identification	Type	Lithology / Mineral	Re	Os	Common Os	$^{187}\text{Re}/^{188}\text{Os}$	$^{187}\text{Os}/^{188}\text{Os}$	γOs
Type 1 (B1)								
Whole Rocks								
CO005	B1	granular pyroxenite (WR)	0.4687	0.3132	0.3049	7.40 ± 7	0.3319 ± 20	-34
ECBV19DL	B1	granular pyroxenite (WR)	0.7852	0.3579	0.3443	11.13 ± 11	0.4297 ± 6	-63
ECBV49a	B1	pyroxenitic norite (WR)	0.6585	0.1847	0.1726	18.41 ± 18	0.6576 ± 19	-85
ECBV50	B1	pyroxenitic norite (WR)	0.5341	0.4973	0.4880	5.43 ± 5	0.2759 ± 6	-23
CD01	B1	microtextured pyroxenite (WR)	0.6212	0.1755	0.1635	18.29 ± 18	0.6767 ± 28	-65
ECBV105	B1	microtextured pyroxenite (WR)	0.8306	0.1757	0.1604	24.98 ± 25	0.8481 ± 14	-119
ECBV111	B1	microtextured pyroxenite (WR)	0.4901	0.2746	0.2659	8.88 ± 9	0.3737 ± 6	-43
DI204	B1	microtextured pyroxenite (WR)	0.6974	0.0758	0.0633	53.30 ± 53	1.6307 ± 24	-299
Oxides								
ECBV111_OX	B1	chr / mt concentrate (MS)	1.9900	10.8536	10.8266	0.89 ± 1	0.1463 ± 2	0.56
ECBV111_OXrpt	B1	chr / mt concentrate (MS)	2.0761	9.9983	9.8664	1.01 ± 1	0.1519 ± 4	3.14
ECBV17CHR	B1	chr concentrate (MS)	0.2956	6.9557	6.9632	0.20 ± 2	0.1195 ± 2	-0.61
ECBV50CHR	B1	chr concentrate (MS)	0.3240	3.8323	3.8330	0.40 ± 1	0.1262 ± 21	-0.77
DI326CHR	B1	chr concentrate (MS)	0.4765	44.8187	44.8955	0.05 ± 1	0.1146 ± 3	-0.14
Type 2 & 3 (B2/B3)								
Whole Rocks								
ECBV26	B2	gabbro-norite (WR)	0.3860	0.1231	0.1156	16.10 ± 16	0.6152 ± 9	-52
ECBV58	B2	fine grained gabbro-norite (WR)	0.1473	0.0610	0.0578	12.53 ± 13	0.5492 ± 23	0
ECBV13	B3	fine grained gabbro-norite (WR)	0.0502	0.0419	0.0409	5.97 ± 6	0.3221 ± 136	1
ECBV63	B3	fine grained gabbro-norite (WR)	0.4165	0.0464	0.0385	52.21 ± 52	1.6874 ± 27	-215
ECBV64	B3	gabbro-norite (WR)	0.2889	0.0461	0.0401	34.77 ± 35	1.2548 ± 23	-61
Oxides								
ECBV26_OX	B2	mt concentrate (MS)	3.6164	0.3333	0.2608	67.03 ± 67	2.2352 ± 34	-187
ECBV27_OX	B2	mt concentrate (MS)	2.4459	0.0678	0.0235	574 ± 6	16.55 ± 6	-3134
ECBV58_OX	B2	mt concentrate (MS)	4.0563	0.5453	0.4475	43.79 ± 44	1.7835 ± 29	129
ECBV58_OXrpt	B2	mt concentrate (MS)	4.0537	0.4268	0.3411	57.28 ± 57	2.0276 ± 30	-70
ECBV64_OX	B3	mt concentrate (MS)	6.3179	0.2346	0.1111	274 ± 3	8.58 ± 16	-94

Notes: Abundances are in parts per billion (ppb). Uncertainties (2s) are in the last digits quoted. γOs is the percentage deviation of the samples from the calculated chondritic reservoir at the Bushveld emplacement age of 2054 Ma ($^{187}\text{Os}/^{188}\text{Os}_{2054} = 0.1131$; Shirey & Walker, 1998). Codes: MS, Mineral Separate; WR, Whole Rock; chr, chromite; mt, magnetite; tmt, titanomagnetite; B1, Bushveld Type 1; B2, Bushveld Type 2; B3, Bushveld Type 3 (see text for explanation).

groups of rocks are markedly different. As expected for more tholeiitic melts, the B2 and B3 samples both have consistently lower concentrations of both Re and Os. The Re concentrations in the B1 samples are in the range 0.4-0.9 ppb, whereas the B2 and B3 samples fall in the range 0.05-0.4 ppb, the Os concentrations are in the range 0.07-0.5 ppb for the B1 samples and the B2 and B3 samples in the range 0.04-0.12 ppb. These ranges place both groups of samples in the field expected for typical basaltic melts. Despite the markedly different concentrations of Re and Os in the melts their $^{187}\text{Re}/^{188}\text{Os}$ ratios are indistinguishable all being in the range $^{187}\text{Re}/^{188}\text{Os} = 5-55$. The similarity in $^{187}\text{Re}/^{188}\text{Os}$ and the fact that there is no correlation between either Re or Os concentration and the $^{187}\text{Re}/^{188}\text{Os}$ ratio suggests that the elemental concentrations of both Re and Os are controlled by similar geological processes.

Whole rock Re-Os isochrons (Fig. 6.1) define ages of around 1700 Ma, which is approximately 350 Ma younger than the age of Bushveld emplacement. In view of SHRIMP age determinations made as part of this study these isochrons are clearly secondary in nature, having no age significance with respect to the emplacement age of the rocks, further supported by the high mean square of the weighted deviates value (MSWD).

Initial isotopic compositions (γOs) of the whole rock samples from the B1, B2 and B3 groups calculated at the age of emplacement (2054 Ma) are not geologically realistic, being in most cases well below the initial of the bulk earth at 4.5 Ga. The likely cause for this is an over estimation of the production of ^{187}Os since the time of emplacement resulting in the subtraction of too much radiogenic ^{187}Os in the calculation of the initial (Equation 6.1). This could result from an increase in the Re/Os ratio occurring after the age of emplacement. To investigate this further the γOs was considered as a function of the $^{187}\text{Re}/^{188}\text{Os}$ ratio (Fig. 6.2a), the Re concentration (Fig. 6.2b) and the Os concentration (Fig. 6.2c). The broadly negative correlation between $^{187}\text{Re}/^{188}\text{Os}$ and the γOs value confirms that the low initials are the product of increased $^{187}\text{Re}/^{188}\text{Os}$ ratios. A broadly negative correlation between γOs and Re concentration suggests that the elevation of the $^{187}\text{Re}/^{188}\text{Os}$ is likely to have been the product of addition of Re. As expected the addition of Re has had the most profound effect on the samples with the lowest Os concentrations particularly in the B1

suite (Fig. 6.2c).

In an attempt to circumvent the problem of isotopic resetting in the determination of initial Os isotopic composition in the B1 rocks, mineral separates were analysed. Spinel was selected because of their high concentrations of Os and their potential to resist the effects of isotopic resetting

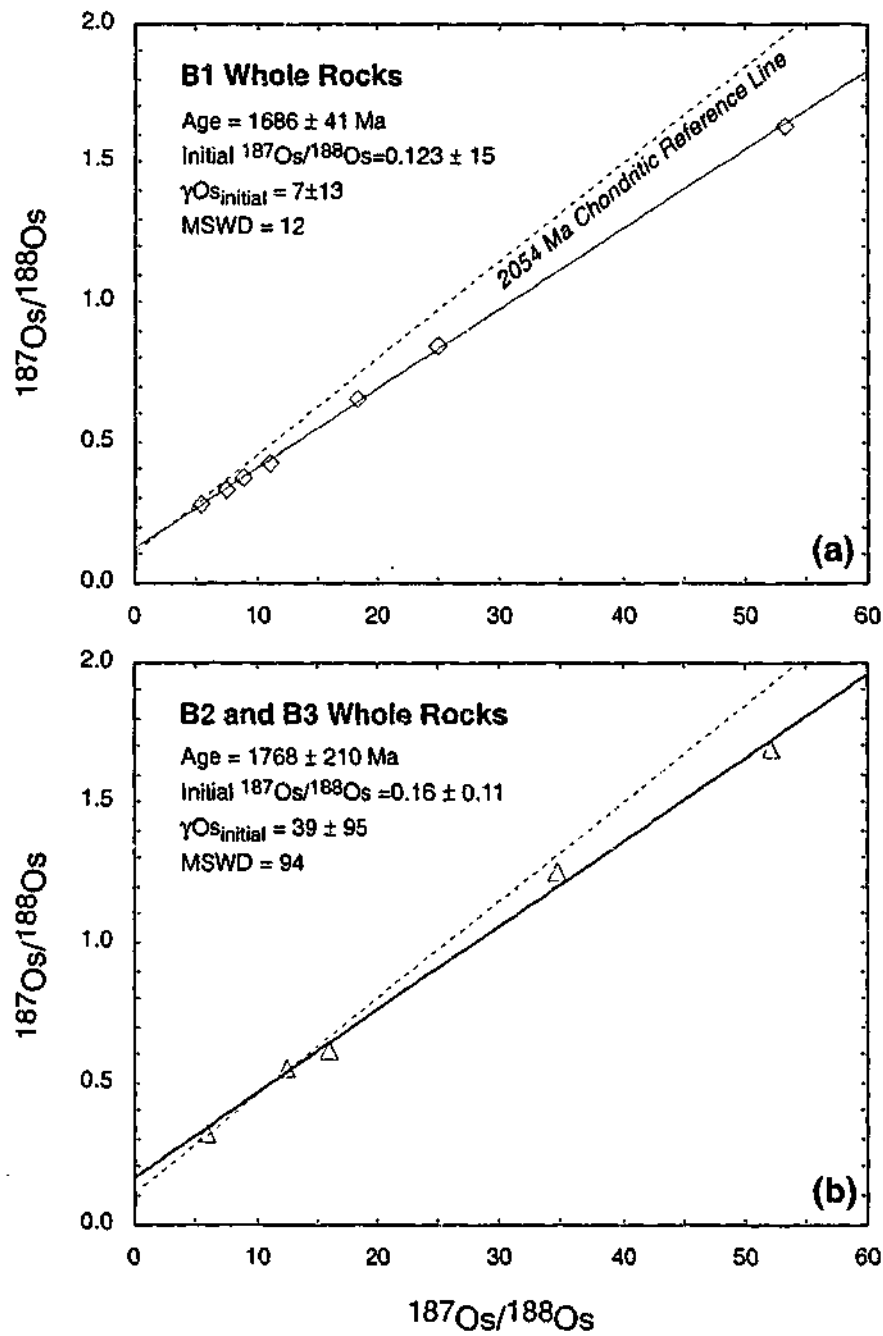


Table 6.1 Re-Os abundances and Os isotopic compositions for whole rock samples and mineral separates from the Bushveld marginal rocks. Notes: Abundances are in parts per billion (ppb). Uncertainties (2s) are in the last digits quoted. γ_{Os} is the percentage deviation of the samples from the calculated chondritic reservoir at the Bushveld emplacement age of 2054 Ma ($^{187}\text{Os}/^{188}\text{Os}_{2054} = 0.1131$; Shirey & Walker, 1998). Codes: MS, Mineral Separate; WR, Whole Rock; chr, chromite; mt, magnetite; tmt, titanomagnetite; B1, Bushveld Type 1; B2, Bushveld Type 2; B3, Bushveld Type 3 (see text for explanation).

(Graham, 1999). The spinels separated from the B1 samples were chrome spinels, with the exception of the quench textured samples which contained dominantly magnetites and those from the B2 and B3 samples which contained titanomagnetites. Os concentrations in the B1 chromites were 1-2 orders of magnitude greater than the whole rocks (4-45 ppb). This confirms the high bulk compatibility of Os in chromite, not discounting the possibility that the Os could be contained in

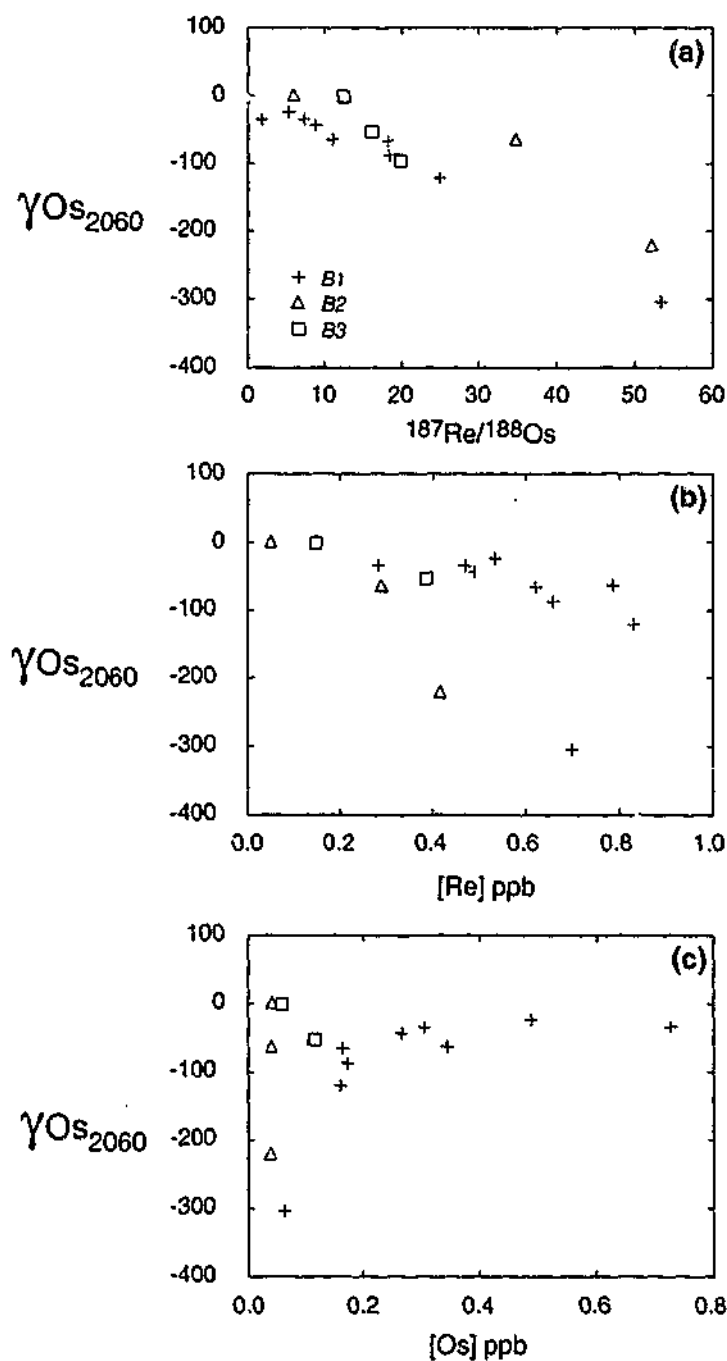


Figure 6.2 γ_{Os} as a function of (a) $^{187}Re/^{188}Os$, (b) Re concentration, and (c) Common (unradiogenic) Os. Illustrating the broad dependence of the γ_{Os} on the concentration of Os and the resulting Re/Os ratio.

platinum group minerals (PGM) included in the chromites. The converse relationship was observed for the analyses of the titano-magnetite separates from the B2 and B3 samples. The observed Re/Os ratio and the Re concentrations were much higher than that of the whole rocks and the Os concentration was much lower, suggesting a high compatibility of Re and a lesser compatibility of Os in this mineral.

The chromite mineral separates from the B1 samples define a 3 point isochron (Fig 6.3a) with a precise chondritic initial γ_{Os} of -0.03 ± 0.50 at 2054 Ma. The very limited spread in the $^{187}Re/Os$

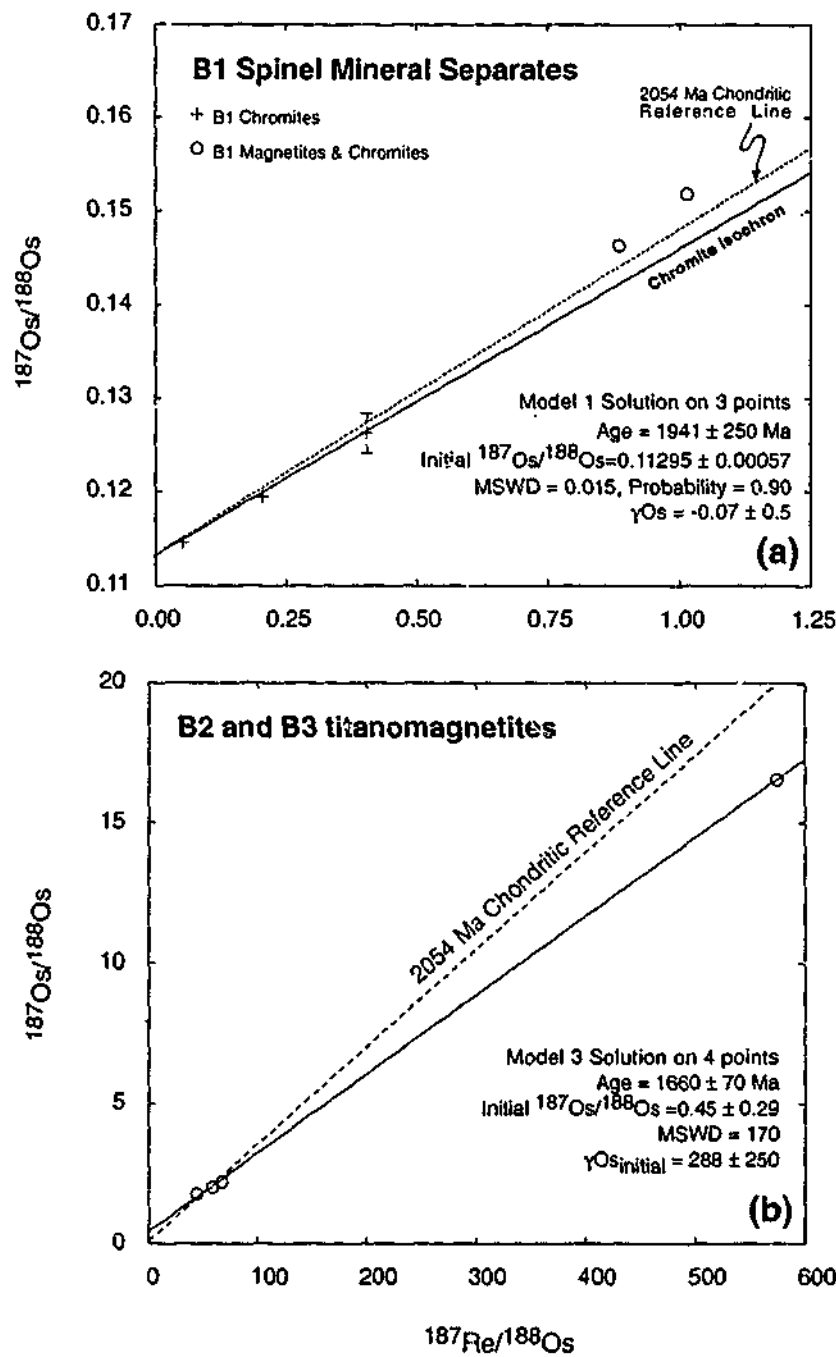


Figure 6.3 (a) Isochron diagram of spinel mineral separates from B1 samples, showing regression for 3 B1 chromite separates, (b) Isochron diagram of titanomagnetite mineral separates taken from B2 and B3 samples. (parameters and regression methods as for Fig. 6.2).

^{188}Os ratios (0.05 – 0.4) poorly constrains the age of the isochron (slope), which is nonetheless within error of the age of the Bushveld Complex.

The spinels separated from the B2 and B3 samples were titanomagnetites and secondary oxides/hydroxides thereof. In contrast to the B1 spinels, the B2 and B3 separates exhibited extremely high concentrations of Re (2.5-6.5 ppb) and relatively low concentrations of Os (0.06-0.40 ppb). The resulting extremely high $^{187}\text{Re}/^{188}\text{Os}$ ratios have led to the evolution of very high measured $^{187}\text{Os}/^{188}\text{Os}$ ratios and extremely low calculated γOs initial values. Similar to the whole rock Re-Os systematics, a plot of the $^{187}\text{Os}/^{188}\text{Os}$ versus $^{187}\text{Re}/^{188}\text{Os}$ yields an age of around 1700 Ma (Fig. 6.3b), significantly younger than the crystallisation age of the Bushveld Complex.

6.2.2 Sr-Nd Isotopes

Analytical Methods

Rb-Sr and Sm-Nd concentrations and isotopic determinations were determined on a single aliquot of sample powder (100 mg) for each sample. Digestion was performed using an "open beaker" digestion method. Primary ion exchange columns were used to separate Rb, Sr and the REE elements from the remainder of the dissolved rock matrix. This was followed by a secondary column separation which separated Sm and Nd from each other and from the remainder of the REE. Analyses were also performed using the Finnigan MAT 262 TIMS in the VIEPS Department of Earth Sciences at LaTrobe University, Melbourne Australia (Appendix 1e). Sr isotopic data are reported relative to a value of 0.71025 for the SRM 987 strontium standard (measured value was 0.71028), and is fractionation corrected to $^{86}\text{Sr}/^{88}\text{Sr} = 0.1194$. Nd data are fractionation corrected to $^{146}\text{Nd}/^{144}\text{Nd} = 0.72190$ (measured value was 0.722163). Oxygen fractionation corrections are made according to the parameters reported by Nier, (1950). Data are reported relative to the La Jolla Standard ($^{143}\text{Nd}/^{144}\text{Nd} = 0.511860$) with the laboratory average of the La Jolla standard being $^{143}\text{Nd}/^{144}\text{Nd} = 0.511842$ at the time the measurements were made.

Rb-Sr Results

The Sr isotopic results for the 16 whole rock samples analysed, including a duplicate analysis, are presented in Table 6.2. In general the B1 samples have higher concentrations of Rb and lower concentrations of Sr than the B2/B3 samples (Fig. 6.4a), resulting in substantially higher $^{87}\text{Rb}/^{86}\text{Sr}$ for the B1 samples (0.4-0.9) compared with the B2/B3 samples (0.01-0.1) (Fig. 6.4b). In general the quenched textured B1 samples exhibit slightly higher concentrations of Sr, and lower Rb/Sr than the remainder of the suite.

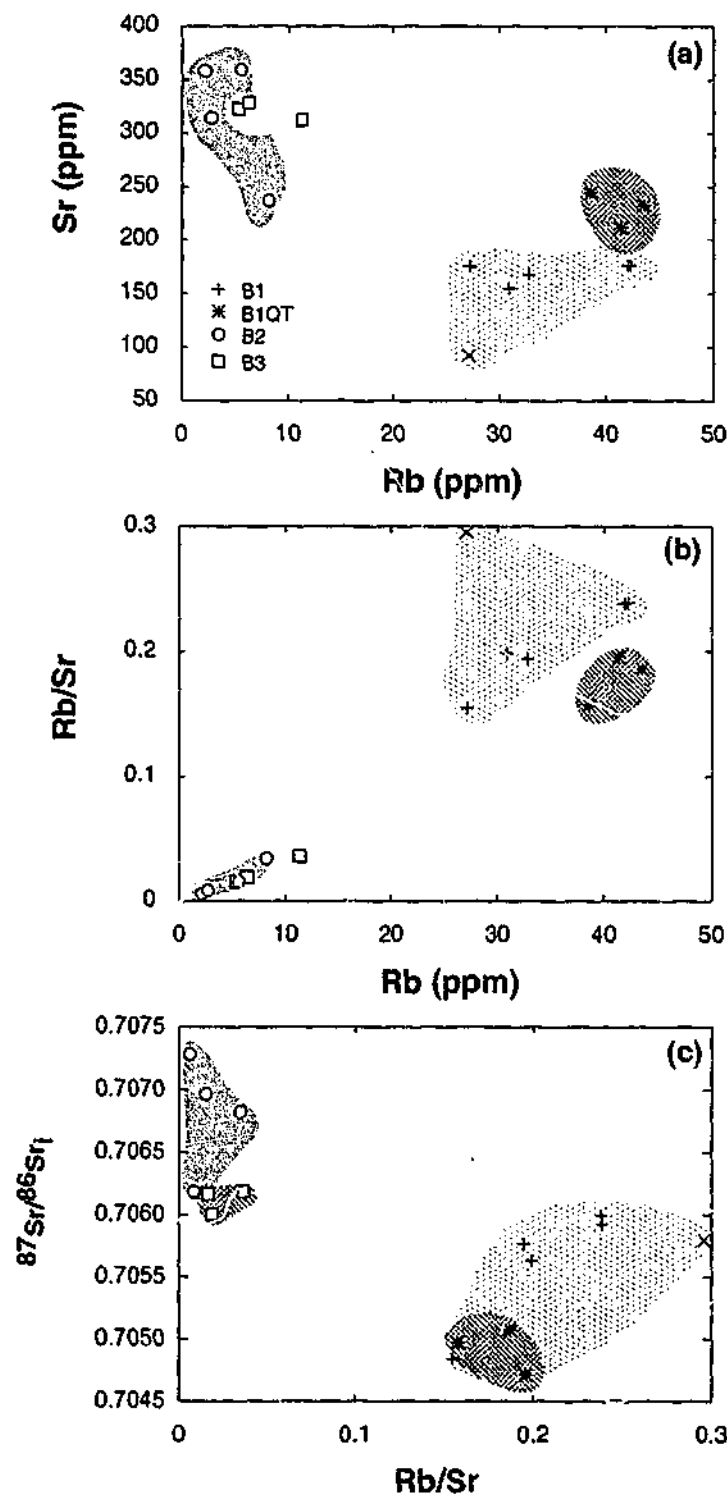


Figure 6.4 Rb-Sr variation diagrams, (a) Sr variation as a function of Rb, (b) Rb/Sr variation as a function of Rb, and (c) $^{87}\text{Sr}/^{86}\text{Sr}$ (2054 Ma) as a function of Rb/Sr.

Table 6.2: Rb-Sr isotope determination on the Bushveld marginal rocks.

Sample	Lithology	Rb (ppm)	Sr (ppm)	$^{87}\text{Rb}/^{86}\text{Sr}$	$^{87}\text{Sr}/^{86}\text{Sr}$	$^{87}\text{Sr}/^{86}\text{Sr}_{\text{initial}}$
Type 1 (B1)						
ECBV16	peridotite sill	27.08	91.6	0.85530 ± 10	0.731104 ± 24	0.70579
ECBV18	granular pyroxenite	30.89	155.3	0.57568 ± 3	0.722668 ± 19	0.70563
ECBV19	granular pyroxenite	32.69	168.0	0.56291 ± 12	0.722416 ± 18	0.70576
ECBV49a	granular pyroxenite	27.18	175.6	0.44772 ± 2	0.718090 ± 16	0.70484
ECBV21	microtextured pyroxenite	38.57	244.3	0.45691 ± 3	0.718491 ± 21	0.70497
ECBV105	microtextured pyroxenite	43.47	232.6	0.54073 ± 2	0.721073 ± 22	0.70507
ECBV106	microtextured pyroxenite	41.32	211.0	0.56656 ± 5	0.721482 ± 19	0.70471
ECBV111	microtextured pyroxenite	42.21	176.6	0.69174 ± 5	0.726393 ± 14	0.70592
ECBV111rpt	microtextured pyroxenite	41.96	176.1	0.68954 ± 9	0.726399 ± 21	0.70599
Type 2 (B2)						
ECBV15	gabbro	8.14	236.4	0.09960 ± 0.4	0.709764 ± 33	0.70682
ECBV26	gabbro	5.51	359.2	0.04441 ± 0.3	0.708272 ± 23	0.70696
ECBV25	fine grained gabbro	2.16	358.4	0.01748 ± 0.1	0.707801 ± 20	0.70728
ECBV58	fine grained gabbro	2.73	314.0	0.02515 ± 0.2	0.706922 ± 18	0.70618
Type 3 (B3)						
ECBV64	gabbro	11.25	312.2	0.10430 ± 1	0.709267 ± 20	0.70618
ECBV13	fine grained gabbro	5.23	322.3	0.04693 ± 1	0.707554 ± 20	0.70616
ECBV63	fine grained gabbro	6.25	328.7	0.05498 ± 0.4	0.707626 ± 20	0.70600

Notes: Uncertainties on the isotopic compositions are 2s in the last digits quoted based on in-run statistics. $^{87}\text{Sr}/^{86}\text{Sr}_i$ is calculated for the SHRIMP emplacement age of the Bushveld marginal rocks (2054 Ma), using the Bulk earth parameters of (DePaolo & Wasserburg, 1979).

When the marginal rocks are plotted on an $^{87}\text{Rb}/^{86}\text{Sr}$ versus $^{87}\text{Sr}/^{86}\text{Sr}$ they define a broadly linear trend which is not sufficiently correlated to define an isochron (Fig. 6.5). However, regressions for the individual groups of rocks and the marginal rocks on the whole define errorchrons with ages in the vicinity of the accepted age of Bushveld crystallisation (2054 Ma).

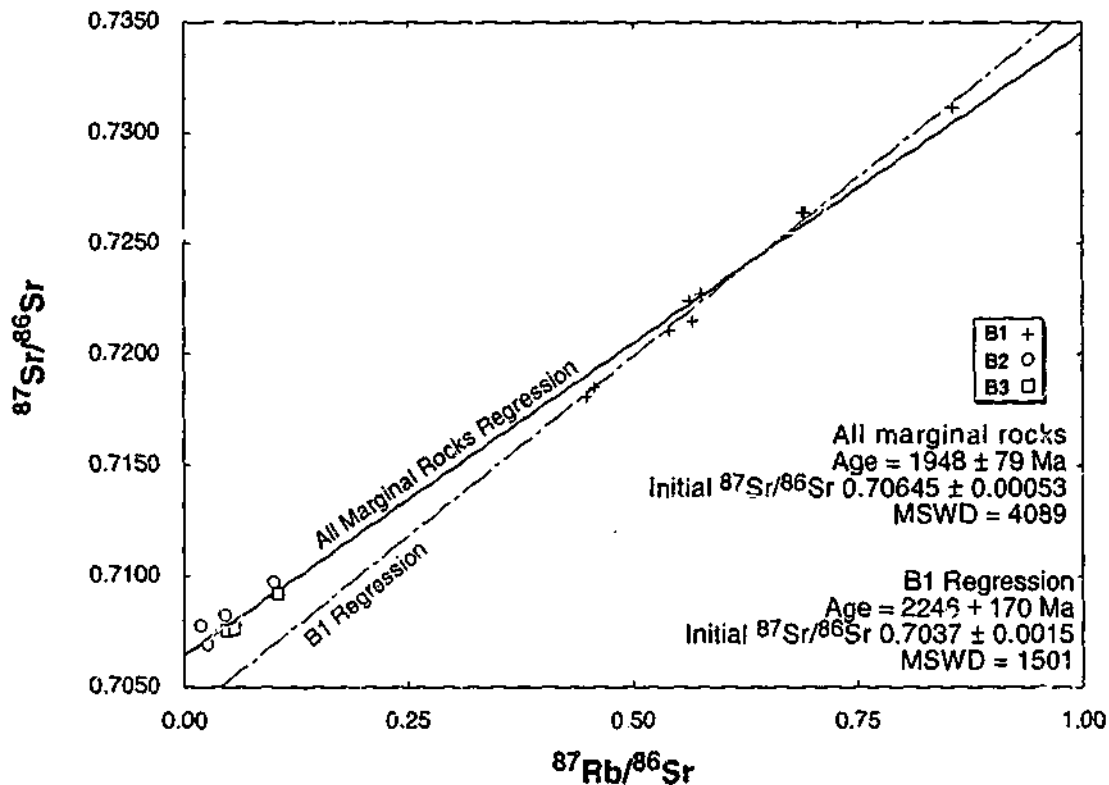


Figure 6.5 $^{87}\text{Sr}/^{86}\text{Sr}$ versus $^{87}\text{Rb}/^{86}\text{Sr}$ isochron diagram for marginal rocks. Regression parameters are as for Figure 6.2.

The calculated initial isotopic composition of Sr ($^{87}\text{Sr}/^{86}\text{Sr}_i$) in the B1 samples is lower than that of the B2 and B3 samples, despite the higher Rb/Sr values. The values for B1 fall into the range 0.7047-0.7060 in comparison to the B2 and B3 samples (0.7060-0.7073) (Fig. 6.5c). This suggests that the parent daughter ratio may have been decoupled from the initial isotopic composition at some stage during the genesis or post emplacement history of the Bushveld suite of rocks. Variable initials are also probably the principal causes of scatter in the $^{87}\text{Rb}/^{86}\text{Sr}$ versus $^{87}\text{Sr}/^{86}\text{Sr}$ isochron plot.

Sm-Nd Results

The results of Sm-Nd isotopic determinations on the marginal rocks are presented in Table 6.3. The concentrations of Sm and Nd are in the range 1.3-2.5 ppm and 8-16 ppm respectively (Table

6.3). There is significant overlap in the concentration ranges of Sm and Nd for the B1, B2 and B3 rocks (Fig. 6.6a). However, as expected the $^{147}\text{Sm}/^{144}\text{Nd}$ ratios for the B1 rocks are generally lower than those for the B2 and B3 rocks (Fig. 6.6b).

Similar to the $^{87}\text{Sr}/^{86}\text{Sr}_i$ ratios a plot of $^{143}\text{Nd}/^{144}\text{Nd}$ versus $^{147}\text{Sm}/^{144}\text{Nd}$ defines an overall linear correlation, although the correlation within the various groups is nowhere near as strong, leading to age estimates with no geological significance. A regression of all of the marginal rocks is shown on Figure 6.7, which yields an age approaching that of the Bushveld Complex (1847 ± 30 Ma).

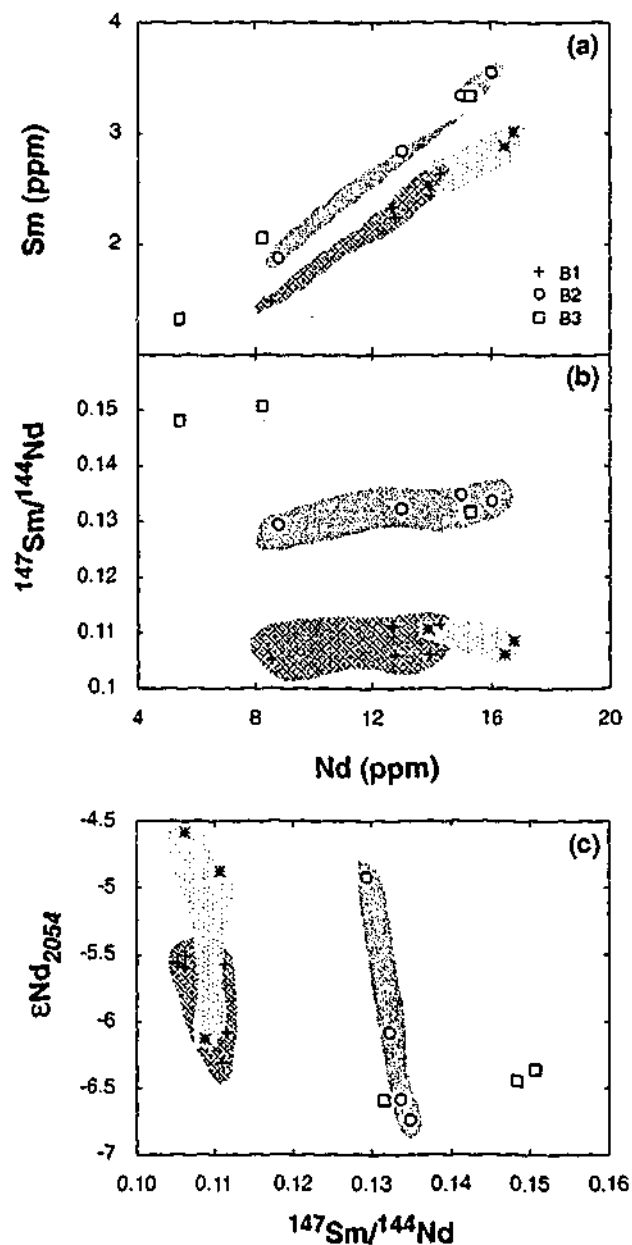


Figure 6.6 Sm-Nd variation diagrams, (a) Sm variation as a function of Nd, (b) $^{147}\text{Sm}/^{144}\text{Nd}$ variation as a function of Nd, and (c) ϵNd_{2054} as a function of $^{147}\text{Sm}/^{144}\text{Nd}$.

There is significant variability in the Nd initial isotopic composition (ϵ_{Nd}) (Fig. 6.7c). The ϵ_{Nd} values for the B1 rocks are in the range -4.5 to -6.3 , whereas the B2 and B3 rocks are slightly less radiogenic, falling within the range -4.9 to -6.7 . Similar to the Sr system is the apparent decoupling of the REE trends and the Nd isotopic systematics. Despite the fact that the B1 magmas on the whole have significantly lower Sm/Nd ratios, they are similar or perhaps slightly more radiogenic as a group than the B2 and B3 magmas, which have higher Sm/Nd and are less LREE enriched.

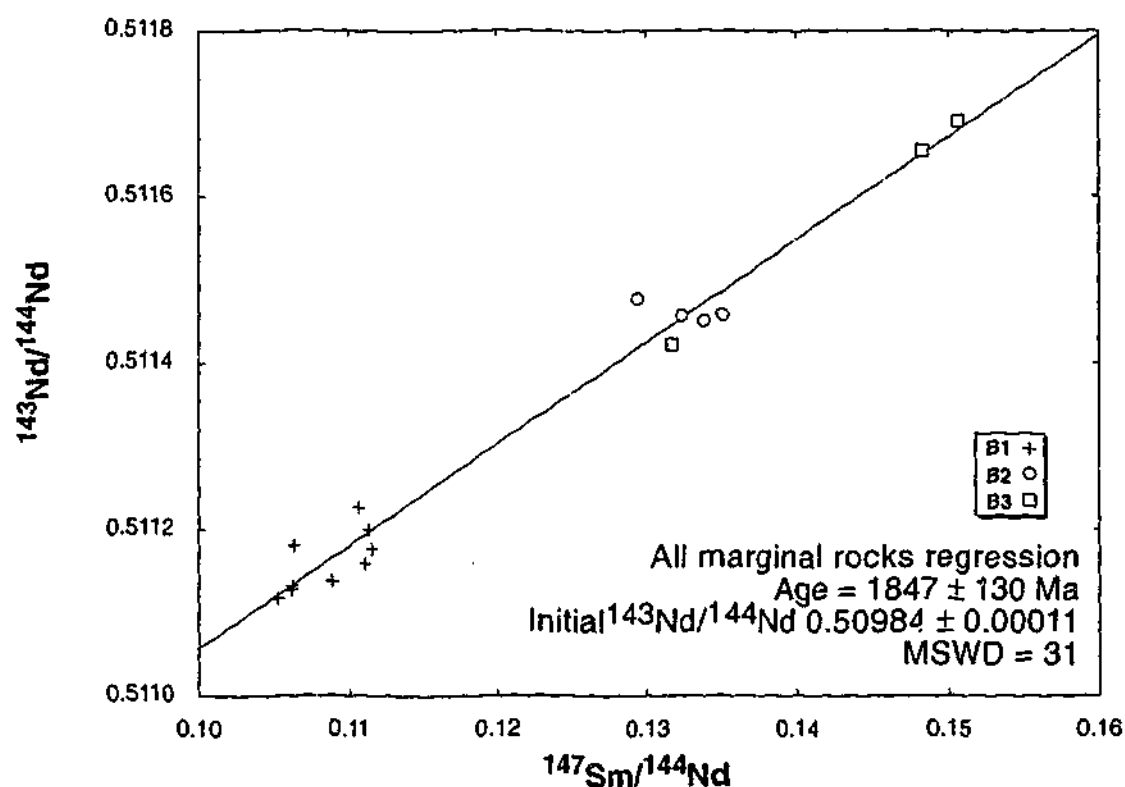


Figure 6.7 $^{143}\text{Nd}/^{144}\text{Nd}$ versus $^{147}\text{Sm}/^{144}\text{Nd}$ isochron diagram for marginal rocks. Regression parameters are as for Figure 6.2.

Oxygen isotopes

The contrast in the oxygen isotopic compositions of crustal and mantle reservoirs makes them useful in the identification of the roles of the reservoirs in magma genesis. Mantle reservoirs typically have $\delta^{18}\text{O}$ values of approximately 6 ‰ (relative to V-SMOW; Vienna Standard Mean Ocean Seawater), whereas crustal rocks, although more variable are generally higher often with an average of approximately 12 ‰ (James, 1981).

Analytical Methods

Oxygen isotope ratios were determined in the Department of Earth Sciences at Monash University on whole rock powders following the procedures of Clayton & Mayeda (1963) but using ClF_3 , in

Table 6.3 Sm-Nd isotope data on the Bushveld marginal rocks.

Sample Identification	Lithology	Sm (ppm)	Nd (ppm)	$^{147}\text{Sm}/^{144}\text{Nd}$	$^{143}\text{Nd}/^{144}\text{Nd}$	Initial $^{143}\text{Nd}/^{144}\text{Nd}$	ϵNd	T_{DM} (Ma)
Type 1 (B1)								
ECBV16	peridotite sill	1.49	8.54	0.1052 ± 1	0.511117 ± 7	0.509694	-5.56	2794
ECBV18	granular pyroxenite	2.24	12.76	0.1061 ± 1	0.511131 ± 8	0.509697	-5.51	2796
ECBV19	granular pyroxenite	2.44	13.92	0.1060 ± 1	0.511126 ± 7	0.509692	-5.60	2802
ECBV49a	granular pyroxenite	2.63	14.26	0.1116 ± 0.5	0.511176 ± 7	0.509668	-6.08	2879
ECBV21	microtextured pyroxenite	3.02	16.76	0.1088 ± 0.4	0.511136 ± 8	0.509665	-6.13	2861
ECBV105	microtextured pyroxenite	2.89	16.45	0.1062 ± 1	0.511180 ± 9	0.509744	-4.59	2731
ECBV106	microtextured pyroxenite	2.53	13.84	0.1107 ± 1	0.511226 ± 11	0.509729	-4.88	2782
ECBV111	microtextured pyroxenite	2.34	12.71	0.1111 ± 1	0.511158 ± 10	0.509656	-6.31	2892
ECBV111rpt	microtextured pyroxenite	2.33	12.66	0.1113 ± 1	0.511199 ± 10	0.509694	-5.57	2839
Type 2 (B2)								
ECBV15	gabbroonorite	1.88	8.79	0.1294 ± 1	0.511477 ± 5	0.509727	-4.92	2948
ECBV26	gabbroonorite	3.34	14.96	0.1349 ± 0.5	0.511458 ± 7	0.509634	-6.74	3187
ECBV25	fine grained gabbroonorite	3.55	16.02	0.1337 ± 0.5	0.511450 ± 6	0.509642	-6.59	3156
ECBV58	fine grained gabbroonorite	2.84	12.97	0.1323 ± 1	0.511457 ± 8	0.509668	-6.08	3089
Type 3 (B3)								
ECBV64	gabbroonorite	3.33	15.28	0.1316 ± 1	0.511422 ± 8	0.509642	-6.59	3129
ECBV13	fine grained gabbroonorite	1.33	5.41	0.1483 ± 2	0.511655 ± 7	0.509649	-6.44	3384
ECBV63	fine grained gabbroonorite	2.05	8.24	0.1507 ± 1	0.511691 ± 8	0.509653	-6.36	3425

Notes: Uncertainties on the isotopic compositions are 2s in the last digits quoted based on in-run statistics. ϵNd is calculated for the SHRIMP emplacement age of the Bushveld marginal rocks (2054 Ma). T_{DM} model age is the age of intersection of the sample evolution curve with that of the depleted mantle. Calculated depleted mantle evolution is based on the parameters of (Michard *et al.*, 1985).

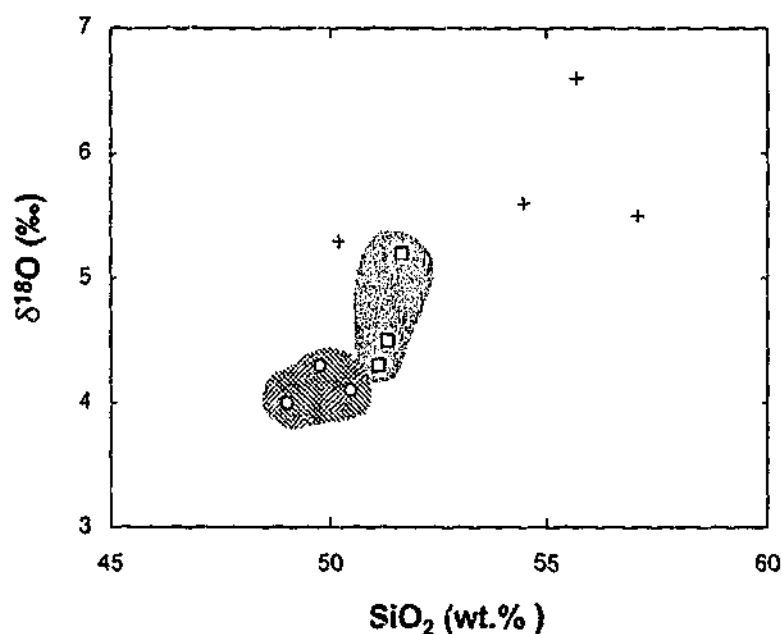
place of BrF_5 as the oxidising reagent. Standardisation was made against the internal standard BHQ that has an $\delta^{18}\text{O}$ value of $10.24 \pm 0.21\text{‰}$. This standard was calibrated against NBS-28 (Coplen *et al.*, 1983) that has a long-term laboratory average $\delta^{18}\text{O}$ value of $9.58 \pm 0.12\text{‰}$. $\delta^{18}\text{O}$ values are expressed relative to V-SMOW, and reproducibility is generally about $\pm 0.2\text{‰}$.

Table 6.4 Oxygen isotope data

Sample	Classification	$\delta^{18}\text{O}$
ECBV16	B1	5.3
ECBV49A	B1	5.6
ECBV105	B1	5.5
ECBV111	B1	6.6
ECBV25	B2	4.0
ECBV26	B2	4.1
ECBV58	B2	4.3
ECBV13	B3	4.5
ECBV63	B3	4.3
ECBV64	B3	5.2

O-isotope Results

The results of 10 oxygen isotopic determinations on a representative suite of marginal rocks are presented in Table 6.4. Results for the B1 samples were slightly higher (5.3-6.6 ‰) than those for the B2 and B3 samples (4.0-5.2 ‰). The oxygen isotopic ratios ($\delta^{18}\text{O}$) were found to be positively correlated with SiO_2 (Fig. 6.8), suggesting a mineralogical control on the whole rock values determined, with the higher abundance of quartz in the B1 samples perhaps controlling this fractionation. However, as a group the marginal rocks exhibit $\delta^{18}\text{O}$ that are suggestive of a mantle source.

Figure 6.8 $\delta^{18}\text{O}$ versus SiO_2

6.3 Discussion

6.3.1 Re-Os Isotope Systematics

The B1 chromites appear to yield a primary chondritic Os signature suggesting that the B1 magmas themselves were essentially chondritic. The uncertainty in the age derived from the chromite isochron is due primarily to the very limited spread in $^{187}\text{Re}/^{188}\text{Os}$ ratio, meaning that relatively minor deviations of individual samples in terms of their $^{187}\text{Os}/^{188}\text{Os}$ translate into large uncertainty. This suggests that the calculated isochron presented (1941 ± 250 Ma) has limited age significance, although it is within error of the Bushveld age. Despite the uncertainty surrounding the isochron slope, the initial remains relatively constant due to the close proximity of the data points to the origin of the graph.

It is apparent that the whole rock Re-Os isotope systematics of the B1, B2 and B3 samples have suffered some post emplacement disturbance. The similarity between the secondary age of the whole rocks and the age yielded by the titanomagnetite mineral separates, coupled with the high Re abundance in this phase may indicate that the secondary products of the titanomagnetites may be the mineralogical control on the resetting of the Re-Os system. For this reason the B1 spinel mineral separates containing appreciable magnetite were excluded from the regression of the chromites.

The possibility that the disturbance observed in the Re-Os system occurred during emplacement can be discounted on the basis that the samples approximate an isochron that is of younger age than the emplacement age. For this to be a process operating at the time of emplacement is impossible because it would require systematic addition of Re, proportional to the Os concentration and the existing Re/Os ratio in the sample such that the isochron started with a negative slope.

It seems most likely that the disturbance of the Re-Os systematics was due to hydrothermal redistribution of either Re and/or Os about 350 Ma after emplacement. The very high Re abundances of the titanomagnetite separates suggest that the alteration event probably involved the addition of significant Re to the samples. Brenan *et al.* (1998) and Xiong & Wood (1998) report experimental

findings on the solubility of Re and Os in medium temperature, low pressure brines under oxidising conditions at temperatures as low as 500°C, and even lower under more saline fluids. This indicates that it is possible to reset the Re-Os system at temperatures not uncommon in the Earth's crust. The derivation of fluid bearing significant concentrations of Re and relatively low concentrations of Os, is not difficult to envisage given the high concentrations of Re and the high Re/Os ratios of typical crustal rocks (Esser & Turekian, 1993). Circumstantial evidence for the existence, if not abundance, of these types of fluids in crustal settings is found in the high Re concentrations and extremely high Re/Os ratios of hydrothermal sulphides such as pyrite and chalcopyrite from meso/epithermal gold deposits (Stein *et al.*, 1999a; Stein *et al.*, 1999b). There is also evidence from metasomatised xenolith suites analysed by proton microprobe that Re is often found along the grain boundaries of granular minerals further rendering the Re budget of a rock susceptible to alteration (Brenan *et al.*, 1998). Thus, it seems plausible that the Re-Os system in the Bushveld rocks may have been reset with minimal textural evidence for hydrothermal alteration.

There is some complimentary evidence for long-lived thermal / hydrothermal activity in the Bushveld rocks after the emplacement and crystallisation of the layered rocks and coincident with the age implied by the secondary Re-Os isochrons. An $^{40}\text{Ar} / ^{39}\text{Ar}$ step-heating analysis performed by FM Consulting on a magnetite gabbro drill-core sample collected from the Upper Zone of the Western Bushveld (Ref: GSSA LW139), yields an argon step heating plateau age of 2096 ± 12 Ma, with partial overprints at 1750 and 1216 Ma (Burger & Walraven, 1976; F. Fitch, FM Consulting, pers. com. 2000). A large degree of discordancy as well as cryptic age determination on bulk zircon fractions from a variety of locations in the Bushveld granites has also been interpreted to be the product of long lived hydrothermal systems in the Bushveld granites (McNaughton *et al.*, 1993).

6.3.2 Correlations between the marginal rocks and the Bushveld Complex cumulates

Sr-Nd

Initial Sr isotope variation in the layered rocks of the Bushveld Complex led to the original suggestion by Harmer & Sharpe (1985) that the more mafic lower part of the cumulate series crystallised from a different melt to the upper more leucocratic rocks. The Bushveld Complex shows a slow but

steady increase in $^{87}\text{Sr}/^{86}\text{Sr}_i$ up to the base of the Upper Critical zone, after which several positive peaks or 'spikes' in the $^{87}\text{Sr}/^{86}\text{Sr}_i$ are observed coupled with a more rapid increase up to the level of the Merensky and Bastard reefs. The $^{87}\text{Sr}/^{86}\text{Sr}_i$ remains high but much more uniform throughout the Main and Upper Zones of the Complex, with a slight drop in $^{87}\text{Sr}/^{86}\text{Sr}_i$ marking the base of the Upper Zone (Fig. 6.9) (Kruger, 1994; Kruger & Anonymous, 1997; Kruger & Barnes, 1992). Recent Nd isotope determinations by Maier *et al.* (2000) show that there is a broadly negative correlation between $^{87}\text{Sr}/^{86}\text{Sr}_i$ and ϵNd in the layered rocks, suggesting that the Nd isotope systematics were controlled by the same process as that which controlled the Sr.

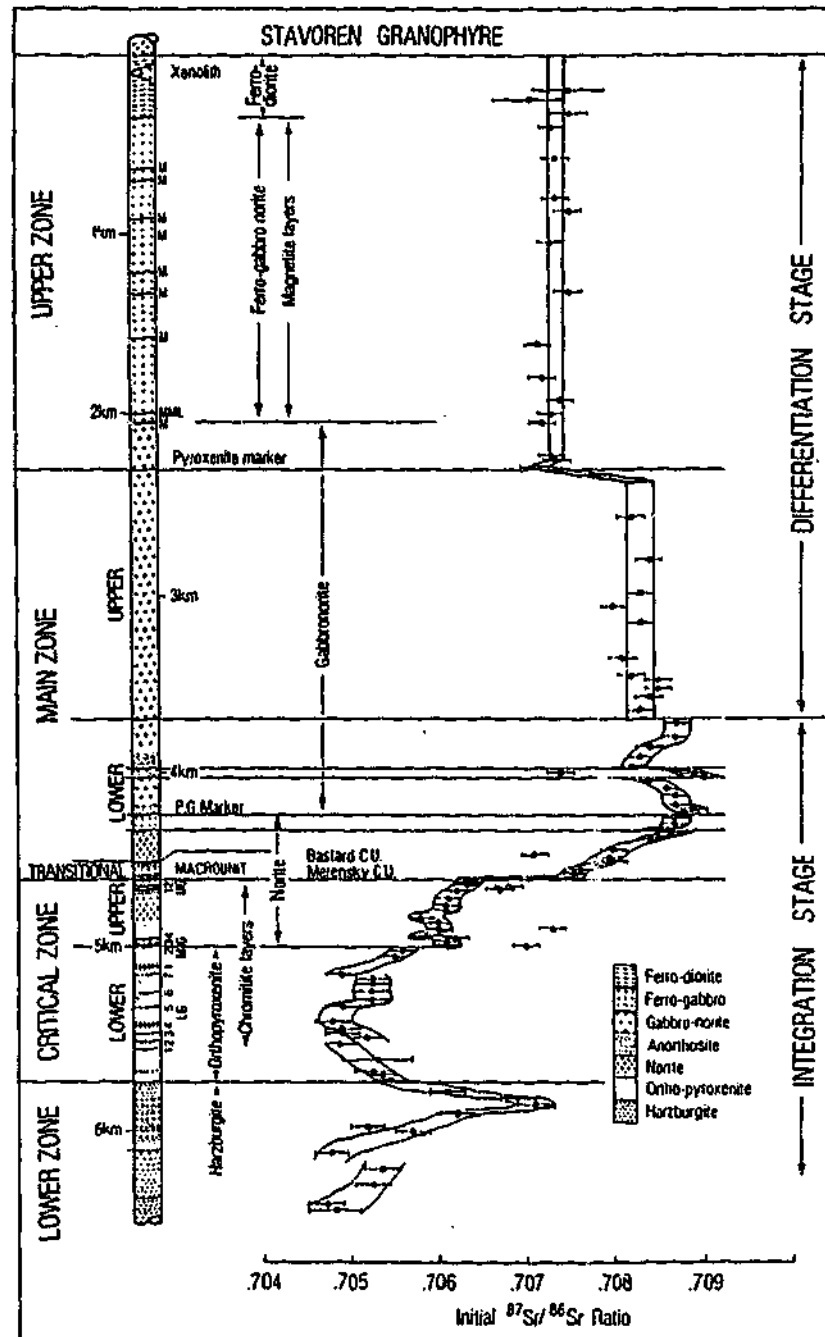


Figure 6.9 Initial $^{87}\text{Sr}/^{86}\text{Sr}$ ratio as a function of stratigraphic height above the base of the Bushveld Complex (Kruger, 1994).

Although direct stratigraphic correlation between the marginal rocks and the cumulate series is difficult, a broad stratigraphic correlation can be made (Fig. 6.10). This correlation shows that the ϵNd and $^{87}\text{Sr}/^{86}\text{Sr}_i$ systematics of the marginal rocks broadly mirror those of the layered complex, with the exception of $^{87}\text{Sr}/^{86}\text{Sr}_i$ in the Main Zone. Our analyses of the B3 marginal rocks have considerably lower $^{87}\text{Sr}/^{86}\text{Sr}_i$ values than the Main Zone, with the Main Zone rocks plotting above 0.7070 and the marginal rocks plotting in general around 0.7060. A similar observation was made by Harmer & Sharpe (1985) and appears to be at odds with a model which proposes that the B3

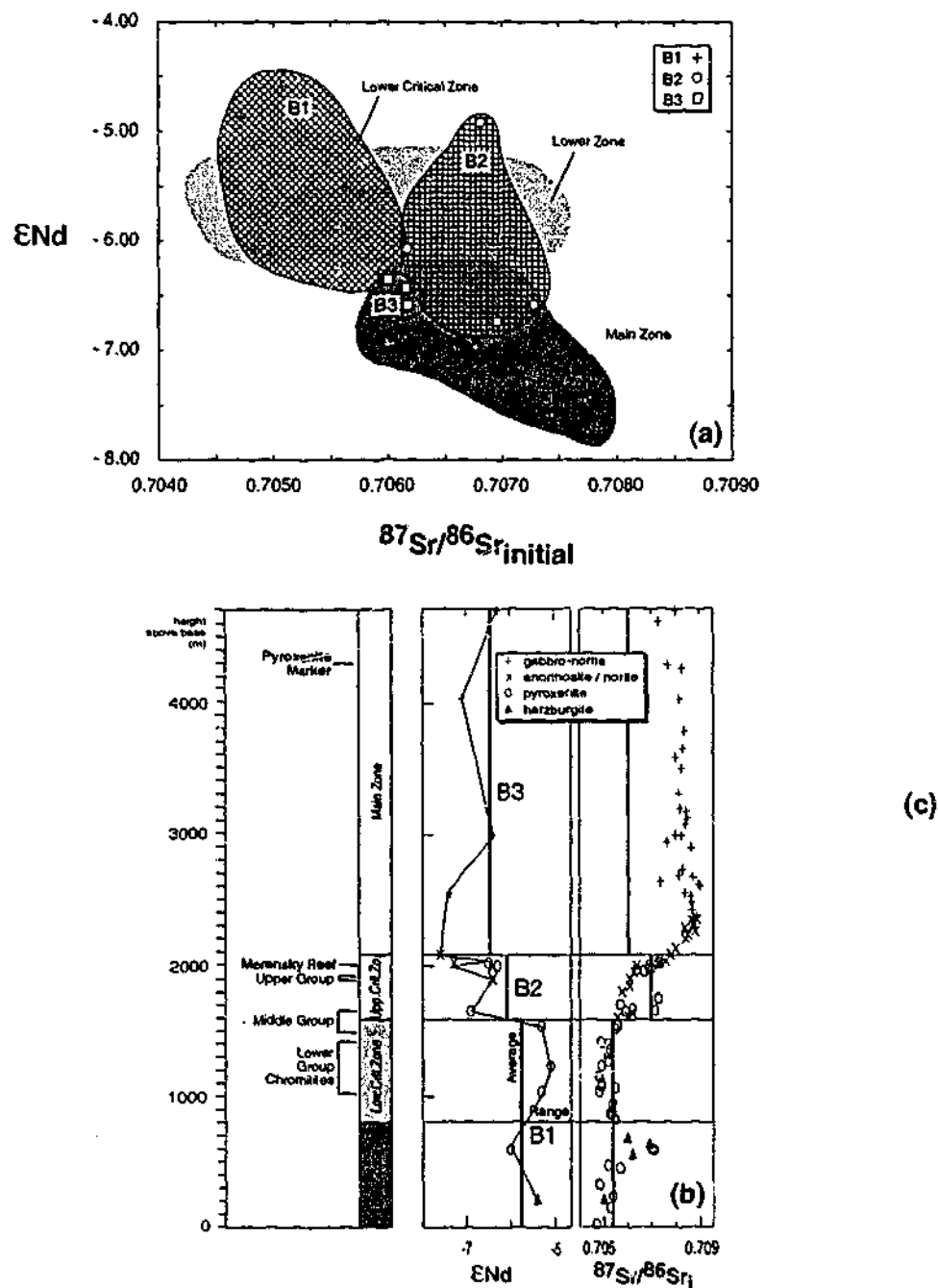


Figure 6.10 Correlation of the marginal rocks with the cumulate series, (a) ϵNd as a function of $^{87}\text{Sr}/^{86}\text{Sr}_i$ for the marginal rocks and Bushveld Complex cumulates], and (b) vertical $^{87}\text{Sr}/^{86}\text{Sr}_i$ and ϵNd variation in the Bushveld cumulates compared with average and range values of the marginal rocks (values and Figure (b) adapted from Maier *et al.* 2000).

rocks are the direct antecedents of the Main Zone, cumulates. It is possible that either the samples analysed in this study are not entirely representative of the B3 rocks, or that the B3 rocks are not directly representative of the parental melts to the Main Zone, most probably the latter. Hatton (1996) saw this conundrum as reason to propose a fourth Bushveld magma, which was designated B4 as was considered as parental to the Main Zone. However, Hatton (1996) went on to propose that the B2 rocks were parental to the Lower Critical Zone and the B3 were parental to the Upper Critical Zone. While Sr isotopic data are consistent with the "redesignation" of the parental melts to the various zones of the complex the Nd data are not, with the Nd isotopic data paralleling those for the Main Zone (Fig 6.10).

Re-Os

While the Re-Os database for the cumulate series of the Bushveld Complex is limited, available data show that chromites from the Bushveld B1 rocks have slightly lower $^{187}\text{Os}/^{188}\text{Os}$ isotopic compositions than the ore bearing rocks of the Merensky reef and associated chromitites (Fig. 6.11). McCandless *et al.* (1999) and Schoenberg *et al.* (1999) propose that the slightly supra-chondritic Os isotopic compositions of the ore bearing sulphides and chromitite horizons ($\gamma\text{Os} \sim +1-30$) are the products of minor crustal contamination during emplacement. The positioning of the B1 chromites below the mineralised samples in terms of their γOs is consistent with them representing the uncontaminated magma composition.

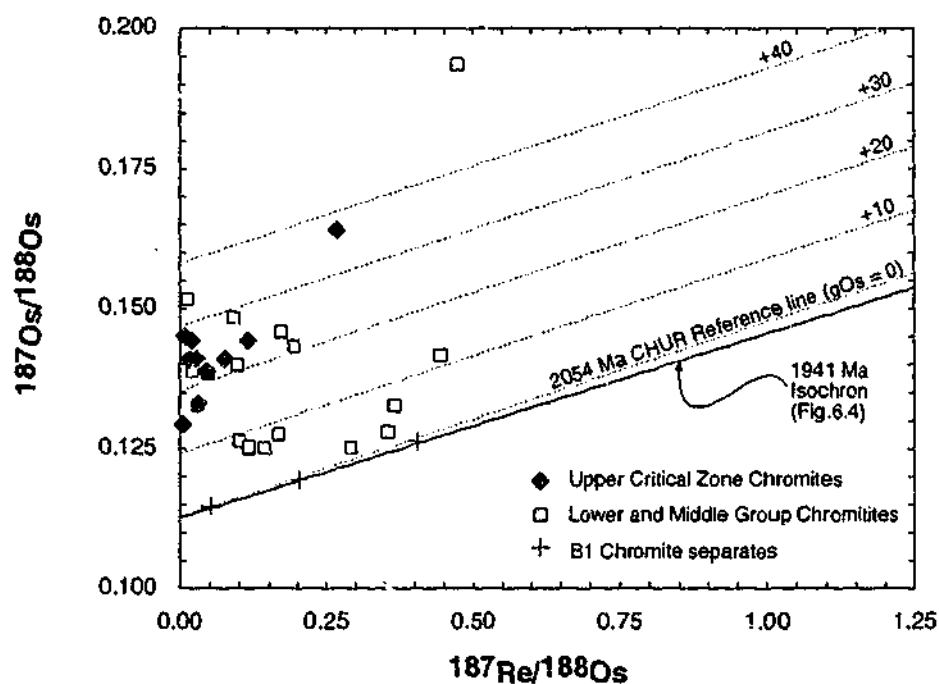


Figure 6.11 Comparison of Re-Os analyses of chromite and magnetite separates from B1 marginal rocks with determinations made on Upper Critical Zone chromitites (McCandless *et al.*, 1999) and Lower and Middle Group chromitites (Schoenberg *et al.*, 1999).

6.3.3 Sm-Nd depleted mantle model ages

Depleted mantle model ages (T_{DM}) are defined as the calculated age of the intersection of a sample evolution curve with that of the depleted mantle. In the case of rocks derived directly from melting in the depleted mantle these ages are equivalent to the age of melting. In samples, or suites of rocks with a more complicated history of crustal contamination or melting of enriched source regions these ages can be more difficult to interpret. However, in view of the fact that the process of partial melting in most instances increases the degree of LREE enrichment (decreases the Sm/Nd ratio), even in rocks with a more complex history T_{DM} model ages may be used as an estimate of the minimum age of separation from the depleted mantle reservoir.

The Nd evolution trajectories of the marginal rocks have been calculated and are presented graphically in Figure 6.12. Depleted mantle model ages on the whole range from 3.4 Ga in the least LREE enriched B3 sample to 2.7 Ga in the most LREE enriched B1 sample. The fact that the model ages are significantly older than the age of Bushveld emplacement reconfirms the fact that the Bushveld melts were derived from an enriched source, or were contaminated with enriched material. The significance of the T_{DM} ages to this argument is that in either case these data suggest

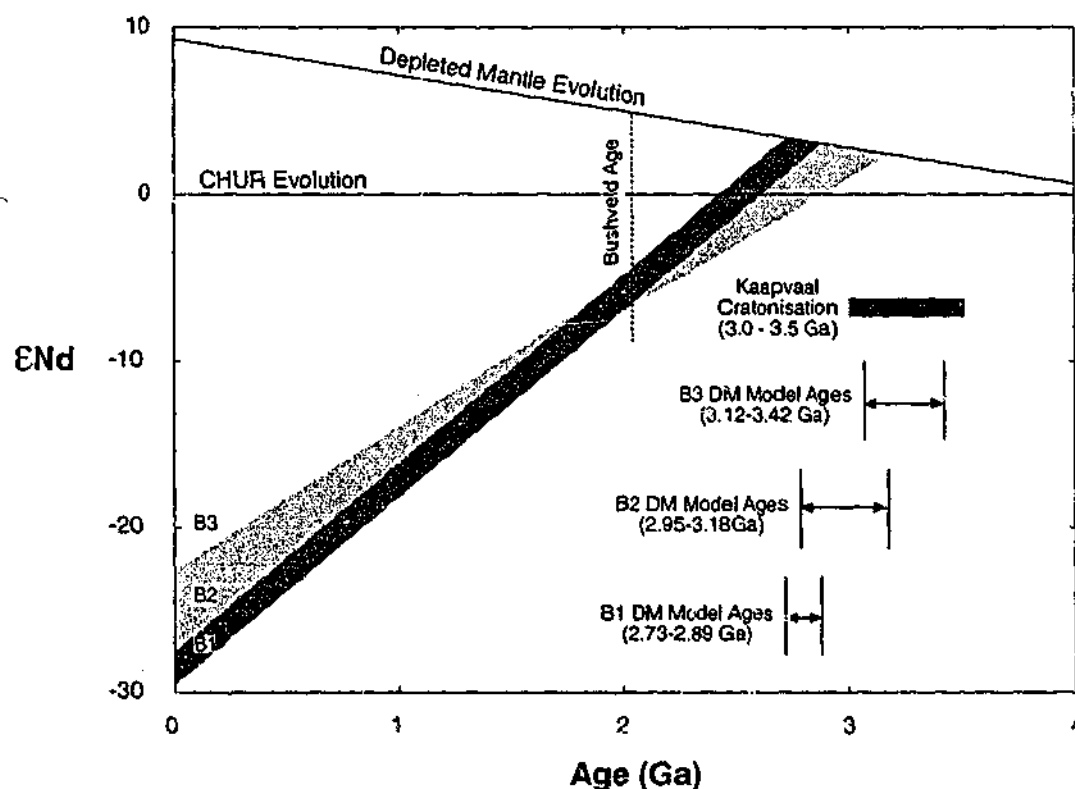


Figure 6.12 Plot of Nd isotopic evolution and intersection with the depleted mantle reservoir and resulting depleted mantle model ages. Depleted mantle evolution parameters are those of Michard *et al.* (1985). Position of Kaapvaal cratonisation age also shown (de Wit *et al.*, 1992).

that the enriched source, or crustal material, separated from the depleted mantle at an age that was probably significantly older than 2.7 Ga in the case of the B1 samples and at an age of greater than *c.a.* 3.0 Ga for the B2 and B3 samples. However, these data have limited scope for distinguishing between these two sources of enrichment in view of the fact that available age data for enrichment of the Kaapvaal SCLM (Pearson *et al.*, 1995a; Pearson *et al.*, 1999; Richardson *et al.*, 1993; Walker *et al.*, 1989) and crust formation (de Wit *et al.*, 1992; de Wit *et al.*, 1990) suggest that the two events may have been coincident in time, and perhaps even related (Anderson, 1995a; de Wit *et al.*, 1992; de Wit *et al.*, 1990; Jordan & Anonymous, 1981).

6.4 Sr-Nd Modelling

6.4.1 Previous models for the generation of the Bushveld magmas

Recent work by Maier *et al.* (2000) has shown that the Sr-Nd isotope systematics of the parental magmas to the Bushveld Complex may be modelled by assimilation of upper crustal material in the case of both B1 and B2/B3. Their model, based on the work of Sharpe *et al.* (1986), models the isotope and trace element characteristics of the B1 magmas as products of contamination of a mantle derived picritic-komatiitic magma with a small degree partial melt (5-12%) of 3.0-3.5 Ga Archaean upper crust. This partial melt is modelled as being highly enriched in trace elements, but with low Sr concentration, as much of this element would have been retained in residual plagioclase. The Upper Critical and Main Zone melts were then formed through further magma being injected into an upper crustal staging chamber where as much as 50 % of the residual material after the contamination of the B1 magmas was assimilated through an AFC type process. This imparts the more Al-rich tholeiitic major element chemistry to the melt, as well as adding a large amount of relatively radiogenic Sr. In addition the residence of the melt in a crustal staging chamber may have provided the opportunity for homogenisation of the B2 and/or B3 magmas to produce the consistent $^{87}\text{Sr}/^{86}\text{Sr}_i$ signature observed in the Main Zone. Although 50 % assimilation is large, the initial extraction of the first partial melt could be expected to heat the residual material close to melting, such that the heat budget required is much less than in a primary AFC system.

6.4.2 Sr-Nd modelling of the marginal rocks

The Sr-Nd systematics of the marginal rocks have also been modelled (Fig. 6.13). The Sr isotopic composition of the crustal endmember was based on the extraction of average continental crust (Taylor & McLennan, 1985) from the Bulk Earth reservoir at 3.2 Ga, which evolved with a Rb/Sr ratio of 0.17 until the age of Bushveld emplacement (Fig. 6.13a). The depleted mantle component was calculated according to the model of Ben Othman *et al.* (1984) which is based on separation of the depleted mantle from the Bulk Earth reservoir at 2.8 Ga. Nd was calculated for the depleted mantle on the basis of the parameters given by DePaolo & Wasserburg (1979). The crustal estimate was again based on extraction of average continental crust extracted from the chondritic mantle at 3.2 Ga. Concentration estimates for the crustal endmember were similar to those calculated by Maier *et al.* (2000) based on a calculated small degree partial melt of the crust (<10 %). The mantle endmember is a calculated picritic melt of the depleted mantle.

The curves generated by modelling (Fig. 6.13b) pass through the approximate centre of the calculated initial field for the marginal rocks, with a calculated 30 wt.% of the crustal endmember required to produce these melts. Quantitative assessment of the degree of contamination relies heavily on the selection of endmember concentration values, which in this case are speculative, thus these estimates should be treated cautiously. However, this modelling does serve to illustrate that there is a likely role for a crustal component in the genesis of the marginal rocks, and that these melts can be modelled as a possible mixture between continental crust and depleted mantle.

6.5 Oxygen-Sr modelling

Trace element and radiogenic isotope modelling hinges on our understanding of the behavior of minor constituents of most rocks in processes of partial melting, element partitioning between mineral phases and reaction relations, thus there are a relatively large number of uncertainties. In contrast oxygen isotope systematics rely on an element that makes up 45-50 wt.% of most terrestrial silicate rocks. Thus, this technique has the potential to provide better insights into *bulk* processes of exchange between source rocks, magma and contaminants. James (1981) derived a series of mixing lines that model the contamination of a mantle derived melt with representative silicate

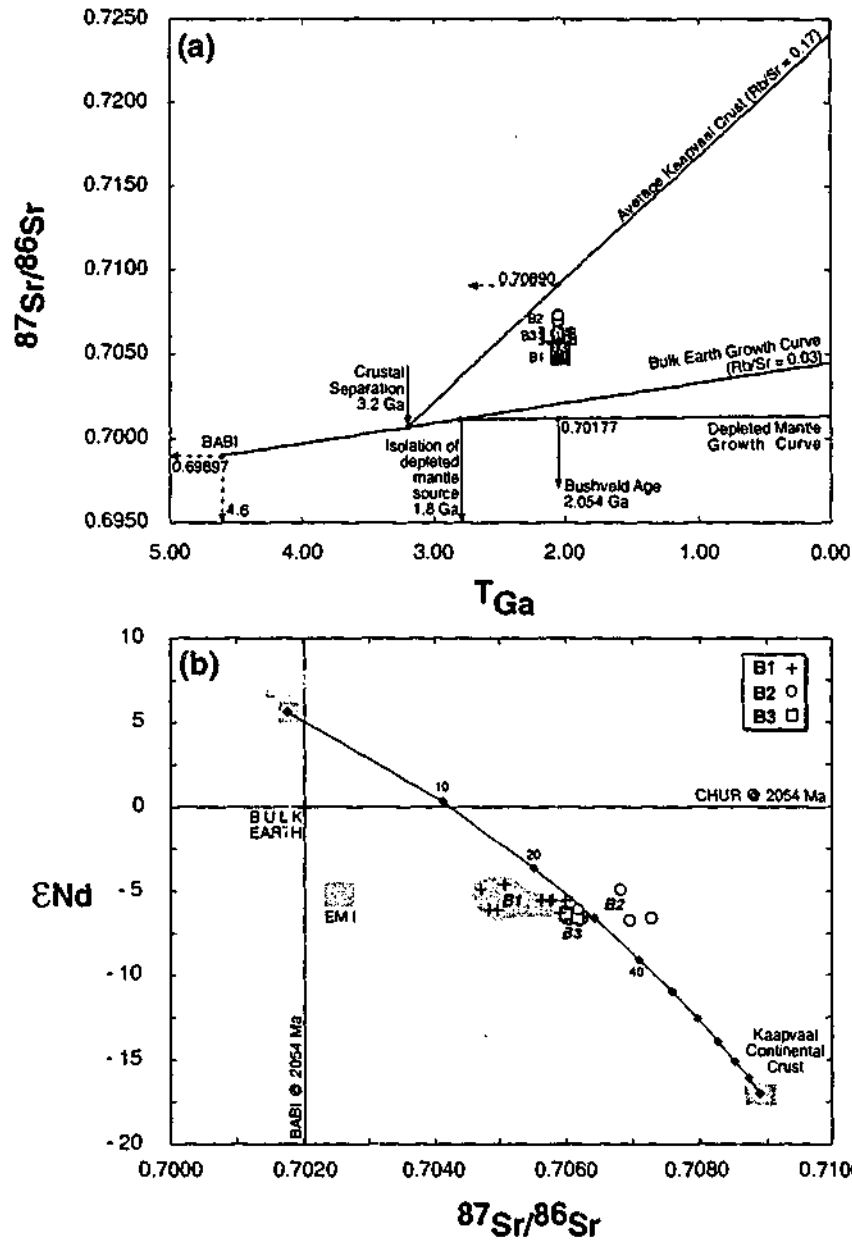


Figure 6.13 Sr-Nd Modelling (a) $^{87}\text{Sr}/^{86}\text{Sr}$ versus Time (Ga) growth curves for Bulk Earth, Depleted Mantle and estimated Kaapvaal continental crust, with position of marginal rocks calculated for age of emplacement and positions of modelled endmembers also shown, and (b) ϵNd versus $^{87}\text{Sr}/^{86}\text{Sr}$ modelling of the marginal rocks as a function of mixing between depleted mantle picrite and 12% partial melt of the estimated Kaapvaal upper crust. All initial values calculated at 2054 Ma. Reservoir parameters are from (Ben Othman *et al.*, 1984; DePaolo & Wasserburg, 1979; McCulloch & Black, 1984; O'Nions *et al.*, 1977; Taylor & McLennan, 1985).

crustal material (Fig. 6.14). There are two fields shown which model source contamination (convex down) and direct crustal contamination of a mantle derived melt (convex up). The source contamination process is envisaged as infiltration of a partial melt derived from enriched rocks, in this case subducted oceanic slab. Because the concentration of Sr (and other trace elements) is high in the partial melt and low in the mantle source, the Sr isotopic signature of the source is

quickly dominated by the infiltrating melt, even when the melt:mantle ratio (x) is low. Meanwhile this has limited effect on the $\delta^{18}\text{O}$ because of the similar concentrations of O in either endmember. In the case of source contamination the degree of convexity is governed by the $[\text{Sr}]_{\text{mantle}}/[\text{Sr}]_{\text{contaminant}}$ ratio, as indicated on Figure 6.14. In contrast crustal contamination of a mantle derived melt is convex-up on account of the higher concentrations of Sr in the mantle derived melt, thus the effects of a given value of x is less due to the lower $[\text{Sr}]_{\text{mantle}}/[\text{Sr}]_{\text{contaminant}}$ ratio.

Modelling Results

The low, mantle like $\delta^{18}\text{O}$ values of the marginal rocks and their positioning close to or below the modelled field for source contamination suggests that bulk contamination is not a likely cause of the observed elevated $^{87}\text{Sr}/^{86}\text{Sr}_i$ values. Their positioning suggests that the elevated $^{87}\text{Sr}/^{86}\text{Sr}_i$ is the product of source contamination, or another process that decouples $^{87}\text{Sr}/^{86}\text{Sr}_i$ from $\delta^{18}\text{O}$ to a similar extent. This essentially means that the contaminant has to have a sufficiently contrasted Sr concentration to the material it is contaminating, be it source or melt. Maier *et al.* (2000) propose a partial melt of the upper crust as a contaminant, which in light of the oxygen/Sr modelling is possible if the contaminant had a sufficiently high concentration of Sr. However, Maier *et al.* (2000) propose that the partial melt which contaminated the B1 melts, contained relatively low concentrations of Sr, leaving residual plagioclase which was assimilated to form the more Al-tholeiitic B2 and B3 melts. This was proposed on the basis that the B1 melts have higher Rb/Sr ratios and lower $^{87}\text{Sr}/^{86}\text{Sr}_i$ than the B2 and B3 melts. Hence the product of the early melting event were required to be enriched in Rb, but not radiogenic Sr. The oxygen isotope data are clearly at odds with this explanation.

6.6 Os-Nd Modelling

Although the Sr-Nd systematics of the marginal rocks suggest a role for the crust, the mantle-like (chondritic) Os signature may suggest otherwise. Thus, a model that involves the derivation of much of the Sr and Nd from an enriched reservoir such as the crust and much of the Os from a near-chondritic reservoir seems the most plausible. In addition, any model for the Bushveld melts must

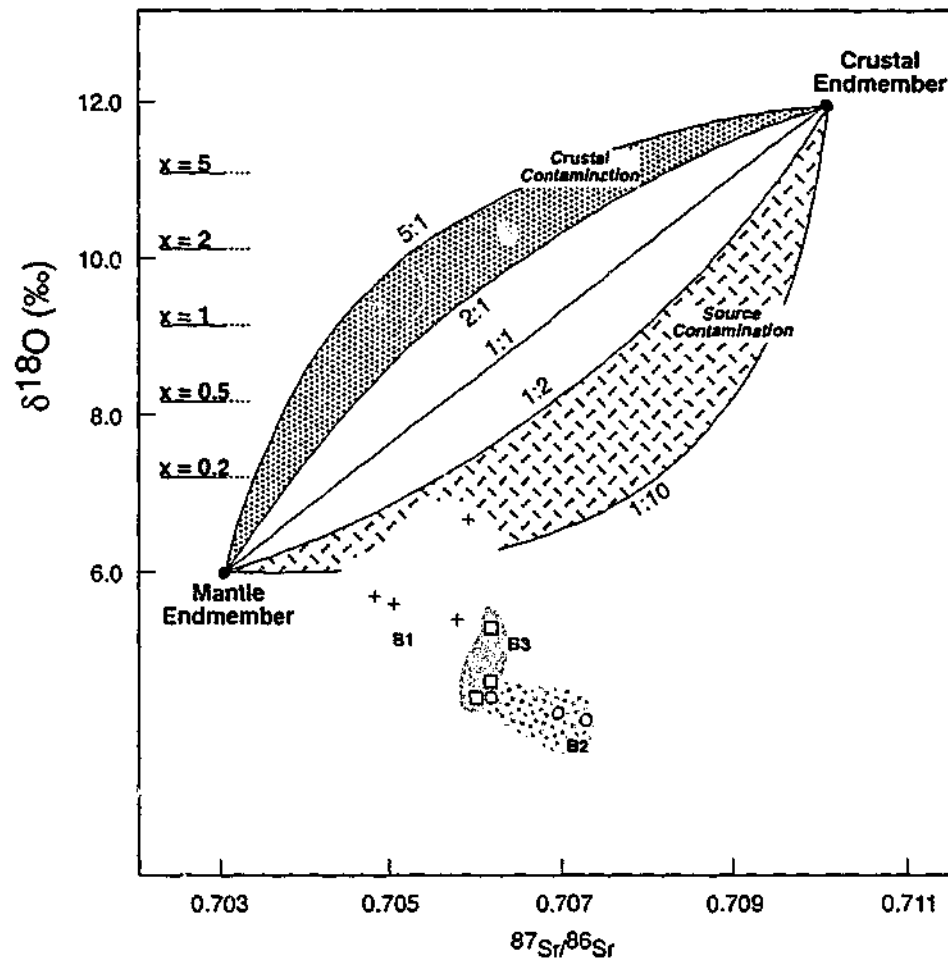


Figure 6.14 $\delta^{18}\text{O}$ versus $^{87}\text{Sr}/^{86}\text{Sr}$ modelling of mantle melt contamination, showing Bushveld marginal rocks plotted in the position of their calculated $^{87}\text{Sr}/^{86}\text{Sr}$, (2054 Ma). Ratio values shown on the curve represent the concentration ratios of Sr in the mantle component/crustal component. The parameter x represents the mass proportion of the crustal endmember in the modelled derivative melt (diagram after James, 1981).

consider a heat source or mechanism for melting which accounts for the massive volume of magma in the complex generated over a relatively short time (*c.a.* km^3 over 1-3 Ma; Harmer & Armstrong, 2000), which may imply a role for a plume. As will be demonstrated presently there is well developed SCLM under much of the Kaapvaal craton, with substantial evidence for re-enrichment beneath the Bushveld Complex which may amount to circumstantial evidence for melting in the SCLM during the Bushveld event. Os-Nd modelling provides a unique opportunity to study the interaction of these three reservoirs because of the unique Os-Nd signature of each. In light of these considerations we will model several different possibilities for the genesis of the Bushveld B1 magmas and the subsequent genesis of the B2 and B3 magmas. Those possibilities are: (a) the B1 magmas were primarily plume derived, (b) the B1 magmas were sourced by melting of depleted mantle with a possible role for the SCLM and /or the continental crust, and finally (c) the B1 magmas are primarily the product of melting in the SCLM with a minor role for crustal assimilation.

Once the possibilities for the B1 magmas have been investigated, a model for the derivation of the B2 and B3 magmas from the B1 magmas will be considered.

Modelling Methods

The principal parameters used here in the modelling of the derivation of the Bushveld melts are the concentration and isotopic composition of Os and Nd. These two systems when used in concert provide modelling which incorporates contrasts between the crustal and mantle reservoirs in terms of siderophile (Re-Os) and lithophile (Sm-Nd) elements. Whilst $^{87}\text{Sr}/^{86}\text{Sr}$ initial data provide useful information relating the marginal rocks to the Bushveld Complex and they are useful in understanding the emplacement and mixing dynamics of the layered complex, their application in modelling crustal and mantle reservoirs as an ultimate source for the Bushveld rocks is limited. This is primarily a function of a less well constrained understanding of the time integrated evolution of the Rb/Sr system in those environs. In contrast the Re-Os system is well constrained in terms of our understanding of the evolution of crust and mantle primarily on account of the large and consistent contrast in Re/Os ratios between the crust and mantle (Pearson *et al.*, 1999; Shirey & Walker, 1998). Similarly the Sm-Nd system is well understood in terms of crust and mantle reservoirs and their time integrated evolution.

Modelling in the Re-Os system provides some unique challenges in terms of isotopic mass balance of endmember compositions. When modelling the mixing of two endmembers in the Re-Os system it is important to consider the mass balance of the changing isotopic composition of Os, particularly when there is a large contrast between the isotopic compositions of the two endmembers. In one case modelled here of contamination of an SCLM melt with Archaean upper crust the abundance of ^{187}Os in the SCLM melt is 1.4%, compared with 12% in the crustal endmember. Thus, simple mixing of two endmembers on the basis of concentration alone may lead to erroneous results, and this is amplified in mixing cases where the contrast in γOs is even larger. The method of mixing adopted here was similar to that of Horan *et al.* (1995b), which accounts for the mass balance of ^{187}Os in the two endmembers. The abundance of ^{187}Os and ^{188}Os is calculated in the two endmembers on the basis of the measured/assumed $^{187}\text{Os}/^{188}\text{Os}$ ratios. The molar concentration of

the two isotopes was then mixed separately by simple mixing and the $^{137}\text{Os}/^{188}\text{Os}$ are calculated for each increment of mixing. For consistency a similar approach was adopted for Nd.

The reservoirs

Plume Source

The mantle endmember proposed in the model of Maier *et al.* (2000) is a picritic composition. Most models for these high MgO primitive melts propose plume derived melting (Walker *et al.*, 1997). Furthermore the sheer volume of the Bushveld melts implies the role of a plume in providing (a) the heat source for melting, and/or (b) the melts themselves (Hatton, 1995). A similar line of reasoning is invoked for the genesis of some continental flood basalt provinces (Gallagher & Hawkesworth, 1992; Hawkesworth *et al.*, 1994; Hawkesworth & Turner, 1994).

Analyses of modern oceanic island basalts (OIB) indicates that plumes may be sourced from a region of the mantle with elevated Re/Os ratios. This has led in time to elevated γOs for these reservoirs with estimates of modern OIB magmas falling in the range $\gamma\text{Os}(T) = +5$ to $+20$ (Hauri & Hart, 1993; Widom *et al.*, 1999). It has been proposed that a subduction-related oceanic crustal component resident in the mantle source regions for these melts for up to 1.3 Ga is responsible for their enriched Os isotopic signatures (Hauri & Hart, 1993; Widom *et al.*, 1999). It is arguable whether these types of reservoirs would have been fully developed with sufficient residence times to evolve radiogenic isotopic signatures at the time of the Bushveld event (2.06 Ga). However there is substantial evidence to support the existence of radiogenic plumes at that time. Walker *et al.* (1997) showed that 1980 Ma uncontaminated ferropicrites from the Pechenga had γOs values of $+6 \pm 0.7$. Os isotopic analyses of younger plumes at 1100 Ma (Shirey, 1997) and 250 Ma (Horan *et al.*, 1995b) show them to fall in a similar range to those of the Pechenga picrites suggesting the long term isolation and stability of the plume source (Frick, 1998).

The origin of the enriched Re/Os and consequent elevated γOs in late Archaean / Early Proterozoic plumes may not necessarily be the same as that for modern OIB basalts. Walker *et al.* (1995) proposed that differential partitioning of Os into the siderophile core of the earth during core

formation may have led to elevated Re/Os ratios in the region surrounding the core, termed D' by Walker et al. (1995). The possible sourcing of early plumes from this region of the mantle may explain their positive γ_{Os} values. The similarity in age of the Pechenga plume and the Bushveld event is sufficient to suggest that if the Bushveld was sourced from a "plume source", that it probably had a radiogenic γ_{Os} composition. Similarly published analyses (Table 6.5) of plume basalts and picrites suggest that their source regions have $^{143}Nd/^{144}Nd$ ratios slightly more radiogenic than the CHUR reservoir, possessing recalculated ϵ_{Nd} of $\sim +2$ at the age of the Bushveld. The elemental concentrations used in the modelling of the plume component were estimated from published data on plume picrites and basalts (Table 6.5).

Table 6.5 Os-Nd Modelling parameters

	[Os] ppb	γ_{Os}^f	[Nd] ppm	ϵ_{Nd}^f	References
Plume					
Picrite	0.5	+6	12	+2	Hauri & Hart, 1993; Horan et al., 1995; Martin et al., 1991; Pegram & Allegre, 1992; Reisberg et al., 1993.
Depleted mantle					
Picrite	0.5	0	12	+5.6	DePaolo & Wasserburg, 1979; Lambert et al., 1994; Shirey & Hanson, 1986.
SCLM					
Bulk	3.5	-2.5	3.5	-3	Carlson & Irving, 1994; Carlson et al., 1999; Pearson et al., 1995; Pearson et al., 1999; Richardson et al., 1993; Smith, 1983; Walker et al., 1989.
SVM (Lamproite component)	0.2	-2.5	50	-3	
Crust					
Bulk	0.05	+823	26	-17	Maier et al., 2000; Esser & Turekian, 1993; Taylor & McLennan, 1985.
12 % partial melt	0.005	+823	33	-17	
Residue from 12 % partial melt	0.056	+823	25.2	-17	

^f γ_{Os} and ϵ_{Nd} calculated for age of emplacement of the Bushveld complex (2054 Ma)

The Crust

The estimates for Archaean upper crustal rocks of the Kaapvaal are more speculative, based on the age and estimated parent/daughter ratios in the Kaapvaal upper crust at the age of emplacement of the Bushveld Complex. The age of the basement in the northeast region of the Kaapvaal shield is thought to range from 3.5-3.0 Ga (de Wit *et al.*, 1992). In the absence of Re-Os data on the predominantly tonalitic, trochhemitic and granitic rocks that make up the basement estimates of average Archaean crustal rocks have been used (Esser & Turekian, 1993). The initial osmium isotopic composition of these rocks is projected from their chondritic separation age of 3.5-3.0 Ga forward in time to the age of formation of the Bushveld Complex at 2054 Ma, giving them crustal residence ages between 1 and 1.5 Ga, resulting in an estimated average γ_{Os} of +823 (Fig 6.15). A

similar process was adopted for the Nd isotopic composition calculated for the age of the Bushveld.

The Nd concentrations of the 12% partial melt and melting residual of the Archaean upper crust are taken from Maier *et al.* (2000) who estimated them on the basis of melting experiments on a biotite gneiss (Patiño Douce & Beard, 1995) following the procedure of Rudnick *et al.* (1990). The concentration of Os in a partial melt of the Archaean upper crust was estimated assuming Os was compatible during the melting of average continental crust (Esser & Turekian, 1993). The concentration of Os in this component is critical to the results of the modelling. The concentration depends on the partitioning behavior of Os during partial melting of the crust. As a first order estimate for crustal D_{Os} values a similar value for that of mantle melting could be adopted. Naldrett *et al.* (1986) recommend a D value for Os and Ir of ~10 during mantle partial melting. A considerable proportion of the Os in the mantle resides in high temperature refractory alloys, which are often included in minerals such as olivine and chrome spinel and importantly immiscible sulphide. Recent work by Lassiter & Luhr (2001) confirm that Os is also compatible during fractional crystallisation of these minerals in a crustal setting, exhibiting D values similar to nickel. The lower abundances of these minerals in the crust may mean that Os is less compatible, having a bulk D value of less than 10. However, the lower temperatures that could be expected during crustal melting may mean that the alloys would be melted to a lesser extent, rendering Os more compatible. This leads to a considerable degree of uncertainty in the selection of an appropriate D_{Os} value for modelling Os during crustal melting. More empirical estimates of Os partitioning behavior during crustal melting may be obtained by looking at Os in acid / intermediate melts considered to be the product of crustal melting. Although hampered by a limited database on these types of melts, available data do suggest low concentrations of Os in partial melts of the crust. Walker *et al.* (1994) and Walker *et al.* (1991) in Frick (1998) report values for granitoids in the range 3-20 ppt (average 11 ppt). If these melts were derived by melting of crustal rocks with Os concentrations of 50 ppt (Esser & Turekian, 1993), then a D_{Os} value in the range 2-17 for melting of crustal rocks seems reasonable, thus a median value of 10 has been adopted. This results in melts of the crust with an estimated Os concentration of 0.005ppb (Table 6.4).

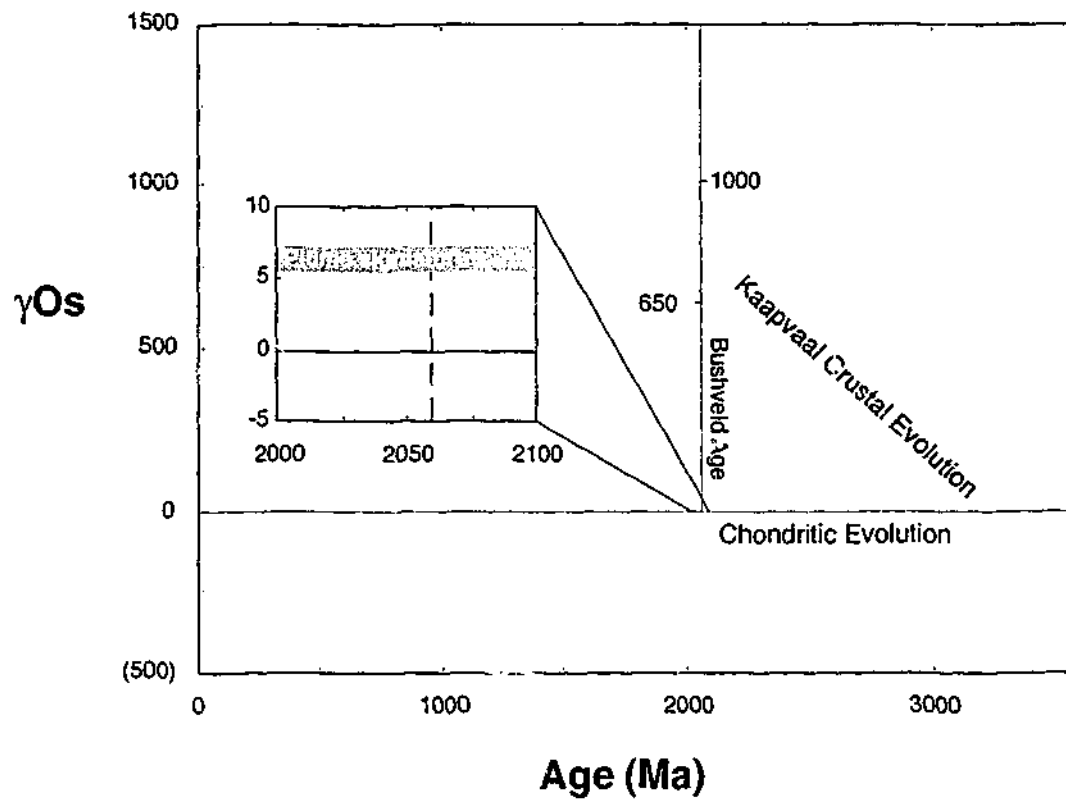


Figure 6.15 Projection of average Archaean continental crust from age of Kaapvaal shield formation (3.0-3.5 Ga i.e. age of separation from chondritic mantle) forward in time to the age of Bushveld melting. Projection yields $\gamma\text{Os}(2054)$ values for average Archaean crust in the range 650-1000 (average = 823) using $R_e = 500$ ppt and $O_s = 50$ ppt (Esser & Turekian, 1993).

SCLM

The SCLM is the portion of the upper mantle that is mechanically coupled to the base of the continental crust and is chemically isolated from the underlying convecting asthenosphere (Anderson, 1995). The refractory nature of the SCLM is thought to be the product of ancient melt depletion. Studies of xenoliths brought to the surface by kimberlites and other ultra-potassic rocks erupting onto the Kaapvaal craton indicate the presence of a thick refractory keel beneath the continent for most of its history (Pearson *et al.*, 1995a; Pearson *et al.*, 1999; Walker *et al.*, 1989). Estimates of the antiquity of the SCLM beneath the Kaapvaal craton are as old as the continent itself (3-3.5 Ga; Pearson *et al.*, 1999), perhaps suggesting a relationship between crustal stabilisation and development of the SCLM (McBride *et al.*, 1996). So while the primitive mantle has a near chondritic Re-Os composition (Shirey & Walker, 1998) and the crust has a high Re/Os ratio and with time a high $^{187}\text{Os}/^{188}\text{Os}$ (Esser & Turekian, 1993) the SCLM has a complimentary relationship to the crust, having a lower Re/Os and $^{187}\text{Os}/^{188}\text{Os}$ as a product of the extraction of partial melts during crust building.

While the SCLM may be a possible source for the enriched trace element and isotopic signature of the Bushveld melts, the actual dynamics of melting in the SCLM may be more difficult to explain. The persistence of the Kaapvaal SCLM for over 3.5 Ga of cratonic history attests to the refractory nature of the SCLM. However, Gallagher & Hawkesworth (1992) proposed that the addition of as little as 0.4 wt. % water to the SCLM could lower the solidus by several hundred degrees. While this may provide a melting mechanism for the SCLM the absence of hydrous minerals (Eales & Cawthorn, 1996) from the Bushveld assemblage may argue against this. Although, if the Bushveld magma system was open, dissolved water in the magma may have been carried through the system or was degassed during emplacement and would not be represented in the assemblage of the cumulate sequence (Boudreau & McCallum, 1992). The possibility of synchronous intrusive and extrusive magmatism during the Bushveld event was recognised by Hatton & Schweitzer (1995). Thus it appears possible that the Bushveld magmas did contain minor concentrations of water, and that hydrous melting of the SCLM may have been an important factor in the genesis of the Bushveld magmas.

Recent seismic experiments on the Kaapvaal craton confirm the presence of a thick (300-400 km) refractory keel under most of the Kaapvaal and Zimbabwe cratons (James *et al.*, 2001). Cross-sectional models of the S and P-wave seismic data reveal a zone of markedly lower seismic velocities (-1% velocity perturbation) beneath some Proterozoic terranes such as the Limpopo belt and in particular beneath the Bushveld Complex. James *et al.* (2001) suggest a link between the velocity perturbation beneath the Bushveld Complex and the magmatic event that formed the Bushveld Complex. The possibility that the SCLM is lacking beneath these terranes is unlikely, particularly in the case of the Bushveld Complex. The 1180 ± 30 Ma (Richardson *et al.*, 1990) Premier kimberlite intrudes the margin of Bushveld Complex and sampled diamondiferous harzburgitic, lherzolitic and eclogitic SCLM, indicating the presence of thick (>150 km) SCLM beneath the Bushveld Complex at 1180 Ma. The more likely explanation for the low velocity zone is the re-fertilisation (addition of Fe) of the SCLM, lowering the rigidity and seismic velocity. This re-fertilisation hypothesis is also given support by the virtual absence of sub-calcic Cr-rich garnets from heavy mineral separates of the Premier kimberlite. Sub-calcic Cr-rich garnets are typical of and only

found within melt-depleted Archaean lithospheric mantle peridotite (Gurney 1984), and their absence from Premier kimberlite concentrate suggests the presence of an anomalous mantle. The fact there has been a major refertilisation event may imply a preceding depletion event, correlated with the Bushveld event.

Inclusions in diamond are important samples of the lithospheric mantle because the diamond acts to shield the inclusion from re-equilibration with other mantle phases at the high ambient temperatures. For the three suites of diamond at Premier Sm-Nd isotope data clearly indicate three different crystallisation ages. Harzburgite sub-calcic garnets yield Archaean model ages, lherzolite Ca-saturated garnets yield an isochron age of 1938 ± 98 Ma and eclogite garnet-cpx pairs suggest an age of ~ 1200 Ma (Richardson *et al.*, 1993). For comparison a garnet-cpx isochron from lherzolite xenoliths at Premier yields an age of 1194 ± 77 Ma (recalculated from Pearson *et al.* (1995a) suggesting isotopic equilibrium at emplacement. Significantly this age is much younger than the age determined from inclusions in diamond. However, the most important information that may be obtained from isotopic studies of inclusions in diamond that of the initial isotopic compositions, as these may be used to infer what kind of processes have occurred within/to the lithospheric mantle.

In the case of the Bushveld Complex the most important inclusions are those of the harzburgite and lherzolite parageneses. The Premier Archaean sub-calcic garnets included in diamond yield model ages and hence their initial is the same as that of the asthenospheric mantle. Sub-calcic garnets are extremely rare in Premier kimberlite concentrates (suggesting the presence of anomalous Ca-rich mantle), however, sub-calcic concentrate garnets from the Cretaceous Finsch and Bultfontein kimberlites yield an age of 600 Ma and an initial ϵ_{Nd} value of -8.4, suggesting re-equilibration. The initial ϵ_{Nd} value from the Premier lherzolite 1938 ± 98 Ma diamond inclusions is -3.1 and the ~ 1200 Ma lherzolite xenolith samples is 1.3, implying continued SCLM modification and equilibration following diamond crystallisation. Asthenospheric mantle ϵ_{Nd} values at this time were -5.7 - 7.5, respectively, hence the lherzolite inclusions in diamonds must have crystallised from an old enriched source. Importantly this -3.1 initial ϵ_{Nd} value places a firm constraint on the

Nd isotopic composition of the SCLM at ~2000 Ma. If it is assumed that the lherzolite xenoliths and diamond inclusions represent the same source then in order to obtain a ~1.3 1200 Ma ϵ_{Nd} value the source must have had an Sm/Nd ratio of ~0.24. In contrast to the isotopic constraint we have on the SCLM, concentration data is more limited. To circumvent this problem, significant weight was placed on the Nd concentration of Group II kimberlite melts emplaced into the Kaapvaal craton (Smith, 1983), similar to the adoption of a the "lamproite component" of Ellam & Cox (1991).

Osmium isotopic studies on the xenolith suites derived from the Premier kimberlite reveal different systematics to those derived from other kimberlites from the Kaapvaal Craton. The most recent compilation of Kaapvaal xenolith data from Carlson *et al.* (1999) reveals some interesting aspects concerning the state of the lithospheric mantle beneath the Bushveld Complex compared to other regions of the craton. The Re-Os T_{RD} and T_{CHUR} model ages of most xenoliths from the Carlson *et al.* (1999) data set are older than the age of the Bushveld Complex. Hence xenolith isotopic compositions can be calculated for 2050 Ma for the majority of xenoliths. Some Re may have been introduced during emplacement, however, the close correspondence in T_{RD} and T_{CHUR} model ages and the presence of only a few samples with unreasonable T_{CHUR} model ages suggests that this is minimal. For xenoliths from the Kimberley, Lesotho and Letlhakane areas the average 2050 Ma γ_{Os} value is -5.7 ± 6.7 (2SD $n = 20$). For samples from the Limpopo belt the average 2050 Ma γ_{Os} value is -7.1 ± 7.3 (2SD $n = 4$). In all cases the xenoliths have sub-chondritic initial γ_{Os} values. However, at Premier the xenoliths yield a significantly higher initial γ_{Os} value of -2.5 ± 4.0 (2SD $n = 11$) implying that the lithospheric mantle beneath the Bushveld Complex was of significantly different age and composition to that beneath the rest of the craton and the Limpopo Belt. Average 2050 Ma T_{RD} model ages for the xenoliths also differ and for the samples with the -5.7 γ_{Os} value the average T_{RD} model age is ~2500 Ma, compared to the average T_{RD} at Premier which is ~2200 Ma.

These data, like the Sm-Nd data from inclusions in diamonds place constraints on the SCLM beneath the Bushveld Complex during its emplacement. Two lines of evidence suggest that there

was at some stage Archaean lithospheric mantle beneath the Bushveld Complex: 1) some diamond inclusions contain Archaean sub-calcic Cr-rich garnets, and 2) T_{RD} model age average for the Premier xenoliths is 2200 Ma, which is older than the Bushveld Complex. The fact that the average γ_{Os} value for the xenoliths is -2.5 suggests that the lithospheric mantle beneath the Bushveld was not of asthenospheric composition, as its γ_{Os} value would be 0, or typical Archaean SCLM but suggests that the mantle was re-worked and re-fertilised at some stage. The obvious event based on the seismic, and inclusion in diamond data for this re-working is that it occurred during the emplacement of the Bushveld Complex. Moreover, knowing that the Bushveld event likely altered the composition of the lithospheric mantle, and knowing the isotopic compositions of this lithospheric mantle following re-fertilisation allows constraints on the source of the initial magmas and of the metal enrichment in the Bushveld Complex to be thoroughly investigated.

Projection of a xenolith's sub-chondritic initial isotopic composition back in time to its age of separation from the chondritic mantle reservoir yields an estimate of the age of melt depletion referred to as the rhenium depletion model age (T_{RD}). The projection is accomplished by assuming that all of the Re was removed during melt depletion resulting in a $Re/Os=0$ and cessation of production of radiogenic ^{187}Os which in turn results in a constant $^{187}Os/^{188}Os$ since the age of melt depletion (Fig. 6.16). The complete removal of Re from peridotite mantle does not occur until ~30 partial melting which is higher than is commonly assumed in the formation of basalt. This means that in many cases some Re remains in the mantle after melt extraction which leads to continued evolution of the $^{187}Os/^{188}Os$ ratio. Thus, in many cases it means that T_{RD} ages are minimum estimates of the age of mantle depletion and the actual age of depletion may be much older. Estimates of the actual age of depletion (as opposed to the minimum age) can also be gained by projecting the measured $^{187}Re/^{188}Os$ back in time to its age of separation from the chondritic mantle, referred to as a mantle model age (T_{MA}). However, interpretation of T_{MA} ages is complicated by metasomatism of xenoliths during kimberlite transport. Addition of Re during transport can lead to falsely elevated Re/Os and over-estimation of depletion ages, sometimes yielding ages older than that of the Earth (Pearson *et al.*, 1999). T_{RD} and T_{MA} ages of mantle xenoliths are the principal constraint that we have on the age and evolution of the SCLM. T_{RD} ages of Kaapvaal xenoliths

extend all the way back to the age of stabilisation of the craton (3-3.5 Ga), confirming the enrichment/depletion relationship deduced on the basis of diamond inclusion ages.

The broad range of osmium isotopic compositions of xenolith suites from Southern African kimberlites suggests that the Archaean SCLM beneath the Kaapvaal was also heterogeneous. Thus, the question must be raised as to the validity of the adoption of an average value for the γ_{Os} of the SCLM or a partial melts of the SCLM used in modelling. A similar question could be asked of the adoption of an average value for Archaean crust. The rationale behind the adoption of average values is that the Bushveld event, being one of the single largest magmatic events in the earth's history, must have sampled, in its interaction with either crust or mantle, a massive volume of either reservoir. The volume of interaction of the Bushveld event could have been expected to transcend the relatively local heterogeneities of the crust and mantle reservoirs hence averaging their composition.

The Depleted Mantle

The depleted mantle reservoir is well constrained in terms of both Os and Nd, being equivalent to the chondritic reservoir for Os ($\gamma_{Os} = 0$) and it is a well defined reservoir for Nd (DePaolo & Wasserburg, 1979). In modern day terms the depleted mantle is equivalent to a mid ocean ridge basalt (MORB) source (Zindler & Hart, 1986).

The mode of generation of a possible depleted mantle component is in need of some consideration. Recent geochronological work of Harmer & Armstrong (2000) suggests that the entire Bushveld magmatic event occurred over a relatively short period of time (1-3 Ma), indicating relatively high eruption rates. Gallagher & Hawkesworth (1992) proposed a role for "decompression" melting, that is adiabatic decompression of the source region during rifting causing melting in the asthenospheric mantle during the generation of CFB. There is evidence for considerable rift related basinal subsidence and sedimentation in the Transvaal basin (Cheney, 1996; Eriksson & Reczko, 1995), perhaps suggesting that this part of the Kaapvaal was under an extensional regime at the time of Bushveld emplacement. There is also some possible evidence for rift related magmatism

provided by the geochronology of the Bushveld Complex magmatism. Hawkesworth *et al.* (1994) noted the proportionality between rates of eruption and rates of continental extension in the derivation of high volume melts, perhaps lending support to a model that invokes continental extension and decompression melting in the generation of the Bushveld melts. Another possibility for the generation of asthenospheric mantle melts is through a similar mechanism to that which forms komatiites. Although they are commonly thought of as being the product of melting in the head of a plume (Campbell *et al.*, 1989), the non-radiogenic Os signature of Archaean komatiites (Foster *et al.*, 1996) suggests that their source is non-radiogenic, perhaps providing a mantle source for the Bushveld melts.

Modelling Results

Derivation of the Bushveld from a predominantly plume source?

Whilst the contamination of a picritic plume derived melt with a partial melt of the crust satisfies the low ϵNd of the B1 melts, the positive γOs of the plume source argues against the derivation of the B1 melts from a plume source in the absence of a component with low γOs (Fig. 6.16a). However, in view of the strong geological arguments for the role of a plume in the derivation of the Bushveld melts, either providing a heat source, or the source of the melts themselves, the possibility that the plume melts were contaminated by a low γOs component has also been investigated. Results of modelling (Fig 6.16b) suggest that it is possible to derive a melt approaching the composition of the Bushveld melts by contaminating a plume derived picrite with a small volume melt (SVM) of the SCLM, particularly if the considerable uncertainty involved in the estimation of the ϵNd of the SCLM component is considered. A relatively high degree of contamination (80-90 %) is suggested by this model. Such a high level of contamination indicates that the main role of the plume would be in providing the heat source for melting with minimal contribution of actual melt. The contamination of an asthenospheric melt, in this case a plume derived melt, with a SVM of the lithospheric mantle was proposed by Ellam *et al.* (1992) and Ellam & Cox (1991) for the derivation of the Karoo picrites. They termed this component the "lamproite" component, basing its estimated composition on that of kimberlites erupted onto the Kaapvaal craton. A similar approach was adopted here which also follows the work of Horan *et al.* (1995b) (Table 6.5).

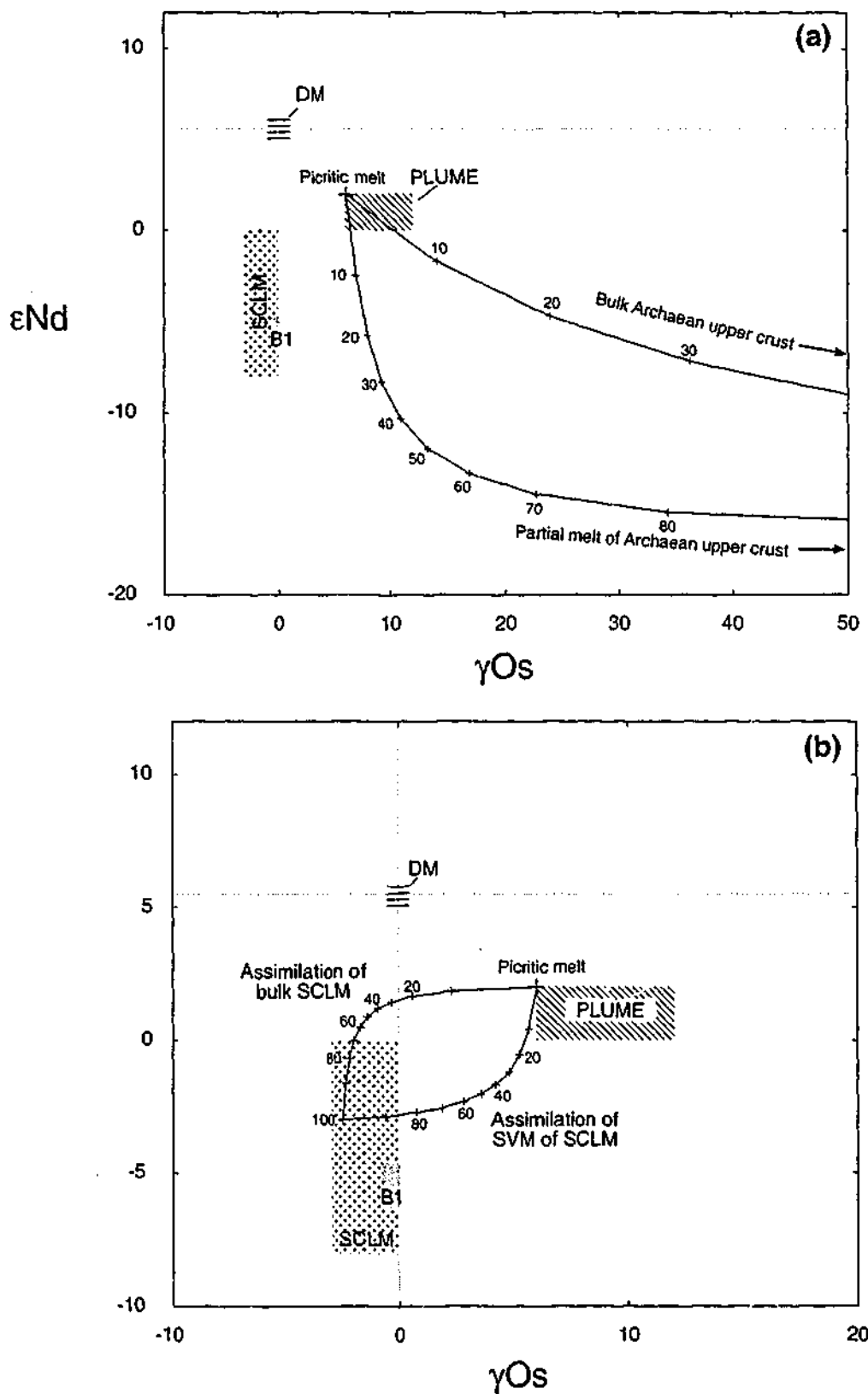


Figure 6.16 Modelling the Os-Nd systematics of Bushveld B1 melts from a plume derived melt. (a) Contamination of a plume picrite with bulk Archaean upper crust and a partial melt of the Archaean upper crust, and (b) Contamination of a plume basalt with bulk Kaapvaal SCLM and a small volume melt of the SCLM. Composition of B1 melts derived from the range of ϵ_{Nd} calculated for whole rock samples and the γ_{Os} calculated for chromite separates. Endmember compositions detailed in Table 6.5.

The implied minimal contribution of plume derived melt is consistent with several other aspects of the melting regime beneath thick continental lithosphere. Hawkesworth *et al.* (1994) noted that melting in the asthenospheric mantle at depths greater than 70 km can be problematic on the basis that with increased pressure (*i.e.* depth) the liquidus temperature of asthenospheric mantle is increased, such that melting will not occur in the absence of an anomalously high heat contribution. Given that estimates of the depth of the Kaapvaal SCLM are as great as 400 km (James *et al.*, 2001), it may be suggested that even if a plume impinged on the base of such thick continental lithosphere extensive melting in the asthenosphere may not take place. On the contrary melting in the lithospheric mantle can take place in the absence of melting in the asthenospheric mantle through conductive heat transfer, provided that the lithosphere is >70 km thick. This type of melting is locally enhanced by the presence of water in the SCLM. Thus, plume driven melting of the SCLM beneath the Bushveld Complex is possible in the absence of extensive asthenospheric mantle melting.

A role for the depleted mantle?

The relatively high ϵNd of the depleted mantle reservoir calculated for the age of the Bushveld (DePaolo & Wasserburg, 1979; Lambert *et al.*, 1994; Shirey & Hanson, 1986) limits the role of the depleted mantle in the genesis of the Bushveld melts, in the absence of a low ϵNd component (Fig. 6.17). The modelled curve for a picrite derived from the depleted mantle contaminated with a partial melt of the upper Archaean crust again passes close to the upper limits of the field of B1 melts (Fig. 6.17a). However, it is difficult to explain the negative γOs of the B1 melts in the absence of a component with negative γOs . In a similar way to the modelling performed for a plume derived melt the contamination of a depleted mantle melt with SCLM has also been modelled (6.17b). Again it requires 80-90 % contamination of a depleted mantle picrite to produce a melt that even approaches the composition of the Bushveld melts. At these levels of contamination it would be difficult to say with any certainty whether the mantle endmember was of depleted mantle or plume origin, or indeed that there was necessarily any asthenospheric mantle component.

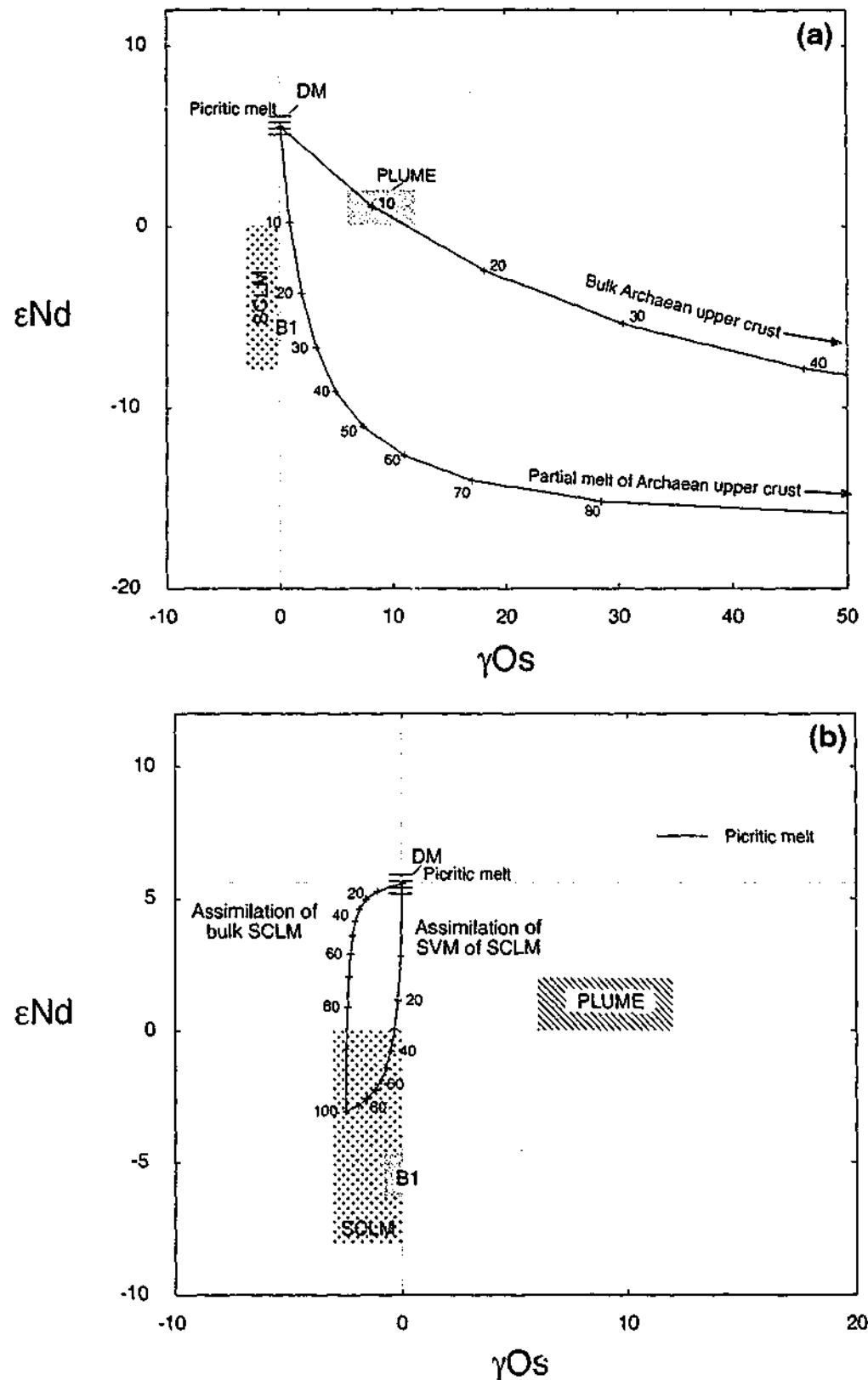


Figure 6.17 Modelling the Os-Nd systematics of Bushveld B1 melts from a depleted mantle derived melt. (a) Contamination of a depleted picrite with bulk Archaean upper crust and a partial melt of the Archaean upper crust, and (b) Contamination of a depleted mantle basalt with bulk Kaapvaal SCLM and a small volume melt of the SCLM. Endmember compositions detailed in Table 6.5.

SCLM Component in the Bushveld melts?

The sub-chondritic osmium isotopic composition of the Bushveld marginal rocks coupled with recent seismic evidence of melting in the SCLM imply a role for the SCLM in the genesis of the Bushveld melts. Thus, there is some possibility that the B1 melts are simply the product of melting in the SCLM. The position of estimates of the Os-Nd isotopic composition of the Kaapvaal SCLM

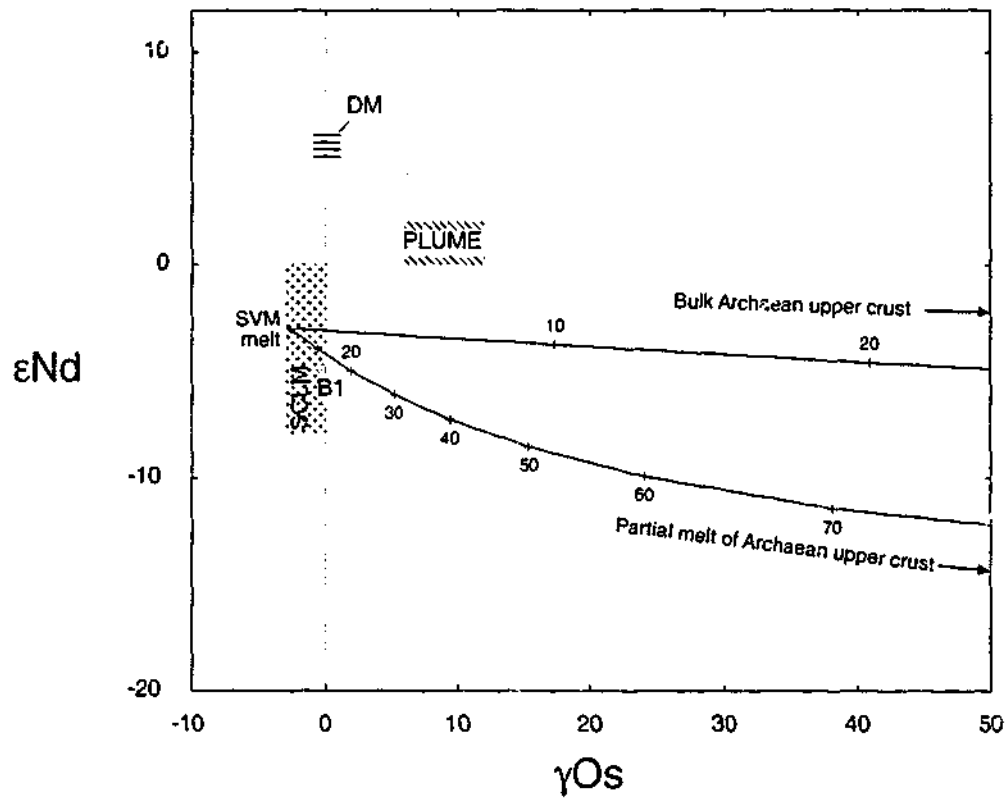


Figure 6.18 Modelling the Os-Nd systematics of Bushveld B1 melts by contamination of an SVM of the SCLM with bulk Archaean crust and a partial melt of the Archaean crust. Endmember compositions detailed in Table 6.5.

are shown relative to the B1 melts on Figure 6.18. The positioning of the B1 melts with respect to the SCLM in Os-Nd space does suggest that the B1 melts could simply be derived by melting in the SCLM. However the slightly lower ϵNd of the B1 melts with respect to the estimated average Nd composition ($\epsilon\text{Nd} \approx -3$) may suggest some role for a crustal component. In consideration of this the contamination of a partial melt of the SCLM with either bulk Archaean upper crust, or a partial melt of the upper crust is considered in Figure 6.18. As shown the contamination of a melt of the SCLM with a partial melt of the upper crust models the B1 melts quite effectively. According to this model a low degree partial melt of the SCLM contaminated by 10-20 wt. % of a partial melt of the upper crust is a plausible means of generating the low ϵNd B1 melts.

Synopsis of generation of B1 melts

Maier *et al.* (2000) proposed the assimilation of a partial melt of the upper crust by a picritic melt, probably derived from a plume. Although this hypothesis may satisfy the Sr and Nd isotopic constraints, the chondritic Os isotopic composition of the B1 melts argues against this in the absence of a negative γOs component. The most obvious source of chondritic Os in the Kaapvaal environment

is the SCLM. A partial melt of the SCLM with some contamination from a partial melt of the Archaean upper crust satisfies the Sr, Nd and Os isotopic composition of the B1 melts. This process is illustrated schematically in Figure 6.19.

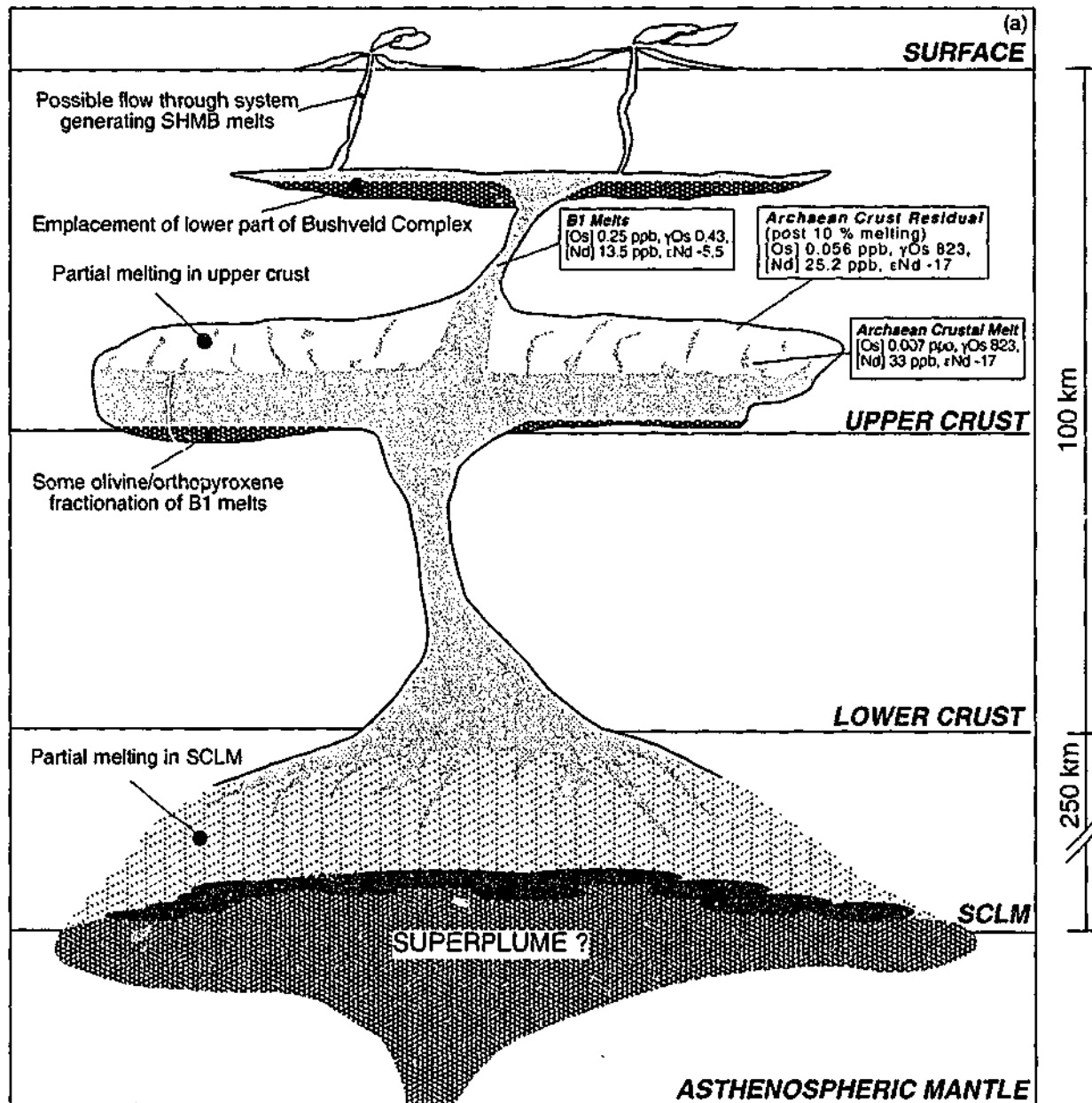


Figure 6.19 Schematic representation of possible process of generation of the Bushveld B1 magmas, envisaged after . 10% partial melt of the SCLM with possible plume picrite component is mixed with 5-7 wt. % of a 12% partial melt of average Archaean crust leading to the B1 melts.

Generation of the B2 and B3 melts

Maier et al (2000) proposed that the B2 and B3 magmas of the Bushveld Complex may have been generated by an AFC process in the upper crust in which the proto B1 melt underwent fractional crystallisation and assimilation of the restitic crustal material left after the initial derivation of a partial melt which they propose led to the generation of the B1 melts. This process is illustrated schematically in Figure 6.20 and can also be modelled in terms of Os and Nd (Fig. 6.21).

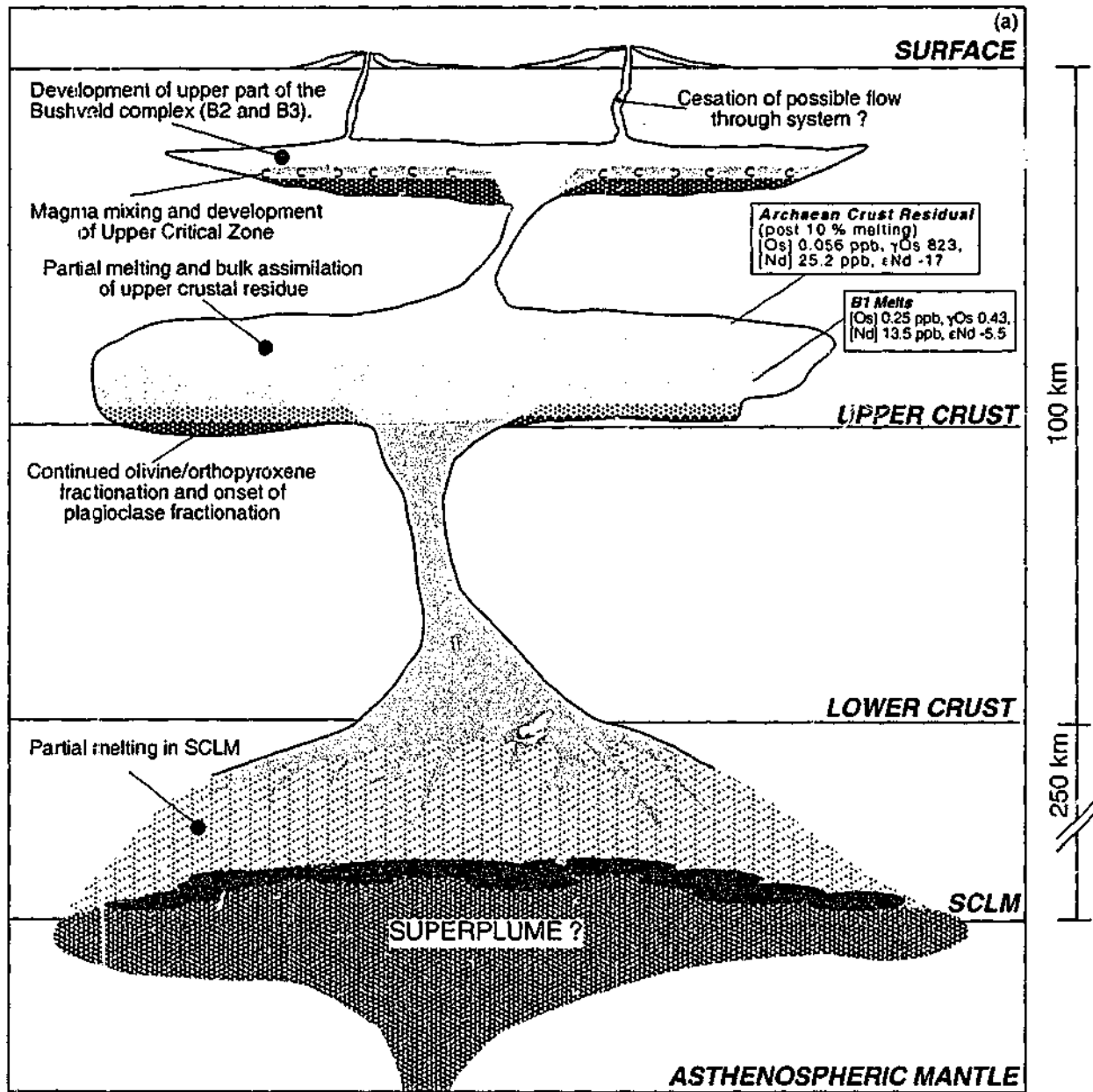


Figure 6.20 Schematic representation of generation of B2 and B3 magmas through contamination of B1 proto-melt with (5-15 wt.%) restitic Archaean upper crust left after a 12 wt.% partial melt of the upper crust possibly generated during contamination of B1 melts.

The composition of the endmembers is that of the measured composition of the B1 melts and the estimated composition of the residual crustal material after partial melt extraction as explained above. The trajectory of the mixing line is significantly flatter primarily as a function of lower Os concentration in the B1 melts (compared to previously modelled mantle derived melts) and the relatively higher concentration of Os in the crustal endmember. The higher concentration of Nd in the B1 melts also renders the melts less susceptible to rapid change as a function of addition of Nd.

Whilst the modelling of the mixing trajectory is relatively well constrained, the composition of the B2 and B3 melts in Os-Nd space is not. The reason for this is the lack of undisturbed whole rock Os isotopic data for both of these series of rocks on account of the post emplacement disturbance

of the isotopic system. The best estimate of the Os isotopic composition of these rocks is from the poorly constrained initial provided by the errorchron for them (γ_{Os} 39 ± 95), which has been used as the best estimate for the Os isotopic compositional field for the B2 and B3 rocks. The modelled curve passes well below the estimated field for B2 and B3 rocks. The discrepancy between the modelled and estimated composition for these rocks is primarily in the isotopic composition of Nd, which is relatively well constrained for the B2 and B3 rocks, which represents a problem in either the modelling or the estimated composition of the B2 and B3 rocks. One likely explanation is that the estimated Os isotopic composition of the B2 and B3 rocks is too radiogenic. The reason for this may be that the elevated γ_{Os} of these rocks is the product of the resetting event. This is supported by the elevated γ_{Os} (*c.a.* 50-500) of the secondary titanomagnetites in these rocks, thus the true primary magmatic isotopic composition of these rocks may lie to the left of the field shown and closer to the modelled curve. Nonetheless this is a highly speculative line of reasoning

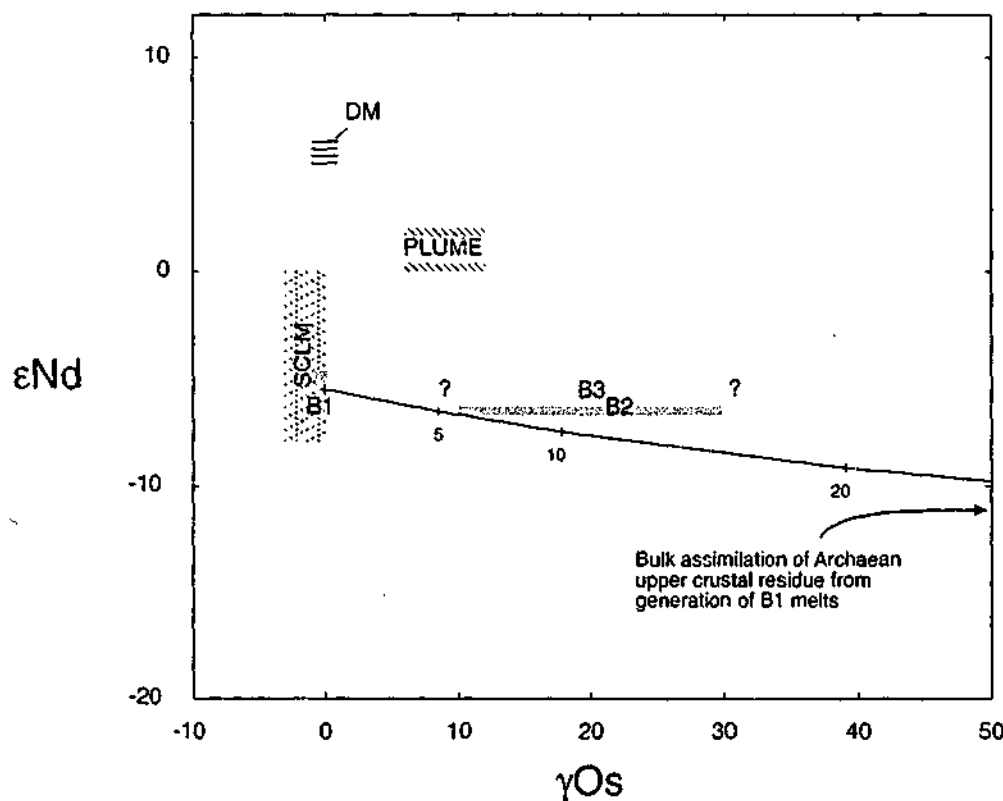


Figure 6.21 Modelling the Os-Nd systematics of B2 and B3 melts by contamination of a B1 proto-melt with restitic Archaean upper crust left after a 12 wt.% partial melt of the upper crust possibly generated during contamination of B1 melts. Endmember compositions detailed in Table 6.4. Compositions of B2 and B3 melts are derived from whole rocks Nd isotopic determinations and estimates of Os isotopic composition based on initial of errorchron and associated error (Figure 6.2).

and the only thing that can be said is that the modelled curve is heading in the right direction for the B2 and B3 rocks, but no quantitative estimation of the extent of contamination according to this model is possible.

6.7 Summary

Re-Os, Sm-Nd, Rb-Sr and oxygen stable isotopic data have been obtained on the fine grained sills and dykes surrounding the Bushveld Complex to further constrain the composition of the parental magmas. Re-Os data on chromite separates from the B1 melts define a five point isochron with a precise chondritic osmium initial of $\gamma_{Os} = -0.03 \pm 0.5$. Whole rock Re-Os data on both the B1 as well as the B2 and B3 rocks, indicate that the whole rock Re-Os isotopic system has not remained closed since the time of primary igneous crystallisation. Secondary isochrons for both groups of rocks suggest that the system did not achieve closure until approximately 350 Ma after the crystallisation of the Bushveld Complex. However, the resistance of chromite to hydrothermal alteration suggests that the initial isotopic composition recorded by the chromites is indicative of the original melts. The relatively unradiogenic initial Os isotopic compositions, coupled with low initial Nd values ($\epsilon Nd < -4$) and high $(La/Yb)_n$ for the B1 melts suggests that the melts were sourced either by melting rocks that had some history of LREE enrichment or were contaminated with material with a history of LREE enrichment as well as near chondritic to slightly depleted Re/Os ratios.

It is apparent from the data presented that no single source can explain all of the isotopic characteristics of the marginal rocks. Data on kimberlite borne-xenoliths indicate that the SCLM beneath the Kaapvaal has, on the whole, a sub-chondritic osmium isotopic composition and in most instances negative ϵNd . However, the values of ϵNd calculated for the marginal rocks are slightly lower than the estimated bulk composition of the SCLM, although not outside the possible range of the SCLM. Similarly, while the Kaapvaal crustal rocks possess the requisite unradiogenic Nd compositions, the Os isotopic composition of the crust is estimated to be well above that of the marginal rocks. In addition, the low $\delta^{18}O$ data may severely limit the possible role of crustal contamination in the genesis of the B1 rocks. It would seem that the most likely explanation for

the genesis of the B1 melts is through partial melting of the SCLM which has undergone source contamination/enrichment in trace elements. There is a possible role for crustal assimilation, through incorporation of a partial melt of the crust that has extremely elevated concentrations of trace elements, in particular Sr and Nd, whilst having low concentrations of Os. Again the role of crustal assimilation in the genesis of the B2 and B3 melts is limited by their low $\delta^{18}\text{O}$ values, suggesting that they may be derived through fractional crystallisation in a crustal magma chamber, but with limited coupled assimilation.

Chapter 7: Discussion and Conclusion

7.1 Introduction

The aims of the project were twofold: (a) to establish the relationship of the marginal rocks of the Eastern Bushveld Complex to the Layered cumulate series, and (2) to gain an understanding of the petrogenetic processes that led to the generation of these magmas and ultimately the generation of the Bushveld Complex.

7.2 Relationship of the marginal rocks to the Layered Complex

One of the fundamental premises of this project was that the marginal rocks of the Eastern Bushveld Complex were in some way representative of the parental magmas of the Layered Complex. The working hypothesis, based on previous studies was that they were related based on their field relations, trace element geochemistry and their Sr isotope systematics (Davies *et al.*, 1980; Harmer & Sharpe, 1985; Kruger, 1994; Sharpe, 1981). Early isotopic analyses yielded ages that were significantly younger than the accepted age of the Bushveld Complex which called into question the premise that these rocks were related to the Layered Complex. In order to address this issue SHRIMP U-Pb age dating on zircons was undertaken. The results of this work revealed that the age of the marginal rocks was statistically indistinguishable from the accepted age of the Bushveld Complex, which in conjunction with other evidence confirmed that the marginal rocks were part of the Bushveld igneous event. Furthermore, trace element and isotope results compare well with previous determinations on the Bushveld layered rocks, confirming that the marginal rocks represent likely parental melt compositions for the Bushveld Complex.

7.2.1 SHRIMP U-Pb age dating

SHRIMP U-Pb ages on a B1 sample (2050 ± 4 Ma) and a B2 sample (2052 ± 6 Ma) are well within error of recent ages on the mafic portion of the Bushveld Complex (Harmer & Armstrong, 2000). All analytical points were between 97 and 101% concordant, with excellent statistical correlation (MSWD 0.66 and 0.73). These ages represent the most precise age determination on the marginal rocks made to date and as such are the best evidence we have for the co-genetic nature of the

marginal rocks and the Bushveld Complex.

7.3 Summary of petrogenetic indicators

7.3.1 Major elements

Geochemically the suite of rocks associated with the lower part of the Bushveld Complex (B1) were found to be high in both SiO_2 (52-56 wt.%) and MgO (8-15 wt.%) rendering them similar to Siliceous High Magnesium Basalts (SHMB). The suite associated with the upper part were less magnesian and more akin to continental tholeiites. The relatively high abundance of alkali metals in both groups of rocks classified them as borderline between the fields of tholeiitic and calc-alkaline according to the classifications of Irvine & Baragar (1971) and Kuno (1968). There is considerable variation in the major element abundances in both suites of rocks indicating that they evolved in some way during their genesis. Negative correlations between the transition metals (Ni and Cr) and MgO in the B1 suite suggests that both olivine and orthopyroxene were important liquidus phases in their evolution. The fact that these metals form a linear trend when plotted against an incompatible element such as Th on a Log-Log plot also suggests that the crystal fractionation of olivine and orthopyroxene can be described by the laws of Rayleigh fractionation (Allegre *et al.*, 1977). Similarly broadly linear correlations between Th and Al_2O_3 , CaO, Na_2O and in particular Sr in the B2 and B3 rocks suggests an important role for plagioclase crystal fractionation/accumulation in these rocks.

Although the major elements provide insight into the evolution of each of the groups of marginal rocks, the relationship between the B1, B2 and B3 melts is not obvious on the basis of this data alone.

7.3.2 Trace elements

The similarity between the B1 magmas and Archaean SHMB occurrences is also found in the trace element concentrations and relative abundances. In particular the high concentrations of LREE, similar levels of overall REE fractionation and negative Nb anomalies as well as the elevated concentrations of highly incompatible elements are similar in the Bushveld B1 rocks and SHMB.

On this basis the interpretation of SHMB as being the product of contamination of a komatiitic or picritic mantle derived melt (Arndt & Jenner, 1986; Barnes, 1989; Sun, 1989) may be applicable for the Bushveld magmas. However, classification on the basis of ternary HFSE classification Wood (1980) places the B1 magmas plot in the field of convergent margin basalts suggesting something like a boninite/shoshonite type source (Pearce *et al.*, 1992), although this field is relatively close to the field for continental crust. Several other aspects of the B1 magmas can also be explained by their derivation from an enriched mantle source, such as, their negative Nb anomalies which although they are commonly associated with crustal rocks, they can also be explained as the product of retention of the mineral titanite (sphene) in the source region (Hellman & Green, 1979). Thus, on the basis of trace element data alone it is difficult to distinguish between rocks from an enriched mantle source, in this case a convergent margin setting (boninite source) and that of the contamination of an asthenospheric mantle derived melt such as a komatiite.

The trace element geochemistry of the B2 and B3 magmas is more akin to an enriched MORB magma, with lower overall abundances of trace elements and less LREE enrichment. Again the genetic relationship between the B1, B2 and B3 magmas is not apparent on the basis of trace element geochemistry alone.

7.3.3 Lithophile isotope systematics

The marginal rocks of the Bushveld Complex exhibit lithophile isotope systematics which suggest that they were sourced from, or have interacted with a reservoir with a protracted history of both LREE enrichment and elevated Rb/Sr ratios relative to the depleted mantle. The calculated ϵ_{Nd} at the age of emplacement are in the range -5 to -8 , which in the absence of other evidence suggests that these rocks were either derived from the crust, or have derived a significant proportion of their LREE budget from a crustal reservoir. Similarly the $^{87}Sr/^{86}Sr_i$ of the marginal rocks on the whole are elevated well above calculated mantle reservoirs of the same age, slightly more so in the B2 and B3 rocks than in the B1. The fact that the B1 magmas have a higher Rb/Sr ratio than the B2 and B3 magmas, despite the fact that on the whole they have lower $^{87}Sr/^{86}Sr_i$ is an unusual feature of the B1 magmas. This suggests that the initial was decoupled from the parent daughter ratio at or

near the age of melt generation and emplacement, perhaps through the addition of a disproportionately large amount of Rb during melting or transport.

Sr-Nd Modelling suggests that the Bushveld B1 magmas could be derived by mixing a depleted mantle melt with approximately 30 wt.% by a partial melt of the upper crust. This modelling serves to demonstrate that the Sr and Nd systematics are consistent with a crustal contamination hypothesis for the derivation of the B1 magmas. Similarly the isotopic composition of the B2 and B3 magmas can be approximated with similar modelling parameters, but perhaps with a slightly higher proportion of crustal contamination. However, the ϵ_{Nd} are also not outside the possible range for the SCLM beneath the Kaapvaal at the age of Bushveld emplacement as suggested by Sm-Nd data on kimberlite borne xenoliths. Sr data on xenoliths provides limited indication of the isotopic composition of the SCLM due to metasomatism during kimberlite borne emplacement (Walker *et al.*, 1989).

Despite the "crust like" signatures of both the Sr and Nd, the oxygen isotopes are distinctly mantle like, with signatures of the B1 magmas in the vicinity of $d^{18}O = 5$, and even lower for the B2 and B3 magmas which is at odds with a model that proposes significant crustal contamination as a means of generating the observed Sr and Nd signatures. Indeed, combined $d^{18}O - ^{87}Sr/^{86}Sr_1$ modelling suggests that the elevated $^{87}Sr/^{86}Sr_1$ coupled with low $d^{18}O$ values may be the product of contamination of the source (James, 1981). This process involves the addition radiogenic Sr without the addition of significant elevated $d^{18}O$ material. This sort of process could occur through the addition of a trace element enriched melt or an enriched metasomatic fluid to the source region (Boettcher *et al.*, 1979; Ellam *et al.*, 1992; Ellam & Cox, 1991; Hawkesworth & Vollmer, 1979; Lambert *et al.*, 1994; Mueller *et al.*, 1983; Pearson *et al.*, 1995b; Vollmer & Hawkesworth, 1980; Wyman, 1999; Yaxley *et al.*, 1997). So while the Sr-Nd isotope systematics are inconclusive in determining the origin of the enriched signature the Oxygen isotope signature may provide the first decisive evidence for derivation of the Bushveld magmas from a predominantly enriched mantle source.

7.3.4 Re-Os isotopes

The Re-Os isotope systematics of the whole rock samples have suffered post emplacement disturbance in the form of hydrothermal addition of Re estimated to have occurred at around 1700 Ma on the basis of secondary isochrons and collateral evidence for a thermal event in the northeast Kaapvaal craton at about this time. Thus, the whole rock analyses provide little insight into the mode of primary igneous petrogenesis. However, analyses of Os enriched chromite mineral separates from the B1 group define a 3 point isochron with a precise chondritic initial and an age that is within error of the age of Bushveld emplacement. This indicates that the B1 magmas had a chondritic Os signature at the time when the chromites crystallised. Notwithstanding the possibility that the chromites were a phenocrystic mineral phase this suggests that the B1 magmas had chondritic Os at or near the time of emplacement. Although this is a strong argument for a mantle source origin for the enriched signature, it does not entirely rule out crustal contamination.

Combined Os-Nd isotopic modelling indicates that despite the chondritic Os isotopic signature of the B1 magmas, there is some limited scope for crustal contamination in explaining the low ϵ_{Nd} , provided that the concentration of Os in the contaminant is sufficiently low. Despite the highly radiogenic Os composition estimated for a partial melt of the upper crust of the Kaapvaal craton at the age of Bushveld emplacement, the low concentrations of Os may render it a plausible contaminant in deriving the low ϵ_{Nd} and elevated $^{87}Sr/^{86}Sr_i$ without upsetting the chondritic Os signature. However, with the crustal assimilation of a partial melt by a komatiitic/picritic melt that begins as a chondritic melt of the depleted mantle the amount of crustal contamination required to sufficiently lower the ϵ_{Nd} from the *c.a.* +5 of the depleted mantle at that age, the Os is driven to values more positive than the B1 magmas, rendering this a non-feasible model for the derivation of the B1 magmas in the absence of a negative γ_{Os} component. The most obvious source of sub-chondritic Os being the SCLM. The results of Os-Nd modelling suggest that by whatever means the bulk of the Bushveld magmas were derived it seems almost irrefutable that there was some contribution of subchondritic Os from the SCLM.

7.4 Origin of the Bushveld parental magmas

7.4.1 "Are Bushveld U-type parent magmas boninites or contaminated komatiites?"

(Barnes, 1989)

Of all of the evidence presented, much of it could be interpreted as the result of either crustal assimilation by a mantle derived melt, or melting of an enriched mantle source. Of that which points to one or the other, the weight of evidence points to a predominantly enriched mantle origin for the enriched characteristics of the parental magmas of the Bushveld Complex – that is to say that the magmas are analogous to boninites. Whilst it is possible to contaminate a mantle derived melt with crustal material to some extent without swamping the chondritic mantle Os signature, the extent required to produce the observed enriched ϵNd and $^{87}\text{Sr}/^{86}\text{Sr}_i$ signatures is too high, thus the weight of Os evidence points to an enriched mantle origin. Similarly, the oxygen stable isotope data points strongly to a mantle source, with a very limited role possible for crustal assimilation. Combined $\text{d}^{18}\text{O} - ^{87}\text{Sr}/^{86}\text{Sr}_i$ modelling also argues strongly for a mantle source enrichment model.

7.4.2 Nature and origin of the enriched source

The requirements of the enriched source component are LREE enrichment, enriched Rb/Sr ratios and chondritic-subchondritic Re/Os ratios, whilst maintaining relatively low d^{18}O . James (1981) proposed infiltration of a highly enriched subduction derived melt into the mantle source region as a means of explaining the elevated $^{87}\text{Sr}/^{86}\text{Sr}_i$ and LREE, whilst not elevating the d^{18}O . Such a melt could also be expected to have a relatively high Re/Os ratio. Similarly the circulation of slab derived fluids through the mantle wedge above a subduction zone could also generate enriched mantle without significantly increasing the d^{18}O . The generation of a suitable reservoir would also require depletion of Re at some time soon after infiltration of the melt, such that the γOs of the source remained relatively low. Jordan (1978) proposed that melt depletion in the SCLM may be related to major episodes of crust building, thereby removing Re from the source region and lowering the Re/Os ratio. Several other authors have proposed such a model of selective enrichment and depletion in the development of the SCLM (McBride *et al.*, 1996; Pearson *et al.*, 1995a; Pearson *et al.*, 1995b; Walker *et al.*, 1989).

Considering the model proposed by de Wit *et al.* (1992) for the formation of the early Kaapvaal craton, (Fig. 2.7) a model in which either slab derived melt and/or fluid infiltrate the SCLM is not difficult to envisage. The generation of large volumes of trondhjemite-tonalite melt early in the development of the Kaapvaal craton may also have provided the necessary depletion of the SCLM. Thus, the early development of suitably enriched SCLM beneath the Kaapvaal craton with sufficient time to isotopically evolve seems plausible. Evidence of the geochronology of enrichment from diamond inclusion assemblages goes some way to confirming the presence of this type of mantle beneath the craton.

7.4.3 Evolution of the Bushveld magma series

The field relations of the marginal rocks suggest that the emplacement of the Bushveld Complex was an episodic event, with possible relatively short time breaks between the emplacement of the various zones. Thus, there may have been time for the various varieties of parental magmas to evolve significantly prior to emplacement within the complex.

Following the generation of the proto-B1 melts through melting of enriched mantle it is proposed that the magmas were subject to some degree of fractional crystallisation as suggested by their major element trends. There is some possibility for minor levels of assimilation of a crustal partial melt concurrent with fractional crystallisation perhaps lowering the ϵ_{Nd} slightly, and perhaps imparting a crustal Nb signature, without significantly affecting the chondritic γ_{Os} . Subsequent generation of the B2 and B3 magmas is less clear on the basis of the data presented. Maier *et al.* (2000) propose a relatively large degree of crustal assimilation of a dominantly plagioclase material, coupled with fractional crystallisation of plagioclase in a crustal staging chamber as a means of explaining the more Al-tholeiitic major element geochemistry and unradiogenic ϵ_{Nd} . The very poor constraint on the γ_{Os} initial provided by the secondary isochron for the B2 and B3 whole rocks provides very little information on the whether or not this could have occurred. However, the $d^{18}\text{O}$ are even lower than those of the B1 magmas, perhaps indicating that crustal contamination is even less

likely in these magmas. Certainly, the major and trace element trends are consistent with the crystal fractionation and accumulation of plagioclase, which based on the oxygen isotope geochemistry may have occurred in the absence of crustal assimilation.

7.5 Exploration/metallogenic significance

This project provides some constraints on the global/regional targeting of ore deposits associated with mafic/ultramafic layered intrusions. The fact that mineralised layered intrusions worldwide possess a similar melt succession and many of the unusual enriched characteristics of the B1 magmas, may suggest that the development of these characteristics is integral to the formation of ore deposits. One of the principal findings of this study was that these features are probably associated with melt derivation in the SCLM. Thus, based on this study, a principal targeting criteria for exploration could be to target Archaean cratons with evidence for well developed SCLM. Further to this, particularly prospective areas would be any that were underlain by SCLM exhibiting regionally low seismic velocities. Intrusions within these areas that exhibit unusual geochemical characteristics similar to the Bushveld B1 magmas should be targeted. In particular, mafic ultramafic magmas with chondritic osmium isotopic compositions ($\gamma_{Os} \approx 0$) coupled with trace element enrichment and moderately unradiogenic Nd ($\epsilon_{Nd} \approx -5$). Specific targeting for reef-type PGE mineralisation should be directed to the contact region between the lower mafic/ultramafic and upper anorthositic zones of a prospective intrusion.

7.6 Conclusions

The first aim of this study was to determine the specific relationship of the marginal rocks to the layered mafic phase of the of the Bushveld Complex. It was found that the marginal rocks represent a compositional spectrum of rocks, of which the granular textured B1 samples approximate the parental magma composition of the Lower mafic/ultramafic portion of the layered complex. Sr isotopic evidence suggests that the parental magma composition of the upper part of the complex is not represented entirely in the marginal group of rocks, but is best approximated by the B3 marginal rocks. Specific findings relevant to the meeting of this aim are:

- SHRIMP U-Pb age of the marginal rocks is within error of the age of the layered rocks
- The rocks and the various zones of the complex that they represent are spatially correlated
- Major and trace element characteristics in the marginal rocks are similar to those documented for the layered rocks
- With the exception of the B3 rocks the lithophile isotope systematics of the marginal rocks were found to be well correlated with their corresponding zones in the layered complex

The second aim of the study was to determine the petrogenesis of the parental magmas as represented by the marginal rocks. Firstly, the study aimed to determine the origin and significance of the elemental and isotopic enrichments observed in the B1 rocks by assessing them in terms of either crustal assimilation or enriched mantle melting. This study concludes that the enriched features of the B1 magmas are the product of melting of enriched SCLM on the basis of several key points:

- A precise chondritic initial isotopic composition determined on the B1 magmas
- Mantle like $d^{18}\text{O}$ values of all of the samples measured

Secondly, to determine the origin and petrogenetic significance of the B2 and B3 marginal rocks and their relationship and likely derivation from the B1 melts. This is less well constrained, but major and trace element evidence for the fractionation and accumulation of plagioclase suggests that they could be derived by extensive fractional crystallisation of a B1 melt, with the possibility of some associated crustal assimilation.

REFERENCES

- Allegre, C. J., Treuil, M., Minster, J.-F., Minster, B. & Albarede, F., 1977. Systematic use of trace element in igneous process; Part I, Fractional crystallization processes in volcanic suites. *Contributions to Mineralogy and Petrology*, **60**(1), 57-75.
- Altermann, W. & Halbich, I. W., 1991. Structural history of the southwestern corner of the Kaapvaal Craton and the adjacent Namaqua realm; new observations and a reappraisal. *Precambrian Research*, **52**(1-2), 133-166.
- Altermann, W., Halbich, W., Horstmann, U. E., Ahrendt, H., Fitch, F. J. & Miller, J. A., 1992. The age of tectonogenesis and metamorphism of the southwestern Kaapvaal Craton. In: *29th international geological congress; abstracts*. (ed Anonymous), pp. 261.
- Anderson, D. L., 1995a. Lithosphere, asthenosphere, and perisphere. *Reviews in Geophysics*, **33**, 125-149.
- Anderson, D. L., 1995b. Lithosphere, asthenosphere, and perisphere. *Reviews of Geophysics*, **33**(1), 125-149.
- Arndt, N. T. & Christensen, U., 1992. The Role of Lithospheric Mantle in Continental Flood Volcanism: Thermal and Geochemical Constraints. *Journal of Geophysical Research*, **97**(7), 10967-10981.
- Arndt, N. T. & Jenner, G. A., 1986. Crustally contaminated komatiites and basalts from Kambalda, Western Australia. *Chemical Geology*, **56**(3-4), 229-255.
- Barnes, S. J., 1989. Are Bushveld U-type parent magmas boninites or contaminated komatiites? *Contributions to Mineralogy and Petrology*, **101**, 447-457.
- Ben Othman, D., Polve, M. & Allegre, C. J., 1984. Nd-Sr isotopic composition of granulites and constraints on the evolution of the lower continental crust. *Nature (London)*, **307**(5951), 510-515.
- Birck, J. L., Roy-Barman, M. & Capmas, F., 1997. Re-Os isotopic measurements at the femtomole level in natural samples. *Geostandards Newsletter*, **20**, 19-27.

- Boettcher, A. L., O'Neil, J. R., Windom, K. E., Stewart, D. C. & Wilshire, H. G., 1979. Metasomatism of the Upper Mantle and the Genesis of Kimberlites and Alkali Basalts. In: *The Mantle Sample: Inclusions in Kimberlites and Other Volcanics - Proceedings of the 2nd International Kimberlite Conference* (ed Boyd), pp. 173-182, American Geophysical Union, Washington.
- Boudreau, A. E. & McCallum, I. S., 1992. Concentration of platinum-group elements by magmatic fluids in layered intrusions. *Economic Geology*, **87**, 1830-1848.
- Brenan, J. M., Cherniak, D. J., Rose, L. & Anonymous, 1998. Diffusion of rhenium and osmium in pyrite and molybdenite; implications for closure of the Re-Os isotope system. In: *Geological Society of America, 1998 annual meeting*, pp. 91, Toronto, ON, Canada.
- Burger, A. J. & Walraven, F., 1976. Summary of age determinations carried out during the period April 1975 to March 1976. *Annual Report of the Geological Survey of South Africa*, **11**, 323-329.
- Campbell, I. H., Griffiths, R. W. & Hill, R. I., 1989. Melting in an Archaean mantle plume; heads it's basalts, tails it's komatiites. *Nature (London)*, **339**(6227), 697-699.
- Carlson, R. W. & Irving, A. J., 1994. Depletion and enrichment history of subcontinental lithospheric mantle; an Os, Sr, Nd and Pb isotopic study of ultramafic xenoliths from the northwestern Wyoming Craton. *Earth and Planetary Science Letters*, **126**(4), 457-472.
- Carlson, R. W., Pearson, D. G., Boyd, F. R., Shirey, S. B., Irvine, G., Menzies, A. H. & Gurney, J. J., 1999. Re-Os Systematics of Lithospheric Peridotites: Implications for Lithosphere Formation and Preservation. In: *Proceedings of the VIIIth International Kimberlite Conference* (eds Gurney, J. J., Gurney, J. L., M.D., P. & Richardson, S. H.), pp. 99-108, Red Roof Design, Cape Town, 1999.
- Cawthorn, R. G., 1998. Initial liquid to the Bushveld Complex sampling site. Personal communication - *8th International Platinum Symposium roadside field stop Johannesburg-Rustenburg*.
- Cawthorn, R. G., Davies, G., Clublely-Armstrong, A. & McCarthy, T. S., 1981. Sills associated with the Bushveld Complex, South Africa: an estimate of parental magma composition. *Lithos*, **14**(1), 1-16.

- Cawthorn, R. G. & Lee, C., 1998. Field Guide - Bushveld Complex excursion, 8th International Platinum Symposium. In: *Field Guide - Bushveld Complex excursion, 8th International Platinum Symposium*, Rustenburg, South Africa.
- Cheney, E. S., 1996. Sequence stratigraphy and plate tectonic significance of the Transvaal succession of Southern Africa and its equivalent in Western Australia. In: *Geology and geochemistry of the Transvaal Supergroup, Southern Africa*. (eds Kaufman, A. J. & Danielson, A.) *Precambrian Research*, pp. 3-24, Elsevier, Amsterdam, International.
- Clayton, R. N. & Mayeda, T. K., 1963. The use of bromine pentafluoride in the extraction of oxygen from oxides and silicates for isotopic analysis. *Geochimica et Cosmochimica Acta*, 27(1), 43-52.
- Cohen, A. S. & Water, F. G., 1996. Separation of osmium from geological materials by solvent extraction for analysis by thermal ionisation mass spectrometry. *Analytica Chimica Acta*, 332, 269-275.
- Compston, W., Williams, I. S., Meyer, C. E., Boynton, W. V. e. & Schubert, G. e., 1984. U-Pb geochronology of zircons from lunar breccia 73217 using a sensitive high mass-resolution ion microprobe. In: *Fourteenth lunar and planetary science conference; Part 2*, pp. 525-534, Houston, TX, United States.
- Condie, K. C., 1981. Archaean Greenstone Belts. In: *Developments in Precambrian Geology* (ed Windley, B. F.), pp. 434, Elsevier Scientific Publishing Company, Amsterdam-Oxford-New York.
- Coplen, T. B., Kendall, C. & Hopple, J., 1983. Comparison of stable isotope reference samples. *Nature (London)*, 302(5905), 236-238.
- Crawford, A. J., Falloon, T. J. & Green, D. H., 1989. Classification, petrogenesis and tectonic setting of boninites. In: *Boninites* (ed Crawford, A. J.), pp. 2-49, Unwin Hyman, London.
- Davies, G., Cawthorn, R. G., Barton, J. M. J. & Morton, M., 1980. Parental magma to the Bushveld Complex. *Nature*, 287, 33-35.
- de Wit, M. J., Roering, C., Hart, R. J., Armstrong, R. A., deRonde, E. J., Green, R. W. E., Tredoux, M., Peberdy, E. & Hart, R. A., 1992. Formation of an Archaean continent. *Nature*, 357, 553-562.

- de Wit, M. J., Tredoux, M., Hart, R. & Anonymous, 1990. 3.5 Ga oceanic-like lithosphere; some chemical and geodynamic constraints on (Archaean) Earth models
- 1990 Western Pacific geophysics meeting; abstracts. *1990 Western Pacific geophysics meeting*, 71(28), 969-970.
- DePaolo, D. J. & Wasserburg, G. J., 1979. Sm-Nd age of the Stillwater Complex and the mantle evolution curve for neodymium. *Geochimica et Cosmochimica Acta*, 43, 999-1008.
- DuPlessis, C. P. & Walraven, F., 1990. The tectonic setting of the Bushveld Complex in Southern Africa, part 1. structural deformation and distribution. *Tectonophysics*, 179, 305-319.
- Durrheim, R. J. & Green, R. W. E., 1992. A seismic refraction investigation of the Archaean Kaapvaal Craton, South Africa, using mine tremors as the energy source. *Geophysical Journal International*, 108(3), 812-832.
- Eales, H. V. & Cawthorn, R. G., 1996. The Bushveld Complex. In: *Layered Intrusions* (ed Cawthorn, R. G.), pp. 181-229, Elsevier Science, B.V.
- Ellam, R. M., Carlson, R. W. & Shirey, S. B., 1992. Evidence from Re-Os isotopes for plume-lithosphere mixing in Karoo flood basalt genesis. *Nature*, 359, 718-721.
- Ellam, R. M. & Cox, K. G., 1991. An interpretation of Karoo picrite basalts in terms of interaction between asthenospheric magmas and the mantle lithosphere. *Earth and Planetary Science Letters*, 105, 330-342.
- Eriksson, P. G., Hattington, P. J. & Altermann, W., 1995. An overview of the geology of the Transvaal Sequence and Bushveld Complex, South Africa. *Mineralium Deposita*, 30, 98-111.
- Eriksson, P. G. & Reczko, B. F. F., 1995. The sedimentary and tectonic setting of the Transvaal Supergroup floor rocks to the Bushveld Complex. *Journal of African Earth Sciences*, 21(4), 487-504.
- Esser, B. K. & Turekian, K. K., 1993. The osmium isotopic composition of the continental crust. *Geochimica et Cosmochimica Acta*, 57, 3093-3104.
- Evensen, N. M., Hamilton, P. J. & O'Nions, R. K., 1978. Rare-earth abundances in chondritic meteorites. *Geochimica et Cosmochimica Acta*, 42, 1199-1212.

- Foster, J. G., Lambert, D. D., Frick, L. R. & Maas, R., 1996. Re-Os isotopic evidence for genesis of Archaean nickel ores from uncontaminated komatiites. *Nature*, **382**, 703-706.
- Frick, L. R., 1998. Application of Re-Os Isotopes to the Study of Lithospheric processes in Archaean Terrains. *Unpub. Ph.D. Thesis, Monash University, Melbourne*.
- Gallagher, K. & Hawkesworth, C., 1992. Dehydration melting and the generation of continental flood basalts. *Nature*, **358**, 57-59.
- Gibson, R. L. & Stephens, G., 1997. Regional metamorphism due to anorogenic intracratonic magmatism. *Information Circular, University of the Witwatersrand, Economic Geology Research Unit*, 311.
- Gibson, R. L. & Wallmach, T., 1995. Metamorphism of the Witwatersrand basin: a perspective from the Vredefort dome. *Information Circular, University of the Witwatersrand, Economic Geology Research Unit*, 288.
- Gurney, J. J., 1990. The diamondiferous roots of our wandering continent. *South African Journal of Geology*, **93**(3), 423-437.
- Hamilton, P. J., 1977. Sr isotope and trace element studies of the Great Dyke and Bushveld mafic phase and their relation to Proterozoic magma genesis in Southern Africa. *Journal of Petrology*, **18**, 24-52.
- Harmer, R. E., 1985. Rb-Sr Isotopic Study of the Pienaars River Alkaline Complex, North of Pretoria, South Africa. *Transactions of the Geological Society of South Africa*, **88**, 215-223.
- Harmer, R. E., 1999. The Petrogenetic Association of Carbonatite and Alkaline Magmatism: Constraints from the Spitskop Complex, South Africa. *Journal of Petrology*, **40**, 325-348.
- Harmer, R. E. & Armstrong, R. A., 2000. Duration of Bushveld Complex (*sensu lato*) magmatism: Constraints from new SHRIMP zircon chronology. In: *Workshop on the Bushveld Complex - Abstracts and Programs*, Gethlane Lodge, Burgersfort, 18-21 November 2000.
- Harmer, R. E. & Sharpe, M. R., 1985. Field Relations and Strontium Isotope Systematics of the Marginal Rocks of the Eastern Bushveld Complex. *Economic Geology*, **80**, 813-837.

- Hatton, C. J., 1995. Mantle plume origin for the Bushveld and Ventersdorp magmatic provinces. *Journal of African Earth Sciences*, **21**(4), 571-577.
- Hatton, C. J., 1996. The Bushveld Complex, a product of interaction among magmas derived from a mantle plume. *Communications of the Geological Survey of Namibia*, **10**, 93-98.
- Hatton, C. J. & Schweitzer, J. K., 1995. Evidence for synchronous extrusive and intrusive Bushveld magmatism. *Journal of African Earth Sciences*, **21**(4), 579-594.
- Hauri, E. H. & Hart, S. R., 1993. Re-Os isotope systematics of HIMU and EMII oceanic island basalts from the South Pacific Ocean. *Earth and Planetary Science Letters*, **114**, 353-371.
- Hawkesworth, C., Gallagher, K. & Turner, S., 1994. Causes of melt generation in the sub-continental mantle. *Mineralogical Magazine*, **58A**, 394-295.
- Hawkesworth, C. & Turner, S., 1994. The composition of the sub-continental mantle: evidence from magmatic rocks. *Mineralogical Magazine*, **58A**, 396-297.
- Hawkesworth, C. J., Gallagher, K., Hergt, J. M. & McDermott, F., 1993. Mantle and slab contributions in arc magmas. *Annual Reviews in Earth and Planetary Sciences*, **21**, 175-204.
- Hawkesworth, C. J. & Vollmer, R., 1979. Crustal contamination versus enriched mantle; $^{143}\text{Nd}/^{144}\text{Nd}$ and $^{87}\text{Sr}/^{86}\text{Sr}$ evidence from the Italian volcanics. *Contributions to Mineralogy and Petrology*, **69**(2), 151-165.
- Hellman, P. L. & Green, T. H., 1979. The role of sphene as an accessory phase in the high-pressure partial melting of hydrous mafic compositions. *Earth and Planetary Science Letters*, **42**, 191-201.
- Hickey, R. L. & Frey, F. A., 1982. Geochemical characteristics of boninite series volcanics: implications for their source. *Geochimica et Cosmochimica Acta*, **46**, 2099-2115.
- Hoal, B. G., Hoal, K. E. O., Boyd, F. R. & Pearson, D. G., 1995. age constraints on crustal and mantle lithosphere beneath the Gibeon kimberlite field, Namibia. *South African Journal of Geology*, **98**(2), 112-118.

- Horan, M. F., Walker, R. J., Fedorenko, V. A. & Czamanske, G. K., 1995b. Osmium and neodymium isotopic constraints on the temporal and spatial evolution of Siberian flood basalt sources. *Geochimica et Cosmochimica Acta*, **59**, 5159-5168.
- Horan, M. F., Walker, R. J., Fedorenko, V. A. & Czamanske, G. K., 1995a. Osmium and neodymium isotopic constraints on the temporal and spatial evolution of Siberian flood basalt sources. *Geochimica et Cosmochimica Acta*, **59**(24), 5159-5168.
- Irvine, T. N., 1970. Crystallisation sequences in the Muscox intrusion and other layered intrusions. I. Olivine-pyroxene-plagioclase relations. *Geological Society of South Africa, Special Publication No.1*, 441-476.
- Irvine, T. N. & Baragar, W. R. A., 1971. A guide to the classification of the common volcanic rocks. *Canadian Journal of Earth Sciences*, **8**, 523-548.
- Irvine, T. N., Keith, D. W. & Todd, S. G., 1983. The J-M Platinum-Palladium Reef of the Stillwater Complex, Montana: II. Origin of Double-Diffusive Convective Magma Mixing and Implications for the Bushveld Complex. *Economic Geology*, **78**(7), 1287-1333.
- Irvine, T. N. & Sharpe, M. R., 1982. Source-Rock Compositions and Depths of Origin of Bushveld and Stillwater Magmas. *Carnegie Institution of Washington Yearbook - Papers From the Geophysical Laboratory*, **81**, 294-303.
- Jackson, E. D., 1967. Ultramafic cumulates in the Stillwater, Great Dyke and Bushveld Intrusions;. In: *Ultramafic and Related Rocks* (ed Wyllie, P. J.), pp. 20-30, John Wiley and Sons, New York.
- James, D. E., 1981. The combined use of oxygen and radiogenic isotopes as indicators of crustal contamination. *Annual Review of Earth and Planetary Sciences*, **9**, 311-344.
- James, D. E., Fouch, M. J., VanDecar, J. C., van der Lee, S. & Kaapvaal Seismic Group, 2001. Tectonospheric structure beneath southern Africa. *Science*, **submitted**.
- Jochum, K. P., Arndt, N. T. & Hofmann, A. W., 1991. Nb-Th-La in komatiites and basalts: constraints on komatiite petrogenesis and mantle evolution. *Earth and Planetary Science Letters*, **107**, 272-289.

- Jones, M. Q. W., 1988. Heat flow in the Witwatersrand Basin and environs and its significance for the South African Shield geothermal and lithosphere thickness. *Journal of Geophysical Research, B, Solid Earth and Planets*, **93**(4), 3243-3260.
- Jordan, T. H., 1978. Composition and development of the continental tectosphere. *Nature (London)*, **274**(5671), 544-548.
- Jordan, T. H., 1988. Structure and formation of the continental tectosphere. In: *Oceanic and continental lithosphere; similarities and differences*. (eds Menzies, M. A. & Cox, K. G.) *Journal of Petrology*, pp. 11-37, Clarendon Press, Oxford, United Kingdom.
- Jordan, T. H. & Anonymous, 1981. Continents as a chemical boundary layer; the origin and evolution of the Earth's continental crust. In: *The origin and evolution of the Earth's continental crust; discussions meeting*, pp. 359-373, London, United Kingdom.
- Kerrick, R. & Wyman, D. A., 1997. Review of developments in trace-element fingerprinting of geodynamic settings and their implications for mineral exploration. *Australian Journal of Earth Sciences*, **44**, 465-487.
- Kruger, F. J., 1994. The Sr-isotopic stratigraphy of the Western Bushveld Complex. *South African Journal of Geology*, **97**, 393-398.
- Kruger, F. J. & Anonymous, 1997. The Bushveld Complex; an isotopic perspective. *American Geophysical Union, 1997 fall meeting*, **78**(46, Suppl.), 800.
- Kruger, F. J. & Barnes, S. J. e., 1992. The origin of the Merensky cyclic unit; Sr-isotopic and mineralogical evidence for an alternative orthomagmatic model. In: *Proceedings of the Sixth international platinum symposium*, pp. 255-261, Perth, West. Aust., Australia.
- Kruger, F. J., Cawthorn, R. G. & Walsh, K. L., 1987. Sr-isotopic evidence against magma addition in the Upper Zone of the Bushveld Complex. *Earth and Planetary Science Letters*, **84**, 51-58.
- Kruger, F. J. & Marsh, J. S., 1982. Significance of $^{87}\text{Sr}/^{86}\text{Sr}$ ratios in the Merensky cyclic unit of the Bushveld Complex. *Nature*, **298**, 53-55.
- Kuno, H., 1968. Differentiation of Basaltic Magmas. In: *Basalts: The Poldervaart treatise on rocks of basaltic composition* (eds Hess, H. H. & Poldervaart, A.), pp. 623-688, Interscience, New York.

- Lambert, D. D., Foster, J. G., Frick, L. R., Hoatson, D. M. & Purvis, A. C., 1998. Application of the Re-Os isotopic system to the study of Precambrian magmatic sulfide deposits of Western Australia. *Australian Journal of Earth Sciences*, **45**, 265-284.
- Lambert, D. D., Frick, L. R., Foster, J. G., Li, C. & Naldrett, A. J., 2000. Re-Os Isotopic Systematics of the Voisey's Bay Ni-Cu-Co Magmatic Ore System, Labrador, Canada: II. Implications for Parental Magma Chemistry, Ore Genesis and Metal Redistribution. *Economic Geology*, **65**(5), in press.
- Lambert, D. D., Morgan, J. W., Walker, R. J., Shirey, S. B., Carlson, R. W., Zientek, M. L. & Koski, M. S., 1989. Rhenium-Osmium and Samarium-Neodymium Isotopic Systematics of the Stillwater Complex. *Science*, **244**, 1169-1174.
- Lambert, D. D. & Simmons, E. C., 1987a. Magma evolution in the Stillwater Complex, Montana: I. Rare Earth Element Evidence for the Formation of the Ultramafic Series. *American Journal of Science*, **287**, 1-32.
- Lambert, D. D. & Simmons, E. C., 1987b. Magma evolution in the Stillwater Complex, Montana: II. Rare Earth Element Evidence for the Formation of the J-M Reef. *Economic Geology*, **83**(6), 1109-1126.
- Lambert, D. D., Walker, R. J., Morgan, J. W., Shirey, S. B., Carlson, R. W., Zientek, M. L., Lipin, B. R., Koski, M. S. & Cooper, R. L., 1994. Re-Os and Sm-Nd Isotope Geochemistry of the Stillwater Complex, Montana: Implications for the Petrogenesis of the J-M Reef. *Journal of Petrology*, **35**(6), 1717-1735.
- Lassiter, J. C. & Luhr, J. F., 2001. Osmium abundance and isotope variations in mafic Mexican volcanic rocks: Evidence for crustal contamination and constraints on the geochemical behavior of osmium during partial melting and fractional crystallization. *G3: Geochemistry, Geophysics, Geosystems*, **2**, Paper No. 2000GC000116.
- Le Maitre, R. W., Bateman, P., Dudek, A., Keller, J., Lameyre, L. B. M. J., Sabine, P. A., Schmid, R., Sorensen, H., Strekeisen, A., Wooley, A. R. & Zanettin, B., 1989. *A classification of igneous rocks and glossary of terms*. Blackwell, Oxford.
- Lin, P. N., Stern, R. J. & Bloomer, S. H., 1989. Shoshonitic volcanism in the northern Mariana Arc; 2, Large-ion lithophile and rare earth element abundances; evidence for the source of incompatible element enrichments in intraoceanic arcs. In: *Special section on alkaline volcanism in island arcs*. (eds Box, S. E. & Flower, M. F. J.) *Journal of*

- Geophysical Research, B, Solid Earth and Planets*, pp. 4497-4514, American Geophysical Union, Washington, DC, United States.
- Ludwig, K. R., 1998. Isoplot/Ex - A geochronological toolkit for Microsoft Excel (Ver. 1.00b), Berkley Geochronology Centre, Berkley, California.
- Maier, W. D., Arndt, N. T. & Curl, E. A., 2000. Progressive crustal contamination of the Bushveld Complex: evidence from Nd isotopic analyses of the cumulate rocks. *Contributions to Mineralogy and Petrology*, **140**, 316-327.
- Maier, W. D. & Barnes, S.-J., 1997. Concentration of Rare Earth Elements in silicate rocks of the Lower, Critical, and Main Zones of the Bushveld Complex. *in prep.*
- Marsh, J. S., Hooper, P. R., Rehacek, J., Duncan, R. A., Duncan, A. R., Mahoney, J. J. e. & Coffin, M. F. e., 1997. Stratigraphy and age of Karoo basalts of Lesotho and implications for correlations within the Karoo igneous province
- Large igneous provinces; continental, oceanic, and planetary flood volcanism. *Geophysical Monograph*, **100**, 247-272.
- Martin, C. E., Esser, B. K. & Turekian, K. K., 1991. Re-Os isotopic constraints of the formation of mantle and crustal reservoirs. *Australian Journal of Earth Sciences*, **28**, 569-576.
- McBride, J. S., Lambert, D. D., Greig, A. & Nicholls, I. A., 1996. Multistage evolution of Australian subcontinental mantle: Re-Os isotopic constraints from Victorian mantle xenoliths. *Geology*, **24**(7), 631-634.
- McCandless, T. E., Ruiz, J., Adair, B. I. & Freydier, C., 1999. Re-Os isotope and Pd/Ru variations in chromitites from the Critical Zone, Bushveld Complex, South Africa. *Geochimica et Cosmochimica Acta*, **63**(6), 911-923.
- McCourt, S., 1995. The crustal architecture of the Kaapvaal crustal block South Africa, between 3.5 and 2.0 Ga - A synopsis. *Mineralium Deposita*, **30**, 89-97.
- McCulloch, M. T. & Black, L. P., 1984. Sm-Nd isotopic systematics of Enderby Land granulites and evidence for the redistribution of Sm and Nd during metamorphism. *Earth and Planetary Science Letters*, **71**(1), 46-58.
- McDonough, W. F., McCulloch, M. T. & Sun, S. S., 1985. Isotopic and geochemical systematics in Tertiary-Recent basalts from southeastern Australia and implications for the

- evolution of the sub-continental lithosphere. *Geochimica et Cosmochimica Acta*, **49**, 2051-2067.
- McDonough-W-F, 1990. Chemical and isotopic systematics of continental mantle. *Eos, Transactions, American Geophysical Union.*, **71**(43), 1670.
- McNaughton, N. J. & Pollard, P. J., 1993. Cassiterite; potential for direct dating of mineral deposits and a precise age for the Bushveld Complex granites: Comment. *Geology (Boulder)*, **21**(3), 285-286.
- McNaughton, N. J., Pollard, P. J., Groves, D. I. & Taylor, R. G., 1993. A long-lived hydrothermal system in Bushveld granites at the Zaaiplaats tin mine; lead isotope evidence. *Economic Geology and the Bulletin of the Society of Economic Geologists*, **88**(1), 27-43.
- Michard, A., Gurriet, P., Soudant, M. & Albarede, F., 1985. Nd isotopes in French Phanerozoic shales: external vs. internal aspects of crustal evolution. *Geochimica Cosmochimica et Acta*, **49**, 601-610.
- Mueller, P. A., Wooden, J. L., Schulz, K. & Bowes, D. R., 1983. Incompatible-element-rich andesitic amphibolites from the Archaean of Montana and Wyoming: Evidence for mantle metasomatism. *Geology*, **11**, 203-206.
- Naldrett, A. J., Gasparini, E. C., Barnes, S. J., G., v. G. & Sharpe, M. R., 1986. The Upper Critical Zone of the Bushveld Complex and the origin of Merensky-type ores. *Economic Geology*, **81**, 1105-1117.
- Nelson, D. R. & Myers, J. S. e., 1997. Evolution of the Archaean granite-greenstone terranes of the Eastern Goldfields, Western Australia; SHRIMP U-Pb zircon constraints. In: *Precambrian Research*, pp. 57-81.
- Nier, A. O., 1950. A redetermination of the relative abundances of the isotopes of carbon, nitrogen, oxygen argon and potassium. *Physics Reviews*, **77**, 789-793.
- O'Nions, R. K., Hamilton, P. J. & Evensen, N. M., 1977. Variations in $^{143}\text{Nd}/^{144}\text{Nd}$ and $^{87}\text{Sr}/^{86}\text{Sr}$ ratios in oceanic basalts. *Earth and Planetary Science Letters*, **34**(1), 13-22.
- O'Reilly, S. Y., Griffin, W. L. & Ryan, C. G., 1991. Residence of trace elements in metasomatized spinel hercynite xenoliths; a proton-microprobe study. *Contributions to Mineralogy and Petrology*, **109**(1), 98-113.

- Patiño Douce, A. E. & Beard, J. S., 1995. Dehydration-melting of biotite gneiss and quartz amphibolite from 3 to 15 kbar. *Journal of Petrology*, **36**(3), 707-738.
- Pearce, J. A., van, d. L. S. R., Arculus, R. J., Murton, B. J., Ishii, T., Peate, D. W. & Parkinson, I. J., 1992. Boninite and harzburgite from Leg 125 (Bonin-Mariana forearc); a case study of magma genesis during the initial stages of subduction. In: *Proceedings of the Ocean Drilling Program, Bonin/ Mariana region; covering Leg 125 of the cruises of the Drilling Vessel JOIDES Resolution, Apra Harbor, Guam, to Tokyo, Japan, sites 778-786, 15 February 1989-17 April 1989*. (eds Fryer, P., Pearce, J. A., Stokking, L. B., Ali, J. R., Arculus, R., Ballotti, D. L., Burke, M. M., Ciampo, G., Haggerty, J. A., Haston, R. B., Heling, D., Hobart, M. A., Ishii, T., Johnson, L. E., Lagabrielle, Y., McCoy, F. W., Maekawa, H., Marlow, M. S., Milner, G. J., Mottl, M. J., Murton, B. J., Phipps, S. P., Rigsby, C. A., Saboda, K. L., Stabell, B., van, d. L. S., Xu, Y., Dearmont, L. H., Mazzullo, E. K., Stewart, N. J. & Winkler, W. R.) *Proceedings of the Ocean Drilling Program, Scientific Results*, pp. 623-659, Texas A & M University, Ocean Drilling Program, College Station, TX, United States.
- Pearson, D. G., Carlson, R. W., Shirey, S. B., Boyd, F. R. & Nixon, P. H., 1995a. Stabilisation of Archaean lithospheric mantle: A Re-Os isotope study of peridotite xenoliths from the Kapvaal craton. *Earth and Planetary Science Letters*, **134**, 341-357.
- Pearson, D. G., Shirey, S. B., Carlson, R. W., Boyd, F. R., Pokhilenko, N. P. & Shimizu, N., 1995b. Re-Os, Sm-Nd, and Rb-Sr isotope evidence for thick Archaean lithospheric mantle beneath the Siberian craton modified by multistage metasomatism. *Geochimica et Cosmochimica Acta*, **59**(5), 959-977.
- Pearson, D. G., van der Hilst, R. D. e. & McDonough, W. F. e., 1999. The age of continental roots. In: *International symposium on Composition, deep structure and evolution of continents*, pp. 171-194, Cambridge, MA, United States.
- Pegram, W. J. & Allegre, C. J., 1992. Osmium isotopic compositions from oceanic basalts. *Earth and Planetary Science Letters*, **111**(1), 59-68.
- Potgeiter, G. J., 1992. Tectonism along the Northeastern margin of the Bushveld Complex, South Africa (in Afrikaans). *University of Pretoria, Pretoria*.
- Reisberg, L., Zindler, A., Marcantonio, F., White, W., Wyman, D. & Weaver, B., 1993. Os isotope systematics in ocean island basalts. *Earth and Planetary Science Letters*, **120**(3-4), 149-167.

- Richardson, S. H., Erlank, A. J., Harris, J. W. & Hart, S. R., 1990. Eclogitic diamonds of Proterozoic age from Cretaceous kimberlites. *Nature (London)*, **346**(6279), 54-56.
- Richardson, S. H., Gurney, J. J., Erlank, A. J. & Harris, J. W., 1984. Origin of diamonds in old enriched mantle. *Nature (London)*, **310**(5974), 198-202.
- Richardson, S. H., Harris, J. W. & Gurney, J. J., 1993. Three generations of diamonds from old continental mantle. *Nature (London)*, **366**(6452), 256-258.
- Rudnick, R. L., Presper, T., Vielzeuf, D. e. & Vidal, P. e., 1990. Geochemistry of intermediate/- to high-pressure granulites
- Granulites and crustal evolution. *The NATO ARW granulite conference*, **311**, 523-550.
- Russell, R. D., 1975. Mass discrimination in the measurement of lead isotope reference samples. *Geochemical Journal*, **9**(1), 47-50.
- Schoenberg, R., Kruger, F. J., Nögler, T. F., Meisel, T. & Kramers, J. D., 1999. PGE enrichment in chromitite layers and the Merensky Reef of the western Bushveld Complex; a Re-Os and Rb-Sr isotope study. *Earth and Planetary Science Letters*, **172**, 49-64.
- Sharpe, M. R., 1978. "Cone-type" diabases from the eastern Transvaal-representatives of a quenched magma. *Transactions of the Geological Society of South Africa*, **81**, 373-378.
- Sharpe, M. R., 1981. The chronology of magma influxes to the eastern compartment of the Bushveld Complex as exemplified by its marginal border groups. *Journal of the Geological Society of London*, **138**, 307-326.
- Sharpe, M. R., 1982a. Classification, distribution and chronology of intrusion of mafic sill suites beneath the eastern Bushveld Complex, Pretoria University, Bushveld Institute of Geological Research, Pretoria.
- Sharpe, M. R., 1982b. Noble Metals in the Marginal Rocks of the Bushveld Complex. *Economic Geology*, **77**, 1286-1295.
- Sharpe, M. R., 1982c. Petrography, classification and chronology of intrusion of mafic sills beneath the Eastern Bushveld Complex, Institute for Geological Research on the Bushveld Complex, Pretoria.

- Sharpe, M. R. & Chadwick, B., 1982. Structures in Transvaal sequence rocks within and adjacent to the eastern compartment of the Bushveld Complex. *Transactions of the Geological Society of South Africa*, **85**, 29-41.
- Sharpe, M. R., Evensen, N. M. & Naldrett, A. J., 1986. Sm/Nd and Rb/Sr evidence for liquid mixing, magma generation and contamination in the Eastern Bushveld Complex. In: *Geocongress, Conference abstracts, University of the Witwatersrand*, pp. 621-624, Johannesburg.
- Sharpe, M. R. & Hulbert, L. J., 1985. Ultramafic Sills beneath the Eastern Bushveld Complex: Mobilized Suspensions of Early Lower Zone Cumulates in a Parental Magma with Boninitic Affinities. *Economic Geology*, **80**, 849-871.
- Sharpe, M. R. & Snyman, J. A., 1980. A model for the emplacement of the eastern compartment of the Bushveld Complex. *Tectonophysics*, **65**, 85-110.
- Shirey, S. B., 1997. Re-Os isotopic compositions of Midcontinent rift system picrites: implications for plume-lithosphere interaction and enriched mantle sources. *Canadian Journal of Earth Sciences*, **34**, 489-503.
- Shirey, S. B. & Hanson, G. N., 1986. Mantle heterogeneity and crustal recycling in Archaean granite-greenstone belts; evidence from Nd isotopes and trace elements in the Rainy Lake area, Superior Province, Ontario, Canada. *Geochimica et Cosmochimica Acta*, **50**(12), 2631-2651.
- Shirey, S. B. & Walker, R. J., 1995. Carius Tube Digestion for Low-Blank Rhenium-Osmium Analysis. *Analytical Chemistry*, **67**, 2136-2141.
- Shirey, S. B. & Walker, R. J., 1998. The Re-Os isotope system in cosmochemistry and high-temperature geochemistry. *Annual Reviews of the Earth and Planetary Sciences*, **26**, 423-500.
- Smith, C. B., 1983. Pb, Sr and Nd isotopic evidence for sources of southern African Cretaceous kimberlites. *Nature (London)*, **304**(5921), 51-54.
- Smith, H. S. & Erlank, A. J., 1982. Geochemistry and petrogenesis of komatiites from the Barberton greenstone belt, South Africa. In: *Komatiites* (eds Arndt, N. T. & Nisbet, E. G.), pp. 347-397, Allen & Unwin, London/Boston.

- Smoliar, M. I., Walker, R. J. & Morgan, J. W., 1996. Re-Os ages of Group IIA, IIIA, IVA, and IVB iron meteorites. *Science*, **271**(5252), 1099-1102.
- Stein, H., Morgan, J., Markey, R. & Hannah, J., 1999a. Re-Os dating of Au deposits in Precambrian Terranes. In: *Gold '99 Trondheim* (ed Abstract, K.), Trondheim Norway.
- Stein, H. J., Morgan, J. W. & Robert, F., 1999b. $^{187}\text{Re} - ^{187}\text{Os}$ Dating of Archaean Au Deposits in the Val d'Or District, Abitibi Belt, Quebec. In: *AGE spring meeting*, EOS, Transactions, American Geophysical Union, Boston.
- Sun, S.-s., 1989. Geochemistry and petrogenesis of Archaean and early Proterozoic siliceous high-magnesian basalts. In: *Boninites* (ed Crawford, A. J.), pp. 148-173, Unwin Hyman, London.
- Sun, S.-s. & McDonough, W. F., 1989. Chemical and isotope systematics of oceanic basalts: implications for mantle composition and processes. In: *Magmatism in the Ocean Basins* (eds Saunders, A. D. & Norry, M. J.), pp. 313-345, Geological Society Special Publication.
- Taylor, S. R. & McLennan, S. M., 1985. *The Continental Crust: It's Composition and Evolution*. Blackwell, London.
- Vollmer, R. & Hawkesworth, C. J., 1980. Lead isotopic composition of the potassic rocks from Roccamonfina (South Italy). *Earth and Planetary Science Letters*, **47**(1), 91-101.
- Wager, L. R. & Brown, G. M., 1968. *Layered Igneous Rocks*. Oliver and Boyd, Edinburgh.
- Walker, R. J., Carlson, R. W., Shirey, S. B. & Boyd, F. R., 1989. Os, Sr, Nd and Pb isotope systematics of the southern African peridotite xenoliths: Implications for the chemical evolution of the subcontinental mantle. *Geochimica et Cosmochimica Acta*, **53**, 1583-1595.
- Walker, R. J., Morgan, J. W., Eero, J. H. & Smolkin, V. F., 1997. Re-Os systematics of Early Proterozoic ferropicrites, Pechenga Complex, northwestern Russia: Evidence for ancient ^{187}Os -enriched plumes. *Geochimica et Cosmochimica Acta*, **61**(15), 3145-3160.
- Walker, R. J., Morgan, J. W. & Horan, M. F., 1995. ^{187}Os enrichment in some mantle plume sources: Evidence for core-mantle interaction? *Science*, **269**, 819-822.

- Walker, R. J., Morgan, J. W., Horan, M. F., Czamanske, G. K., Krogstad, E. J., Fedorenko, V. A. & Kuniyov, V. E., 1994. Re-Os isotopic evidence for an enriched-mantle source for the Noril'sk-type, ore-bearing intrusions, Siberia. *Geochimica et Cosmochimica Acta*, **58**, 4179-4197.
- Walker, R. J., Morgan, J. W., Naldrett, A. J., Li, C. & Fassett, J. D., 1991. Re-Os isotope systematics of Ni-Cu sulfide ores, Sudbury igneous complex, Ontario; evidence for a major crustal component. *Earth and Planetary Science Letters*, **105**(4), 416-429.
- Walraven, F., 1997. Geochronology of the Rooiberg Group, Transvaal Supergroup, South Africa. *Information Circular, University of the Witwatersrand, Economic Geology Research Unit*, **316**.
- Walraven, F., Armstrong, R. A. & Kruger, F. J., 1990. A chronostratigraphic framework for the north-central Kaapvaal craton, the Bushveld Complex and the Vredefort structure. *Tectonophysics*, **171**, 23-48.
- Walraven, F. & Hattingh, E., 1993. Geochronology of the Nebo Granite, Bushveld Complex. *South African Journal of Geology*, **96**, 31-41.
- Walraven, F., Retief, E. A., Burger, A. J. & Swanepoel, D. J., 1987. Implications of new U-Pb zircon age dating on the Nebo Granite of the Bushveld Complex. *Transactions of the Geological Society of South Africa*, **90**, 344-351.
- Widom, E., Hoernle, K. A., Shirey, S. B. & Schmincke, H. E., 1999. Os isotope systematics in the Canary Islands and Madeira; lithospheric contamination and mantle plume signatures. *Journal of Petrology*, **40**(2), 279-296.
- Willemsse, J., 1959. The "floor" of the Bushveld Igneous Complex and its relationships, with special reference to the Eastern Transvaal. *Transactions of the Geological Society of South Africa*, **62**, 21-80.
- Williams, I. S. & Claesson, S., 1987. Isotopic evidence for the Precambrian provenance and Caledonian metamorphism of high grade paragneisses from the Seve Nappes, Scandinavian Caledonides; 2, Ion microprobe zircon U-Th-Pb. *Contributions to Mineralogy and Petrology*, **97**(2), 205-217.
- Wood, D. A., 1980. The application of a Th-Hf-Ta diagram to problems of tectonomagmatic classification and to establishing the nature of crustal contamination of basaltic lavas

- of the British Tertiary volcanic province. *Earth and Planetary Science Letters*, **50**(1), 11-30.
- Wyman, D. A., 1999. Palaeoproterozoic boninites in an ophiolite-like setting, Trans-Hudson Orogen, Canada. *Geology (Boulder)*, **27**(5), 455-458.
- Xiong, Y. & Wood, S. A., 1998. Experimental evidence for the mobility of Os under hydrothermal conditions. In: *Proceedings of the 8th International Platinum Symposium*, pp. 457-459, Rustenburg, South Africa.
- Yaxley, G. M., Crawford, A. J. & Green, D. H., 1997. Evidence for carbonatite metasomatism in spinel peridotite xenoliths from western Victoria, Australia. *Earth and Planetary Science Letters*, **107**, 305-317.
- York, D., 1969a. The best isochron. *Eos, Transactions, American Geophysical Union*, **50**(4), 337.
- York, D., 1969b. Least squares fitting of a straight line with correlated errors. *Earth and Planetary Science Letters*, **5**(5), 320-324.
- Zindler, A. & Hart, S., 1986. Chemical geodynamics. *Annual Review of Earth and Planetary Sciences*, **14**, 493-571.

Appendix I Analytical Methods

Appendix I(a) Sample Preparation

This study relied on the accurate determination of precise trace element and isotopic determination of samples that potentially have low Re and Os concentrations, a clean crushing technique was considered essential. Because both Re and Os are usually concentrated into minor and accessory phases concentrations can vary on the hand specimen scale, to address this the maximum amount of material was prepared at any given time to ensure homogeneity.

All samples selected for major, trace and isotopic analyses were thin sectioned before cut into smaller pieces to remove the outer coating. Samples were then polished on a diamond lap to produce a fresh, flat surface free of any saw marks and saw residue. These blocks were then repeatedly washed in MQ-H₂O, before being dried in an oven at 90°C overnight. A ceramic faced jaw crusher was used to further reduce the size of the pieces down to an aggregate of ~2-5 mm sized pieces. This material was then pulverized in a natural crystalline agate mill. The mill was cleaned between samples by crushing quartz sand to a fine powder, followed by an initial charge of sample which was pulverised to a fine powder in order to pre-contaminate the mill. The sample was then loaded in a charge of ~50 g and pulverized for approximately 40 minutes.

Appendix I(b) X-Ray Fluorescence Analysis

An ARL 8420 X-ray fluorescence spectrophotometer was employed for whole rock major and trace element analysis. A low-dilution fusion method was used to produce glass discs (Haukka and Thomas, 1977; Thomas and Haukka, 1978) which were polished and analysed for both major and trace elements in a single analysis. This technique provides detection limits of approximately 0.5 wt.% for the major elements and 10 ppm for most trace elements. A Si-Ca-Fe standard was analysed along with the samples. Accuracy was monitored by measuring major and trace element abundances of international rock standards.

Appendix I(c) High Resolution Inductively Coupled – Mass Spectrometry (HR ICP-MS)

Whole rock trace elements analyses for this study have been analysed using a Finnigan MAT ELEMENT high resolution magnetic sector ICP-MS. Drift corrections were minimal for the Finnigan MAT ELEMENT (~2 %). The multiple resolution modes and very small amount of in-run drift observed using the Finnigan MAT ELEMENT allows all the elements to be analysed together. One isotope (or two) was chosen for each element of interest based on no or minimal isobaric interferences. The run specifications resulted in approximately 10 sample points per peak.

All wet-chemistry sample preparation was performed in "class 350" clean air cabinets. 50-100 mg of sample powder was weighed into PTFE-teslon bombs and dissolved in a 2HF:HNO₃ mixture. The sample solutions were then dried down under heat lamps. Samples containing highly resilient spinels were then refluxed in aqua regia (3HCl:2HNO₃:MQ) and transferred into steel pressure vessels for further dissolution high pressure at 160°C for 3 days. After evaporation to dryness, the samples were then refluxed twice in 16N HNO₃ to remove fluorides, then re-dissolved in a 2% HNO₃ solution containing 10 ppb In to be used as an internal standard during ICP-MS analysis. Samples which did not contain abundant spinels were refluxed twice in concentrated HNO₃ solution as above. The solution was then diluted to 50 ml of 2% HNO₃ (made with sub-boiled distilled concentrated HNO₃ and 18.2 M-ohm Millipore water). Aliquots of this solution were then taken and diluted to an appropriate dilution factor for presentation to the mass spectrometer, typically 6000. The final solutions contained 10 ppb indium to serve as an internal standard. One analytical blank and 4 standard solutions (based on 50 mg and 100 mg of digested U.S. Geological Survey standard BHVO-1, BIR-1 and/or BCR-1) were typically prepared with each run. BHVO-1 was used as a check standard to monitor accuracy during the analytical procedure.

Appendix I(d) Re-Os Isotopic analyses

A combination of both whole rock and mineral separate Re-Os isotopic analyses were employed in this study. Where estimated sample concentrations were below 0.2 ppb Os the desilicification procedure described below was employed (a), otherwise whole rock powders, and finely ground mineral separate powders were loaded directly into the curius tubes (b).

(i) Desilicification procedure

Sample powder was accurately weighed onto foil and transferred into 250ml Savillex PTFE bombs. 4 ml ethanol: 10 ml 12N HCl : 10 ml 16N HNO₃ was added to the sample powder, the bomb was tightly capped, heated to 90°C overnight and then evaporated to dryness. These steps were repeated twice. Desilification samples were then dissolved in 4ml of 12N HCl, ready for transfer to Carius tubes.

(ii) Carius tube loading

Either sample powder or desilification solution was carefully transferred into a carius tube which had been chilled in a methanol-dry ice mixture. Appropriate amounts of ¹⁸⁵Re and ¹⁹⁰Os spike were then added based on estimated sample concentrations and calculated optimal spike/sample ratios. Milli-Q (MQ) water, HCl and HNO₃ added in the proportions to obtain a 3HNO₃:2HCl:1MQ Reverse Aqua Regia mix. Carius tubes were then sealed using an oxy-acetylene torch and allowed to warm up to room temperature.

(iii) Sample spike equilibration

Loaded tubes were placed into metal jackets, or "pipe bombs" which were covered at both ends with a screw on metal lid in case of catastrophic failure of the tube. Carius tubes were heated to 240°C for between 12-96 hours and slowly cooled.

(iv) Solvent Extraction Technique

The solvent extraction of Os relies on the partitioning of Os from the equilibrated (post carius tube) solution into an organic solvent (CCl₄), the Os is then "back extracted" into a HBr acid solution and dried down for final purification. The procedure is performed according to the following series of steps:

- 1) Cool Carius tubes and carbon tetrachloride in refrigerator.
- 2) Prepare Savillex beakers with 4 ml conc HBr for each sample.
- 3) Prepare centrifuge tubes for each sample.
- 4) Open Carius tube and pour contents into centrifuge tube.
- 5) Add 3ml of chilled CCl₄ to each centrifuge tube and cap tightly.

- 6) Shake centrifuge tube vigorously for about 1 minute and centrifuge for 10-15 minutes.
- 7) **OPEN TUBES IN FUME HOOD.**
- 8) Extract the carbon tetrachloride layer and deposit into the Savillex beaker for that sample- ensure that no precipitate or aqua regia is transferred to the HBr.
- 9) Repeat from step 5 two more times.
- 10) Cap the Savillex beakers tightly and put on top of a hotplate at 80-90°C for 1 hour.
- 11) Turn off the hotplate and allow to cool for 2 hours or overnight.
- 12) Open beakers and extract the carbon tetrachloride layer (bottom) and make sure to discard only the carbon tetrachloride layer, no HBr.
- 13) Dry down the HBr under heat lamps for μ -distillation.
- 14) Dry down residual aqua regia solution for Re extraction.

(v) Osmium microdistillation for the clean up of Os samples

The following technique is the final stage of purification of the Os fraction of the sample. This technique follows the work of Birck, Roy Barman, and Capmas, (1997), Geostandards Newsletter 20, 19-27.

- 1) Dry down the Os cut from the distillation or solvent extraction procedure.
- 2) Pick up in 1 (20 μ L) drop of conc HBr (9N) and place in the upturned lid of a 5ml rocket bomb.
- 3) Dry down using heat lamps.
- 4) Place the one drop (20 μ L) conc HBr into the very end of a clean rocket bomb. It will be held up by surface tension when inverted.
- 5) Add one drop of the 8% CrO₃ in 12N H₂SO₄ to the dried Os sample in the lid of the rocket bomb.
- 6) **QUICKLY SEAL THE BOMB KEEPING IT UPSIDE DOWN.**
- 7) Wrap the bottom of the vessel in Aluminium foil, leaving the top uncovered.
- 8) Place on a hotplate at 80°C for 3 hours.
- 9) Discard the lid of the rocket bomb and replace with a clean one.
- 10) Dry down the HBr drop, which should contain all of the Os- ready for mass spectrometry.

(vi) Re concentration and clean-up procedure

The Re fraction after solvent extraction is treated with two stages of ion exchange chromatography.

The standard procedural charts are included below detailing acid molarities and volumes:

Re Primary Column Procedure

Name:
 Sample type: Carius tube acid digestion
 Sample pre-treatment: Dry down 1te aliquot from AR digestion in teflon beaker
 Dry down 2x with concentrated HNO₃ to remove Os
 pick up in 10 ml 0.1N HNO₃
 Column type: New acid-washed BioRad econo-column
 set up columns in PVC column box
 Resin volume: 1 ml in MQ water loaded with Finnpiptette and clean tip
 Resin type: AG1 X8 (100-200) in teflon bottle labelled "for Re"
 Acid types: 8N and 0.1N HNO₃ in 1 litre PP bottles in hood

Procedure	Volume (ml)	Column 1	Column 2	Column 3	Column 4	Column 5	Column 6
Sample Number							
Wash resin with milli-Q	One reservoir						
Wash resin with 8N HNO ₃	Two reservoirs						
Equilibrate resin with 0.1N HNO ₃	10						
Load sample in 0.1N HNO ₃	10						
Wash column with 0.1N HNO ₃	2 x 5 = 10						
Collect Re in 8N HNO ₃	2 x 10 = 20						

Dry down Re cut; ready for N-TIMS (may require clean-up column) or pick up in 5 ml dilute HNO₃ for ICP-MS analysis
 Discard resin and column
 Wash new columns in teflon jar with clean 6N HCl prior to use

NOTES:

Re Clean-up Column Procedure

Name:
 Sample type: Re cut from primary Re column procedure
 Sample pre-treatment: Dry down Re from columns
 Add 1ml 0.1N HNO₃ to sample, to get into solution
 Ultrasonicate or stew gently on hotplate aid dissolution
 Column type: 0.25ml PP columns with slide-in teflon frit assemblies
 Set up columns in PVC column box, use TFE insert supports
 Resin volume: 0.1ml in MQ water loaded with Finnpiptette and clean tip
 Resin type: AG1 X8 (100-200) in teflon bottle labelled "for Re"
 Acid types: 8N and 0.1N HNO₃ in 1 litre PP bottles
 Note: Reservoir volume approx 4ml

Procedure	Volume (ml)	Column 1	Column 2	Column 3	Column 4	Column 5	Column 6
Sample Number							
MQ water to wash resin	One reservoir						
Wash resin with 8N HNO ₃	Two reservoirs						
Equilibrate resin with 0.1N HNO ₃	Two reservoirs						
Load sample in 0.1N HNO ₃	1ml						
Wash column with 0.1N HNO ₃	Two reservoirs						
Collect Re in 8N HNO ₃	5ml						

Dry down Re cut; ready for N-TIMS or pick up in 5 ml dilute HNO₃ for ICP-MS analysis
 Discard resin
 Wash columns in MQ and return to storage wash

NOTES:

(vii) Negative-Thermal Ionization Mass Spectrometry (N-TIMS)

Re and Os were analysed using a Finnigan-MAT 262 multicollector mass spectrometer thermal ionisation mass spectrometer (N-TIMS) after Creaser and others (1991). Os samples were loaded in HBr onto single filaments, heated in high vacuum to convert the Os bromide salt to Os metal. Re was loaded in 4N HNO₃ onto singly Pt filaments and 1 ml of Ba(NO₃)₂ was added to both the Re and the Os metal on the filaments to increase ionisation efficiency. Filaments were heated to running temperatures (>900°C) and O₂ was introduced into the source at a pressure of 2x10⁻⁶ mbar. Osmium was measured as the negative OsO₃²⁻ ion, using a single secondary electron multiplier in peak jumping mode. ¹⁸⁵Re was monitored to check for interference on ¹⁸⁷Os. Mass fractionation corrections were performed off-line to ¹⁹⁰Os/¹⁸⁸Os = 3.09219 (Hauri and Hart, 1993). O₂ correction (Nier, 1950), spike correction and data reduction were also performed off-line using a custom made Excel spreadsheet. Re was measured as the ReO₄²⁻ ion either by static multicollection into Faraday cup collectors or, for extremely low level samples, using a single secondary electron multiplier as for Os. Spike correction and data reduction was performed off-line. Table A. 2.4 shows the long term mean values obtained for the Department of Terrestrial Magnetism (DTM) Os isotopic standard (made using Johnson-Mathey (NH₄)₂OsCl₆ batch 5.56870-A in 6N HCl). Total procedural blanks were < 2 pg for Os and < 6 pg for Re for the majority of samples. Some samples, including magnetite and chromite separates and chromitites were also analysed on the Finnigan MAT HR-ICP-MS.

Appendix I(e) Rb-Sr Isotopic Analysis***(i) Sample preparation***

Analyses of Sm-Nd and Rb-Sr were performed on a single aliquot (50-100 mg) of sample powder was accurately weighed and appropriate amounts of ¹⁵⁴Sm, ¹⁵⁰Nd, ⁸⁷Rb and ⁸⁴Sr spikes were added. Samples were then digested as for ICP-MS trace element preparation above, up until the final 16N HNO₃ reflux when the samples were then dried down and picked up in dilute HCl acid. After centrifuging, the Rb, Sr and REE (containing the Sm and Nd) were separated from the solution by gradient elution on standard cation exchange columns using BioRad AG50Wx8 (200-400 mesh) resin. The REE fraction was dried down and all remaining resins particles are destroyed using hot

HNO₃ acid. Nd and Sm are then separated using 3 ml diameter columns of 2 di-ethyl-hexyl phosphate (HDEHP) on a Kel-F support. Purified Sm and Nd are then ready for mass spectrometry.

(ii) Rb-Sr Mass spectrometry

Rubidium and Sr concentrations and Sr isotopic compositions were determined by isotope dilution analysis. 100 mg of sample powder was accurately weighed and spiked with ⁸⁴Sr and ⁸⁷Rb spikes. The samples were then digested by the same procedure as for the preparation of the samples for ICP-MS analysis. The Rb and Sr fractions were separated from each other by gradient elution on cation exchange columns using BioRad AG50Wx8 (200-400 mesh) resin in hydrochloric acid. Usually the samples required no further treatment, and were ready for mass spectrometry. Separated Rb and Sr were analysed by static multicollection into Faraday cup detectors on a Finnigan-MAT 262 multicollector mass spectrometer at La Trobe University. The Sr samples were dissolved in phosphoric acid and loaded onto single Ta filaments. All spike stripping and isotope dilution calculations were done off-line. The total blanks for this procedure are less than 200 pg for Rb and Sr. Long term precision of the Sr standard SRM987 yields $^{87}\text{Sr}/^{86}\text{Sr} = 0.71023 \pm 4$ (1 sd, n=50). Precision for $^{87}\text{Rb}/^{86}\text{Sr}$ is $\pm 0.8\%$ (2 sd).

(iii) Sm-Nd Mass spectrometry

Sm and Nd were all analysed using a Finnigan-MAT 262 multi-collector mass spectrometer at La Trobe University. All elements were analysed in static mode into Faraday cup collectors. Sm and Nd were loaded in H₃PO₄ doped HNO₃ onto the Ta side of double Re-Ta filament assembly. Raw ratios were corrected for mass fractionation using $^{146}\text{Nd}/^{144}\text{Nd} = 0.7219$ (power law) and $^{152}\text{Sm}/^{147}\text{Sm} = 1.78307$ (linear law). All spike stripping and isotope dilution calculations were performed off-line. Typical blanks are < 200 pg for Nd and Sm. External reproducibility for the La Jolle Nd standard is $^{143}\text{Nd}/^{144}\text{Nd} = 0.511860 \pm 20$ (2 sd). Precision for $^{147}\text{Sm}/^{144}\text{Nd}$ is < 0.2% (2 sd).

Appendix II. Major and Trace Element Data

SAMPLE CLASSIFICATION	ECBV18 B1	ECBV19 B1	ECBV49a B1	ECBV111 B1	D1204 B1	ECBV21 B1 - QT
Major Element Oxides (XRF)						
Fe ₂ O ₃ wt.%	10.92	11.08	11.02	9.96	10.37	10.26
MnO	0.20	0.20	0.19	0.17	0.17	0.17
TiO ₂	0.27	0.30	0.34	0.33	0.29	0.42
CaO	5.88	6.41	6.48	6.32	6.35	7.09
K ₂ O	0.77	0.79	0.76	1.07	0.64	1.09
SO ₃	0.09	0.09	0.10	0.01	0.13	0.14
P ₂ O ₅	0.07	0.07	0.08	0.08	0.05	0.11
SiO ₂	55.54	56.04	54.46	55.67	55.31	57.05
Al ₂ O ₃	10.70	11.77	11.19	11.46	10.95	13.05
MgO	14.10	12.48	13.11	13.36	13.49	8.84
Na ₂ O	1.19	1.31	1.39	1.59	1.58	2.04
Total	99.87	100.27	100.18	100.34	100.53	100.02
loi	-0.16	-0.53	0.76	-0.01	0.95	-0.48
Minor Elements (XRF)						
Cl ppm	307	349	278	34	129	561
Ti	1156	1284	1456	1413	1242	1798
V	159	166	155	152	151	182
Cr	1381	983	906	1874	1136	442
Co	65	68	68	63	58	58
Ni	336	288	324	368	300	130
Cu	33	35	41	32	47	48
Zn	83	91	86	75	72	81
Sr	145	158	164	162	161	223
Zr	62	65	69	65	51	78
Ba	306	301	301	293	229	361
Minor / Trace Elements (HR ICP-MS)						
Sc ppb	32798	35521	28546	22381	33660	29167
Ti	1521285	1545259	1950538	1890544	1680188	2318578
V	165268	162461	172992	153819	151870	172581
Cr	1393007	970246	893015	1782063	1097651	436900
Mn	1417181	1382541	1398409	1205473	1284401	1271116
Co	64990	59994	64398	60476	61320	53555
Ni	308689	245953	295397	331067	339546	160929
Cu	44248	44582	53802	36896	45830	57989
Zn	78129	76442	90806	70012	61648	70819
Rb	37619	38934	30506	41166	27537	45669
Sr	158698	171401	182364	197866	159066	250526
Y	9885	10434	12600	11421	10180	13521
Zr	69777	74480	77407	71450	57132	94842
Nb	4001	3985	4608	4543	2722	5478
Mo	371	342	472	672	371	790
Sn	1211	1151	1125	913	661	1143
Cs	2991	3001	1843	3960	991	2856
Ba	300287	338259	347659	430108	243616	416424
Hf	1759	1840	1958	1919	1377	2356
Ta	502	479	555	657	248	562
Pb	11889	11869	9452	20776	6448	11820
Th	3677	4023	1759	3576	2594	3925
U	898	946	487	1237	694	1220
Rare Earth Elements (HR ICP-MS)						
La ppb	16744	17440	17239	16783	12884	20703
Ce	32534	34343	34275	34309	23858	40612
Pr	3815	4040	4200	4099	2938	4891
Nd	13633	14443	15718	15543	11104	17859
Sm	2353	2397	3076	2844	2022	3142
Eu	690	719	881	943	538	962
Gd	2066	2197	2665	2384	1781	2846
Tb	290	303	365	350	261	401
Dy	1573	1642	2136	2042	1534	2152
Ho	318	332	415	421	319	445
Er	878	938	1143	1135	859	1206
Tm	134	142	175	178	138	180
Yb	927	956	1210	1188	954	1230
Lu	151	159	189	180	154	199

APPENDIX II: MAJOR AND TRACE ELEMENT DATA

SAMPLE CLASSIFICATION	ECBV105 B1 - QT	ECBV106 B1 - QT	CD017 B1 - QT	CD01 B1 - QT	ECBV16 B1 - UM	ECBV20 B1 - UM
Major Element Oxides (XRF)						
Fe2O3 wt.%	10.18	10.29	10.97	9.95	9.67	9.00
MnO	0.18	0.19	0.19	0.16	0.16	0.17
TiO2	0.35	0.32	0.44	0.31	0.16	0.17
CaO	7.14	6.43	6.41	6.51	2.55	2.85
K2O	1.17	1.10	1.00	0.97	0.61	0.59
SO3	0.10	0.07	0.10	0.09	0.04	0.00
P2O5	0.08	0.07	0.08	0.07	0.05	0.04
SiO2	57.05	56.11	53.27	56.85	50.19	56.01
Al2O3	13.76	12.38	10.89	12.01	5.60	5.93
MgO	8.08	10.07	13.99	10.93	28.70	24.08
Na2O	1.86	1.77	1.70	1.85	0.89	0.77
Total	100.32	99.73	100.29	100.35	99.57	100.27
loi	0.10	0.61	0.97	0.43	0.20	0.28
Minor Elements (XRF)						
Cl ppm	838	1076	389	132	20	159
Ti	1498	1370	1884	1327	685	728
V	177	158	148	153	76	70
Cr	392	680	1063	791	5078	2438
Co	48	54	61	51	100	72
Ni	165	220	408	241	1644	646
Cu	43	45	67	46	35	11
Zn	93	97	86	77	83	64
Sr	213	191	194	185	92	97
Zr	76	70	65	68	44	38
Ba	390	362	232	320	212	169
Minor / Trace Elements (HR ICP-MS)						
Sc ppb	27950	23176	28308	33212	15081	20922
Ti	2006677	1853585	2635141	1888198	766867	683470
V	176660	167986	162934	168256	75640	62732
Cr	374822	645938	1092764	800586	5388116	2455095
Mn	1272894	1418315	1432549	1305210	1204743	1149269
Co	48872	54806	68305	58557	93702	69570
Ni	147141	200187	487259	271745	1593058	646268
Cu	53169	54614	69661	47703	22814	16846
Zn	93481	83375	116893	76135	76386	49873
Rb	42588	40494	46746	44365	31155	28356
Sr	250635	226980	207336	199505	94650	88838
Y	12337	10979	13555	11774	5907	5149
Zr	125138	73266	52671	82199	49187	40585
Nb	4613	4218	3211	4116	2896	2578
Mo	600	473	704	619	288	172
Sn	1379	1044	959	797	946	477
Cs	3811	2930	1580	1586	2570	1881
Ba	539231	486494	234626	394582	223385	219829
Hf	2783	1929	1291	1908	1340	934
Ta	633	563	273	329	425	493
Pb	19368	21014	15736	10908	10021	9239
Th	4961	4252	2500	3378	2742	2086
U	1424	1250	745	994	779	680
Rare Earth Elements (HR ICP-MS)						
La ppb	22817	20845	15177	19364	11082	8816
Ce	43302	40343	28635	35810	21504	17291
Pr	5193	4620	3438	4499	2549	2005
Nd	18837	17729	13128	16577	8868	7318
Sm	3649	3222	2501	2787	1547	1315
Eu	1054	973	754	710	438	361
Gd	2806	2534	2331	2367	1349	1091
Tb	399	333	342	327	180	150
Dy	2216	1925	1975	1821	989	781
Ho	428	390	414	362	201	156
Er	1196	1024	1102	1012	540	423
Tm	173	162	176	158	82	65
Yb	1231	1059	1169	1069	552	454
Lu	185	171	187	174	89	72

APPENDIX II: MAJOR AND TRACE ELEMENT DATA

SAMPLE CLASSIFICATION	ECBV50 B1 - UM	CD005 B1 - UM	ECBV17 B1 - UM	DJ326 B1 - UM	ECBV15 B2	ECBV26 B2
Major Element Oxides (XRF)						
Fe2O3 wt.%	11.10	10.79	9.87	8.89	10.92	12.60
MnO	0.18	0.18	0.15	0.15	0.17	0.19
TiO2	0.26	0.24	0.14	0.07	0.38	0.69
CaO	5.13	5.40	2.39	2.69	8.69	11.19
K2O	0.60	0.78	0.22	0.13	0.41	0.22
SO3	0.06	0.09	0.00	0.01	0.00	0.04
P2O5	0.05	0.05	0.03	0.01	0.06	0.14
SiO2	50.80	49.99	42.60	42.27	52.68	50.46
Al2O3	8.28	9.00	4.12	3.97	13.52	15.65
MgO	21.89	18.57	33.88	33.20	10.56	7.35
Na2O	0.70	1.24	0.20	0.17	1.69	1.99
Total	99.84	99.45	99.77	100.21	99.32	100.12
loi	0.21	2.69	4.91	7.75	0.08	-0.55
Minor Elements (XRF)						
Cl ppm	250	173	341	163	155	74
Ti	1113	1028	599	300	1627	2954
V	145	135	82	81	165	243
Cr	3942	2585	9790	6591	443	157
Co	84	74	106	96	51	57
Ni	865	728	2049	2066	168	148
Cu	34	45	8	26	42	88
Zn	73	80	65	51	65	86
Sr	112	141	58	41	233	297
Zr	52	46	27	15	34	48
Ba	157	206	100	52	160	166
Minor / Trace Elements (HR ICP-MS)						
Sc ppb	23354	27808	13502	16925	29592	26800
Ti	1155402	1395841	483317	331856	2023232	3919511
V	127085	140653	68124	58874	163351	240716
Cr	3912813	1411842	10001430	2825430	500250	154599
Mn	1264110	1372878	1028433	1042831	1210402	1316361
Co	85880	77275	109026	101247	57361	58806
Ni	901324	821102	1988003	2441174	183556	130854
Cu	47012	52445	12639	20765	54000	111060
Zn	61897	64708	47892	37385	55859	78043
Rb	24537	37203	10374	7981	9623	5911
Sr	103824	145285	46246	24623	238918	351372
Y	7995	8268	3209	2327	13062	18107
Zr	51992	54641	22719	13087	23978	39282
Nb	2802	2628	1178	642	2654	3592
Mo	316	287	63	107	128	289
Sn	833	1045	269	230	415	731
Cs	1688	1110	749	255	892	359
Ba	219575	257970	98894	63021	237410	151347
Hf	1308	1290	509	322	603	1108
Ta	315	275	135	72	329	382
Pb	9449	9768	3616	2727	5517	3582
Th	2154	2728	1111	619	660	632
U	654	734	283	179	212	243
Rare Earth Elements (HR ICP-MS)						
La ppb	11522	12559	5660	2966	9819	12892
Ce	22925	24311	11273	5686	19607	27837
Pr	2730	2923	1289	708	2403	3668
Nd	10102	10795	4720	2630	9325	15516
Sm	1952	1948	809	484	1954	3340
Eu	535	506	217	125	809	1198
Gd	1589	1653	663	424	1958	3445
Tb	229	230	92	61	309	524
Dy	1284	1295	487	349	1821	3029
Ho	268	253	102	76	402	639
Er	745	716	278	204	1118	1651
Tm	116	112	42	34	176	242
Yb	785	748	302	242	1208	1665
Lu	125	122	49	42	190	258

APPENDIX II: MAJOR AND TRACE ELEMENT DATA

SAMPLE CLASSIFICATION	ECBV28 B2	ECBV32 B2	ECBV38 B2	ECBV44 B2	ECBV51 B2	ECBV58 B2
Major Element Oxides (XRF)						
Fe2O3 wt. %	12.01	10.19	12.37	13.31	10.01	12.31
MnO	0.20	0.15	0.18	0.18	0.19	0.22
TiO2	0.60	0.92	0.83	0.53	0.70	0.60
CaO	11.01	7.58	11.02	11.22	8.85	10.80
K2O	0.20	0.56	0.16	0.10	0.83	0.15
SO3	0.00	0.21	0.00	0.00	0.00	0.00
P2O5	0.13	0.22	0.15	0.15	0.16	0.14
SiO2	50.09	59.12	49.96	49.12	55.25	49.76
Al2O3	16.27	14.63	15.41	16.35	14.66	15.04
MgO	8.09	3.49	7.68	7.61	4.47	9.48
Na2O	1.31	2.81	2.11	1.54	1.76	1.52
Total	99.80	100.06	100.05	99.69	100.31	99.96
loi	-0.24	-0.01	0.01	-0.55	3.29	-0.20
Minor Elements (XRF)						
Cl ppm	37	244	135	191	297	4
Ti	2569	3939	3554	2269	2997	2569
V	210	204	220	269	219	224
Cr	173	211	512	111	43	290
Co	44	33	50	52	32	63
Ni	120	36	108	109	40	173
Cu	51	154	24	0	0	42
Zn	97	87	77	32	54	106
Sr	331	359	307	406	331	256
Zr	43	118	88	13	50	24
Ba	109	370	109	73	307	94
Minor / Trace Elements (HR ICP-MS)						
Sc ppb	33083	27148	34543	41042	30855	29423
Ti	3340591	5380144	4711854	2807596	3949566	3616440
V	202084	218647	220620	267765	209763	230867
Cr	205337	231147	558792	130198	50003	289698
Mn	1457302	1151185	1397934	1412236	1469049	1510834
Co	56166	38343	56547	63067	42627	58941
Ni	142593	50894	125430	133850	55735	155236
Cu	74887	197847	48832	55	10303	42462
Zn	86611	85716	80158	28632	53861	96673
Pb	6388	14247	3244	1811	23141	3683
Sr	345043	398229	335695	456392	356509	294253
Y	15710	26638	20448	12243	19413	14679
Zr	29979	133226	84441	11394	39524	28438
Nb	3373	9547	5211	2198	2769	2422
Mo	135	2933	253	38	326	217
Sn	544	537	476	175	615	450
Cs	329	434	185	223	781	222
Ba	158060	448974	156068	113196	457650	127079
Hf	733	2937	1683	394	1150	871
Ta	324	486	370	257	234	362
Pb	10932	5627	2011	3455	12377	2992
Th	592	1535	390	258	1683	381
U	225	496	174	83	480	104
Rare Earth Elements (HR ICP-MS)						
La ppb	12451	27229	14084	12687	15234	11708
Ce	26317	56691	31531	25918	31140	23877
Pr	3368	6906	4168	3208	3990	3235
Nd	13843	28522	17501	13081	16395	13118
Sm	2997	5687	3873	2781	3769	2843
Eu	1044	1762	1261	1172	1407	1118
Gd	2830	5082	3760	2499	3505	2898
Tb	428	754	585	371	538	424
Dy	2413	4138	3331	2080	3127	2608
Ho	517	843	706	434	645	511
Er	1373	2269	1875	1156	1722	1398
Tm	204	334	277	175	264	206
Yb	1369	2218	1818	1222	1701	1371
Lu	213	340	274	191	284	217

APPENDIX II: MAJOR AND TRACE ELEMENT DATA

SAMPLE CLASSIFICATION	ECBV25 B2 N	ECBV27 B2 N	ECBV31 B2 N	ECBV60 B3	ECBV61 B3	ECBV62 B3
Major Element Oxides (XRF)						
Fe2O3 wt.%	13.80	14.12	12.53	10.13	9.59	10.37
MnO	0.23	0.20	0.19	0.18	0.17	0.19
TiO2	0.82	0.83	0.80	0.34	0.38	0.49
CaO	11.59	12.31	10.79	11.39	9.48	11.60
K2O	0.15	0.06	0.16	0.31	0.52	0.37
SO3	0.01	0.16	0.00	0.00	0.00	0.00
P2O5	0.17	0.17	0.15	0.03	0.07	0.05
SiO2	49.01	46.99	50.33	51.57	53.92	50.99
Al2O3	16.29	16.34	15.41	16.35	16.24	16.25
MgO	6.68	7.11	7.23	7.17	7.07	7.75
Na2O	1.93	1.26	2.11	1.53	1.66	1.44
Total	100.41	99.13	99.35	99.52	99.51	99.80
loi	-0.41	-0.55	-0.47	0.40	0.27	0.17
Minor Elements (XRF)						
Cl ppm	120	166	27	15	60	63
Ti	3511	3554	3425	1456	1627	2098
V	277	274	232	159	159	159
Cr	92	78	279	269	408	263
Co	61	52	44	47	41	44
Ni	122	84	91	103	115	109
Cu	64	71	48	1	7	15
Zn	114	77	88	67	64	74
Sr	298	350	298	310	325	332
Zr	48	41	68	25	38	40
Ba	124	47	26	125	149	126
Minor / Trace Elements (HR ICP-MS)						
Sc ppb	21206	39893	35238	32593	24959	31337
Ti	4744725	4566574	4837150	1784758	2031348	2755584
V	270128	268216	226914	150286	153253	149174
Cr	82500	99951	314114	331560	464770	313905
Mn	1579631	1552822	1436881	1455088	1339855	1482795
Co	57122	60870	55881	56250	54614	60639
Ni	102666	103416	115417	122752	132744	135017
Cu	84370	108891	78059	12030	21380	30602
Zn	99506	77255	87479	64178	56475	69041
Rb	2735	1876	2431	7535	26933	12337
Sr	347883	362519	319162	334485	352722	355011
Y	19125	19036	22859	12352	9361	13598
Zr	53122	49615	75705	28579	37744	40419
Nb	3112	1854	5748	1118	3045	2383
Mo	332	134	652	307	812	261
Sn	739	434	397	318	393	482
Cs	140	165	164	331	1264	572
Ba	130351	107296	193380	179714	197866	177427
Hf	1380	1103	1731	802	924	1086
Ta	290	208	354	130	260	220
Pb	2483	2622	4162	3412	4761	4342
Th	417	299	422	601	2129	760
U	199	149	158	158	633	212
Rare Earth Elements (HR ICP-MS)						
La ppb	13998	12323	14765	7914	8052	8961
Ce	29900	27186	31899	15434	15433	18928
Pr	4023	3590	4179	1987	1811	2420
Nd	17073	15963	17487	8134	7030	9774
Sm	3750	3597	3948	1904	1521	2322
Eu	1338	1278	1289	855	723	912
Gd	3758	3498	3747	1903	1473	2278
Tb	561	533	594	306	234	357
Dy	3257	3010	3434	1873	1396	2172
Ho	665	621	734	405	306	459
Er	1772	1628	1963	1118	854	1253
Tm	254	234	292	172	130	190
Yb	1728	1520	1943	1167	881	1268
Lu	268	230	300	179	143	188

APPENDIX II: MAJOR AND TRACE ELEMENT DATA

SAMPLE CLASSIFICATION	ECBV64 B3	ECBV13 B3 N	ECBV61N B3 N	ECBV63 B3 N	ECBV109 HORNFELS
Major Element Oxides (XRF)					
Fe2O3 wt.%	11.99	10.62	10.05	11.62	6.73
MnO	0.20	0.18	0.19	0.19	0.03
TiO2	0.72	0.41	0.27	0.59	0.47
CaO	10.18	11.37	11.52	11.10	0.23
K2O	0.50	0.22	0.19	0.27	5.73
SO3	0.00	0.00	0.00	0.13	0.00
P2O5	0.13	0.03	0.01	0.06	0.09
SiO2	51.63	51.32	50.55	51.10	63.73
Al2O3	15.42	16.33	16.12	15.57	15.40
MgO	6.95	7.79	8.99	7.28	5.15
Na2O	2.41	2.25	1.21	2.48	0.81
Total	100.39	100.35	99.58	100.47	99.89
loi	0.10	-0.33	0.28	-0.08	1.34
Minor Elements (XRF)					
Cl ppm	0	262	47	0	0
Ti	3083	1755	1156	2526	
V	229	180	158	231	77
Cr	271	325	1095	295	94
Co	51	57	55	60	18
Ni	125	151	145	151	48
Cu	51	16	0	189	24
Zn	106	77	69	91	72
Sr	271	284	307	281	204
Zr	52	23	15	23	116
Ba	228	106	58	172	732
Minor / Trace Elements (HR ICP-MS)					
Sc ppb	24917	32373	30331	21547	15411
Ti	4290056	2230128	1310704	3480155	2573716
V	227495	176893	156139	233118	73561
Cr	257703	339358	1213531	295747	91469
Mn	1373845	1281251	1445616	1327842	202976
Co	52307	54348	63298	60030	15047
Ni	109344	138976	170799	136558	36013
Cu	66913	9896	7893	278844	23736
Zn	184810	70573	65329	77500	65280
Rb	12134	6045	6232	6811	144771
Sr	315587	327164	332101	328648	227346
Y	19757	10381	6995	13781	25660
Zr	49313	25197	10707	23224	133272
Nb	3498	1432	487	1251	12397
Mo	449	111	393	2381	1333
Sn	852	536	182	407	5040
Cs	891	418	413	619	14165
Ba	321927	122355	94844	186526	1013357
Hf	1475	739	325	775	4115
Ta	445	223	101	241	2005
Pb	9311	2490	1878	2987	47771
Th	1146	564	241	457	16227
U	330	146	62	140	3999
Rare Earth Elements (HR ICP-MS)					
La ppb	16174	5138	3035	6979	43543
Ce	33689	10499	6031	15176	86315
Pr	4341	1382	810	2084	9939
Nd	17500	5737	3420	9318	34910
Sm	4089	1359	933	2386	6306
Eu	1537	670	560	1155	1539
Gd	3734	1561	991	2591	5333
Tb	587	257	171	406	766
Dy	3559	1618	1045	2413	4447
Ho	730	348	233	511	883
Er	1959	981	650	1379	2495
Tm	292	144	102	209	374
Yb	1936	993	716	1383	2501
Lu	294	157	107	217	372

Appendix III. Sample Database

Sample	Field Classification	Field Description	Interest	Location	Petrography / Mineralogy	XRF	ICP_TCE	Sm-Nd	Rb-Sr	Re-Os (WR)	Re-Os (OXIDES)	OXYGEN ISOTOPES
						DONE	DONE	DONE	DONE	DONE	DONE	DONE
CD01	B1	Refer Sharpe (1981), Harmer and Sharpe (1985) and Sharpe and Hubert (1985)			DONE	DONE	DONE					
CD005	B1	Refer Sharpe (1981), Harmer and Sharpe (1985) and Sharpe and Hubert (1985)			DONE	DONE	DONE					
DN204	B1	Refer Sharpe (1981), Harmer and Sharpe (1985) and Sharpe and Hubert (1985)			DONE	DONE	DONE					
DI326	B1	Refer Sharpe (1981), Harmer and Sharpe (1985) and Sharpe and Hubert (1985)			DONE	DONE	DONE				DONE	
ECBV-13	B3N	Fine grained B3 norite	Representative of marginal suite to the main zone	D-147room - Roosenekal Rd just Nth. of road junction -200m to the SE of the turnoff to Bernard O'Grady's farm		DONE	DONE	DONE	DONE	DONE	DONE	DONE
ECBV-15	B1 - UM (ie. B1 composition plus a significant contribution of cumulus olivine)	Coarse B1 marginal norite with abundant cumulus phenocrystic OPX and OL	Representative of the lithology	On Steelpoort crosscut Rd. over to the Lydenburg-Burgersfont Rd -5km from Steelpoort on West side of Railway in roadside outcrop on the south side.	DONE	DONE	DONE					
ECBV-16	B1 - UM	Coarse B1 marginal norite with abundant cumulus phenocrystic OPX and OL + B1	Establish continuum from ECBV-17-19 (Varying degrees of cumulus contribution and grain size/textural variations)	West side of quarry on Sth. side of Steelpoort crosscut Rd. over to the Lydenburg-Burgersfont Rd - quarry is located -5km from eastern end of the Rd	DONE	DONE	DONE	DONE	DONE	DONE		DONE
ECBV-17	B1-UM	Coarse B1 marginal norite with abundant cumulus phenocrystic OPX and OL + B1 - significantly more (?) olivine than ECBV-16	Establish continuum from ECBV-17-19 (Varying degrees of cumulus contribution and grain size/textural variations)	East side of quarry on Sth. side of Steelpoort crosscut Rd. over to the Lydenburg-Burgersfont Rd - quarry is located -5km from eastern end of the Rd	DONE	DONE	DONE				DONE	
ECBV-18	B1	Finer grained	Establish continuum from ECBV-17-19 (Varying degrees of cumulus contribution and grain size/textural variations)	East side of quarry on Sth. side of Steelpoort crosscut Rd. over to the Lydenburg-Burgersfont Rd - quarry is located -5km from eastern end of the Rd	DONE	DONE	DONE	DONE	DONE			
ECBV-19	B1	Very fine grained ---CO114	Establish continuum from ECBV-17-19 (Varying degrees of cumulus contribution and grain size/textural variations)	East side of quarry on Sth. side of Steelpoort crosscut Rd. over to the Lydenburg-Burgersfont Rd - quarry is located -5km from eastern end of the Rd (---CO114)	DONE	DONE	DONE	DONE	DONE	DONE		
ECBV-20	B1-UM (Rev. 8/3/99)	Coarse grained marginal norite	Representative of norite from a sill a significant depth into the floor rocks	Along Rd. to Beetskraal (13km) Sample collected from loose boulder on the side of Rd. in the absence of any in-situ outcrop	DONE	DONE	DONE					
ECBV-21	B1 ("Cone Disease")	Cone textured orthopyroxene	Representative of "quench" textured B1 from deep in the floor	10km SW from Lydenburg on the Lydenburg-Roosenekal Rd, up on top of a big hill to the West of the Rd. (D1225)	DONE	DONE	DONE	DONE	DONE			
ECBV-25	B2N Gabro Norite	Very fine grained	"Best B2 samples available" - Sharpe, M.R. Very fresh samples unlikely to be contaminated due to the B2 footwall (?)	Map Loc. 06a - Millies Farm south side of the road, on the northern lobe of the B2 pod 50m from the road	DONE	DONE	DONE	DONE	DONE	DONE		DONE
ECBV-26	B2 Gabro Norite	slightly coarser grained	AS ABOVE	AS ABOVE - Slightly (5m) further south up onto the plateau (top section -3m)	DONE	DONE	DONE	DONE	DONE	DONE	DONE	DONE
ECBV-27	B2N Norite	Very fine grained	Representative B2N	Map locality 08 - Up on high hill north of Millies farm sitting directly (concordant) on the footwall quartzite, and underneath (as a rim) a sheet of B2 that forms the top of the hill.	DONE	DONE	DONE				DONE	
ECBV-28	Norite B2	More coarse grained slightly more plagioclase	Representative B2	Map locality 09 - From sheet above ECBV - 27	DONE	DONE	DONE					
ECBV-31	B2N Micro Norite	Micro fine grained	Representative	Map Loc. 18 - On the west side of the lunchtime outcrop just Nth. of link in dirt Rd.	DONE	DONE	DONE					
ECBV-32	B2 Norite	Medium coarse grained with Bortite	Representative	Map Loc. 19 - On the NE side of the lunchtime outcrop just Nth. of link in dirt Rd.	DONE	DONE	DONE					
ECBV-38	B2 Norite	Coarse grained Norite	Representative of coarse grained norite	Map Loc. 25 - Some way up the side of the 2nd saucer from the base - Sth. side power lines locality	DONE	DONE	DONE					
ECBV-44	B2 (Rev. 8/3/99)	Med / Fine grained	Near contact B1 from marginal series (not sill) difficult to imagine this sample as not being synchronous with the intrusion of the cumulate sequence. In. It appears to be part of a continuum	Map Loc. 33 - Lavoie Hills Street - Further up hill just to the south of the EW trending creek - 50m short of basal quartzite contact.	DONE	DONE	DONE					
ECBV-49 A	B1 Pyroxenite	Coarse grained	Coarse grained B1 representative about half way through the sill	Just east of Map Loc. 35	DONE	DONE	DONE	DONE	DONE	DONE		DONE

Appendix III. Sample Database (cont.)

Sample	Field Classification	Field Description	Interest	Location	Petrography / Mineralogy	XRF	ICP_TCE	Sm-Nd	Rb-Sr	Re-Os (WR)	Re-Os (OXIDES)	OXYGEN ISOTOPES
ECBV-50	B1-UM (Rev. 8/3/99)	Fine grained pyroxenite	Representative	Map Loc.36 - near (<5m) concordant contact basal with quartzite	DONE	DONE	DONE				DONE	
ECBV-51	B2 (Rev. 8/3/99)	Medium grained	Representative of marginal suite (cf. 58)	Map Loc.37 - 10m up strat section from the basal quartzite contact	DONE	DONE	DONE					
ECBV-5a	B2 Notha	Med. grained	Very nice B2 representative and very close to the sampling site of the Wager and Brown (1968 p. 534)	42 4 post on the road Roosenekal to Lydenburg		DONE	DONE	DONE	DONE	DONE	DONE	DONE
ECBV-80	B3 Notha	Fine grained	Very nice fine grained B3N occurring internally within the marginal group	Map Loc. 42 - ~40m west of previous locality is a band of B3N	DONE	DONE	DONE					
ECBV-61	Composite B3 Notha COARSE BIT (B3)	B3N +B3 contact in the sample with B3 coarse grained and B3N fine grained	Composite sample of the two types of B3 in this area	Map Loc. 42 - slightly further to the west again	DONE							